

CHAPTER EIGHT: THE ORLEANS EAST BANK (DOWNTOWN) AND CANAL DISTRICT PROTECTED AREA

8.1 Overview

The most populous of the four major protected areas that suffered significant flooding during Hurricane Katrina was the Orleans East Bank (downtown) protected area. As shown in Figures 2.4, 8.1 and 8.2, the Orleans East Bank (downtown) section is one contiguously protected section. This protected unit contains the downtown district, the French Quarter, the Garden District, and the “Canal” District. The northern edge of this protected area is fronted by Lake Pontchartrain on the north, and the Mississippi River passes along its southern edge. The Inner Harbor Navigation Canal (also locally known as “the Industrial Canal”) passes along the east flank of this protected section, separating the Orleans East Bank protected section from New Orleans East (to the northeast) and from the Lower Ninth Ward and St. Bernard Parish (directly to the east.) Three large drainage canals extend into the Orleans East Bank protected section from Lake Pontchartrain to the north, for the purpose of conveying water pumped north into the lake by large pump stations within the city. These canals, from west to east, are the 17th Street Canal, the Orleans Canal, and the London Avenue Canal.

Figure 8.2 shows how this single, contiguously protected unit can be sub-divided into several localized sub-basins separated by a series of ridges, levees and canals. The base map of Figure 8.2 is the flooding map of Figure 2.17 (repeated here) which shows the flooding on September 2, four days after the passage of Katrina. The elevation of the top of the floodwaters in this figure is Elev. +3 feet (NAVD 88). This is approximately the peak flooding, and the depths of flooding shown at this point in time reflect the underlying basin topography and thus serve well to illustrate how the overall protected zone can be approximately subdivided into four separate zones or sub-basins.

The original city of New Orleans had been founded on the high ground adjacent to the Mississippi River (along the southern edge of this protected area.) The river “climbs” within its own channel, periodically depositing overbank sediment deposits which form “natural levees” to constrain its path, until it rises above the surrounding countryside. Then, periodically, the river breaks through its own “natural levees” and takes a new path to the Gulf. The riverbank deposits thus represent the highest ground locally, and it was here that the city began.

As shown in Figure 8.2, this high ground adjacent to the river now comprises much of the expensive Garden District, and much of downtown New Orleans and the historic French Quarter as well. Due to their elevation (typically Elev. +2 feet above Mean Sea Level and higher) these areas remained largely unflooded. Most of the remainder of this large and densely populated protected zone lies at lower elevations, however, and so most of the rest of this zone was flooded.

As also shown in Figure 8.2, a ridge of high ground known as Metairie Ridge separates the low-lying northern (Canal District) portion of this protected area from the

southern half. Metairie Ridge is the result of a previous river “stand”, and resulting river deposits. The Metairie Ridge did not quite successfully separate the northern and southern halves of this protected section during Katrina; flow passed over the ridge at a number of locations carrying floodwaters from the catastrophic northern drainage canal breaches into much of the rest of the protected area to the south. This flow over (across) the Metairie Ridge was noted by eyewitnesses (Van Heerden, 2006), and is also confirmed by calculations of flows through the various breaches.

As described previously in Chapter 2, the initial breaches in this protected area occurred along the eastern flank (on the west bank of the IHNC). Several breaches occurred along this frontage. These breaches allowed significant amounts of water to flow into the adjacent neighborhoods, but these breaches were non-catastrophic; they breaches did not scour to a depth below mean sea level, so that as the storm surge subsequently subsided the flow inwards through these breaches was eventually halted as the IHNC water levels fell below the (mean sea level plus) “lips” of these breaches. Our current estimates, based on simplistic calculations of flow and surge heights vs. time, suggest that approximately 10% to 20% of the eventual flow into the overall Orleans East Bank (Downtown) protected area came through these breaches. Similar calculations, in a bit more detail, by Team Louisiana suggest that approximately 12 to 15% of the overall floodwaters eventually filling the Orleans East Bank protected area came through the breaches on this east bank of the IHNC (Mashriqui, 2006).

The vast majority of the flow into the Orleans East Bank came through the three subsequent, catastrophic breaches in the drainage canals at the northern edge of the Orleans East Bank protected area. As shown in Figures 8.1 and 8.2, one catastrophic breach occurred on the 17th Street drainage canal and two catastrophic breaches occurred on the London Avenue drainage canal. These all eroded (scoured) to depths well below mean sea level, and so continued to admit flow into the city from Lake Pontchartrain well after the initial storm surge had subsided. The drainage canal located between these two (the Orleans Canal) did not suffer any breaches, but the southern end of this canal was unfinished and a “gap” (low area) in the floodwall at the southern end of this canal allowed water to flow freely into New Orleans for a number of hours during the peak of the storm surge.

It was, however, mainly the flow through the three catastrophic breaches in the 17th Street and London Avenue drainage canals that accounted for approximately 85% of the flooding that slowly filled this Orleans East Bank protected area during and after the storm. Flow from the canals overflowed the northern basin and eventually also flowed over the Metairie Ridge and into the other zones shown as flooded in Figures 8.1 and 8.2. This flooding continued to progress after the initial storm surge had subsided, and flooding in the southern portions of this protected zone continued to worsen overnight and into the three days that followed, finally equilibrating with the slightly inflated water levels in Lake Pontchartrain on Thursday (September 1.)

As discussed in Chapter 2, this flooding had catastrophic consequences, accounting for approximately half of the total loss of life in this event, and a similar share of the economic damages as well. The performance of the flood protection system in this Orleans East Bank

(downtown) basin is thus of great importance, and was studied in some detail by this investigation.

8.2 Performance of the Flood Protection System Along the West Bank of the Inner Harbor Navigation Channel (IHNC)

8.2.1 An Early Breach at About 4:45 a.m.

As described previously in Chapter 2, the first levee breach and failure in the metropolitan New Orleans area appears to have occurred along one of the banks of the IHNC.

Figure 8.3 shows water elevations at three gage stations as well as at a manual water elevation station in the IHNC as the hurricane storm surge initially began to raise the water levels throughout the IHNC region on the morning of August 29th. As the storm began to approach the coast, water levels within the IHNC began to rise. By about 4:30 a.m. the water level within the IHNC had risen to approximately +9 to +9.5 feet (MSL). Then, at approximately 4:45 a.m., two of the gauges near the Highway I-10 bridge registered a sudden change in the otherwise relatively constant rate of rise in water levels. The U.S. Geological Survey (USGS) gage at this location shows a precipitous drop in water levels at approximately 4:45 a.m. The Orleans Levee District gage was “sampled” less frequently, but it also shows a reduction in rate of local water level rise between about 4:45 and about 5:00 a.m.

These gage readings appear to indicate that a levee breach occurred at about 4:45 a.m. near the I-10 Bridge across the IHNC channel, resulting in a local and temporary drawdown of the otherwise rising water levels in the IHNC.

A number of levee breaches occurred during Hurricane Katrina along the north-south channel of the IHNC, so there is no shortage of candidate sites for this breach.

Many of the partial breaches and distressed levee sections of New Orleans East fronting the IHNC (on the east bank of the IHNC) were relatively minor features, with minor flow potential, and could not have accounted for the significant changes observed in the gage readings shown in Figure 8.3. In addition, a number of these features showed evidence of erosion and scour specifically due to overtopping, indicating that water elevations significantly greater than +9 feet (MSL) eventually occurred at their locations.

Similarly, the timing(s) of the occurrences of the two large breaches on the east side of the IHNC at the edge of the Ninth Ward are well-established by eye witnesses as well as by “stopped clock” data, and these two major breaches appear to have occurred considerably later at about 7:45 a.m.

A significant breach occurred on the west side, behind the main Port of New Orleans, due to overtopping and erosion of soil support for an I-wall (see Section 8.2.3.1.). The elevation of the I-wall, and the observed overtopping erosion, indicate that this failure occurred later in the morning as well when the storm surge had risen high enough to pass water over the top of this floodwall (see Section 8.2.3.1.).

That leaves only three candidate breach sites that might have caused the drop in water level rise shown at about 5:00 a.m. in Figure 8.3.

One of these is the breach on the east side of the IHNC at the CSX railroad crossing and roadway crossing over the levee, as described in Chapter 7.

A second candidate site is the pair of breaches that occurred closely adjacent to each other at the south end of the main Port of New Orleans, as described in Section 8.2.3.3. These were large breaches, and might well have had sufficient flow as to account for the drop in water level rise shown in Figure 8.3. In addition, these sections were constructed of highly erodeable lightweight shell-sand fill, and might well have eroded early due to through-passage of seepage flows through the “earthen” levee embankment as the storm surge rose (but prior to full overtopping of the levee embankment at this location.) This is discussed further in Section 8.2.3.3.

A third candidate breach site is the west bank of the IHNC at the CSX railroad crossing, as described in Section 8.2.2. At this location, a steel “storm gate” on rollers had been damaged by a train accident several months prior to Hurricane Katrina, and was away for repair. In lieu of this missing gate, a sandbag levee crest section had been constructed in the opening left by the missing floodgate. The sandbags washed out at some point during Katrina, and this may have been the early breach reflected by the gage readings shown in Figure 8.3. At this same site, flow along the juncture between the railroad embankment and the adjacent embankment fill supporting an asphalt paved roadway passing over the earthen Federal levee resulted in erosion and scour that produced a second breach feature at essentially this same site, as is also described in Section 8.2.2.

In the end, based on the information currently available to this investigation team, any of these three candidate breach sites might have been responsible for the for the observed gage level drops shown in Figure 8.3.

8.2.2 The CSX Railroad Breach

As shown in Figure 8.2, the CSX railroad crosses the IHNC channel immediately to the south of the I-10 Highway bridge. On both the east and west banks of the IHNC, the railroad passes through the levee system by means of a gate through a structural concrete floodwall. Steel gates are used to close these openings during storms.

Figure 8.4 shows the concrete structural floodwall on the west side of the IHNC, at the east edge of the Orleans East Bank (Downtown) protected area. Note that there is no steel gate shown in this photograph. The steel gate at this location had been damaged by a train accident several months prior to Katrina’s arrival, and it was away for repair at the time of the hurricane.

In lieu of this missing steel gate, a temporary sandbag “levee” was erected across the opening. At some point during the storm this sandbag “levee” section either was pushed over by the rising storm surge or was overtopped and washed away.

In addition, erosion occurred at the juncture between the railroad embankment fill and the fill supporting an adjacent roadway passing over the earthen federal levee at this location, as shown in Figure 8.5. This roadway passed over the levee crest to provide access to port facilities on the outboard (water) side of the Federal levee system. This is shown in Figure 8.5, which is a view from the inboard side of this breach showing the erosion of the roadway fill. The elevated I-10 highway bridge is at the left of this photo, and the CSX railroad is just to the left (north) of the roadway. The roadway fill at this location was comprised largely of highly erodeable lightweight “shell sand” fill; a material not suitable for levee fill in a levee protecting a large population (especially without sheetpile cutoff or similar features to prevent erosion.) The flow appears to have passed initially through the pervious gravel ballast supporting the train rails (which is the “low point” at this complicated location), and then undermined the less competent fill beneath the roadway. The resulting flow through the eroded breach then passed to the inboard (protected) side and made its way into the adjacent neighborhood.

The erosion and scour at this conjoined pair of breach locations did not erode the base (lips) of these breach features to a level below mean sea level. Accordingly, although flow passed through this pair of features for a number of hours, the flow eventually ceased as the storm surge (water level rise in the IHNC) eventually subsided.

The failure at this site is an excellent example of a failure produced by multiple adjoining jurisdictions, and a lack of overall coordination of the various system elements constructed and operated by each. The Federal levee system was “penetrated” here by both the railway and the Port roadway, and the interactions of the pervious railway ballast and the highly erodeable roadway fill combined to fail the overall flood protection system at this location. Lack of coordination, and lack of authoritative oversight, of these disparate organizations and their disparate system components was a critical problem here.

It should be further noted that this same site had also failed catastrophically in 1965 during hurricane Betsy, so that the re-failure of this same location represents a daunting case of lack of progress and learning over the intervening 40 years. As discussed in Chapter 7, the east bank CSX rail crossing, which also failed during hurricane Katrina, was also a “repeat” failure (as it, too, had failed during hurricane Betsy in 1965.) The continued failure to recognize and suitably address the hazards associated with these complex “penetrations”, despite their demonstrated history of previous failure, is difficult to understand.

In addition, it is interesting to note that the steel gate was allowed to be removed for repair, rather than requiring it to be fixed in place until a suitable replacement gate (or at least interim replacement gate) could be fabricated and be brought in, so that trains could continue to operate. This created an obvious potential hazard to the safety of the very large community inboard of this rail crossing; placing the safety of many at increased risk. In hindsight; that was a decision that is difficult to justify.

8.2.3 Breaches and Distressed Sections at the Port of New Orleans

Three breaches occurred to the south of the CSX railroad breach on the west side of the IHNC at the main Port of New Orleans. Several additional levee and floodwall sections

were “distressed” or damaged, but did not fully breach along this same section. These breach and distress sites along this reach are jointly indicated as the suite of “Industrial Canal Overwash Sites” in Figure 8.2.

As the storm surge raised the water levels in Lake Borgne, and then pushed the elevated waters (and flow) westward through the “funnel” at the east end of the east/west trending GIWW/MRGO channel between New Orleans East and St. Bernard Parish, large flows and a major rise in water elevations pushed westward along the GIWW/MRGO channel to this channel’s “T” intersection with the IHNC channel, and raised the water levels within the IHNC channel.

This resulted in rising waters rushing directly at the west bank of the IHNC, coupled with overall raising of the water levels throughout the IHNC region. This produced distress, and several breaches, on the west side of the IHNC in the general vicinity of the main Port of New Orleans. The sub-sections that follow will describe each of these in turn.

8.2.3.1 Breach at Rail Yard Behind the Port of New Orleans

The northern-most of these features was a breach in a combined earthen levee and concrete I-wall section, as shown in Figures 8.6 and 8.7. This breach occurred behind the main Port of New Orleans, just to the south of the juncture between the east-west trending GIWW/MRGO channel and the IHNC, so the water pressures and overtopping from the lateral flow from the east-west trending GIWW/MRGO channel were particularly severe at this location, as indicated in hydrodynamic modeling by Team Louisiana (Mashriqui, 2006.)

At the time of our field team’s arrival in late September, this site was already under repair. The field team arrived at this site on the morning of September 30, 2005, and at that time the trench that had been scoured behind the wall on the north end of the breach had been “filled” with clayey backfill and additional backfill had been placed behind the wall to form an additional buttressing berm, as shown in Figure 8.6. A temporary access road had also been placed through the breach, as is also shown in this photo.

Figure 8.7 shows conditions on the north side of this breach, at the same point in time (on September 30.) The interim repair efforts had not yet reached the north side of the breach, and the mechanisms that contributed to this failure were still clearly evident here. As shown in Figure 8.7, significant overtopping had passed over the concrete I-wall and then cascaded down the backside, resulting in erosion of a “trench” at the base of the backside of the I-wall. It should be noted that water falling over an 8 foot high I-wall strikes the ground at a velocity on the order of about 20 to 25 feet per second; sufficient to cause rapid erosion at the point of impact.

The initial height of the compacted embankment fill on the backside of the I-wall prior this erosion can be clearly seen in Figure 8.7 by the soil markings on the I-wall at the left of the photograph. The depth of this erosion (scour) from the elevation of the top of the pre-event I-wall/soil crest contact to the base of the eroded trench was 4.5 feet at the location of the photographer taking the photo of Figure 8.7, and it deepened progressively towards the actual breach location approximately 25 feet to the North. Just before reaching the actual

displaced I-wall section shown in Figure 8.7 this depth of erosion was approximately 5.5 feet, so that the depth of erosion at the location of the actual I-wall failure was likely on the order of 5.5 to 6.5 feet.

The depth of the sheetpiles was unusually shallow at this location, as shown in Figure 8.8. The I-wall “stick-up” had not been large at this location, and it was not felt that very long sheetpiles were needed to support this I-wall by means of cantilever action given its relatively short unsupported length (stick-up). There was no sign of lateral embankment movement at this site, and the sheetpiles and I-wall showed no signs of flexure on their vertical axis (along their length from top to bottom.) The I-wall failed by rigid body “toppling” laterally towards the inboard (protected) side in a “rigid, post-hole” toppling mode as it became progressively unbraced by the erosion of the supporting soil at the inboard toe. Eventually, it became unable to support the water pressures on the outboard (canal) side due to the storm surge and hydrodynamic forces, and the I-wall toppled far enough to permit catastrophic erosion at the main breach section.

As shown in the cross-section of Figure 8.8, the sheetpiles at this section were only 14 feet in length, and were tipped at a base elevation of approximately -6 feet (MSL). As the overtopping water cascaded over the top of the concrete I-wall, the resulting trench eroded to a depth of approximately 6 feet below the original wall/soil crest contact, and the critical section achieved approximately the geometry shown in Figure 8.8. Soil properties are not well established at this location, as site specific investigation was not possible within the budget and time constraints of this independent investigation. Accordingly, soil stratigraphy and soil properties used in our analyses are inferred from the original design data available from the USACE.

Based on the field observation that no major embankment foundation failure was observed, the most significant properties for analysis of this section were the sheetpile sections (which were PZ-22) and the properties of the engineered embankment fill (which was a moderately compacted silty clay of medium plasticity). Shear strength of the embankment fill was modified to determine the strength (and stiffness) at which the observed failure would be expected to occur, and it was found that the I-wall section would be marginally unstable with a fill strength of approximately 600 to 1000 lb/ft². This appeared to be well-representative of the strength of the observed fill, and the failure mode (shown in Figure 8.9) matched well with the field observations. Figure 8.9 shows the results of Finite Element Analyses (FEA) performed using the program PLAXIS; in this case for embankment shear strength of approximately 800 lb/ft², and with a trench to a depth of 6 feet behind the floodwall. This Figure shows calculated displacements, and the rigid toppling mode of wall failure can be clearly seen. Lateral failure of the I-wall results in large part from shearing at the transition between the base of the embankment fill and the underlying foundation soils.

It appears that this failure could have been prevented, simply and at little incremental cost, by installation of concrete “splash pads” or other erosion protection at the base of the inboard side of the I-wall to prevent the observed erosion. Similarly, this failure would have been prevented if the floodwall had been a “T-wall” section, as illustrated in Figure 8.10(b), rather than the less expensive “I-wall” section, as illustrated in Figure 8.10(a). The I-wall sections are supported laterally only by the cantilever action of their supporting sheetpile

walls, and this cantilever action is adversely affected by this erosion. T-walls, on the other hand, have lateral concrete stems at their bases and these are supported both laterally and rotationally by battered piles (providing a much higher level of rotational resistance.)

Instead a significant breach occurred, and floodwaters passed through the adjacent railroad yard and into the adjacent neighborhoods for a number of hours. This breach was located well inboard from the actual edge of the IHNC channel, however, and the breach did not erode its front lip to a depth below mean sea level. Hence, this flow eventually ceased as the storm surge subsequently subsided later in the morning of August 29th.

8.2.3.2 Erosional Distress at Floodgate Structure Behind the Port of New Orleans

Just a few hundred yards to the south of the breach described in the previous section, significant erosional distress occurred at a concrete I-wall and floodgate structure behind the Port of New Orleans. As shown in Figure 8.11, this concrete wall and steel gate structure provided access from the rail yard (on the protected side) to Port facilities (on the water side) which can be closed off by means of a rolling steel floodgate.

Significant erosional distress occurred at each end of this floodgate structure as it “transitioned” to join the earthen levee and floodwall at each end. An example, at the north end of this structure, is shown in Figure 8.12. In this figure, the canal is on the left and the “protected” side is on the right. The trench-like feature at the outboard side toe of the floodwall is the “gap” left when the wall displaced to the right as overtopping eroded a trench on the right side of this wall, laterally unbracing the very short sheetpiles and wall. New fill has been placed on the right side (as an interim repair), so this erosion is no longer visible. The concrete wall of the gate structure has not displaced, as it is supported on a T-wall basis, and the rotational stiffness of the battered piles has been sufficient to prevent wall rotation.

The erosion at the juncture between the concrete gate structure and the adjacent concrete I-wall was locally exacerbated by the disparity in top elevations between these two walls; which acted to locally concentrate the overtopping flow. Erosional distress of this sort, at the “transitions” between differing elements of the flood protection system, was a recurring theme in the damages caused by Hurricane Katrina.

8.2.3.3 Two Adjacent Erosional Embankment Breaches at the North End of the Port of New Orleans

Additional erosional “distress” and two large erosional breaches occurred slightly farther to the south, at the southern end of the main Port of New Orleans.

Figures 8.13 and 8.14 show two views of a large breach through an earthen levee at the contact (“transition”) between the levee and a concrete floodwall section. As shown in Figure 8.14, the embankment fill material is lightweight shell-sand, a material known to be unusually highly erodeable. This type of shell-sand material performed notably poorly at a number of locations during Hurricane Katrina, and is a material not suitable for construction of critical levees protecting large populations. At this location, no provisions (e.g. a sheetpile cut-off, etc.) had been made to prevent catastrophic erosion of this shell-sand fill due to either

overtopping or through-erosion (erosion due to through-flow prior to full overtopping.) In the absence of an eyewitness, it was not possible to discern from evidence at this site whether the embankment was actually overtopped, or whether flow through this highly erodeable fill caused progressive erosional failure prior to full overtopping.

Figure 8.15 shows a second large erosional breach, less than 50 yards from the breach shown in Figures 8.13 and 8.14. This embankment section was also comprised largely of highly erodeable shell-sand fill. A large scour hole can be seen to the right, immediately inboard of this large breach. The massive flows have rippled the asphalt tarmac, and detritus from the eroded shell sand fill is scattered over a large area. As shown in this photo, some of this shell sand detritus has been scooped back into the breach as part of the initial repair.

Although these two adjacent erosional breaches were both of good size, they were both located some distance inboard from the IHNC channel, and neither eroded a pathway all the way back to the IHNC channel that was continuously below sea level. As a result, although both breaches admitted significant volumes of water into the adjacent neighborhoods, flows through these two breaches eventually ceased as the storm surge subsequently subsided.

8.2.4 Summary and Findings

The breaches along the west bank of the IHNC were each “non catastrophic” as none of them eroded or scoured to such depth that their lip dropped below mean sea level. Accordingly, although they admitted significant volumes of floodwaters into the greater Orleans East Bank (downtown) protected area, these flows eventually ceased as the storm surge subsided. Together, these features appear to have contributed approximately 10% to 20% of the overall volume of floodwaters that eventually flowed into the Orleans East Bank (downtown) protected area.

Although they were each “non-catastrophic”, these features each had the potential to cause significant localized flooding and damage. They were also each the result of engineering lapses and/or lapses in oversight during design and construction; none of the failures in this area should have occurred at the storm surge and wind/wave loadings produced at these locations by Hurricane Katrina had proper design and construction features been included.

The removal of the steel floodgate at the CSX Railroad crossing, and the inadequate sandbagging of the resulting “gap” in the overall regional flood protection system should not have been permitted. The steel gate should have been immediately replaced with a suitable and serviceable temporary replacement until the original gate could be repaired and returned. Instead it was missing for approximately three months of the hurricane season. In view of the events during Katrina, it is difficult to justify the decision to remove the gate and thus maintain the “operability” of the railroad line when it placed the “operability” of the flood protection system, and the safety of the community, at risk.

Similarly, the confluence of the CSX railroad embankment and the adjacent roadway both passing over/through the Federal levee system immediately to the south of the I-10

bridge represents one of many “transitions” between disparate flood protection system elements that performed poorly as an apparent result of lack of appropriate oversight and/or poor design with regard to how abutting elements of the system joined at their edges. In addition, highly erodeable shell sand fill was used at this roadway location without suitable cut-off by means of sheetpiles, etc., representing a hazardous condition that should have been caught and remedied prior to Katrina’s arrival.

The erosional “distress” that occurred at the junctures of structural I-wall sections and the structural T-wall gate structure at the rail yard behind the Port of New Orleans represent additional examples of inadequate attention to details at “transitions” between adjacent sections of differing type and geometry.

The two large erosional breaches at the south end of the Port of New Orleans were clearly the result of use of inappropriate fill materials (highly erodeable lightweight shell-sand fill) in earthen embankment sections with no suitable provisions to reduce the obvious risk of catastrophic erosion and breaching. This, too, should have been spotted and remedied prior to Katrina’s arrival. It is not clear whether these two breach sections were overtopped by the rising storm surge, or whether the embankment sections eroded as a result of “through flow” prior to full overtopping as the waters rose within the IHNC.

Finally, the I-wall section breach behind the Port of New Orleans was largely the result of overtopping and subsequent erosion at the base of the inboard toe of the concrete I-wall. This failure could have been prevented, at relatively little incremental cost, by installation of concrete splash pads or other erosion protection at the inboard toe of this floodwall. In addition, there was ample right of way available to construct a somewhat wider (and heavier) levee embankment on the inboard side of this I-wall. The incremental cost of doing so would have relatively small, and that too would likely have prevented this failure.

8.3 The Canal District Failures

8.3.1 Introduction

As the eye of the hurricane began to pass to the northeast of New Orleans, the counterclockwise swirl of the storm winds caused a surge in water levels along the southern end of Lake Pontchartrain. The storm surge along the Pontchartrain lakefront (which peaked at about 9:00 to 9:30 a.m. at an elevation of about +10 feet, MSL) did not produce water levels sufficiently high as to overtop the crests of the concrete floodwalls atop the earthen levees lining the three drainage canals that extend from just north of downtown to Lake Pontchartrain; the 17th Street Canal, the Orleans Canal, and the London Avenue Canal. Three major breaches occurred along these canals, however, and these produced catastrophic flooding of large areas within the Orleans East Bank protected area (as shown in Figure 8.2.)

The first major breach along the drainage canals occurred near the south end of the London Avenue canal, between about 7:00 to 8:00 a.m. The second breach occurred near the north end of the London Avenue canal, and the best current estimates of the timing of this breach are between about 7:30 to 8:30 a.m. The third major breach occurred near the north

end of the 17th Street canal. The main breach here occurred between about 9:00 to 9:15 a.m., but this may have been preceded by earlier visually observable distress at this same location. All three of these breaches rapidly scoured to depths well below mean sea level, so they continued to transmit water into the main Orleans East Bank (downtown) protected area for three days after the initial peak storm surge subsided. More detailed discussions and analyses of these catastrophic drainage canal breaches are presented in the sections that follow.

The resulting flooding of the main Orleans East Bank (Downtown) protected area was catastrophic, and resulted in approximately half of the 1,293 deaths attributed (to date) to the flooding of New Orleans by this event. Contributions to this flooding came from the overtopping and breaches along the IHNC channel at the east side of this protected area, as described previously in Section 8.2, but the majority of the flooding (approximately 80% to 90% of it) came from the three catastrophic failures along the drainage canals at the northern portion of this protected area.

In addition, one of the drainage canals (the Orleans Canal) had not yet been fully “sealed” at its southern end, so that floodwaters flowed freely into New Orleans during the peak of the storm surge through this unfinished drainage canal. A section of levee and floodwall approximately 200 feet in length had been omitted at the southern end of this drainage canal, so that despite the expense of constructing nearly 5 miles of levees and floodwalls lining the rest of this canal, as the floodwaters rose along the southern edge of lake Pontchartrain, the floodwaters did not rise fully within the Orleans Canal; instead they simply flowed freely into downtown New Orleans.

By about 9:30 a.m. all of the levee failures had occurred, and the main Orleans East Bank (downtown) protected area was slowly filling with water. As the northern end filled from the three catastrophic breaches along the drainage canals, water eventually began to pass over low spots in the Metairie Ridge and flowed into the southern zones within this protected area as well.

The sections that follow present more detailed examinations of the performance of the flood protection system in the “Canal District”.

8.3.2 The Lining of the Drainage Canals

There were a number of lapses, errors and poor decisions that led to the catastrophic breaches along the drainage canals and thus the flooding of the main section of metropolitan New Orleans. Several of these began right at the start, in the aftermath of Hurricane Betsy (of 1965) and the flooding caused in New Orleans by that event.

The decision was made, in the wake of Hurricane Betsy, to raise the level of flood protection throughout the region. The three drainage canals (the 17th Street, Orleans and London Avenue canals) were problematic in this regard, however, due to limited right-of-way adjacent to the existing embankments lining these canals.

As described in Chapter 3, the USACE argued (correctly as it turned out) that the low-rise levees lining the canals were not adequately stable as to sustain a significant raising, and

that the preferred solution would be to place storm gates at the north ends of the three canals which could be closed in the event of a Hurricane to prevent storm surge rise within the canals.

This proposal was bitterly contested by the local Water and Sewerage Board, who were concerned that the gates would be under the control of the local Levee Board, and that they might therefore be impeded in their efforts to operate the massive pumps to “unwater” the city from heavy rainfall (which is also a source of frequent, though non-catastrophic, flooding problems in New Orleans.)

The USACE was, in the end, not allowed to install the floodgates, which would have been the technically superior solution, largely as a result of the internecine distrust between the local Levee Board and the local Water and Sewerage Board. In response, the USACE attempted to “exempt” the three canals from the otherwise contiguous levee system around the main metropolitan Orleans East Bank (downtown) protected area.

As discussed in Chapter 3, lobbying by State and local interests next resulted in a Senate rider (inserted clause) on a bill that un-exempted the three canals and specifically required the USACE to raise the level of flood protection along these three canals. This was the first of a number of causative errors that would prove catastrophic here. The canals would remain open to hurricane-induced storm surges at the south end of Lake Pontchartrain; essentially “allowing the enemy (storm surges) right into the backyard” of metropolitan New Orleans.

A second problem now arose. The existing levees were low, and they were relatively narrow as well. Homes had been constructed throughout the area, and the private property at the inboard (protected side) toes of these existing levees left inadequate space for construction of wider levees. Accordingly, a decision was made to raise the level of flood protection by adding reinforced concrete floodwalls to the crests of the existing earthen embankments.

This, in effect, represented a decision to work within the narrow space available rather than purchasing additional property to allow construction of wider, and more stable, levee sections. That was a second issue that contributed significantly to the catastrophic failures that occurred along the drainage canals.

It also resulted in difficulties with regard to both maintenance and inspection, as private homes at the toes of the levees often had property lines interfering with inspection of conditions at the inboard (protected side) toes. In some locations, private property (mainly people’s back yards) extended up the inboard slope faces of the levee embankments, and trees grown on these faces and at the inboard toes of the levees represented an obvious hazard both with regard to seepage erosion and also with regard to the possibility that trees would blow over (in water softened ground) during hurricanes. This would leave large voids (the sizes of their root balls) at a very dangerous location (right at the inboard toes of the levees) at a time when storm surges in the canals were simultaneously rendering seepage erosion, and inboard slope stability, very tenuous. During Hurricane Katrina a number of large trees did indeed topple, leaving dangerous voids at the toes and on the inboard slope faces of the levees along these canals.

In addition, along some sections private homeowners excavated and constructed in-ground swimming pools in close proximity to the inboard toes of these levees, effectively partially undermining them and rendering them less stable. This, too, should have been prevented.

The abutting private properties also led to inspection difficulties, as inspection of conditions immediately inboard of the levee toes is of great importance and private property rights largely prevented inspectors from walking these critical areas. Reports of seepage and wetness at some locations were made to the local Water and Sewerage Board (who were responsible for “unwatering”, and were thus the group to whom such reports were made), but this investigation team has not been able to determine whether these were then passed along to the local Levee Board or to the USACE, to whom they might have represented unanticipated seepage problems warranting further investigation. Certainly the USACE has stated that they were unaware of such reports.

Lack of appropriate control of conditions at the inboard levees toes, and lack of suitable access for inspection and maintenance at the inboard toes, represented additional inadvisable sources of increased hazard.

8.3.3 The E-99 Sheetpile Wall Test Section:

In order to effect the raising of the flood protection levels within the narrow right-of-way available, the decision was made to erect concrete floodwalls at the crests of the existing earthen levee embankments. To facilitate the analysis and design of these challenging sections (on narrowly confined rights-of-way, and on very difficult foundation soil conditions) the New Orleans District of the USACE made an admirable decision to construct a test section and perform a full-scale test of this type of design.

Very similar (difficult, swampy, riverine delta) soil conditions exist nearby in the Atchafalaya river basin (approximately 80 miles to the west), and a site in this area was selected. A sheetpile “I-wall” and contiguous sheetpile curtain, was constructed on the inboard side stability berm of a federal levee in the Atchafalaya basin in a configuration that was very similar to the eventual installation of similar sheetpile-supported concrete floodwalls at the crests of the low-rise levees along the drainage canals in New Orleans (Foott and Ladd, 1977). The swampy foundation soils at this test site were remarkably similar to those at the north end of the 17th Street canal in New Orleans. A sheetpile cofferdam was constructed adjacent to the full-scale test section, and was filled with water to load the test section’s I-wall and its supporting sheetpile curtain.

Two important lessons were learned from this test, and from subsequent analyses (e.g.: Jackson, 1988; Foott and Ladd, 1977; Oner, Dawkins and Mosher, 1997; Oner, Dawkins, Mosher and Hallal, 1997). One was that a gap opened between the sheetpile curtain and the outboard side earthen embankment during loading (by raising of the outboard side water level), and then water penetrated into this gap. This effectively cut the supporting embankment in half, and the water pressures applied against the lower sheetpile sections helped to push the inboard half of the embankment, as well as the I-wall and its supporting sheetpile curtain, towards the inboard (protected) side. This was a failure mechanism that had

not traditionally been considered in the local design of floodwall systems in the New Orleans District. The other lesson was the shape of the failure surface, which was more curved than the deeply plunging three-wedge “planar” failure surfaces considered in the “method of planes” used for analysis of these types of sections in the New Orleans District of the USACE.

Unfortunately, despite publication of these important findings in both internal USACE reports as well as in electronic professional journals (e.g.: Oner, Dawkins and Mosher, 1997; Oner, Dawkins, Mosher and Hallal, 1997), and despite the fact that these studies had been undertaken to facilitate the design of the challenging floodwalls along the drainage canals and the IHNC, neither of these lessons were then incorporated in the subsequent design of the floodwalls along the 17th Street, Orleans and London Avenue drainage canals, nor along the IHNC.

8.3.4 Field Tests for Assessment of Underseepage Risk at the Canals

The USACE also commissioned a pair of local permeability tests at two selected sections along the drainage canals to assess the rate at which changes in water levels within the canals were transmitted through the soils beneath the embankments. The intent here was to assess whether or not it would be necessary to drive the sheetpile curtains deep enough to “cut off” such underseepage flows for the transient loading conditions represented by a storm surge that would raise and then lower the canal water levels within a matter of hours.

The two sections selected were instrumented with piezometers at a series of stations orthogonal to the canals so that the water levels (phreatic surface) could be observed. The canal sections were then excavated to increase the cross-section available for pumping flows. It was assumed that this excavation and deepening would remove the sediment that “sealed” the canals, and would result in an increase in the observed phreatic surface. If little rapid rise was observed, then that would indicate that the increased hydraulic pressures of a transient storm surge would not propagate rapidly under the levees.

There were two critical flaws to this reasoning. One was the assumption that two such tests could suitably characterize the highly variable soil conditions along many miles of the three drainage canals (and also the IHNC). The other was that this testing program failed to note the alternate possibility that the canals were not well “sealed” at all; in which case simply excavating the canals to greater depth would result in no net change in the observed phreatic surface in the piezometers installed inboard at the test sections (the canal water levels would be unchanged by the excavation of the canal bases, and if “steady state” seepage conditions were already established based on full connectivity between the canals and the inboard toe areas then no net change in phreatic surfaces would be observed.)

When the canals were excavated, no significant change in inboard water levels was noted, and it was concluded that underseepage would not pose a significant risk for a short-lived (transient) storm surge. That would prove to be a very serious error, and would result in sheetpiles throughout the system (the three drainage canals and the IHNC as well) routinely being far too short to adequately cut off underseepage. Several major failures along the

drainage canals and the IHNC would result from underseepage during Hurricane Katrina, and the short sheetpiles continue to pose a risk to the remaining sections today.

8.3.5 Water Levels Within the Canals During Hurricane Katrina

Figure 8.16 shows the calculated peak storm surge heights along the southern shore of Lake Pontchartrain based on the most recently available IPET analyses (IPET Report No. 2: April, 2006). These are in close agreement with similar analyses by Team Louisiana along the canal frontage (Kemp and Mashriqui, 2006). As shown in this figure, the storm surge was estimated to be a bit higher at the west end of the “Canal District” than at the east. The water elevations shown in Figure 8.16 are based on the NGVD 29 datum, and must be reduced by about 1 foot to be compatible with the approximate local Mean Sea Level datum used in this report. With this adjustment, the projected peak water levels at the northern ends of the drainage canals are on the order of +10 to +11 feet (MSL) based on these hydrodynamic analyses.

Figure 8.17 shows locations at which relatively reliable high water marks near the mouth of the 17th Street Canal [IPET Report No. 2, 2006]. These high water locations were selected so as to be affected as little as possible by wave action, so that the water levels recorded would be the mean surge height (without wave action.) Based on these data, the IPET study concluded that the maximum storm surge rise at the mouth of the 17th Street Canal was on the order of +11 feet (NAVD 88-2004.66 datum, which is approximately MSL).

Figure 8.18 shows a hydrograph of estimated water elevations vs. time within the 17th Street Canal, based on the hydrodynamic calculations performed by IPET and on observations of water levels at nearby sites [IPET Report No. 2; April, 2006]. This hydrograph peaks at an assumed height of approximately +11 feet, and it peaks fairly sharply between about 9:00 to 10:00 a.m.

Based on the watermark data, our own field observations, and observations and data provided by Team Louisiana (Kemp, Mashriqui and Van Heerden, 2006), our team feel that these are realistic estimates of the surge heights near the mouths of the three key drainage canals (the 17th Street, Orleans, and London Avenue canals), but that they likely slightly overestimate the water levels. Our team has assumed a peak surge height of approximately +10 to +10.5 feet (MSL) at the mouth of the 17th Street Canal, and slightly lesser heights of on the order of +9.5 to +10 feet (MSL) at the mouths of the Orleans and London Avenue canals.

Accordingly, the hydrograph of Figure 8.18, but with a slight reduction of peak surge height (to approximately +10 to +10.5 feet, MSL in the 17th Street Canal, and +9.5 to +10 feet, MSL in the Orleans and London Avenue Canals) will be used for these current studies.

8.3.6 The Orleans Canal

As described previously in Chapter 3, the U.S. Army Corps of Engineers had lobbied and fought for many years to install floodgates to close off the three drainage canals (the 17th Street, Orleans, and London Avenue canals) during hurricanes so that storm surges would not push their way up into these canals. That would have been a superior technical solution, but it was not allowed as there was internecine fighting between the local Levee Board (who are in charge of “protection”; including levees, walls and floodgates) and the local Water and Sewerage Board (who are in charge of “unwatering” by means of pumping for both rainfall and other flooding.) The Water and Sewerage Board were concerned that the floodgates would not be under their control, and so their ability to pump out rainwater from rainstorms (also a cause of flooding in New Orleans) might be obstructed.

As a result of the two disparate local Boards being unable to resolve their differences in the interest of the greater Public good (and safety), the sides of all three drainage canals were instead lined with floodwalls topping the earthen levees along both sides. This, in effect, opened many additional miles of narrow levees and floodwalls atop difficult (and often marshy) foundation soil conditions to storm surges; greatly increasing vulnerability by “allowing the enemy right into the backyard” of this protected area.

An extreme example of the dangers resulting from the poor interaction between the local Water and Sewerage Board and the local Levee Board occurred at the south end of the Orleans Canal.

At the south end of this canal, the main pumping plant crosses the end of the canal as a “T”. Levees and floodwalls provide storm surge protection to an elevation of approximately +13 feet (MSL) along essentially the full length of both sides of the canal, except at the southern end.

The pumping plant is a brick masonry building that was constructed in 1903, and it houses several of the large capacity Woods pumps of that same era. When the water level within the canal rises three to four feet above normal, the operators report that water seeps through the wall of the building that fronts the canal. It is clear that raising the water level significantly higher against the brick face of this old structure would induce water pressures that could collapse this wall.

The obvious solution would have been either: (1) for the Levee Board to construct a floodwall across the south end of the canal, joining to the levees and floodwalls lining the east and west banks of the canal, thus sealing the end of the canal and simultaneously protecting the ancient structure, or (2) for the Water and Sewerage Board to construct a stronger wall, to achieve the same two purposes.

Neither happened.

The Levee Board did not construct the wall to protect the property of the Water and Sewerage Board (and the safety of the Public by closing the base of the canal), and the Water and Sewerage Board did not assist the Levee Board by closing off the end of the canal (and

protecting their own building at the same time.) Instead, an opening of approximately 200 feet in length was left “open” on the east side at the south end of the otherwise continuous levee and floodwall system lining the rest of this canal. A concrete “spillway” section occupies this gap, to prevent erosion from further exacerbating the flows emanating from this hole in an otherwise continuous flood protection system.

Figure 8.19 is a view of the south end of the Orleans canal, showing the brick masonry pumping house, the levees and floodwalls on both sides of the canal, and the “gap” at the south end of the east bank (on the left side of this photo.) Figure 8.20 shows this “gap” from the outboard side, with elevations of key features indicated. Figure 8.21 shows an oblique view from rotation of three-dimensional LIDAR survey measurements (see Appendix A) of this same section. All dimensions, and elevations, are captured by this LIDAR dataset to an accuracy of approximately ± 0.1 feet (or less). The “spillway” section across the open gap has a crest elevation of approximately +6.8 feet (MSL), with a marginally lower “low spot” slightly to the north of the concrete “spillway” section at Elev. +6.5 feet (MSL). The “gap” thus represents a long opening in the otherwise contiguous levees and floodwalls along many miles of both sides of this canal, and with a top elevation of approximately 6 feet below the top of the adjacent floodwalls topping the levees (permitting overflow at approximately Elev. +6.5 to +6.8 feet, MSL.)

As a result, while the storm surge along the southern shore of Lake Pontchartrain was raising the water levels within the full lengths of the adjacent 17th Street and London Avenue drainage canals, the rising storm surge (after reaching an elevation of approximately +6.5 feet, MSL) simply caused floodwaters to flow freely into the heart of New Orleans through this “gap” in the flood protection system.

The opening left at the south end of the Orleans canal resulted in lower water levels toward the south of the canal, but did little to alleviate the storm surge rise at the north end. The lack of failures along the north end of the canal must therefore have been the result of more favorable embankment and floodwall geometries and/or foundation soil properties than occurred along failed sections of the nearby London Avenue and 17th Street drainage canals.

On both sides of this canal there was considerably more right of way available, and the earthen levee embankments along the Orleans canal are considerably wider than those along either the 17th Street or London Avenue canals. Figures 8.22 and 8.23 show views of these levee and floodwall sections along the east and west sides of the Orleans canal. The embankment widths shown in these photos are in strong contrast to the narrower embankments (and crowding from adjacent homes and yards) along the London Avenue and 17th Street canals, as shown for example in Figures 8.109, and 8.24 and 8.30, respectively.

An additional factor working in favor of the stability of the Orleans Canal levees and floodwalls was the fact that the relationship between effective soil overburden stress and resulting soil shear strength in the soft clayey and organic marsh soils near the north end of the Orleans Canal embankments and floodwalls had been better treated during initial analysis and design than it was for 17th Street Canal embankments and floodwalls for similar soils.

8.3.7 The 17th Street Canal

8.3.7.1 *The Breach on the East Bank*

(a) Introduction

One of the most catastrophic failures during Hurricane Katrina was a breach near the north end of the 17th Street Canal, on the east side, just to the south of the Hammond Highway bridge. The location of this breach is shown in Figures 8.1 and 8.2.

Figure 8.24 (which is a repeat of Figure 2.14) shows the use of military helicopters to place oversized bags of gravel into this breach. This photo shows a number of important features at this breach site. In this photo, it can be clearly seen that the inboard side of the levee embankment (on the “protected” side of the floodwall) has translated laterally to the east (to the right in this photo, which is taken looking north.) The translated embankment section is relatively intact along the northern two-thirds of this breach, and appears to have swung much like a door about the northern end. Severe scour and damage to structures on the inboard (“protected”) side at the south end of this feature support this mode; the major rush of inflow was concentrated near the southern end of this breach.

A number of borings and Cone Penetration Test (CPT) probes were performed at this site by the IPET investigation, by Team Louisiana, and by the ILIT investigation team. In addition, several borings had been performed earlier, as part of the initial design studies for the raising of the floodwalls at this location. Figure 8.25 is an approximate plan view of this site, showing the locations of the borings and CPT performed by our (ILIT) investigation. This plan view also shows the locations of a number of important features that help to shed light on the causes and mechanism of this failure. Figure 8.25(a) shows the approximate locations of borings and CPT probes performed at this site by the IPET investigation.

Figure 8.26 shows two views of a cross-section through the heart of this breach along Section A-A' from Figure 8.25. Figure 8.26(a) shows this cross-section before the failure, and Figure 8.26(b) shows this same section after the failure. Nearby cultural features (including buildings, fences, and floodwall sections) as well as boring logs and CPT probes are projected to this cross section for graphical clarity.

As shown in Figures 8.25 and 8.26, the intact levee segment near the center of the breach moved laterally approximately 49 feet. To the inboard side (“protected” side) of the displaced levee embankment sections, three sets of exiting toe overthrust features were mapped, as also shown in these figures.

As shown in Figure 8.26(b), the breach was the result of a translational failure of the inboard section of the embankment, pushed laterally by the water pressures exerted by the storm surge in the canal acting on the outboard face of the floodwall and sheetpile curtain. Figure 8.27 illustrates the sequence of movements associated with this failure, again for the cross-section through Section A- A'. As discussed in the text sections that follow, the rising waters in the canal pushed laterally against the floodwall and eventually (progressively) opened a gap between the floodwall and the outboard section of the levee embankment, as

illustrated in Figure 8.27(b). Water then entered this gap, and increased the lateral push against the sheetpile curtain and floodwall. A shear failure then occurred in the foundation soils beneath the embankment, and the embankment section along with the sheetpile curtain/floodwall slid inboard, pushed laterally by the storm surge as illustrated in Figures 8.27(c) and (d).

Figure 8.28 is an oblique aerial view of this breach section, showing tops of the I-wall sections that “pushed” the inboard section of the earthen embankment (driven by water pressures on their outboard sides), and then toppled backwards towards the canal as the translating levee embankment section finally came to rest and as water pressures equilibrated when the neighborhood filled with water and the storm surge eventually subsided. It also shows two sections of floodwall at the northern end of the failure (the near end in this photo) toppled forward (toward the “protected” side) by the intruding floodwaters at the north end of this breach.

Figure 8.29 shows the tops of the I-wall sections at the very southern end of the breach, which were also left “toppled forward” (towards the inboard, or “protected” side) by the intruding floodwaters passing through the breach opening.

Figure 8.30 shows a collapsed metal shed, with a corrugated roof, that was pushed against the side of the home at 6914 Belaire Drive by “plowing” at the toe of the laterally translating earthen embankment section, as is also shown in Figures 8.26 and 8.27.

Figure 8.31 shows a foundation slab at the toe of the failed section, immediately to the south of the home at 6914 Belaire Drive. The final exiting toe thrust feature rises just at the near end of this slab, which was partially laterally displaced despite being supported by piles, as shown previously in Figures 8.26 and 8.27. Scour caused by the floodwaters also left an erosional depression beneath and behind this slab, resulting in the “pond” shown in the background of Figure 8.31. Also clearly visible in this photo are blocks of peat that were scoured from the foundation strata by the intruding floodwaters.

Figure 8.32 shows a piece of one of the exiting toe thrusts (Toe Thrust #1, from Figure 8.26(b)) at a location between the slab of Figure 8.31 and the home and collapsed shed of Figure 8.30. Figures 8.33 and 8.34 show two views of the other two toe thrust features which occur farther to the inboard (protected) side of the failure (Toe Thrusts #2 and #3, from Figure 8.26(b)).

The general failure mode involved water pushing on the canal side of the floodwall, resulting in the opening of a gap between the sheetpile curtain/floodwall and the outboard side of the earthen embankment. Water then flowed into this gap, and the resulting water pressures pushed the inboard half of the earthen embankment (and the sheetpile curtain/floodwall) sideways. This “cutting the embankment in half, opening a gap, filling it with water, and then pushing the inboard half of the embankment (along with the sheetpile curtain/floodwall)” mode of failure had not been considered or analyzed during the original design of the floodwalls along the drainage canals. It was, however, not an unexpected mode of failure as it had been clearly evinced in the E-99 full-scale test section experiment near

Morgan City in the nearby Atchafalaya basin in 1977 (as described previously in Section 8.3.3.)

In the second IPET interim report (IPET; April 1, 2006) this mode was selected as the likely mode of failure based on stability analyses and centrifuge model testing performed as part of the IPET studies. Our own investigation team had favored this failure mode from the time of the initial post-event field observations in September and October of 2005. It was apparent that this mode had been in operation at this site based on the field observations made at that time. In addition, the same mode had also been in operation, and was “frozen” in place as a partially developed or incipient failure, on the east bank near the north end of the London Avenue drainage canal (see Section 8.3.8), and the field evidence also clearly indicated that this same “half embankment with a water-filled crack pushing laterally” had been the mode of failure at the large breach on the west bank near the north end of the London Avenue Canal (see Section 8.3.8). Also, we had read the E-99 full-scale test section reports, and were aware of the likelihood of this mechanism.

The deeper question is: What was the underlying mechanism that produced the observed failure within the foundation soils beneath the embankment?

Here the findings of our investigation differ significantly from those of the second IPET interim report, and those of the IPET Draft Final Report of June 1, 2006 as well. The IPET report’s finding was that the failure was the result of a largely rotational failure, shearing mainly through the soft gray clays occurring beneath the organic, marshy layers that support the base of the embankment. Our own studies found that there were two mechanisms that were each capable of producing the failure and breach, and that the margins of safety associated with each of these did not differ by large amounts. The actual failure that occurred followed the weakest and least stable of these two mechanisms, and was a largely translational failure along a relative thin but laterally continuous stratum of weak and highly sensitive organic clayey silt silty clay embedded within the “marsh” layer as shown in the cross-sections of Figures 8.26 and 8.27.

An examination of the various soil units, the various potential failure modes, and analyses and explanation of the findings as to the nature of the actual failure mechanism, follow.

(b) Geotechnical Analyses of the Failure

As shown previously in Figures 4.14 through 4.17, the north end of the 17th Street Canal is situated atop largely paludal marsh clays and organic marsh deposits, in an area long riven with erosional drainage features associated with the Lake Pontchartrain basin.

Figures 8.35(a) and (b) present two additional cross-sections showing conditions prior to the failure along Sections B-B and C-C in Figure 8.25. As shown, the foundation soil conditions differed somewhat, but were largely similar along the width of the breach (failure) section.

As shown in Figures 8.26, 8.27 and 8.35, the levee embankment was comprised of two distinct soil fill zones. The upper embankment was a moderately compacted imported brown

clay fill, placed in the early 1970's. This fill had raised the pre-existing levee, which was comprised largely of locally available gray clay fill from the local swamp deposits. Placement of the original layer of gray clay fill dated back to the previous century, and these earlier "historic" fills had consisted of simply piling up locally available gray paludal marsh clays without compaction.

These two embankment fill zones were underlain by a layer of "marsh" deposits. This was actually a relatively complex and layered zone, consisting of strata of peaty organics interbedded with soft, sensitive organic clayey silts and plastic clays with very high water contents, and of varying organic and fibrous organic contents. Cypress tree root systems were common in this mixed "marsh" layer, apparently representing two distinct "stands" or levels of cypress marsh as shown in Figure 8.26(a), and these root systems often interfered with drilling and sampling.

The "marsh" layer was underlain by a transitional layer of progressively less organic soils, with fewer fibrous and peaty inclusions and an increasing fraction of soft, plastic gray clays. Beneath this transitional "intermixing" zone, the foundation consisted of soft, weak gray paludal marsh clays (CH) of high natural water content (natural water contents of $w_o \approx 85$ to 95 %.) These marsh clays were both weak and "sensitive". Sensitivities (the ratio of peak undrained shear strength vs. residual undrained shear strength) were typically on the order of 2 to 6.

These soft gray clays were underlain by fine sands. These sands are adequately strong and competent relative to the softer (and weaker) overlying soil units that they were not involved in the failure. Similarly, although these sands were relatively pervious, this was not a significant issue at this site as they occurred at sufficient depth that they were effectively "capped" by the relatively thick low permeability layer of soft gray clays.

The plan views of Figures 8.25 and 8.25(a) show the locations of borings and CPT probes performed for the original design studies, as part of the IPET investigation, and as part of our own studies. The pre-design and IPET borings generally used 5-inch diameter thin-walled fixed-piston samplers to obtain samples. Most shear strength data reported from both efforts that are currently available to our investigation team are the result of unconsolidated-undrained triaxial tests (UUTX) performed on these samples, although some samples were tested in unconfined compression (q_{unc}). A limited number of in-situ vane shear test results (VST) were also reported for some sites.

Our own field investigations involved primarily the use of 3-inch diameter thin-walled, fixed-piston Shelby tube samples, and laboratory UUTX tests were performed on many of these samples. The Shelby tubes were "modified" prior to use to eliminate the "roll-in" at the cutting end that produces overcutting and then allows lateral expansion of the sample during sample entry into the tubes. It has been shown (e.g. Lunne and Lacasse, 1994) that the use of this type of constant tube diameter, sharp-edged, thin-walled fixed piston sampling with good technique can greatly reduce the disturbance otherwise associated with sampling of the soft, sensitive clayey soils of principal concern at this site.

Some of the borings were sampled continuously and the samples were extruded onsite to examine the stratigraphy and geology in detail. Some of the borings were not sampled at all; instead in-situ vane shear tests were performed at selected depths within these boreholes. Some of the samples were retrieved and brought to the laboratory for testing. Finally, some of the samples were subjected to rather unusual laboratory vane shear testing, and this will be discussed in detail a bit later in this section.

The boring logs for all borings performed as part of these current studies are presented in Appendix B. Laboratory test data, including laboratory vane shear strength test data, are presented in Appendix D. In-situ vane shear strength test data for tests performed within the borings is summarized in Appendix D, and on the boring logs in Appendix B.

In addition to the borings, in-situ and laboratory vane shear and laboratory testing, both the IPET investigation and our own team performed a number of piezocone Cone Penetration Test (CPTU) probes. Logs of the CPTU probes performed as part of our studies are presented in Appendix C.

Figure 8.36 shows a summary of the shear strength test data available to our investigation team for the embankment fill at and near the 17th Street drainage canal breach site. Shear strength of the embankment fill is not of significant direct importance for the conventional overall stability analyses that will follow, as the embankment fill “went for the ride” and was carried along on shear surfaces that sheared through lower, weaker foundation soil units. The strength data from Figure 8.36 was of some importance, however, in selection of properties to model the nonlinear stiffness of these embankment soils in finite element modeling of this levee and floodwall section. The heavy line shown in Figure 8.34 is the shear strength modeled through the embankment fill along the embankment centerline (directly beneath the levee crest) in these studies. The strength lines representing CPT data in Figure 8.36 are based on interpretation of the CPT data using a cone tip factor of $N_k = 12$ in the upper, brown clay fill and $N_k = 12$ in the lower, gray clay fill as well.

Figure 8.37 shows an example of the available CPTU data beneath the central portion of the levee embankment, for “Marsh”, “Intermixing Zone” and “Gray Clay” strata shown in the cross-sections of Figures 8.27 and 8.35. Figure 8.38 shows a similar example of CPTU data, but this time for locations outboard of the toe of the levee embankment. As expected, shear strengths are notably lower here, due to lesser effective vertical stresses resulting from lesser overburden loads.

As shown in Figures 8.37 through 8.40, there are distinct differences between the “gray clay” strata and the “marsh” strata, and these will therefore be treated separately.

Beginning with the deeper unit, the gray clays, it must be observed that our interpretation differs somewhat from that presented in the second IPET interim report. The IPET report assumed that these clays were normally consolidated as they had been protected from desiccation by the overlying swamp deposits. Our interpretation differs, as we found three separate “stands” in the evolution of this layer of soft gray clays and the overlying marsh deposits, with three corollary desiccation-induced overconsolidation profiles associated with these.

The shear strength data based on UUTX tests from the initial design studies, as well as the IPET studies, showed considerable scatter and this was considered likely to reflect the issues associated with sampling disturbance for these soft, sensitive soils. The CPTU data from both the IPET and our own (ILIT) studies, on the other hand, appeared far more consistent within this stratum (as shown in Figures 8.37 and 8.38.) Figure 8.39 shows a typical plot of the pore pressure parameter B_q from a CPTU performed through the crest of the levee ($B_q = \Delta u / (q_{t-} - \sigma_{vo})$), highlighting the value of B_q where the clay appears to be normally consolidated. Figure 8.40 then shows these values of transposed onto the relationships of Lunne et al. (1985) and Karlsrud et al. (1996) to determine appropriate values of the cone tip factor N_{kt} for conversion of CPT tip resistance to undrained shear strength. As shown in this Figure, the value determined for this stratum was approximately $N_{kt} = 12$.

Figure 8.41 then shows the values of $[Su/P]_{OC} / [Su/P]_{NC}$ vs. OCR determined for minerologically similar Mississippi River clays of similar depositional history in Atchafalaya as determined by Foott & Ladd (1977). The SHANSEP exponent for these similar clays was found to be $\lambda = 0.75$, a relatively normal value for clays of this plasticity and character.

Using a value of $N_{kt} = 12$, and $\lambda = 0.75$, the CPTU data within the soft gray clay foundation stratum was then processed to develop plots of S_u/P vs. depth, and OCR vs. depth, for CPT beneath the full height of the levee (Figure 8.42) and inboard of the levee toe where effective overburden stresses were significantly lower (Figure 8.43).

As shown in Figures 8.42 and 8.43, the results show a pleasingly consistent pattern. The clay inboard of the levee toe clearly evinces three “stands” of the marsh development, with three OCR profiles associated with surficial desiccation. The clays beneath the levee embankment loads show just the residual tips of these same three OCR “crusts”, as the clays have been further loaded by the placement of the overlying embankment fill and so are more nearly normally consolidated over most of the stratum. Near the base of this stratum, the clays inboard of the levee toe show a minor degree of overconsolidation associated with secondary compression (as verified by subsequent consolidation analyses using the program PLAXIS which successfully modeled the evolution of this site and accurately reproduced this basal OCR profile).

In establishing the plots shown in Figures 8.42 and 8.43, the value of $(S_u/\sigma'_v)_{NC} = 0.31$ was found to best fit the data. This is a fairly normal value for clays of this plasticity, and it was exactly the same value found by Foott & Ladd (1977) for the minerologically similar clays at Atchafalaya.

The green lines in Figure 8.44 shows the resulting profiles of S_u vs depth within the soft gray clay foundation stratum (a) beneath the crest of the levee, and (b) inboard of the levee toe, based on $S_u/P = 0.31$ and $\lambda = 0.75$. Also plotted on this figure are the CPTU tip resistance data converted to S_u based on $N_{kt} = 12$, and the results of UUTX tests on “undisturbed” ILIT samples, lab vane tests (LVT) on ILIT samples and in situ field vane shear strength tests (FVT). The overall “fit” to all the data is generally very good.

Figure 8.45 then repeats Figure 8.44, but adds the rest of the available IPET and pre-Katrina strength data (including UUTX, FVST and CPT data.) For the “toe” region some

adjustment of this data is necessary in viewing this figure, as some of the IPET data is located such that some portion of the embankment overburden stresses slightly increase the shear strengths for some of the “toe” data; as a result these data (including the CPT) tend to drift to the right (to the stronger side) a bit, especially at depth. Overall, these additional data also well support the relationships developed.

Figure 8.46 then shows the selected value of $(S_u/P)_{NC} = 0.31$ for UUTX, field vane and lab vane tests plotted vs. data for other clays (Ladd, 2003). It also shows the value of $(S_u/P)_{NC}$ for direct simple shear (DSS) tests on the mineralogically similar Atchafalaya clays by Foott and Ladd (1973). Both sets of data fit well with the overall background relationship implied for other clays. This suggests that an appropriate scaling factor for the S_u values for conversion from “triaxial” conditions to the DSS stress path conditions that will better represent the stability and deformation analyses for this embankment and floodwall system is approximately 0.80 to 0.84, as shown in Figure 8.46. A value of $S_{u,dss} = 0.82 \times S_{u,tx}$ was used for this soft gray clay in these studies.

As an additional check, the value of $(S_u/P)_{NC} = 0.31$ (for triaxial and in situ vane shear) determined for these clays was also checked against other clays (Figure 8.47.)

Figure 8.48 shows similar treatment of the derivation of the CPT cone factor N_{kt} based on B_q , this time for the “marsh” deposits overlying the soft gray foundation clays. Based on a value of $B_q = 0.25$ to 0.40 , a value of $N_{kt} = 16$ was determined and used to process the CPT data for this unit.

A second approach was also used to also develop profiles of S_u/P vs depth and OCR vs. depth for these marsh deposits, as shown in Figure 8.49. The relationship of Mayne and Mitchell (1978) was used, in conjunction with the available UUTX, LVST and FVST data to iteratively develop relationships for S_u/p vs. depth and OCR vs. depth, as a function of Plasticity Index (PI, %) over the range $PI \approx 55\%$ to 140% , which encompasses the range observed in this complex soil unit. The resulting relationships confirm the classic desiccated OCR crust profile shown previously in Figure 8.41 for this “marsh” deposit.

Figure 8.50 then shows the resulting interpretation, based on all available data, of strength vs. depth within this complex marsh unit for conditions (a) beneath the overburden of the central embankment, and (b) inboard of the toe of the levee. The green lines in this figure represent the final interpreted soil shear strength profiles at these two indicative locations. As with the soft clays, these strengths were, finally, further slightly reduced by multiplying them by a factor of 0.82 to develop the DSS-type strengths needed for the stability analyses performed in these studies.

The red zone near the center of the “marsh” deposits shown in Figure 8.50 is a thin layer of soft, highly sensitive organic silty clay that varies slightly in depth across the profile (and so is thinner than it appears in this figure.) This was the material in which the main lateral translational shear failure occurred at this site.

Figure 8.52 shows a sample of this thin layer at one of three boreholes within the slide region (near to the large, relatively intact displaced levee block) that captured a sheared

sample of this layer. The material is completely remolded and sheared to a fully residual condition with negligible remaining strength, and uni-directional extension and tearing of organic fibers across the sheared zone clearly indicate the shear failure within this sample.

This layer is typically only one to several inches in thickness, but was found to be laterally continuous across essentially the full site (as well as at the distressed section on the opposite, west side of the canal.) It is exceedingly difficult to spot, and to sample, because it is closely overlain (and even partially mixed with) a layer of leaves and twigs and bark that is typically also one to several inches in thickness, as illustrated on the auger stem in Figure 8.51. The very dark, shiny material also coating the auger stem in this photo is the sensitive organic silty clay and indicates that we have just drilled through the layer in question (and so now have to move our hole laterally a few feet and re-drill to attempt to sample it.)

This layer of sensitive organic silty clay is the result of a previous major storm that churned up organics and sediments, mixed them with the locally prevalent clays, and also greatly (temporarily) increased the salinity of the water so that the ensuing deposit is unusually heavily flocculated. The result is a material of low strength and extremely high sensitivity (sensitivities of between about 10 and 20+.)

The same storm was accompanied by winds that knocked down leaves and twigs and bark (and other organic detritus), accounting for the closely overlying layer of organic impediments that “mask” this thin layer.

Figure 8.53 shows a plan view of the site, highlighting with red the 10 locations at which this layer was positively identified. It was not always possible to positively identify this thin layer in CPT, as the strength of this layer is not much less than that of the closely overlying and underlying soils; it is the combination of low strength and high sensitivity that made this thin layer so dangerous. “Thin layer” effects also made spotting this layer in CPT (based on tip resistance) difficult. The best initial “marker” or signature of the presence of this layer was found to be a positive spike in friction ratio; as the sleeve continued to drag through the overlying and underlying deposits but the tip resistance dipped a bit.

Figure 8.54 shows a photo of an “undisturbed” sample of this sensitive organic silty clay. The local clays have a gray, peanut butter-like appearance and consistency. They are not highly shiny, but rather semi-glossy, and their stiffness and texture are not unlike peanut butter. The sensitive organic clay, on the other hand, is dark and has a very shiny and translucent appearance; much like “jelly”, as shown in Figure 8.54. In Figure 8.54, hints of the organic detritus that closely overlies and masks access to this thin layer can also be seen.

Two approaches were taken to attempt to characterize the strength (and stress-deformation) behavior of this material. At any location, the precise depth of this layer was first determined by drilling to encounter it. One approach was then to move the drill rig laterally several feet and to re-drill to within approximately one foot of this layer. A 3-foot long Shelby tube, 3-inches in diameter (and modified to eliminate the turn-in that produces overcutting at the mouth) was then used, with a fixed piston system, to drive the tube approximately two feet past the target layer so that more competent underlying soils would “plug” the bottom of the tube and permit careful withdrawal of a sample. Otherwise, the

samples remoulded upon attempted withdrawal and slopped out of the base of the tube making sample recovery nearly impossible.

The samples thus obtained were then taken to the lab at the University of California at Berkeley, where they were subjected to an unusual process, as illustrated in Figure 8.55. The tubes were cut off in 2-inch increments, and a small spoon was used to carefully dig ahead into the remaining tube. When the tell-tale organic detritus was encountered digging stopped and the organic material was hand-plucked from the tube to daylight the underlying sensitive layer. A lab vane shear test was then performed.

The second method used to evaluate the strength of this material also began by pre-locating the precise depth of this layer, usually by sacrificially “oversampling” it (to plug the base of the tube to foment retrieval) and then extruding the sample to determine the precise location of the layer. A second, adjacent hole was then carefully hand augered, and an in situ vane shear test was performed using a shallow-bladed vane. Insertion disturbance, and obstruction by unremoved organic detritus (mixed in the top of the layer) sometimes defeated this effort, often making multiple attempts necessary. Unacceptable insertion disturbance was apparent when the characteristically brittle peak to residual transition was absent and the material exhibited only residual strength.

Figure 8.56 shows typical stress-displacement plots for tests on the thin layer of highly sensitive organic silty clay, and on the local deposits of sensitive gray clay. As shown in Figure 8.56(b), which shows normalized behavior in the form of shear strength divided by maximum shear strength on the vertical axis, the sensitive organic clay was more highly brittle, failed at lower displacement, and exhibited even more pronounced sensitivity and rapid post-peak strength degradation. It was the combination of low strength, and this very brittle sensitivity, that caused this material to “capture” the failure surface at this site.

Finite element analyses were performed for this levee and floodwall section using the program PLAXIS. Figure 8.57 shows the principal parameters and the mesh used for these analyses. The gray foundation clays (CH) and the “marsh layer” were modeled using the “soft soil” effective stress model within PLAXIS, and the soil parameters used were fitted to the values of S_u/p vs. OCR as described previously to match the evaluated strengths of these units and their distribution.

It was necessary to establish the stress state at the end of incremental construction and consolidation of the embankment and foundation. Initial overconsolidation profiles due to desiccation and secondary compression were input, and embankment construction was modeled in two stages (the “historic” fill, and the more recent engineered top fill), and both the OCR vs. depth and the settlement pattern (the bowl shaped pattern at the base of the oldest fill) were well matched to the observed field conditions. Figure 8.58 shows the settlements calculated at the end of initial construction and consolidation.

The front lip of the embankment was then “excavated” and the floodwall installed (as with the actual field case), and displacements were re-zeroed to prepare for the remaining analyses to follow.

Water levels within the canal were incrementally raised, and within a range of stiffnesses considered reasonable it was found that initiation of “gapping” between the outboard toe of the floodwall and the outboard embankment section typically initiated at a surge elevation of between about 7.5 to 8 feet, as illustrated in Figure 8.59. This Figure shows normalized shear strain contours, with the red color indicating shear strains equal to or greater than the shear strain to “peak” shear strength (and thus localized failure.) As shown in this figure, with a water elevation of +8 feet (MSL) gapping has opened partially down the front face of the sheetpile curtain (on the outboard, or water side), and the thin, sensitive organic silty clay layer has already sheared to failure along a short segment inboard of the crest of the levee.

If one looks very carefully at Figure 8.59, a second “lighter” area can be seen beneath this shear zone, representing the beginning of shear deformations along a more “rotational” shear surface passing through the deeper soft gray foundation clays (CH). A dashed line has been added to indicate this surface. This deeper, and more rotational failure surface has a calculated factor of Safety only slightly higher than that calculated for the upper sensitive organic silty clay layer, and this deeper surface represents the failure mechanism favored by the IPET studies reported to date.

As the analysis began to calculate the progressive development of tensile effective stresses between the front of the sheetpiles and the soil, the mesh was revised to model the development of a “gap” between these, and the intrusion of water into the gap as well. Once this “gapping” began, it then developed rapidly. Figure 8.60 shows the situation with an additional foot of storm surge rise to Elev. + 9 feet (MSL) based on our best estimates of the soil parameters. As shown in this figure, the gap has now extended nearly to the base of the sheetpiles. Further extension of the gap is temporarily held up by the malleability of the marsh soils, but further gapping does not provide significant additional lateral water pressures against the front of the sheetpile curtain because the lateral permeability of the “marsh” deposits is relatively high. At this stage, the shear failure along the thin layer of sensitive organic silty clay is well developed, and embankment movements are now significant. This figure also shows quite clearly the deeper, more rotational failure surface that represents the second least stable mechanism at this site (the mechanism favored to date by the IPET studies.)

Figure 8.61 shows calculated displacements for a surge height of 8.5 feet, with displacements exaggerated times two for clarity. Initially, the floodwall tilts slightly forward as it compresses the soils a bit. As sliding then develops, the floodwall base begins to move along with the displacing embankment and the whole moving mass (inboard embankment section, floodwall and sheetpile curtain) displace laterally together, as shown previously in Figure 8.27.

Figure 8.62 shows the Factors of Safety calculated (by $c-\phi$ reduction) using PLAXIS for a variety of water levels in the canal. Three cases are presented: (1) failure dominated by the thin layer of sensitive organic silty clay, but without gapping between the sheetpile curtain and the outboard side soils, (2) a more rotational failure through the deeper soft gray foundation clays, again without gapping, and (3) failure dominated largely by the upper

sensitive organic silty clay layer, but this time with a water-filled gap on the outboard side of the sheetpile curtain.

As shown in this figure, the Factors of Safety for the upper lateral shear failure, and the deeper more rotational failure, are not very different. The heavy red line shows the best-estimated path to failure at this site. Based on these analyses, it appears that gapping would have developed at a surge height of between about 7.5 to 9 feet (MSL), and the intrusion of water into this gap would have increased the lateral forces and rapidly driven the section to instability.

Figure 8.63 shows the cross-section and principal soil properties used to perform more classical limit equilibrium analyses (using Spencer's Method, cross-checked against Morgenstern's and Janbu's Methods) using the program SLOPE/W.

Figure 8.65 shows the most critical failure mode for the "no gapping" case with a surge height to Elevation +6 feet (MSL). The PLAXIS analyses had shown very little likelihood of gapping at this water elevation, and this probably represents the best estimate of Factor of safety for this surge height. As shown, the calculated Factor of Safety is $FS = 1.51$ for this case, and as shown in Table 8.1, the associated probability of failure for this surge height is approximately $P_f = 0.01$. These calculated low probabilities of gapping and of failure are reassuring, as the water in the canal had previously reached an elevation of approximately +6 to +6.5 feet (MSL) during previous storm surges, and no gapping or failure had occurred in those events.

Figures 8.66 and 8.67 show the most critical failure surfaces for a surge to Elev. +9.5 feet (MSL) for (a) a shallow translational failure dominated by sensitive organic silty clay layer, and (b) a deeper, more rotational failure through the soft gray foundation clays. In both analyses, a water-filled gap was modeled at the outboard side of the sheetpile curtain. This water elevation is approximately the maximum elevation achieved (maximum surge at this location is estimated by our team to be approximately Elev. +9.5 to +10 feet, MSL). The calculated Factors of safety are again similar for both modes, and the shallow lateral translation along the sensitive organic silty clay again provides the lower Factor of Safety.

Figure 8.68 shows calculated Factors of Safety for various water elevations (Spencer's Method) for the four cases of principal interest: (a, b) lateral translation along the sensitive organic silty clay layer, with and without a water-filled gap, and (c, d) deeper and more rotational failure, again with and without a water-filled gap. The solid red line again shows the best-estimated path to failure at this site, this time based on the suite of limit equilibrium analyses.

It is challenging to make an estimate of the probability of failure at any given canal water level, as there are numerous uncertainties involved, and some of these are cross-correlated. The principal uncertainties are those associated with shear strengths of the foundation soils, and also with the "representative" shear strength that can be mobilized at any given moment by the very sharply strain-softening soils (especially the highly sensitive, thin organic silty clay layer.) Additional significant uncertainties are those associated with the likelihood (and severity) of opening of the water-filled gap at the outboard side of the

floodwall and its supporting sheetpile curtain, and the unit weights of some of the soils. These were not all accurately reflected in these probabilistic estimates, and as a result the overall uncertainty is expected to have been somewhat underestimated.

One important set of variables are the shear strengths of the various soil units controlling each of the potential instability modes. Each of the conventional limit equilibrium analyses performed was performed using probabilistic variation of these shear strengths. The coefficient of variability in soil shear strengths was taken as log-normally distributed, and was estimated as approximately $COV \approx 30\%$ for the soft gray clays, and $COV \approx 40\%$ for the thin, sensitive organic silty clay layer. The resulting distributions of probable factor of safety are shown (approximately) graphically in Figure 8.68(a) for both the “un-gapped” case and the case of a water-filled gap at the outboard side of the sheetpile curtain. These are only approximate, as they do not precisely fit themselves to any single well-known distribution.

The next critical uncertainty is the probability of cracking. The probability of cracking cannot be calculated or evaluated in any closed-form manner, and so requires a judgmental estimate based on the preceding finite element analyses (and supported in part by the observed field behavior). It should be noted that the stiffnesses used in the PLAXIS analyses to estimate inception of cracking are a bit time dependent, so that a slower rising and falling storm surge would be a bit more deleterious here. The inception of cracking was not taken as the point at which cracking “occurred”; instead cracking was taken to be significant when the crack propagated more than halfway towards the base of the sheetpile curtain. Figure 8.68(b) shows the judgmentally derived estimates of probability of significant crack formation as a function of rising canal water elevation. The upper and lower bounds shown were inferred to represent approximately $\pm 3\epsilon$ values.

Monte Carlo simulation was used to estimate the distribution of the factor of safety considering the analysis with and without a gap and the probability of a gap forming. The formulation is as follows:

$$P(FS) = P(FS_{NG}|NG)P(NG) + P(FS_G|G)P(G)$$

This equation reads; the distribution of the factor of safety is equal to the conditional distribution of the factor of safety for the levee with no gap multiplied by the probability of there being no gap, plus the conditional distribution of the factor of safety for the levee with gap multiplied by the probability of there being a gap. The conditional distribution of the factor of safety with or without a gap is based on the mean and standard deviation from stability calculations. For the probability of gapping, which can also be considered a transition function from no gap to gap conditions, a mean probability function and upper and lower bounds were estimated from Figure 8.68(b). The above equation is for any single canal water elevation.

All the distributions were treated as Gaussian based on observation of the data. The gap and no gap conditions were considered statistically independent scenarios. A Monte Carlo simulation was run for 10,000 samples. Typical simulation results are shown in Figure 8.68(c) for a single depth increment. The first plot is a histogram of the simulation results of the factor of safety for no gap conditions $[FS_{NG}|NG]$, the second is for gap conditions

[$FS_G|G$], the third is the probability distribution of a gap (no gap) occurring [$P(G)$ and $P(NG)=(1-P(G))$], and the fourth is the total distribution of the factor of safety [$P(FS)$].

Figure 8.68(a) showed the distributions of factor of safety for the gap and no-gap cases (separately) as a function of rising canal water levels. Figure 8.68(d) repeats this figure as a background, but adds the now calculated distributions of conjugate overall factor of safety as a function of rising canal water levels, showing how the conjugate distribution “transitions” from the un-gapped to the water-filled gap case. Based on these approximate simulations, the resulting probabilities of failure at any given canal water elevation are then as shown in Table 8.1.

As shown in Table 8.1, the probability of failure was found to be very low for surge heights of less than about Elev. + 7 feet (MSL), and they rise rather quickly as the surge elevation passes above about + 8.5 feet (MSL). Failure at the estimated actual maximum surge elevation of approximately + 9.5 to + 10 feet (MSL) is calculated to have had a likelihood, on the order of $P_f \approx 0.8$ to 0.9. Failure at the originally intended “design” surge height of Elev. + 12.5 feet (MSL) was essentially certain.

Finally, Figure 8.69 shows a comparison between the observed failure mode and the rotational mode determined by IPET. There have been a number of IPET representations (to date) of their failure mode, each varying slightly as to actual depth and dimensions, but all were semi-rotational failures through the soft gray clay stratum underlying the marsh deposits. The rotational surface shown in Figure 8.69 is a somewhat “average” representation of these various failure surfaces, from both the second interim report (IPET, April 1, 2006) and the more recent Draft Final Report (IPET, June 1, 2006.) The rotational IPET failure is superimposed, as carefully as possible, onto our own investigation’s more detailed cross-section. The two modes are not wholly dissimilar, and both lead to low factors of Safety.

More detailed examination of the IPET mode, however, shows it to be problematic with regard to agreement with key field evidence. The rotational IPET mode would have left the chain link fence at the edge of the crest road (on the displaced intact levee block) rotated backwards, but as shown clearly in Figure 8.26 (and Figure 8.69(a)) this crest fence was essentially perfectly vertical at the end of the displacements. Massive rotation would have been necessary to produce the observed very large lateral displacement of the upper “intact crest” section of the levee (lateral displacement of up to 50 feet), and this would not have been feasible with the IPET failure mode. Also, the IPET rotational mode would have significantly back-rotated the floodwall; but the floodwall instead traveled the full lateral distance (50 feet) in contact with the displacing levee embankment section, and then toppled backwards as the water pressures began to equilibrate (as illustrated in the top of Figure 8.69, and in Figures 8.28 and 8.69(a)). The IPET mode also fails to explain the large lateral extent of the mapped toe exit features, and the multiple toe thrust features, as shown in Figures 8.26, 8.27, and 8.32 through 8.34.

Most importantly, the shear failure along the thin, highly sensitive organic silty clay stratum was confirmed at several locations based on remoulding and also uni-directional extension and tearing of organic fibers; conclusive evidence as to the occurrence of massive uni-directional shear failure along this stratum within the marsh sequence.

The failure of the IPET investigation to discover the critical thin stratum of sensitive organic silty clay that was the principal culprit in the failure at this site represents an important lesson both for current geotechnical practice at large, and also for subsequent design studies for the levees and floodwalls of the new Orleans regional flood protection system. The IPET studies drove numerous geotechnical borings and CPT probes right through this stratum (see Figure 8.25(a)) but did not discover it. That was, in large part, because the crews performing the field borings and CPT were “separated” from those who had performed the initial IPET post-event forensic field studies, and both sub-teams were separated from the expert “engineering geology” team also working on the IPET studies. The analysis sub-team was a fourth, separate group. There were geological experts on the IPET team who could certainly have pointed out the possibility, and even likelihood of such a layer if they had been asked. Instead the four sub-teams performed their tasks largely separately, without adequate interchange of knowledge and findings.

Our own investigation team took a wholly different approach. We began by carefully assessing the visually observable surface forensic evidence at this site in the wake of the failure, and by back-tracking through the original (pre-Katrina) field and lab data for this site. We also studied the challenging geology of the region (including seminal publications by the USACE’s geological experts.) Based on all of this, our site team (which included senior investigative team members right out on the drill rigs) went in search of an unusual layer, of high sensitivity, and considerable lateral extent, that would have been capable of producing a lateral translational stability failure with toe thrust features extending to unusually great distances inboard of the original levee toe. The suspected depth of this stratum, inboard of the levee toe, was fairly shallow; probably between several feet to as much as 10 feet at most. We encountered and identified the critical layer with our first boring, and then sampled and tracked it across the site in a total of 11 borings and CPT’s.

Two important lessons here are: (1) the importance of fully integrating all phases of field investigation, laboratory testing, analysis and design (and the team members performing these), and (2) the importance of suitably involving expert engineering geologists in all phases of site investigation and site characterization, as well as the other project phases. These two things are, unfortunately, not always done in contemporary geotechnical practice, and they are also not the norm for many contemporary Corps design studies which tend to be relatively segmented (as were the IPET studies in this case.)

Overall, it can be concluded that there were two potentially critical failure modes at this site, but that the lateral translational failure along the sensitive organic silty clay layer within the “marsh” deposits was the weaker of the two, and that this was the mode of failure that actually occurred at this site.

(c) Initial Section Design Studies

The obvious next question to address is then how the original design studies failed to note this. The answer is a bit complex as a number of poor judgements and errors contributed to the mis-perception of the original “design” section as being adequately stable (and reliable)

for targeted design canal water elevations significantly higher than those that caused the actual failure (the design canal water level was Elev. +12 feet, MSL). The original design studies have been reviewed, and the following are significant errors and poor judgements during initial design that contributed to this failure:

1. Figure 8.70 shows the longitudinal cross section along the segment of the east bank of the 17th Street Canal as developed for the original design studies. An early error in the design process was the use of borings that were too widely spaced to attempt to characterize challenging and complex foundation geology. The savings achieved by not performing more borings now appear miniscule relative to the cost of the catastrophe that has ensued. [It should also be noted, however, that even the borings that were performed appear to have been sufficient as to correctly predict the failure, if the resulting data had been suitably processed and then used in the ensuing analyses.]
2. The longitudinal section of Figure 8.70 was prepared by the USACE, and was based on a number of assumptions; including the assumption the “marsh” deposits were typically flat-bottomed. The history of previous drainage channel erosion across this area would lead to the expectation of likely non-level transitions even for swamp bottoms, and Figure 8.71 shows our own team’s re-interpretation of the original (sparse) longitudinal data to develop an alternative longitudinal subsurface soil profile. This difference in interpretation might be considered the second problem at this site during original design.
3. The USACE then passed the design on to outsourced engineers, who developed the strength data and interpretations for analysis of stability of the intended levee and floodwall section. A major problem occurred here, as data from far too large a lateral distance was eventually transposed to the design analysis cross-section. In the vicinity of the actual failure, there are only 5 sample locations shown within the critical “marsh deposits” (in the 4 borings shown intersecting this unit.)
4. Two of the sample locations shown within the “marsh” deposit of Figure 8.69 were non-recovered samples, and at approximately the same depth in nearly adjacent borings. This is the location of the sensitive organic silty clay layer that actually caused this failure and breach. Failure to note the importance of the non-recovery of testable samples, and in two nearly adjacent borings at essentially the same elevation, should have represented a red flag and an effort should have been made to further investigate this location.
5. Figure 8.72 shows the stability calculations for the critical section nearest to the actual breach and failure. The limit equilibrium method used for these was the “Method of Planes”, a three-wedge analysis with conservative side force assumptions. This method continues to be preferred by the New Orleans District of the USACE, but it is now a relatively archaic anachronism given the availability of more accurate methods and the availability of the simple computer programs necessary to run these. The method itself provides a slightly conservative answer so long as the most critical failure surface can be closely represented by the steeply plunging wedges at the front and back, and by the horizontal surface in between. In the original design analyses, layers were assumed to be laterally horizontal, so

this analysis was a good fit for the cross-sections analyzed. Unfortunately, the actual stratigraphy was not horizontally layered (see for example any of the cross-sections analyzed in these current studies), so this method was poorly suited to the finding of the failure mechanism that was actually most critical.

6. And the assumption of laterally horizontal layering was itself a major problem too. It was born of necessity, as no borings had been performed significantly off the embankment centerline alignment to permit development of full lateral cross-sections. Again, the minimal savings on exploration and testing costs here pale relative to the costs of the catastrophe that ensued. Stratigraphy is a vitally important issue, especially given the low strengths of many of the foundation soils. Looking at the cross-sections at the 17th Street canal breach site as analyzed in this current study, for example, one will note a subtle “bowl shaped” settlement pattern at the base of the embankment fill, and a corresponding bowl shape to the critical sensitive organic silty clay layer just beneath it. Without this “bowl shape”, the original embankment would have been unstable during initial construction; it would have slid sideways on the sensitive layer if that layer had been horizontal. Instead the layer dipped in the center, so that the evolving embankment would have had to slide up a small slope (up a hill) to fail during construction. Minor changes in stratigraphy details can have a major impact on overall stability on these soft, weak soils. Use of “assumed” horizontal layers therefore missed a vitally important element of the problem.
7. Figure 8.73 shows the now well-circulated summary of strength data for stability analyses at this section. The data are based on UU triaxial tests and on vane shear tests. Scatter in the data is considerable, and is likely due in large part to sampling disturbance issues for these sensitive soils. Most samples were obtained from borings through the crests of the levees (the most accessible location) and so represent strength information for locations under full embankment overburden stresses. The solid lines in this figure show the strength interpretation used in the actual design analyses. This line represents an unconservative assessment of the data points presented, in both sides of the figure, even without allowance for the additional effects of overburden stress reduction away from the levee centerline. This interpretation is especially unconservative at elevations of between + 10 feet to – 10 feet (Cairo datum) in the figure at the right, and between -10 feet to -30 feet (NGVD datum) in the figure at the left. These both represent the same 20 foot range of critical elevations, which correspond approximately to Elev. -10 feet to -30 feet (MSL), and this is the region in which strengths are important in the “Method of Planes” analysis performed for this location in the original design studies. As shown in Figure 8.74, a majority of the available shear strength data is lower than the shear strength actually used for the stability analyses in this critical depth range; violating customary “Corps” procedures in this regard. (Corps procedures generally require that approximately 1/3 of the data fall below the strength used for analysis and design, and that 2/3 of the data be greater.) As shown in Figure 8.70, the resulting calculated Factor of Safety was found to be FS = 1.30....., barely enough to satisfy the design criteria which required a FS of at least 1.3 for the case of “transient” storm surge loading. It is very difficult to

justify the apparently unconservative strengths selected in this critical elevation range based on the data presented.

8. Figure 8.74 is a repeat of Figure 8.73, but with additional red and blue lines added to illustrate another major error made in determination of shear strengths for stability analyses. Shear strengths of soils are very strongly a function of effective overburden stress, so the samples obtained from beneath the overburden of the embankments would consistently overestimate the strengths under the levee toes, and in the “free field” out beyond the levee toes. This fundamental principle of soil mechanics was well-known in local practice in the New Orleans region at the time that these analyses were performed. However, it was ignored in the original design studies at this section, and the result was a massive additional increase in the unconservative error in the overall stability analyses. The blue lines on Figure 8.74 represent our own team’s assessment (as described in preceding sections) of the shear strength vs. depth beneath the crest of the levee, and the red lines represent our assessment of the shear strength vs. depth inboard of the levee toe. The contrast is very significant, and the unconservatism involved in the mis-use of strengths from “beneath the full levee overburden” to model conditions beneath and inboard of the levee toe is readily apparent.
9. Despite having adroitly invested significant funds and effort in the E-99 test section (near Atchafalaya; see Section 8.3.3) to perform a very well-designed full-scale field test on appropriate foundation soil conditions, the results of this field test of a model floodwall/sheetpile curtain in a levee embankment founded on weak marshy soils were not subsequently used (as had been intended.) The failure mechanism disclosed by this field test was the opening of a gap at the outboard side of the sheetpile curtain, the filling of this gap with water, and thus the resulting exertion of increased lateral water pressures against the sheetpile curtain. This mechanism, which proved to be the actual field failure mechanism at this site, was not among the suite of cases/mechanisms analyzed in the original design studies.
10. And the use of a design Factor of Safety of only 1.3 was also a major problem. As discussed in detail in Chapters 11 and 12, this was far too low a value for a system protecting a large urban population. This value has a history of development that is traced in Chapter 12 back to use for design of levees protecting agricultural lands in the first half of the last century, and failure to update this in the face of both the passage of time and the increased level of potential consequences associated with flood protection of a major urban area was a significant lapse that left little room for the other errors and poor judgements cited above.

Calculations using the data available at the time of the initial design, and using analysis methods widely available and in common use at that time (though not necessarily within the new Orleans District of the USACE), clearly indicate that this section would be expected to be unstable at canal water levels less than those for which the design was intended (water level of less than Elev. +12 feet, MSL). The more sophisticated analyses employed in these current (ILIT) studies give more precise answers, but this level of sophistication was not necessary to demonstrate overall deficiency of the original design.

8.3.7.2 Distressed Section on the West Bank

There is a “distressed” levee and floodwall section on the west bank of the 17th Street Canal, across from the large breach discussed above. This “distress” was visually minor, but this section was studied both as a check of the ramifications of “minor” visually observable distress, and also because it provided an opportunity to see if the same analysis methods that correctly predicted the failure on the east bank could also accurately predict the observed performance of a second section that it was hoped would be somewhat similar.

Figure 8.75 shows measurement of observed lateral wall offset at the point of maximum offset. Wall tilt is less than 0.75 inches, and the maximum lateral offset is approximately 3.5 inches.

As shown previously in Figure 8.25, only a few borings and CPT were performed at this distressed section on the west bank of the canal, so data is sparse. Figure 8.77 presents the interpreted cross-section used for analysis at this site. The same basic sequence of strata observed on the east bank are again present, but the details of the stratigraphy differ a bit.

Passing quickly through intermediate details (as were presented in detail in Section 8.3.6), the same procedures were used to process and interpret the limited available data, and this was supplemented by the knowledge gained from across the canal. Figures 8.78 and 8.79 show an example determination of the value of $N_{kt} = 12$ for the soft gray foundation clay (CH), and this matches with this same deposit on the east bank. Using the same methods, and the same SHANSEP exponent $\lambda = 0.75$, Figure 8.80 shows the iterative processing of the CPTU data to develop profiles of S_u/p vs depth, and OCR vs depth for this clay unit. These too match well with the east bank deposit data.

Figure 8.81 then presents our SHANSEP-based profiles of strength vs. depth (a) beneath the crest, and (b) at the toe, along with the available strength and CPT data. The fit with the available data is excellent.

Figure 8.82 shows the use of the correlation proposed by Mayne and Mitchell to develop profiles of S_u/P vs depth and OCR vs. depth within the “marsh” deposits overlying the soft gray clays. This matches well with the CPTU-based interpreted OCR profile within this stratum, and with the data from the east bank as well.

Figure 8.83 presents the resulting overall profiles of strength vs. depth within the marsh deposits (a) beneath the crest, and (b) at the toe, along with all available data (including CPT tip resistances interpreted using $N_{kt} = 16$). The thin layer of sensitive organic silty clay was encountered in one boring, again at the approximate mid-point in the “marsh” deposits, and again closely overlain by leaves and twigs. This sample is shown in Figure 8.76. Strengths for this thin layer were based on S_u/P values from the east bank deposit. This thin layer was not critical at this west bank site, as the sheetpiles penetrated well below this sensitive layer and so forced a deeper, more rotational failure through the soft gray clays to be the most critical mode.

Once again, all shear strengths determined represented triaxial or vane shear strengths, and these were reduced slightly (multiplied by a factor of 0.84) to develop shear strengths suitable for the direct simple shear (DSS) dominated shear surfaces to be evaluated.

Figures 8.84 and 8.85 show the most critical failure surfaces (without gapping) for a storm surge level of +9 feet (MSL) for failure (a) to the top of the soft gray clay, and (b) within the lower marsh deposits. These both give low Factors of Safety, but the failure through the lower marsh strata is the more critical case.

Figures 8.84 and 8.85 show these same two potential failure modes, again for a storm surge elevation of +9 feet (MSL), but this time with an assumed water-filled gap at the outboard face of the sheetpile curtain. Once again the lower marsh units present the more critical mechanism.

Figure 8.88 shows calculated Factors of Safety vs. canal water elevation for the failure through the lower marsh stratum, both with and without gapping. The heavy red line in this figure shows the best estimate of the likely critical failure path, based on these limit equilibrium analyses. It is judged that gapping is most likely to be initiated at surge elevations of approximately +10 to +11 feet (MSL) as the Factor of Safety (without gapping) drops below about 1.25 to 1.35. Gapping was relatively unlikely during Katrina (max surge level ~ +10 feet, MSL), and indeed no gap could be seen.

Based on these analyses, probabilities of failure were again estimated using the same procedure as described previously in Section 8.3.7.1. Figure 8.88(a) shows distributions of factor of safety as a function of rising canal water elevations for the “water-filled gap” and the “ungapped” cases, and Figure 8.88(b) shows the resulting estimated distributions of the overall conjugate factor of safety for this west bank section.

Table 8.2 then presents the resulting estimated probabilities of failure vs. canal water elevation. The probability of failure at the actual peak Katrina water elevation of approximately + 10 feet (MSL) was low, but it was not negligible. Moreover, it would have increased rapidly with even minor additional increase in canal water level. The probability of failure becomes very high at the “design” water level of +12.5 feet (MSL).

It should also be noted that the marsh soils have likely been sheared (and thus softened) a bit, and that the overall strength of this section was therefore likely somewhat degraded by the loading it received during Katrina. Accordingly, it may not perform quite as well in subsequent loading in the future.

This levee and floodwall section protects the large population of the still undamaged Jefferson Parish. If the canal floodgate currently being installed, and future control of pumping, cannot guarantee that canal water levels will never exceed about Elev. +5 to 6 feet (MSL), then this section should be remediated.

8.3.8 The Breach Near the South End of the London Avenue Canal

A major breach occurred on the east bank, near the south end of the London Avenue Canal, as shown in Figures 8.1 and 8.2. Figure 8.89 shows an oblique aerial view of this breach under repair. The breach was approximately 80 feet in length, and it scoured to significant depth. Sands eroded and transported by the inrushing floodwaters blanketed the neighborhood inboard of the breach to considerable depth over a surprisingly wide area, as shown for example in Figure 8.90.

Figures 8.91 and 8.92 show the floodwall sections at the south and north ends of the breach, respectively. In these photos it can be seen that these wall sections have not displaced (translated) laterally towards the inboard (“protected”) side; instead they have simply “dropped” into the hole eroded by the scour of the breach flow.

Clearance for the footprint of the levee and floodwall was very limited, and the neighboring homes and their back yards encroached closely on the levee. Levee maintenance was very poor along this section, and numerous large trees had been allowed to grow along the inboard toe. Many of these were actually rooted part way up the inboard slope face of the levee embankment itself, as shown in Figure 8.93 which is a view looking north from the breach location. These trees at the inboard toe represented an unacceptable risk as they can be blown over by storm winds, creating sudden voids that represent favorable paths for concentration of seepage flows and erosion in the critical toe area. Also, when they die the rotting root system can leave voids that can pose a significant hazard with regard to seepage and erosion in the critical inboard toe area.

Several large trees did topple at this site during Katrina, but in the absence of eyewitnesses it is not possible to be certain if they toppled before the breach, or as a result of erosion and scour after the breach opened. Figure 8.94 shows toppled trees at this site. Two large trees from the levee toe area within the breach footprint toppled during this event.

This breach was much shorter in length than the large breaches at the 17th Street Canal, the north end of the London Avenue Canal, and the southern breach on the IHNC at the west side of the Ninth Ward (each of which were hundreds of feet in length.) Instead, like the northern breach at the IHNC at the west end of the Ninth Ward, this was a narrow and deep breach; suggesting that underseepage rather than foundation instability may have been the key issue here.

As discussed previously in Chapter 4, the geology of the London Avenue canal differs significantly from that of the north end of the 17th Street Canal. The buried sand “ridge” runs laterally across the canal region, as shown in Figure 4.10 in Chapter 4, and relatively thick sand strata occur at shallow depths in the London Avenue Canal (and the south Orleans Canal) region. On the south side of this buried sand ridge, the sands tend to be dense as a result of wave action and energy from the Gulf side. On the lee side (the north side), the sands, especially at shallow depth, were protected and tend to be looser.

Figure 8.95 shows the locations of borings and CPT probes performed by the ILIT investigation at this site. Figure 8.96 shows a cross-section through the breach, based on our

own (ILIT) data as well as IPET data and data available prior to Katrina. The embankment has a modern (engineered fill) crown consisting of lightly compacted clay and silty clay, underlain by older fill of more variable composition. The embankment section rests atop variable “marsh” deposits consisting primarily of variably interbedded clays and organics. This “marsh” stratum is relatively thin, with a thickness of only 3 to 4 feet at the inboard toe, and it is underlain by about 2 to 3 feet of soft gray clay (CH).

This thin surficial marsh and clay “crust” is underlain by deep deposits of medium dense and then dense sands. In addition to the sheetpile curtain supporting the current concrete floodwall, there is an older sheetpile curtain on the outboard side that used to support a previous small floodwall at this location.

Strengths of the marsh deposits and the thin layer of underlying clay were determined based on the available data, and the resulting strength characterizations are summarized in the table within Figure 8.97, along with the estimated friction angles for the underlying sand units. Stability analyses showed high factors of safety with regard to “landslide type instability failure”, even for steady state seepage conditions at the maximum storm surge height of approximately Elev. +9 feet (MSL). Figure 8.106 shows the most critical potential slide surface for these worst case steady state seepage conditions. It was concluded that this breach was unlikely to have resulted from conventional foundation stability failure.

Numerous analyses of seepage were performed, varying the horizontal and vertical permeabilities of the various soil units and strata (in both the horizontal and vertical directions) over ranges considered reasonable for these soils. For all reasonable ranges of conditions, it was found the soils in the inboard toe area were vulnerable to erosion and potential piping at storm surge levels of less than Elev. +9 feet (MSL).

An example is shown in Figure 8.98, which shows the flownet and flow velocity vectors for a surge to Elev. +9 feet (MSL). Ranges of values of in situ permeability were modeled for the sandy strata (in transient flow analyses), and it was concluded for reasonable ranges of lateral permeabilities that nearly full equilibration of pore pressures (greater than 90 to 95% equilibration) at the inboard side levee toe region would occur within 30 minutes or less of outboard side canal water level rises. Given the rate at which the outboard side canal waters rose (see Figure 8.18), steady state seepage analyses were considered to provide an accurately (to slightly conservative) basis for assessment of underseepage pore pressures. The analysis shown in Figure 8.98 thus represents steady state flow conditions.

Figure 8.99 is a close-up from this figure showing localized conditions in the vicinity of the levee and floodwall. The sheetpiles are nowhere near deep enough to be effective in reducing massive underseepage flows through the pervious sands, and exit gradients near the inboard toe are unsafe with regard to erosion and the initiation of potential piping.

Figure 8.100 shows pore pressure contours from this same flow analysis. Hydraulic uplift forces at and just inboard of the toe exceed the weight of soil overburden, suggesting the possibility that hydraulic uplift ruptured the less pervious thin clay and marsh crust causing a “blowout” failure in this toe area.

Figure 8.101 shows hydraulic gradients for this same flow analysis. The exit gradients at the inboard toe are on the order of $i_o \approx 0.5$, representing a factor of safety with respect to erosion of approximately

$$FS = \gamma_b / (i_o \cdot \gamma_w)$$

where γ_b is the buoyant unit weight of soil, γ_w is the unit weight of water, and i_o is the exit gradient. For the lightweight marsh soils, with light buoyant unit weights, the calculated factor of safety is on the order of $FS \approx 0.8$ to 1.05 for the conditions shown in Figure 8.101. Any “bunching” or localized constriction of the flownet near the exiting face would further exacerbate the tendency to initiate erosion and the beginning of piping. Given the high variability of the thin surficial marsh deposits that “cap” this site, erosion and piping are highly under these conditions.

Figures 8.101 through 8.105 illustrate how such erosion can rapidly escalate as the flownet converges on even a slight void (Figure 8.102) to rapidly increase the localized exit gradient and accelerate the erosion process (as occurs progressively as the erosion enlarges the hole at the inboard toe in Figures 8.103 through 8.105.) This is actually a three-dimensional process, so the rate of acceleration of this erosion and “piping” process is actually more severe than can be properly illustrated in these two-dimensional figures.

Figure 8.107 is a schematic illustration of this process. As the flownet increasingly converges, and erosion continues to accelerate, and the erosion literally tries to “tunnel” back under the levee embankment. This produces slumping and periodic collapses into the opening void, and the process continues to accelerate until the crest is finally breached, at which point the intruding flows rapidly further scour the breach.

An additional possibility is that this type of erosion process may have been exacerbated by the toppling of a tree near the levee toe, as illustrated schematically in Figure 8.108. Flow towards the toe (and the trees rootball zone) weakens the ground and thus weakens the tree’s resistance to pullout failure under storm wind loading. Many trees toppled in this manner during the hurricane. If the tree near the toe topples, it created a large void toward which the exiting flownet would rapidly converge, initiating or greatly accelerating the type of erosion and piping process described above.

Figure 8.109 shows another view of this breach section, this time from the waterside and in late September of 2005. In this photo it can be clearly seen the breach is a very narrow feature, deeper at the north end (to the left in this view). On the inboard side our field team felt that the evidence suggested that the breach initiated either as a seepage erosion “blowout” or similar near the north end of the feature. There was a large tree that was uprooted at that location, but it could not be determined whether the tree fell before or after (as a result of) this failure and breach.

In the end, this breach scoured to significant depth and was then rapidly buried by the emergency embankment repair section, so there is no conclusive evidence left with which to determine which of the above described possible mechanisms (in detail) caused the actual

failure. It is apparent, however, that this failure was the result of underseepage and erosion of some form. The lack of sufficient sheetpile depth as to adequately reduce underseepage flows and toe exit gradients was an engineering lapse, and so was allowing the rampant growth of large trees in the inboard toe area.

The original design analyses for this section were performed by an outsourced engineering consultant, and were reviewed by the USACE (USACE; DM-19A.) In these analyses, the canal-side phreatic level was taken at the full design level (Elev. +12 feet, MSL), and the phreatic level at the inboard side levee toe was taken at Elev. -5 feet (MSL). Based on our investigation's transient flow analyses, for reasonable ranges of in situ lateral permeability, for the full (design) canal water elevation of +12 feet (MSL), the phreatic level at the inboard side levee toe due to underseepage would have actually been on the order of +2 to +5 feet (MSL). This represents a large increase in underseepage-induced uplift pore pressures and exit gradients, and is the principal difference between the pre-Katrina "design" analyses and our investigation's post-Katrina forensic analyses at this section.

8.3.9 The Breach and Distressed Sections Near the North End of the London Avenue Canal

An additional major breach occurred on the west bank near the north end of the London Avenue Canal, as shown in Figures 8.1 and 8.2. This too was a catastrophic breach as it rapidly scoured below mean sea level and so was one of the three large drainage canal breaches that continued to push water into downtown New Orleans for three days after Hurricane Katrina's passage.

Figure 8.110 shows an aerial view of the breach on the west bank. There was also a "distressed" section on the opposite side (on the east bank) that represents an incipient failure in progress; this failure was arrested in a partially developed state by the failure of the west bank section (which drew down the water level and thus saved the east bank.)

Figure 8.111 shows a view looking south along the canal, with the emergency repair embankment section on the west bank on the right, and the incipient failure section on the left side. If one looks closely, the floodwall on the left (east) side can be seen to be leaning away from the canal in this photo.

This was one of the most challenging sites for our investigation. Foundation soil conditions, and embankment and floodwall geometries, were similar on both sides of the canal. One side failed catastrophically, and the other appears to have begun to fail but to have been saved by the failure on the opposite bank. It was a challenge to develop a model that would predict the failure of the west bank before the east bank failure was able to fully develop. There are also a variety of data and evidence suggestive of a number of potential failure and distress modes evident at both sites (both sides of the canal), and sorting through these posed a significant challenge as well.

Figure 8.112 shows a view of the main breach on the west bank, taken from the south end of the breach on the outboard (water) side. In this photo it can be clearly seen that the water-side toe section of the earthen embankment is still in place, and that the

floodwall/sheetpile curtain and the inboard side of the earthen levee have been separated from it and pushed to the inboard side.

Figure 8.113 shows conditions at the inboard toe of the failed embankment section on the west shoreline. The small clubhouse shown had originally been at the same elevation as the nearly adjacent house, but was lifted nearly 7 feet vertically by the displacements during the failure. Some initial field investigators suggested that this was evidence of rotational movement, but our investigation found that this clubhouse (and the ground upon which it stood) was raised vertically by heave due to “plowing” as the main levee embankment displaced laterally (without rotation.) The confined uplift region, and its “humped” nature, are clearly evident beneath the small clubhouse in this photo.

Figure 8.114 shows a view of the inboard toe of the “distressed” (displaced) embankment and floodwall section on the east shoreline, taken on the outboard (water) side. As shown in this photo, the concrete floodwall leaned away from the canal, and a gap with a maximum width of 2.5 feet (and a common width of 1.5 to 6 feet) opened between the outboard side of the earthen levee embankment and the concrete floodwall (and its supporting sheetpile curtain.)

Figure 8.115 shows the other side of this same floodwall section. As shown in this photo, the displaced floodwall leaned to the inboard with a readily discernable tilt of up to 8°. The next photo, Figure 8.116, shows conditions along the inboard base of the floodwall (at the feet of the photographer who took the photo of Figure 8.115.) A series of apparent “sinkholes” occurred along the inboard side contact between the concrete floodwall and the crest of the earthen levee at this location.

Figure 8.117 shows conditions at the inboard toe immediately below the sinkholes of Figure 8.116. A prominent sand boil feature, with sandy ejecta, occurred at this location. Less apparent, but important, was the hummocky wrinkling of the nearly level ground inboard of the toe of the levee, and the slight overthrust feature adjacent to the sand boil. This overthrust feature was apparently missed by many field investigators, but our team noted it and went back and excavated it during our subsequent field boring, sampling and CPT program and found that it was indeed the toe thrust of the beginning of a translational instability feature.

Figure 8.118(a) shows a cross-section through the west side breach prior to Katrina, and Figure 8.118(b) shows this same section after the failure. The failure on the west side was a translational failure of the embankment, sliding along the interface between the foundation sands and the overlying less pervious layer of silty clay (CL/ML).

Figure 8.119(a) shows a cross-section through the east side “distressed” section prior to Katrina, and Figure 8.119(b) shows this same section after the hurricane. The displacement and tilting of the floodwall was the result of the initiation of slippage, once again at the interface between the foundation sands and the overlying less pervious layer of silty clay. Unlike the west bank, this slippage progressed only enough to produce displacements of approximately 1.5 to 2.5 feet, whereupon these movements were arrested as the failure and breaching on the opposite bank rapidly drew down the canal water level and reduced the lateral push against the sheetpile curtain and floodwall.

Figure 8.120 shows a plan view of both sides of the canal, indicating the locations of the borings and CPT performed as part of this investigation.

Figure 8.121 shows the longitudinal subsurface soil profile developed along this section of levee on the west bank during the original design studies, and Figure 8.122 shows the re-interpretation of this section by this study team based on the original boring data. Figures 8.123 and 8.124 show the same pairing of profiles for the east bank side.

Processing of the available geotechnical data was performed using essentially the same methods and procedures as were described in detail in the preceding sections, and much of the detail will be omitted here in the interest of brevity.

Figures 8.125 and 8.126 show the best estimated profiles of strength vs. depth and Su/P vs depth on the west bank (breach) side for profiles (a) beneath the full levee embankment overburden, and (b) inboard of the levee toe.

Figure 8.127 shows estimated friction angles across the transition from the base of the silty clay stratum (CL/ML) into the underlying clayey sands and sands. Friction angles were estimated from the CPT data using two correlations, and they were also estimated based on the SPT data available from the borings. Also shown are the results of two direct shear tests performed on “undisturbed” samples as part of these studies.

Figure 8.109(a) shows an “undisturbed” sample from the transition across the silty clay into the underlying sands. As shown in this figure, this transition was semi-gradational rather than abrupt. The base of the silty clay layer is underlain by fine clayey sands with variable fines content. Near the contact the fines content is high enough that the clayey fines dominate the shear strength behavior. The fines content rapidly decreases over the next 6 inches or so, and eventually the fines content of the remainder of the layer remains relatively stable at between 5% to 10%. The green line in this figure represents our best estimate of the approximate operative effective friction angle through this zone.

It was not possible to discern with certainty the elevation to which pore pressures arising from underseepage passing beneath the sheetpile curtain through the more open, pervious sands at depth due to the transient rising storm surge penetrated (vertically) upwards into this transition zone. Accordingly, various combinations of partial pore pressure development may be postulated at different elevations across this transition, and these may be paired with various effective friction angles to evaluate the shear strength within this narrow, and critical zone.

Several combinations were postulated and analyzed in these studies. Higher (more completely penetrating) pore pressures more nearly approaching steady state flow are clearly appropriate at the base of this transition zone, and these would be paired with friction angles on the order of $\phi \approx 30$ to 32° . A few inches higher in the transition zone the effective friction angle would be somewhat lower, but this would be offset by reduced penetration of pore pressures, resulting in largely similar estimates of resultant frictional shear strength. In the end, an effective friction angle of 31° was selected, and this was coupled with assumed rapid

development of steady state pore pressures as the storm surge rose. (For reasonable ranges of in situ permeability of the deeper, more open and pervious sands and with reasonable ranges of specific storage for these initially saturated deposits; pore pressure development at the inboard side toe region within the pervious deeper sands was approximately 65 to 90% developed within two hours of outboard side (canal) water level increases.)

Figures 8.128 through 8.130 show the same sequence of figures, this time for conditions on the east bank (distressed) side of the canal. Once again the transition between the silty clay and the underlying clayey sand is the critical region. As with the west bank, an effective friction angle of 31° was selected for analysis, and this was coupled with assumed rapid development of full steady state underseepage as the storm surge rose within the canal.

Figure 8.131 shows the analysis cross-section and principal soil properties modeled for analysis of the west bank breach site. Analyses were performed using both finite element analysis methods (again using the program PLAXIS) and limit equilibrium methods (Spencer's Method).

Figure 8.132 shows normalized shear strain contours for the west bank (breach) section at a storm surge level of Elev. +9 feet (MSL). Gapping initiated at the outboard side of the floodwall and its supporting sheetpile curtain initiated in this analysis at a canal surge elevation of between +7 to +8 feet (MSL), and was fully developed by a surge elevation of +9 feet, as shown in this figure.

Figure 8.133 shows normalized shear strain contours for the east bank (distressed) section, this time for a slightly higher surge to elevation +10 feet (MSL). This the upper bound estimate of the surge elevations achieved during Katrina. Gapping developed in this east bank section at a surge elevation of between +7 to +8 feet, and was fully developed by a surge elevation of +9.5 feet (MSL).

These conditions produce a predicted failure of the west (breach) side at a surge elevation of approximately +9.5 feet (MSL) in these PLAXIS analyses, and the east side displaces a bit (with associated lateral displacement and tipping of the floodwall) but remains barely stable to a surge elevation of +10 feet (MSL).

Figures 8.134 and 8.135 show a simultaneous analysis of both sides of the canal, and the predicted ("best estimated" properties and flow) conditions for a storm surge to elevation +9 feet (MSL). Figure 8.134 shows normalized shear strain contours, and Figure 8.135 shows the associated predicted deformations and displacements. The west side has failed catastrophically, and the east side section is "distressed" (with lateral displacements of approximately 2 to 3 feet and some tilting of the floodwall. This closely matches the field observations.

Figure 8.136 shows the associated PLAXIS-based prediction of the critical path to failure for each side of the canal. Once gapping occurs, the extra "push" of the water in the gap is sufficient to destabilize the west bank at a surge height of approximately +9 to +9.5 feet (MSL), but the east bank section remains barely stable until a surge height of +10 feet (the upper bound of the estimated surge height that actually occurred).

Figures 8.137 through 8.159 repeat these same analyses, this time using classic seepage analyses to predict pore pressures and gradients resulting from the underseepage flows as the storm surge rises, and limit equilibrium analyses (Spencer's Method) coupled with these predicted pore pressure and gradient conditions to evaluate overall stability for both sides of the embankment. Once again, rapid development of essentially full steady state underseepage was assumed, and an effective friction angle of 31° was modeled at the interface between the silty clay and the underlying clayey sand.

Figures 8.142 and 8.146 show the most critical failure surfaces on the west bank (breach) side for a surge elevation of +9 feet (MSL), with and without gapping respectively. Figures 8.153 and 8.157 show the same two cases for the east bank (distressed) side, again for a surge height of +9 feet (MSL).

Figure 8.159 summarizes the results of these limit equilibrium analyses for both sides of the canal, and the heavy red lines show the estimated most critical paths to failure. Once again the west bank side fails at a surge height of slightly less than +9 feet, but the east bank (distressed) side remains barely stable at this surge elevation. The blue horizontal dashed line in this figure represents our investigation team's best estimated surge elevation in the canal at the time of the breach and failure of the west bank section.

These analyses show that the observed behaviors were not the result of underseepage and resultant piping erosion. The behaviors on both sides of the canal were, instead, the result of lateral translational instability (and incipient instability), with the critical potential failure mode on both banks being lateral translational sliding on the interface between the silty clay and the underlying clayey sands. This sliding was made possible by the high porewater pressures in the foundation soils at and near the base of the inboard-side levee toe due to underseepage.

This exactly fits with the observed field data. The "sinkholes" at the crest of the embankment on the east side were the result of tilting of the slightly displaced floodwall, and the resulting opening of a gap between the floodwall and the embankment into which embankment soils could fall. This correlates with the observation the "sinkhole features" were all narrow, and were all parallel and adjacent to the floodwall (see Figures 8.114 and 8.117.)

8.3.10 Summary and Findings

A large number of critical errors and poor judgements jointly contributed to the catastrophic failures that occurred along the drainage canals. There were conceptual errors in the layout and fundamental design of the levees and floodwalls, there were policy and funding issues that greatly reduced the level of safety of the overall system, and there were engineering errors in the analysis and design of individual sections.

No one organization, agency or group of individuals had a monopoly on their contribution to this disaster. Federal government (including the Congress), the Corps of

Engineers, local government and local oversight agencies (including the local Levee Board and the local Water and Sewerage Board), and outsourced engineering firms all contributed.

The resulting system failed catastrophically, and at multiple locations. And it failed at significantly less than the intended levels of “design” (storm surge) loading. Moreover, it is clear that additional sections were saved from failure only by the catastrophic failures of nearby breaches, which drew down the water levels and so reduced the loading on additional potentially unstable levee and floodwall sections.

The results of these failures were catastrophic. The vast majority (approximately 80%) of the eventual floodwaters that flowed into the main Orleans East Bank (downtown) protected area came through the breaches in the drainage canals. These flows overflowed the sub-basin north of the Metairie Ridge, and then crossed this ridge and flowed into the southern areas as well where they greatly exacerbated flooding that had already occurred as a result of overtopping and failures of levees and floodwalls along the west side of the IHNC. In the absence of the drainage canal failures there would still have been localized flooding and damage near the IHNC, but this would have been minor relative to the eventual damages that resulted when the canal breaches filled a majority of the overall basin.

The localized flooding near the IHNC would have posed relatively little threat of loss of life; the damages would have been (relatively) limited and the floodwaters could have been pumped out in a matter of days. Instead, roughly half of the 1,293 fatalities (to date) attributed to flooding of the New Orleans region occurred in the Orleans East Bank (downtown) protected basin, and a roughly similar fraction of the devastating regional economic damages as well.

The following is a listing of critical errors and poor judgements and decisions that contributed significantly to the poor performance of the drainage canal levees and floodwalls during Hurricane Katrina:

1. The decision not to install floodgates at the north ends of the three drainage canals to prevent uncontrolled water level rise due to storm surge within the canals was largely the result of poor interaction between the local Levee Board and the local Water and Sewerage Board, and their inability to resolve their differences in the interests of the greater Public good (and safety). Lawsuits by environmentalists against this system also worked against the floodgates. As a result, the canals remained open to storm surges; essentially inviting the enemy (storm surge) into a poorly protected section of the interior of the protected ring around metropolitan New Orleans.
2. The decision not to purchase additional land (right of way) to permit widening of the levees required that the system be extended vertically without allowing provision of additional levee width and mass with which to resist the increased floodwater forces associated with the increased height. Short-term savings here resulted in tens of billions of dollars in losses.
3. Similarly, the failure to garner access and control of property at the inboard (protected side) toe of the levees prevented full and proper inspection of this critical area. It also

led to unacceptable risk associated with growth of trees on the inboard side levee slopes and toes, and the literal undermining of levee toes by excavation of in-ground swimming pools in this critical inboard toe area.

4. The designers failed to take advantage of critical lessons from an expensive and well-directed research program that involved construction of a full-scale model levee and floodwall on nearly identical foundation soils in the nearby Atchafalya basin. This model was loaded to failure, and the failure mode observed involved opening of a gap on the outboard side of the floodwall, water entering into the gap, and subsequent pressures on the floodwall and sheetpiles pushing the inboard side section of the earthen embankment sideways (the “cut the cake in half and slide it” failure mode). This failure mode was neglected in the subsequent design of the levees and floodwalls lining the canals, and at least two of the catastrophic failures (breaches), and two additional “incipient” failures were the result of this failure mechanism.
5. The designers also failed to take account of the influence of stress history and effective overburden stresses on the strengths of the foundation soils beneath a number of the embankments. Furthermore, they deviated from USACE policy by using average shear strengths (not strengths slightly lesser than the average data), and by “averaging” strengths across lateral distances that were too large. These errors and shortcomings in the determination and selection of soil shear strength parameters played a critical role in the catastrophic failure of the east bank near the north end of the 17th Street canal.
6. Optimistic assumptions, and misinterpretation of two field tests, led to the assumption that system permeability was low enough that underseepage would not be a critical issue during “transient” (short-term) rises in canal water levels during hurricane induced storm surges. This was a critical error, and it resulted in inadequate sheetpile lengths throughout the drainage canals (especially the London Avenue Canal), and along the IHNC. These sheetpile curtains routinely extend to insufficient depths as to adequately “cut off” underseepage flows, and the resulting underseepage flows were principal contributors to the catastrophic failures observed at both of the major breach sections on the London Avenue canal. These inadequate cut-offs continue to be a potentially critical issue at other sections that did not (yet) breach during hurricane Katrina, and they appear to have been a principal factor in the two massive breaches on the east bank of the IHNC (at the edge of the Lower Ninth Ward; see Chapter 6) as well.
7. Insufficient site investigation was performed for the design of these critical systems protecting a major metropolitan population. Given the difficult and complex foundation soil conditions, additional borings and testing would have represented a very modest incremental expenditure, and would have greatly improved the information available as a basis for analysis and design of these important sections.
8. Errors and poor judgements were made in engineering analysis and design of these sections. Soil properties were extrapolated laterally over inappropriately large distances, and without adjustment for the resulting uncertainties. Archaic analysis

techniques were employed (the Method of Planes), and project-specific research (a full scale test embankment and floodwall in the nearby Atchafalya basin) was ignored, resulting in failure to analyze the failure mode (“cut the cake in half and slide it”) that proved critical for at least two of the catastrophic drainage canal breaches, and likely also for the two massive breaches at the east side of the IHNC (adjacent to the Ninth Ward.) This mode was also evident at an additional “incipient” failure section on the London Avenue canal that was saved from failure, by the failure of the even weaker section on the opposite shoreline (which immediately drew down the local water levels.) The stability of the entire canal system should be considered potentially suspect until it can be properly re-evaluated with regard to this potentially critical mechanism.

9. Design review was inadequate. Errors and questionable judgements that would have been expected to be caught and challenged by a properly convened independent external review panel went unchallenged. On one occasion when reviewers from the USACE Division level in Vicksburg did catch and challenge such issues, they were rebuffed by the local District Chief who declared those issues to be a matter of “judgement”.
10. The Factor of Safety (FS) used for design of these vital levees and floodwalls was set at only $FS = 1.3$ for the case of “transient” storm surge loading. As discussed in detail in Section 8.3.7.1 this is inappropriately low for systems critical for the safety of large populations, and for the difficult and challenging foundation soils conditions of the region. This issue is discussed in significantly more detail in Chapters 11 and 12.
11. Congressional funding (appropriations) were problematic. Funding was irregular and somewhat unpredictable, representing a difficult basis for design and construction of a system intended to be contiguous (seamless) and to protect a large metropolitan population. Strategic decisions, and conceptual design, were often driven by a need for frugality. In addition, when appropriations did arrive, some elements of the system had to be further streamlined for economy. The relatively minor savings achieved now pale in comparison to the many tens of billions of dollars in losses that ensued.
12. Pace of funding was also problematic. At the time of Katrina’s arrival, the flood protection system in the canal district was still incomplete.... fully 51 years after the flooding from Hurricane Betsy that inspired the inception of construction of the improved flood protection system. Three of the bridges across the drainage canals still had not yet had their side walls raised, so three “holes” remained in an otherwise contiguous system. These “holes” at the bridges were not critical during Hurricane Katrina only because: (a) the storm surge was less than the full design load case, and (b) catastrophic nearby breaches (failures) occurred. (An additional “hole” in the system, at the south end of the Orleans Canal, was yet another result of dysfunctional interactions between the local levee board and the local water and sewerage board (as discussed previously in item #1 above.)

Many of the issues above, from conceptual design issues through engineering analysis details and even selection of appropriate Factors of Safety would have been expected to be

challenged by a properly convened independent review panel. Unfortunately, in the current system with myriad local interests and no strong local entity able to convene appropriate levels of unbiased expert review capability, this critical element was absent during the design and construction of these important flood protection system elements.

In addition, there was a lack of centralized authority, and of clear areas of responsibility. Involvement of a significant “local” institutional presence of significant stature and resources was lacking. The local levee board lacked the resources and funding to mount serious review of the Federal plans and designs, and the mandate to challenge problems that should have been apparent at early stages.

In the end, the performance of the flood protection system along the three drainage canals was unacceptable, and resulted in catastrophic loss of life and property throughout a major metropolitan region.

8.4 References

- Burk & Associates, Inc (1986) *Geotechnical Investigation of London Avenue Outfall Canal*, OLB Project No 2049-0269, Vol I and II, prepared for the Board of Levee Commissioners of the Orleans Levee District, New Orleans, Louisiana.
- Foott, R and Ladd, C.C (1977) “Behavior of Atchafalaya levees during construction”, *Geotechnique*, 27, No2, pp 137-160.
- GEO-SLOPE/W (2004) “Complete Set of Manuals”, John Krahn (Edit.), Calgary, Alberta, Canada.
- IPET – Interagency Performance Evaluation Task Force (2006) *Performance Evaluation Status and Interim Results*, Report 1 of a Series, Performance Evaluation of the New Orleans and Southeast Louisiana Hurricane Protection System, January 10, US Army Corps of Engineers.
- IPET – Interagency Performance Evaluation Task Force (2006) *Performance Evaluation Status and Interim Results*, Report 2 of a Series, Performance Evaluation of the New Orleans and Southeast Louisiana Hurricane Protection System, March 10, US Army Corps of Engineers.
- Jackson, R. B., (1988), “E99 Sheet Pile Wall Field Load Test Report”, Technical report No.1, US Army Engineer Division, Lower Mississippi Valley, Vicksburg, MS
- Jamiolkoski, M, Ladd, C.C., Germaine, J.T., and Lancellotta, R. (1985) “New developments in field and laboratory testing of soils.” *Proc. 11th International Conf. on Soil Mechanics and Foundation Eng.*, San Francisco, 1, 57-154.
- Karlsrud, K., Lunne, T and Brattlien (1996) “Improved CPTU interpretations based on block samples”, *Nordic Geotechnical Conference*, 12 Reykjavik 1996. *Proc*, Vol.1, pp 195-201.

- Kaufman, R and Weaver, F (1967) "Stability of Atchafalaya Levees", Journal of the Soil Mechanics and Foundations Division, ASCE, SM 4, pp 157 -176.
- Kemp, P., and Mashriqui, H. (2006). Personal Communication
- Lacasse, S., Ladd, C.C., and Baligh, M.M. (1978) "Evaluation of field vane, Dutch cone penetrometer and piezometer probe testing devices." Res. Report R78-26, Dept. of Civil Eng., MIT, 375 pp.
- Ladd, C.C and DeGroot, D. 2003. "Recommended Practice for Soft Ground Site Characterization", Arthur Casagrande Lecture, 12th Panamerican Conference on Soil Mechanics and Geotechnical Engineering, June, Boston.
- Lunne, T., Lacasse, S., and Rad, N.S., (1989) "General report: SPT, CPT, PMT, and recent developments in in-situ testing", Proceedings, 12th International Conference on soilmechanics and foundation engineering, Vol.4, Rio de Janeiro, pp. 2339-2403
- Mashriqui, H., (2006), Personal Communication
- Mayne, P,W and Mitchell, J.K (1988) "Profiling of Overconsolidation Ratio in Clays by Field Vane", Canadian Geotechnical Journal, Vol 25, No 1, February, pp 150-157.
- Oner, M., Dawkins, W.P., and Hallal, I., (1997) "Soil Structure Interaction Effects in Floodwalls", Electronic Journal of Geotechnical Engineering
- Oner, M., Dawkins, W.P., and Mosher, R., (1997) "Shearing Method for Soil Structure Interaction Analysis in Floodwalls", Electronic Journal of Geotechnical Engineering
- Robertson, R.K, and Campanella, R.G. (1983) "Interpretation of Cone Penetration Tests. Part I: Sand", Canadian Geotechnical Journal, Vol 20, No 4, Nov, pp 718-733.
- Seed, R.B. (2005) "CE 270B Class Notes", University of California, Berkeley.
- PLAXIS Finite Element Code for Soil and Rock Analyses (2004). "Complete Set of Manuals", V8.2 , Brinkgreve yVermeer (Edit.), Balkema, Rotterdam, Brookfield.
- USCE (1989) London Avenue Outfall Canal, Design Memorandum No 19A General Design, Vol 1 and Vol 2, Louisiana, Department of the Army, New Orleans District, Corps of Engineers, New Orleans, Louisiana.
- USCE (1990) Orleans Parish (Jefferson Parish) 17th St. Outfall Canal, Metairie Relief, Design Memorandum No 20 General Design, Vol 1 and Vol 2, Louisiana, Department of the Army, New Orleans District, Corps of Engineers, New Orleans, Louisiana.
- Van Heerden, I., (2006), Personal Communication

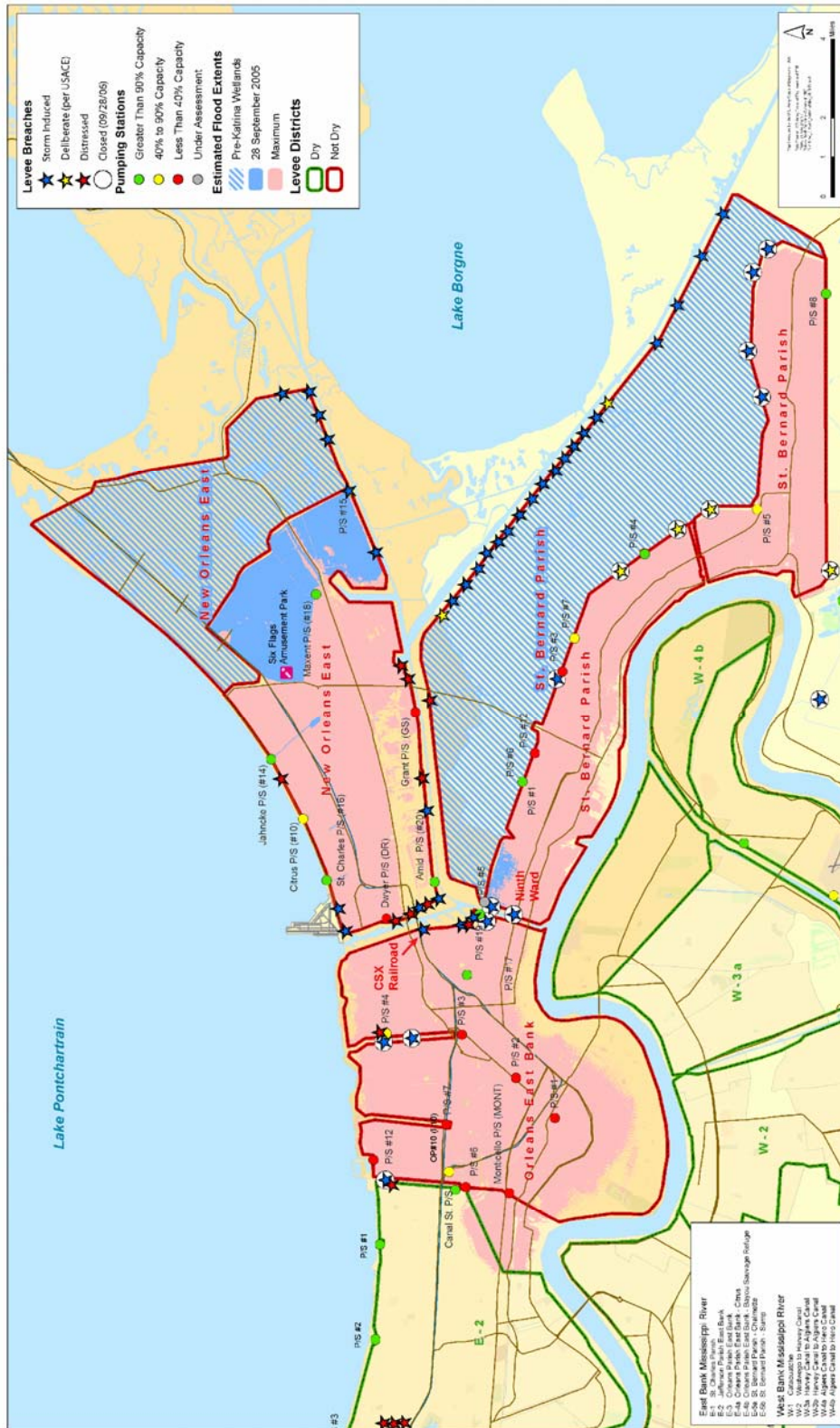


Figure 8.1: Map showing principal features of the main flood protection rings or “protected areas” in the New Orleans area. [Modified after USACE, 2005]

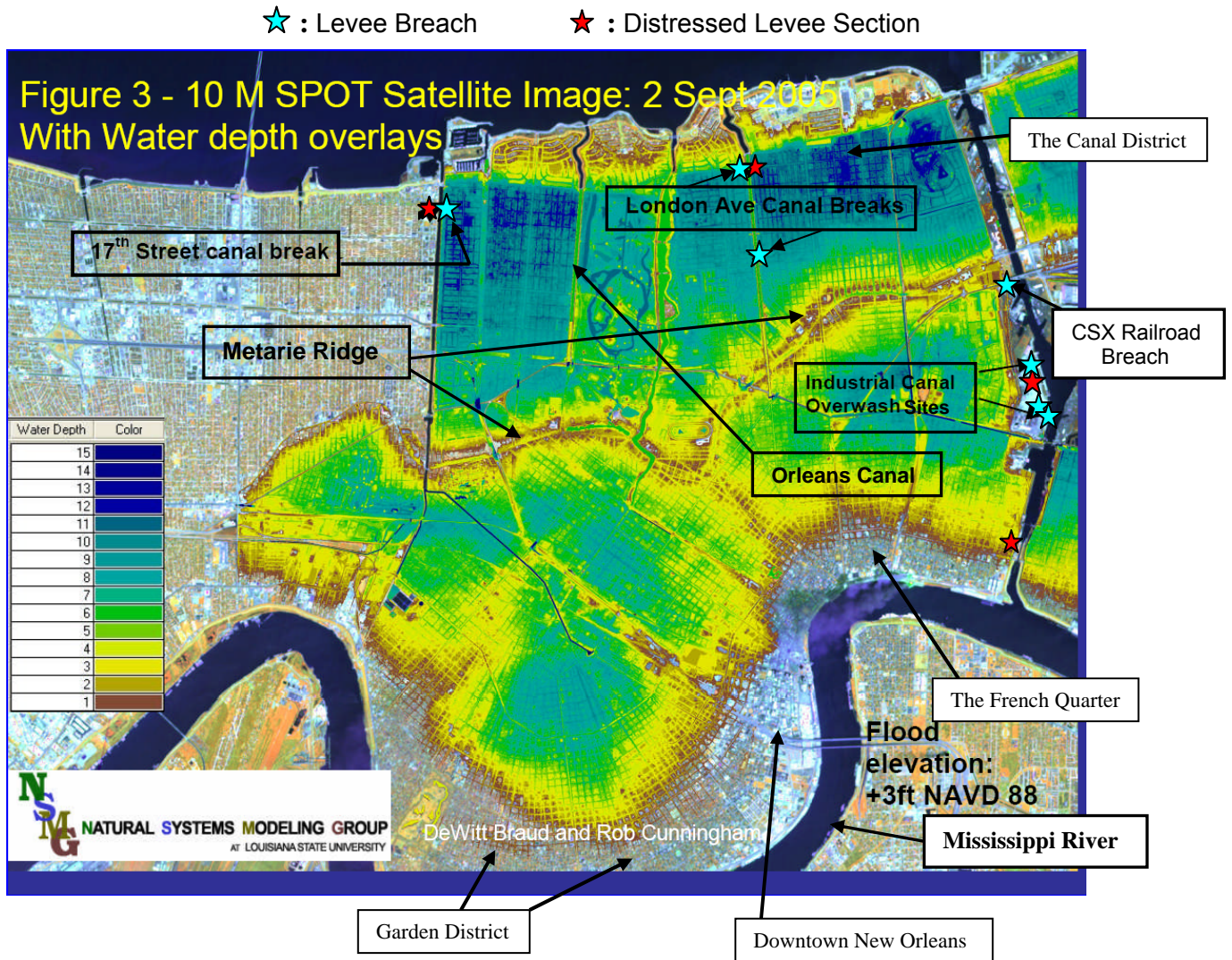
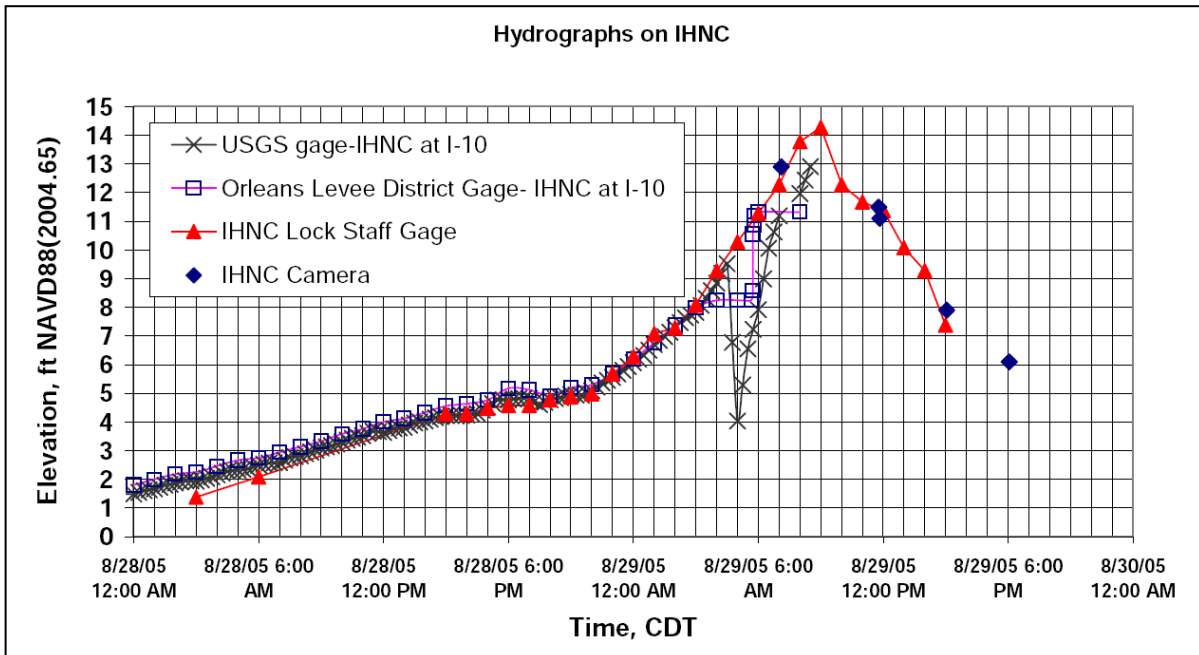


Figure 8.2: Plan View of the Orleans East Bank (Metro) protected area showing approximate depth of flooding on September 2, 2005.

[Modified after Mashriqui, 2006]



Source: IPET Interim Report No. 2; April, 2006

Figure 8.3: Hydrographs showing measured (and photographed) water levels at gage stations along the Inner Harbor Navigation Channel (IHNC).



Photograph by Rune Storesund

Figure 8.4: Concrete storm gate at the west bank of the CSX Railroad crossing of the IHNC, after Hurricane Katrina, showing the steel floodgate missing.



Photograph by Rune Storesund

Figure 8.5: View from the inboard side of the CSX Railroad breach site from Figure 8.4 showing scour of the roadway fill adjacent to the railway embankment fill.



Photograph by Rune Storesund

Figure 8.6: The I-wall section breach behind the Port of New Orleans, showing floodwall failure.



Photograph by Rune Storesund

Figure 8.7: Second view of the I-wall failure at the Port of New Orleans showing the trench scoured by overtopping flows.

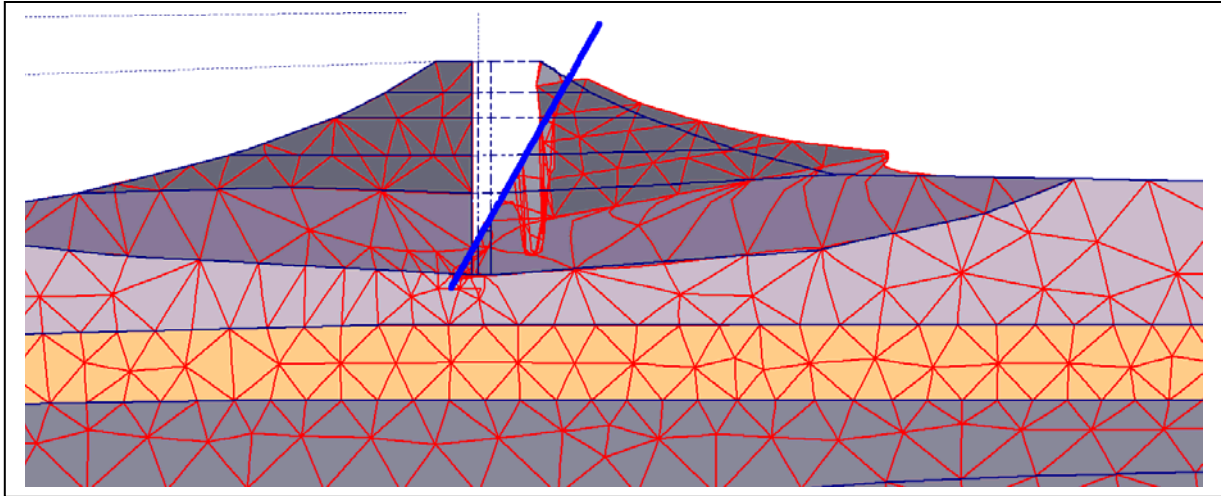


Figure 8.8: Deformed mesh of I-wall failure at the IHNC behind the Port of New Orleans.

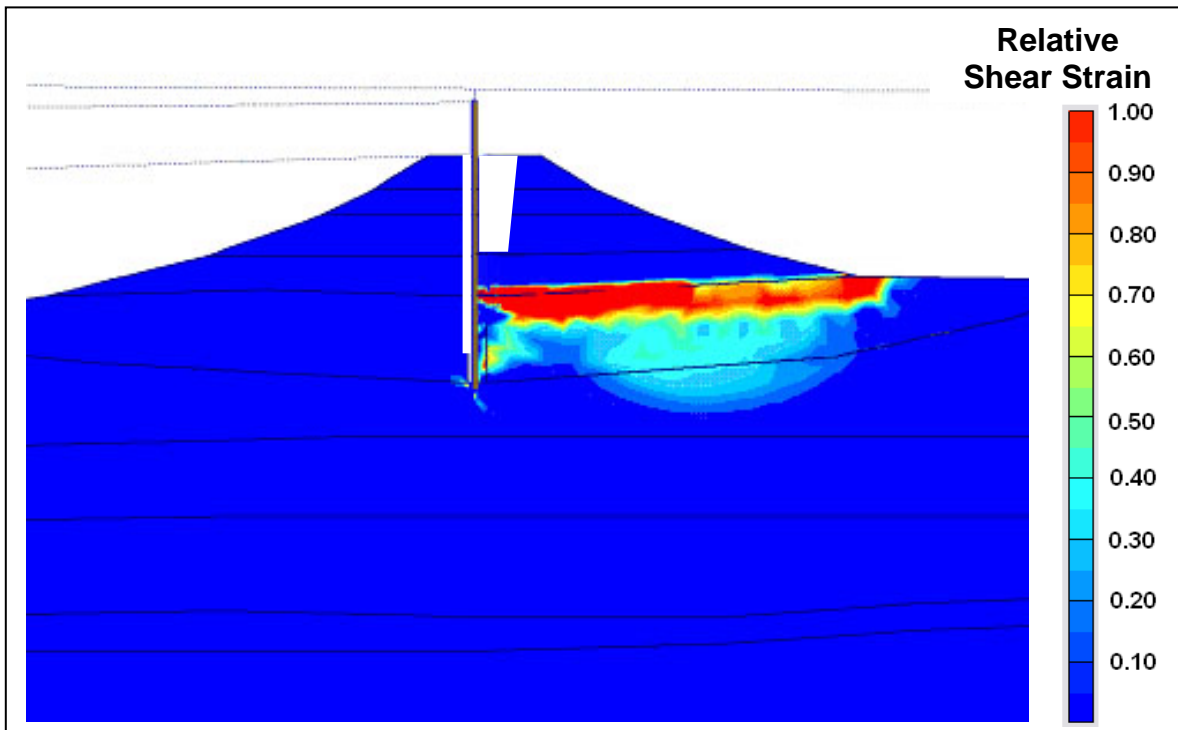


Figure 8.9: Finite element analysis of I-wall failure at the IHNC behind the Port of New Orleans, showing shear strain contours at point of wall failure.

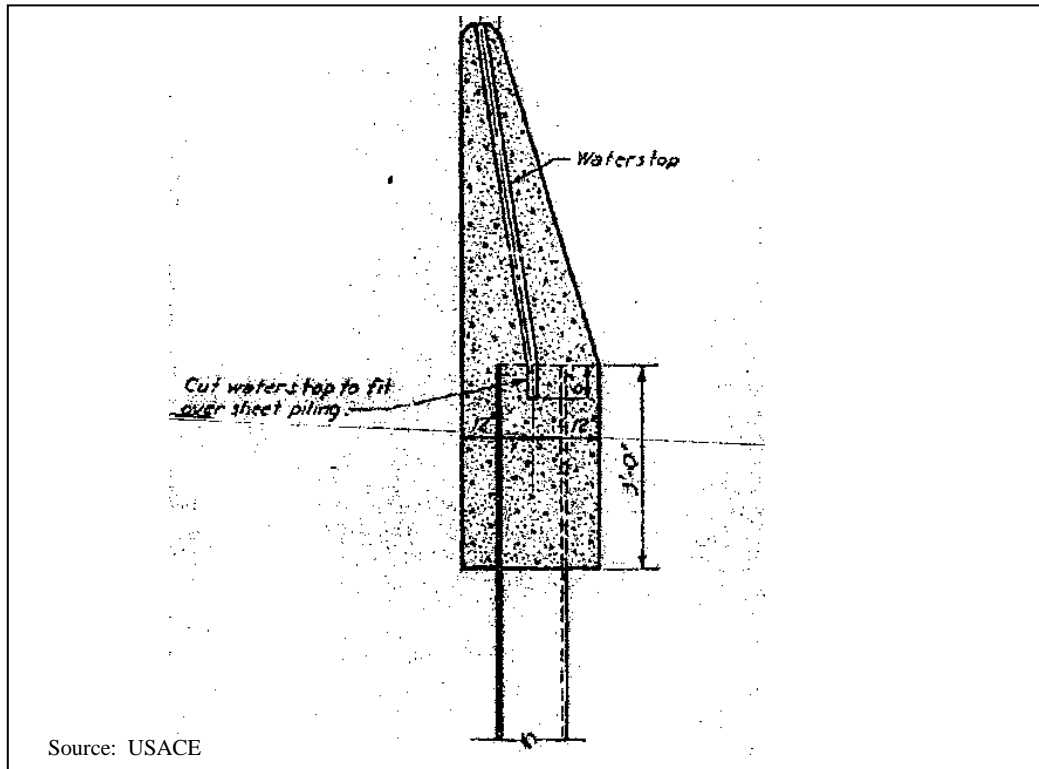


Figure 8.10(a): Typical reinforced concrete I-wall atop a sheetpile curtain.

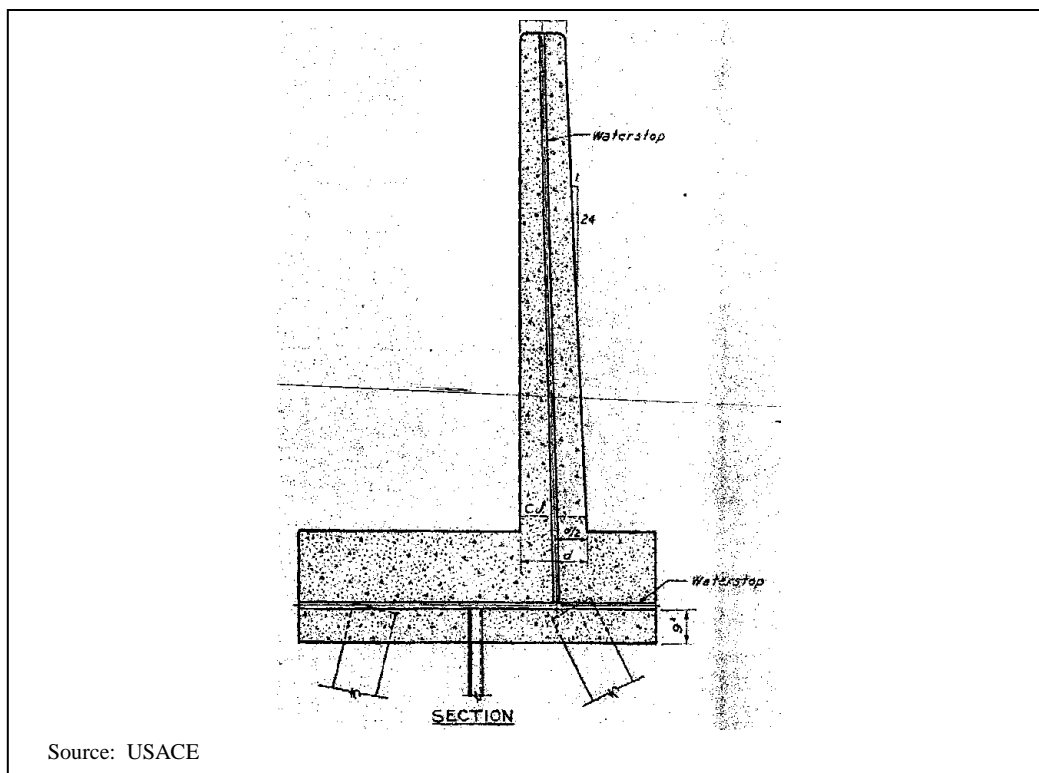


Figure 8.10(b): Typical reinforced concrete T-wall atop a sheetpile curtain.



Photograph by Rune Storesund

Figure 8.11: Concrete floodwall and steel floodgate structure at railroad yard behind the Port of New Orleans.



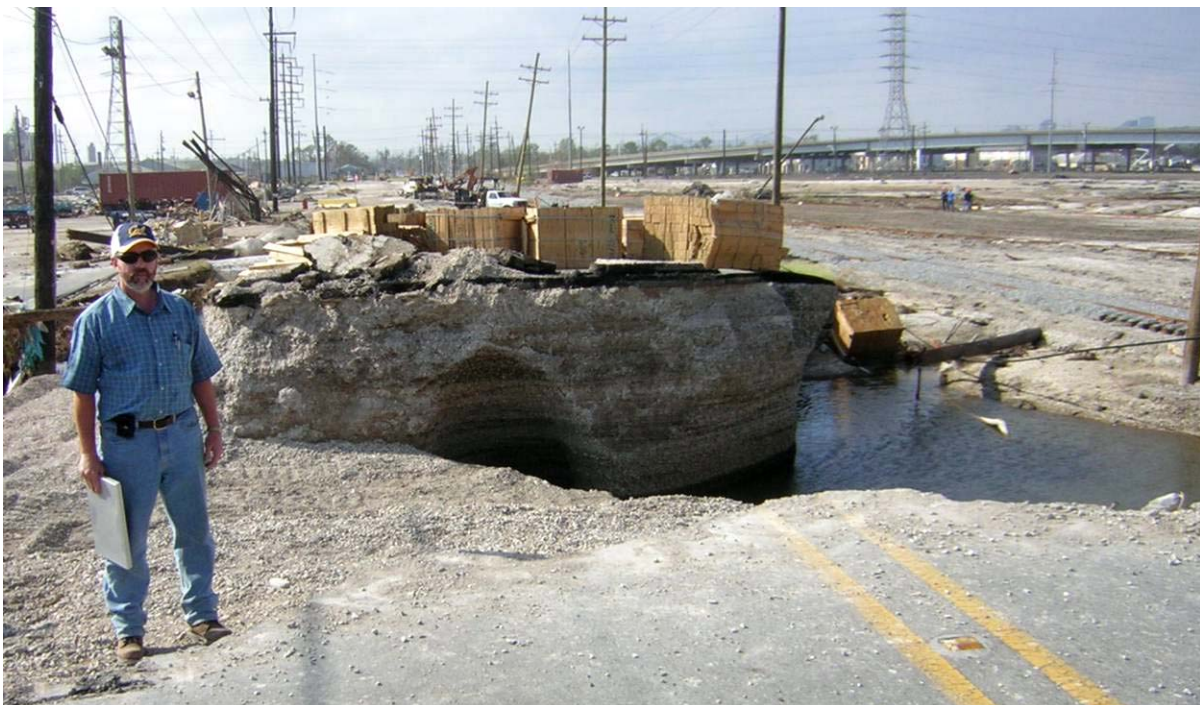
Photograph by Rune Storesund

Figure 8.12: Erosion, gapping and offset of adjacent wall sections at the east end “transition” of the concrete floodwall and gate structure from Figure 8.11.



Photograph by Rune Storesund

Figure 8.13: Erosional breach behind the southern end of the Port of New Orleans at contact between embankment section and structural concrete monolith.



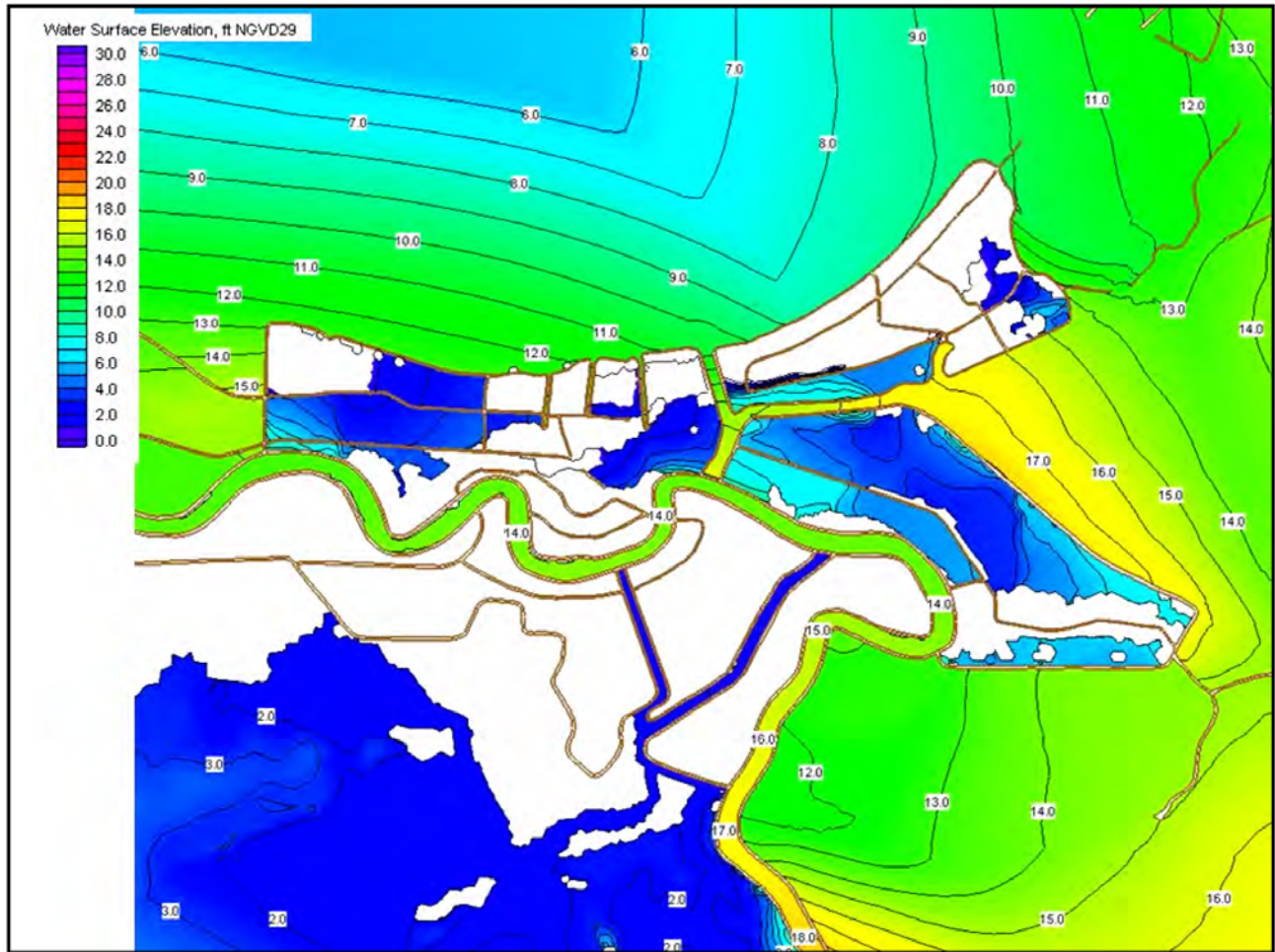
Photograph by Rune Storesund

Figure 8.14: Close-up view of the highly erodeable shell sand fill at the breach shown above in Figure 8.12.



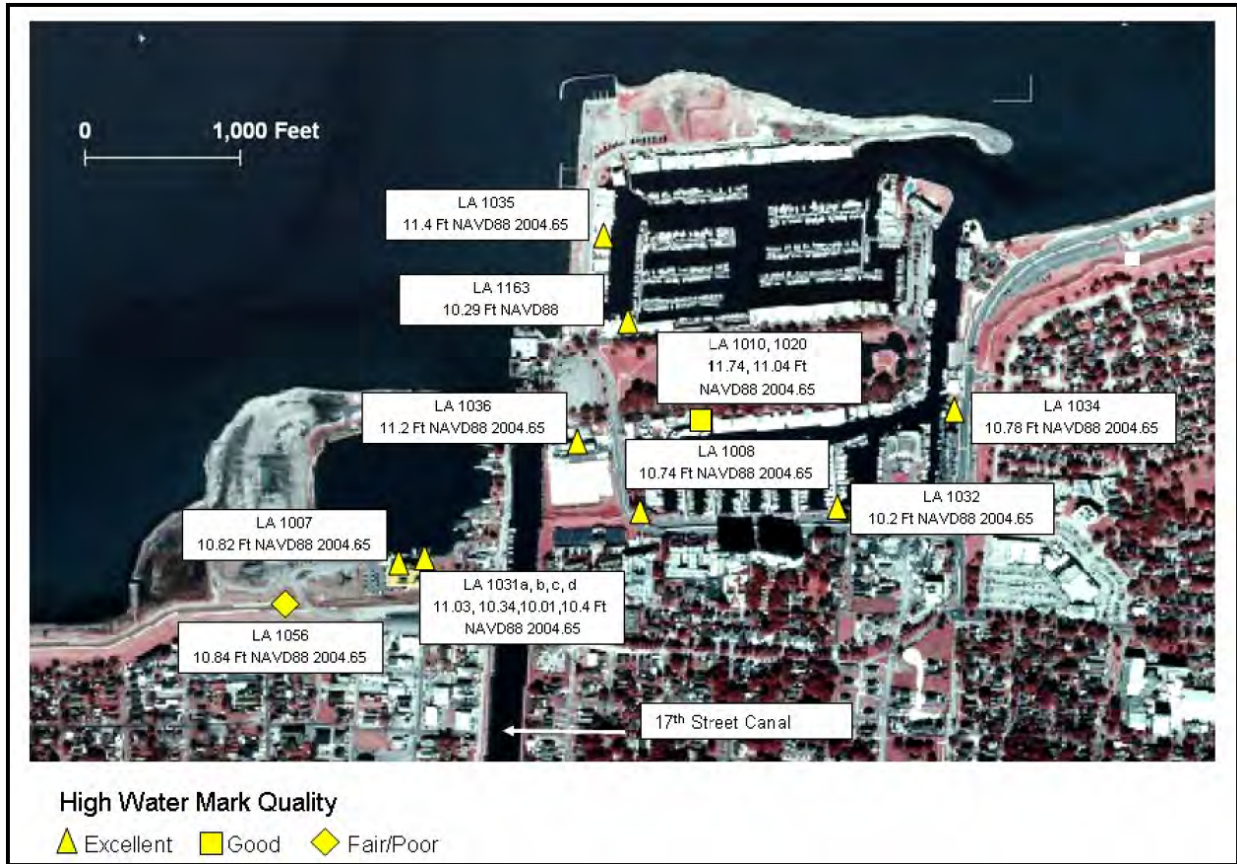
Photograph by Rune Storesund

Figure 8.15: View of second large erosional breach behind the southern end of the Port of New Orleans.



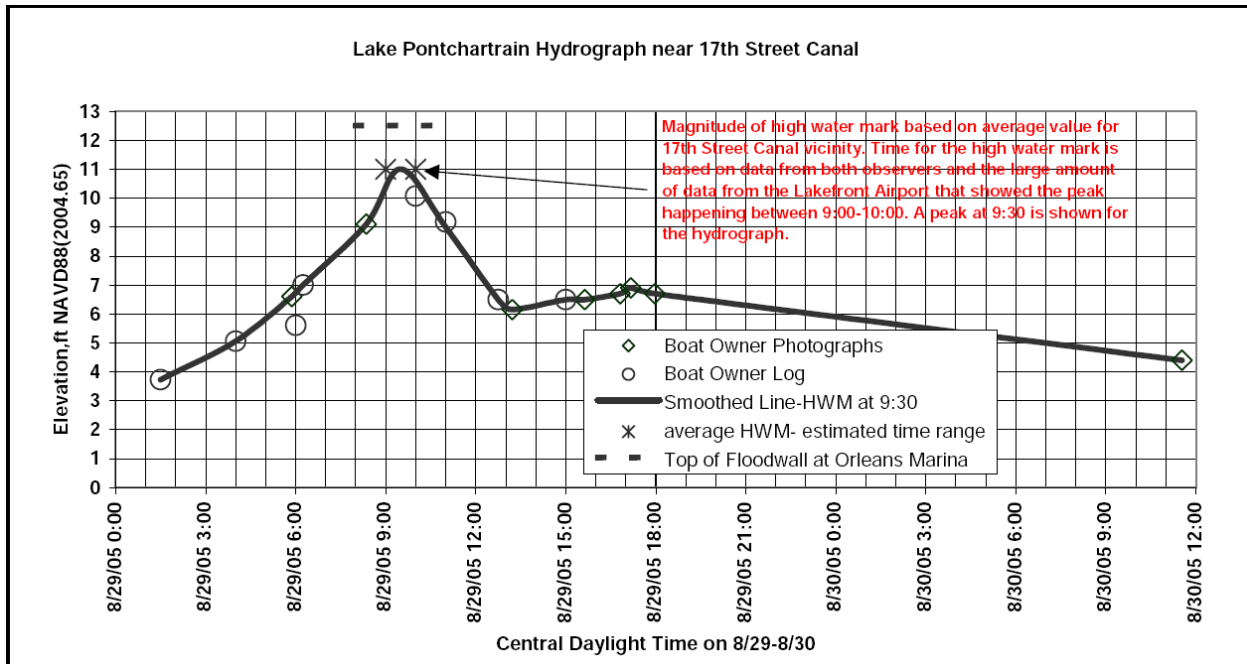
Source: IPET Report No. 2, April, 2006

Figure 8.16: Approximate contours of maximum storm surge heights along the southern end of Lake Pontchartrain. [Note: Elevations in Feet, NGVD29]



Source: IPET Report No. 2; April, 2006

Figure 8.17: High water marks near the mouth of the 17th Street Canal.



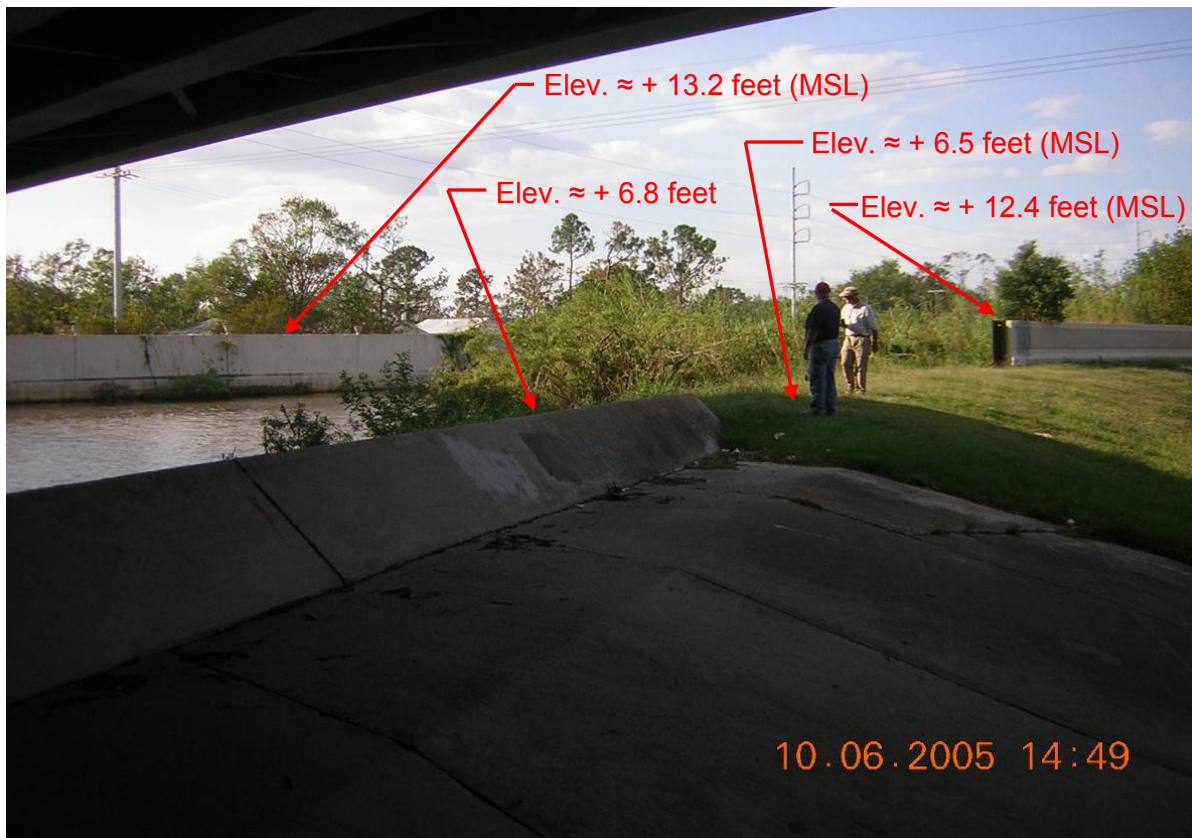
Source: IPET Report No. 2, April, 2006

Figure 8.18: Hydrograph proposed by IPET for the 17th Street drainage canal.



Photograph by Rune Storesund

Figure 8.19: View of the pump house, levees and floodwalls, and the “gap” at the south end of the Orleans canal.



Photograph by Rune Storesund

Figure 8.20: Side view of the “gap” at the south end of the Orleans canal.

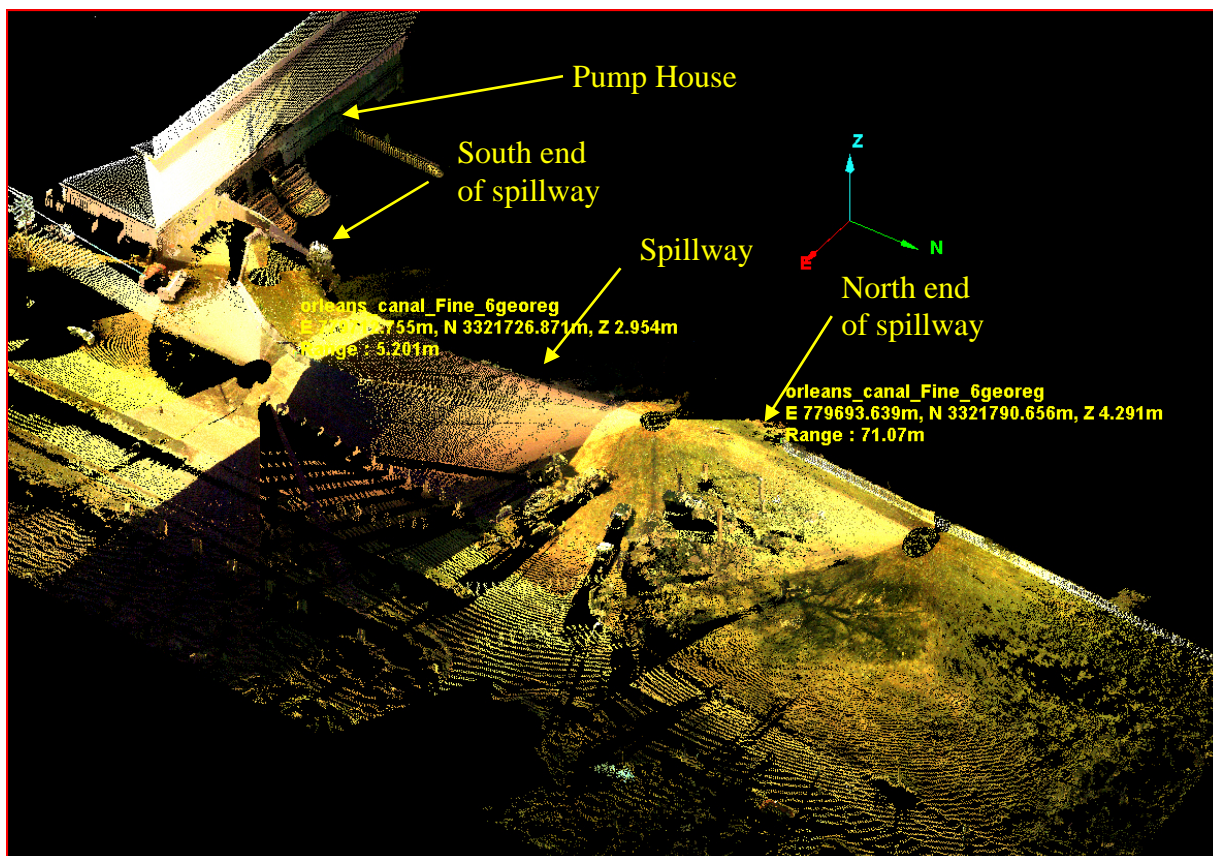


Figure 8.21: Oblique view of LIDAR survey of the southern end of the Orleans Canal, showing the “gap” on the east side where the levee and floodwall that should have sealed the end are omitted, and a “spillway” replaces them.



Photograph by Rune Storesund

Figure 8.22: View of the earthen levee embankments and floodwalls along the east side of the Orleans Canal (view looking to the North.)



Photograph by Rune Storesund

Figure 8.23: View of the earthen levee embankments and floodwalls along the west side of the Orleans Canal (view looking to the North.)



Figure 8.24: Oblique aerial view of the breach at the 17th Street Canal.

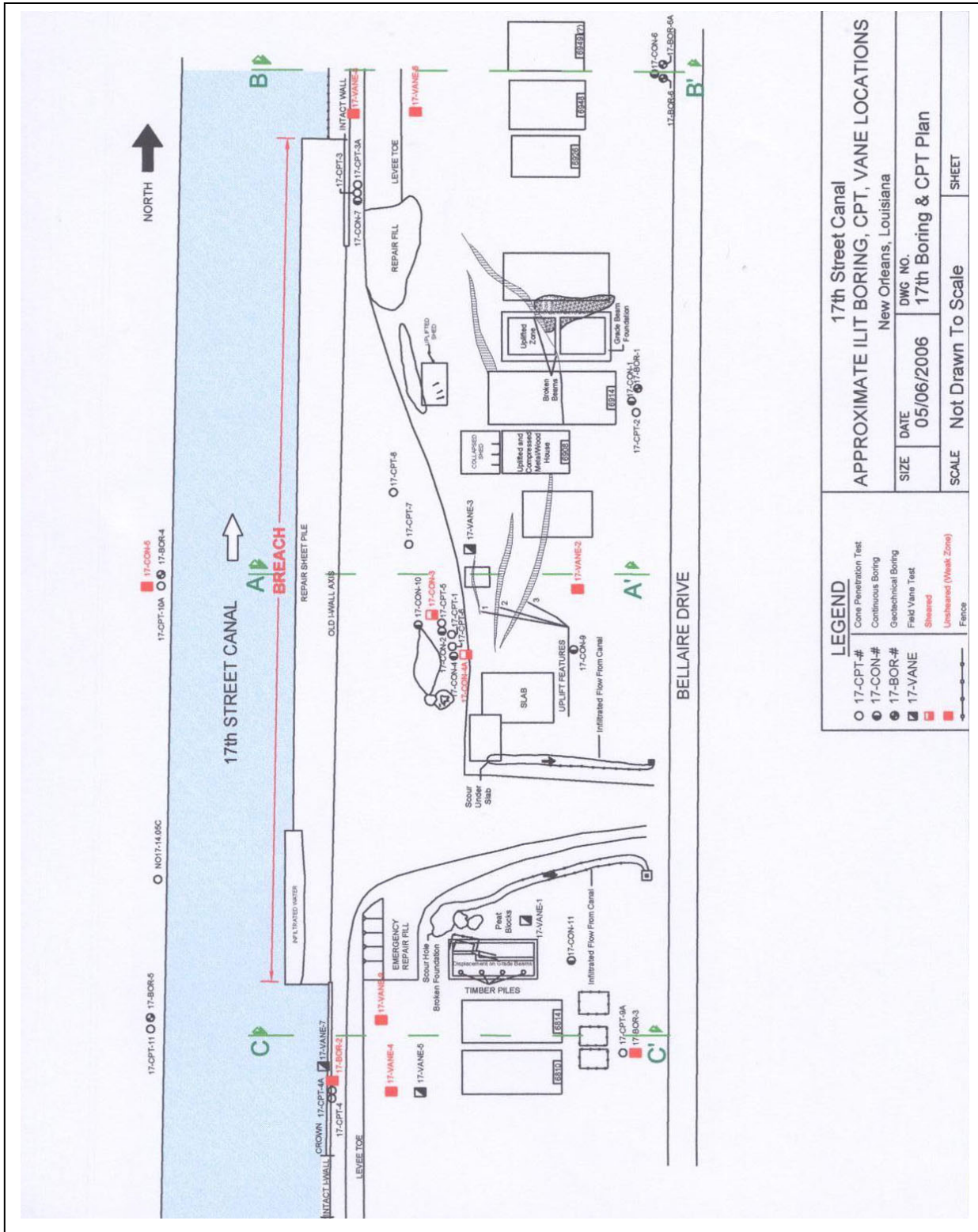


Figure 8.25: Plan view for the 17th Street Canal showing approximate ILIT boring and CPT locations



Figure 25(a): Plan view of 17th Street Canal showing locations of IPET borings and CPT

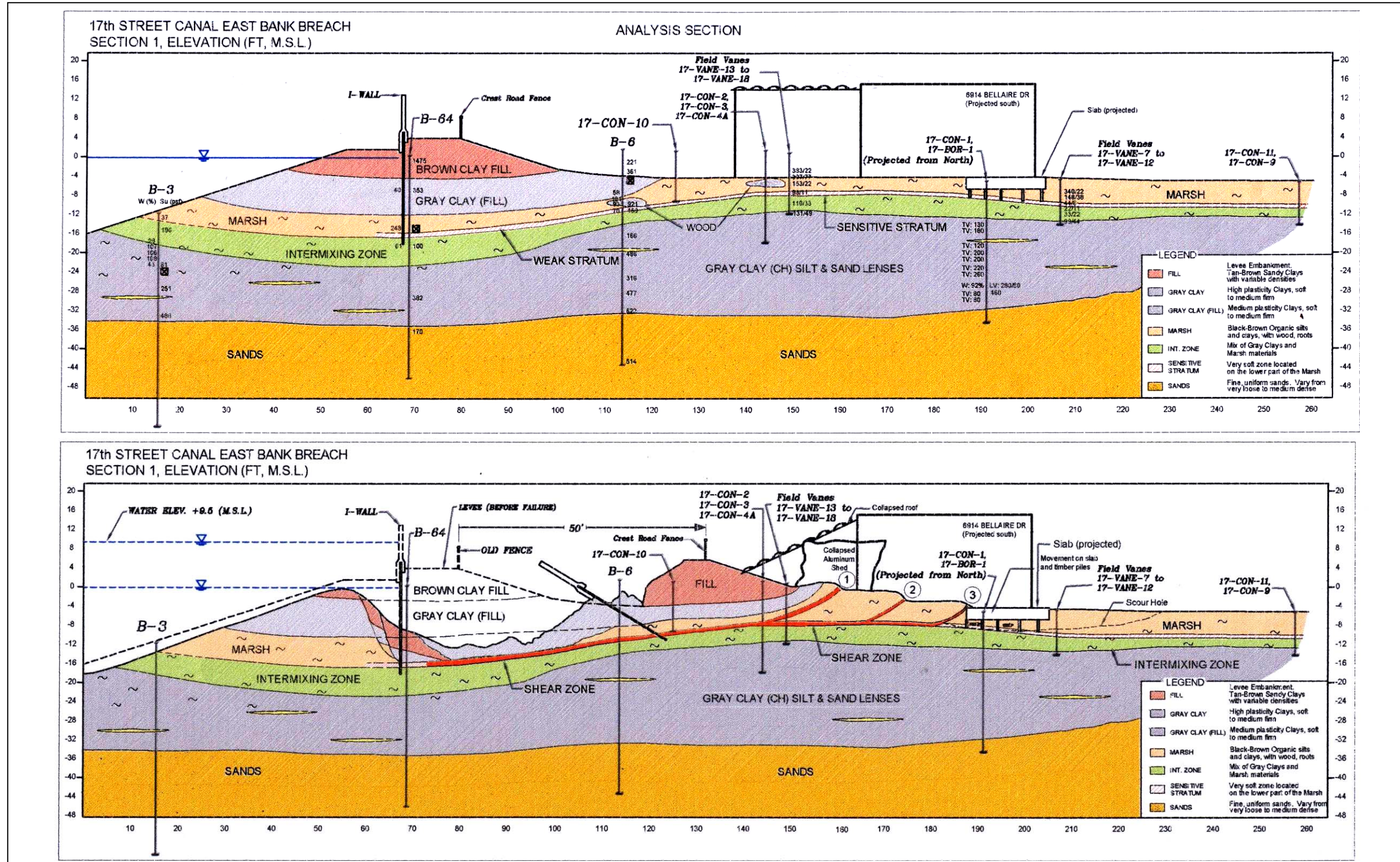


Figure 8.26: Cross-section through the 17th Street Canal breach showing conditions (a) before the hurricane, and (b) after the breach and failure.

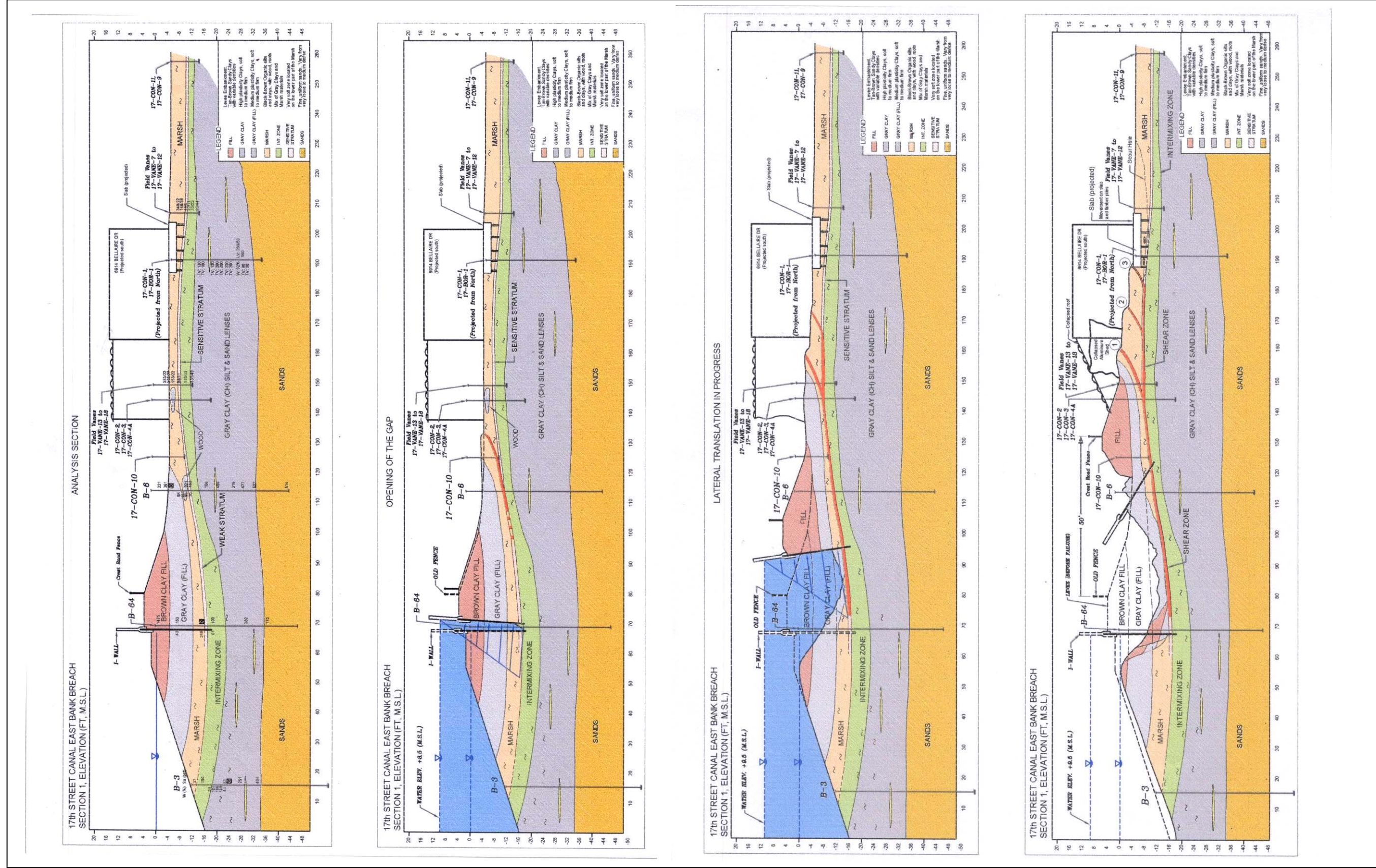


Figure 8.27: Cross-sections through the 17th Street Canal breach showing conditions as: (a) pre-storm surge, (b) a gap opens between the outboard side of the earthen embankment and the sheetpile curtain and the elevated water levels increase within this gap pushing the I-wall and the inboard side of the embankment laterally away from the canal, and (d) final configuration at the end of displacement after I-wall topples backwards towards the canal.



Figure 8.28: View of the 17th Street Canal breach site showing the tops of the I-wall sections that “pushed” (and followed) the displaced levee embankment section, and then toppled backwards towards the canal.



Figure 8.29: View of the 17th Street canal breach site showing the I-wall sections at the south end of the breach toppled forward (to the inboard side) by the inrushing floodwaters. Note the severe scour inboard of the failure at this location.



Figure 8.30: Side view of the collapsed shed pushed into the house at 6914 Bellaire Drive as illustrated in the cross-section of Figure 8.27.



Photograph by Joseph Wartman

Figure 8.31: View of the foundation slab shown in the cross-section from Figure 8.27.



Figure 8.32: View of the exit of the upper failure surface (shear surface No.1 from Figure 8.27) at the inboard toe of the laterally translated embankment (toe scarp No. 1 in Figures 8.26 and 8.27).

[IPET Interim Report No. 2, April 1, 2006]



Figure 8.33: View of toe scarps No's. 2 and 3 at the inboard edge of the lateral translational failure at the 17th Street drainage canal.



Figure 8.34: Additional view of toe scarps No's. 2 and 3 at the inboard edge of the lateral translational failure at the 17th Street drainage canal.

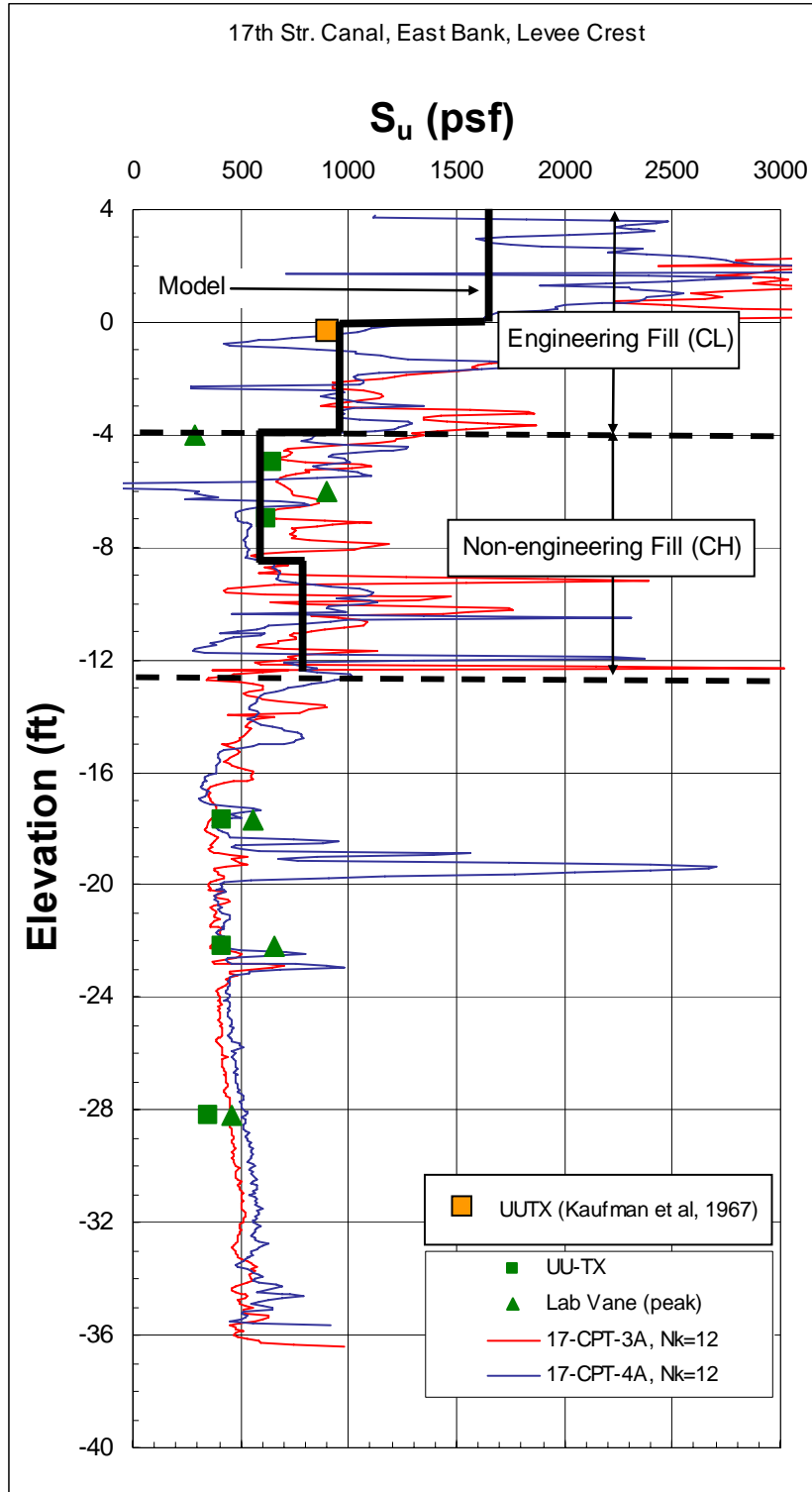


Figure 8.36: Summary of shear strength data within the 17th Street drainage canal levee embankment fill at and near the east bank breach section.

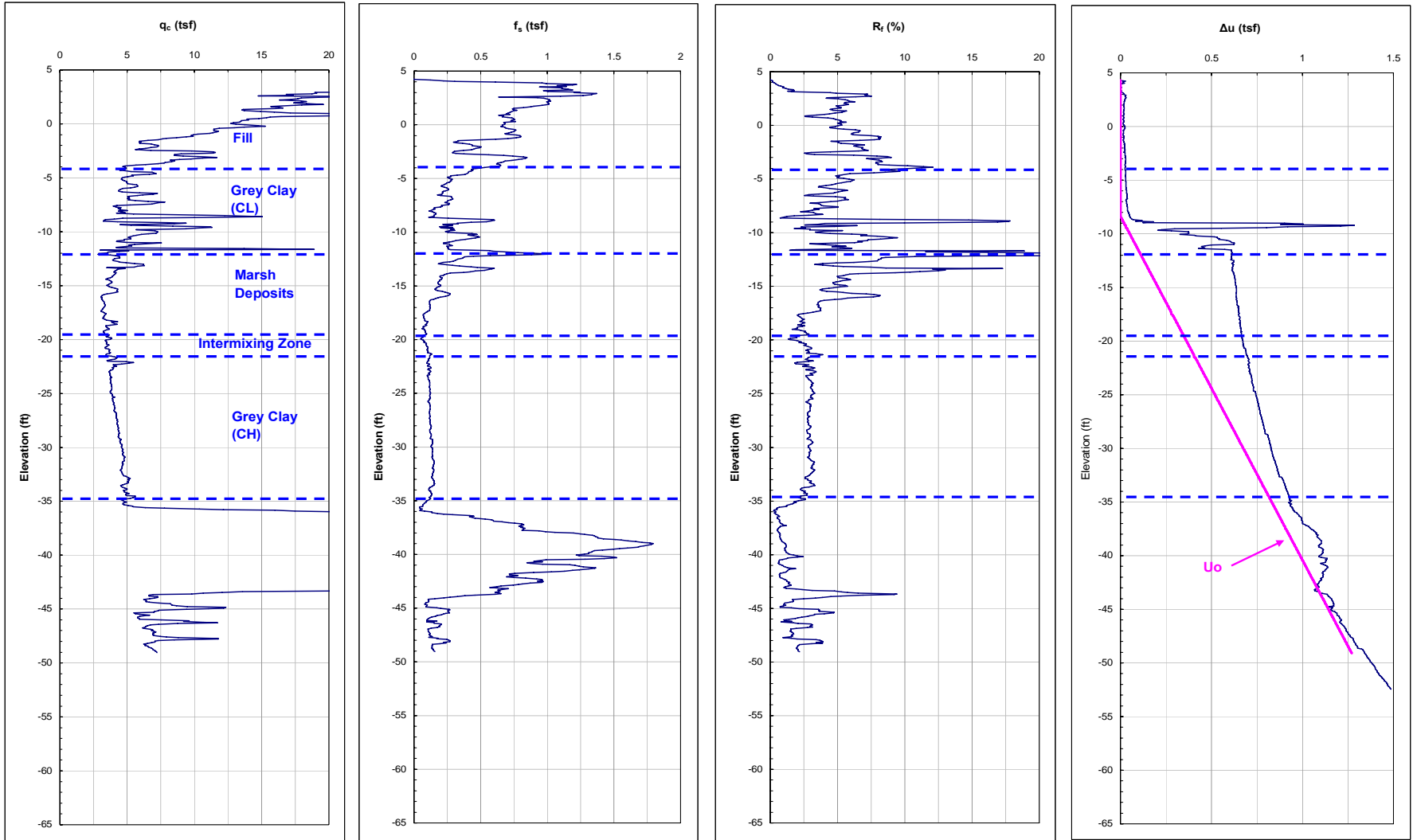


Figure 8.37: Example of CPT test data for locations beneath the levee embankment at and near the 17th Street canal breach section.

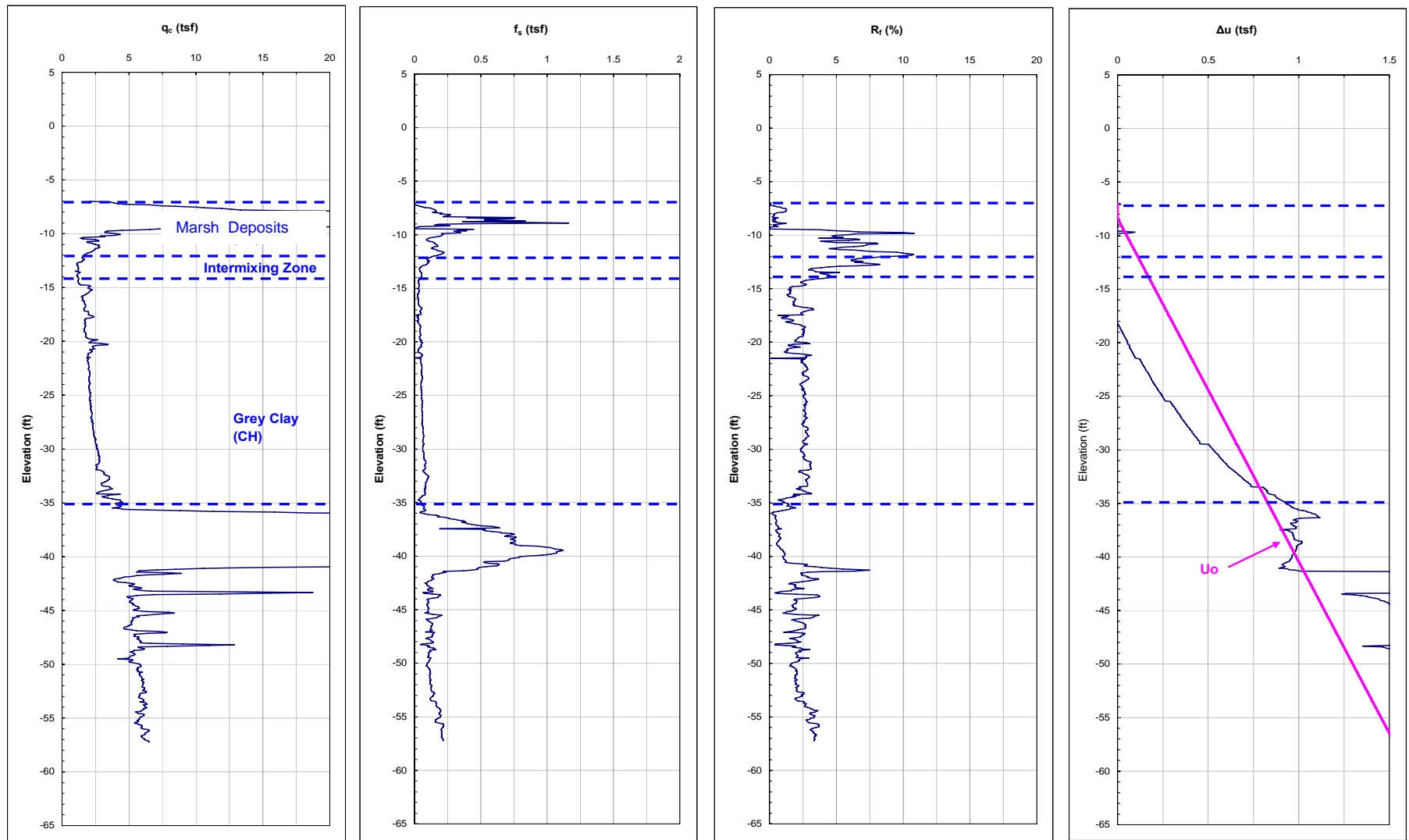


Figure 8.38: Example of CPT test data for locations inboard of the toe of the levee embankment at and near the 17th Street Canal breach section.

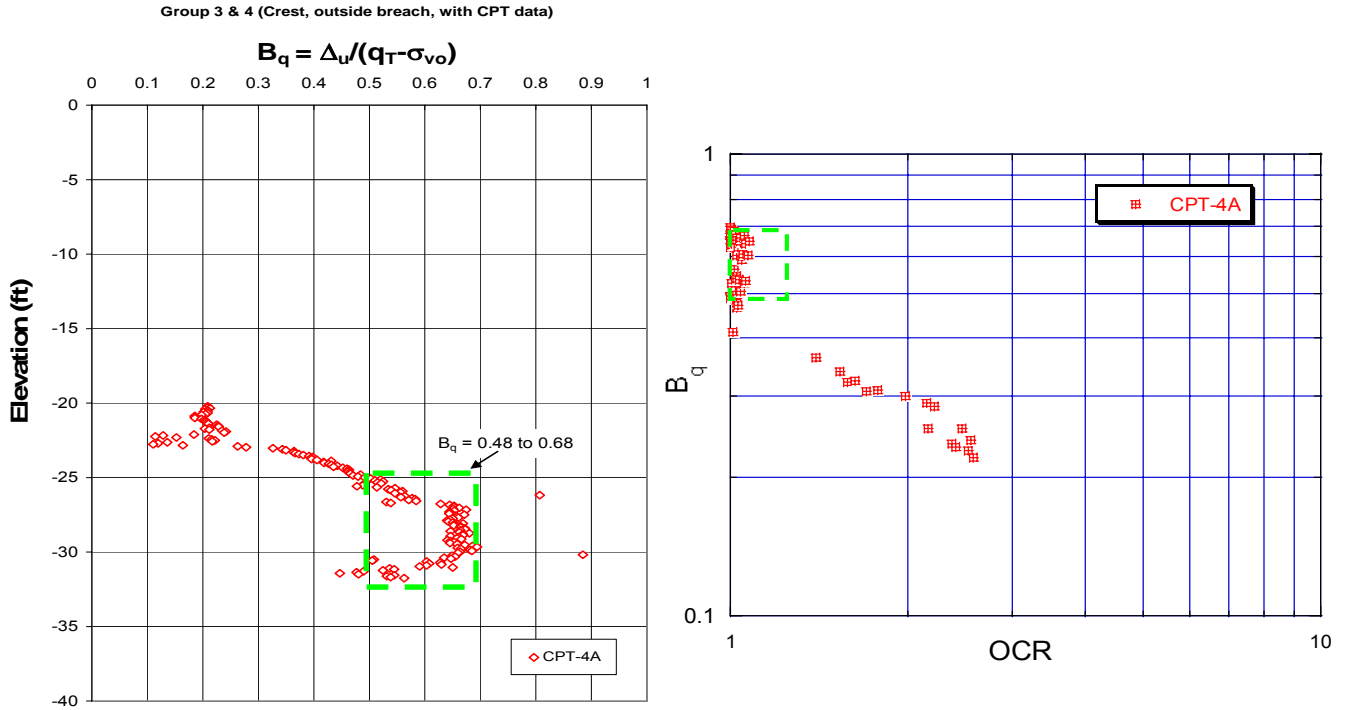


Figure 8.39: Pore Pressure parameter B_q vs. OCR and vs. depth within the soft gray clay (CH) foundation layer under full embankment overburden load.

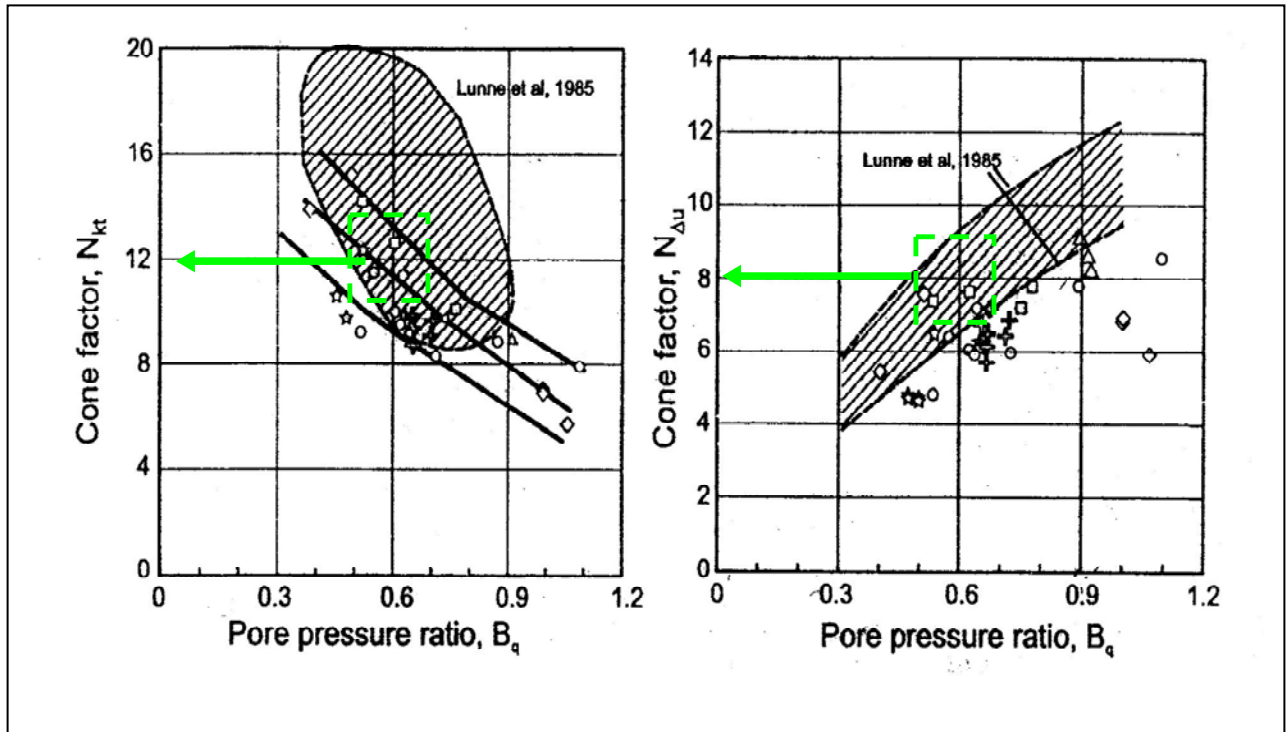


Figure 8.40: CPT cone factor N_{kt} based on B_q (after Lunne et al., 1985 and Karlsrud et al., 1996) for the soft gray clay (CH) under full embankment overburden load.

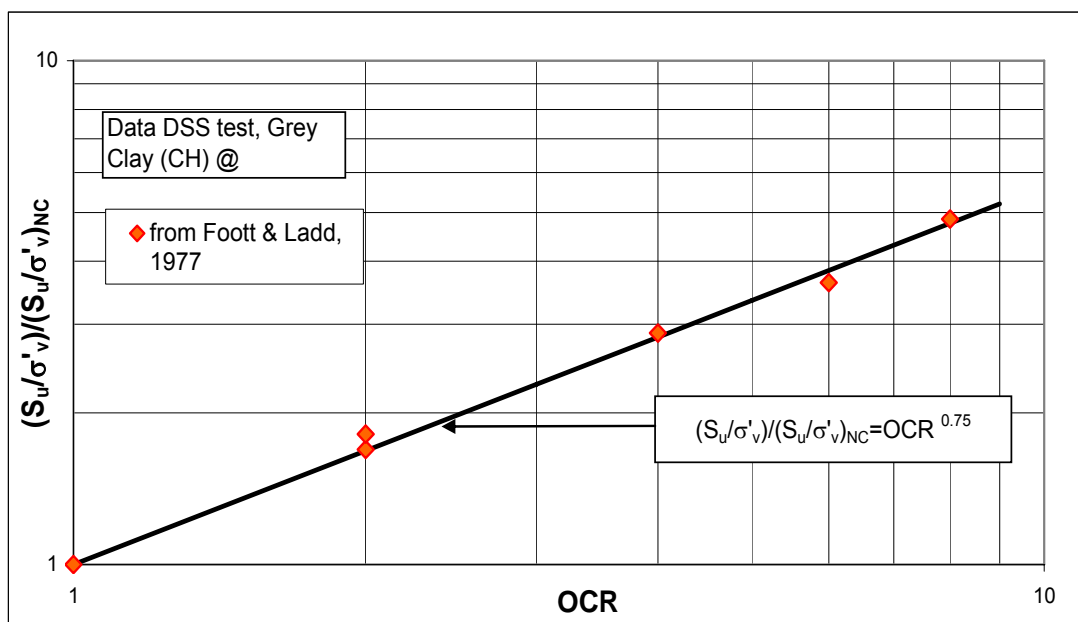


Figure 8.41: Relationship between S_u/P vs. OCR for mineralogically similar gray marsh clays (CH) at Atchafalua.

[Foott & Ladd, 1977]

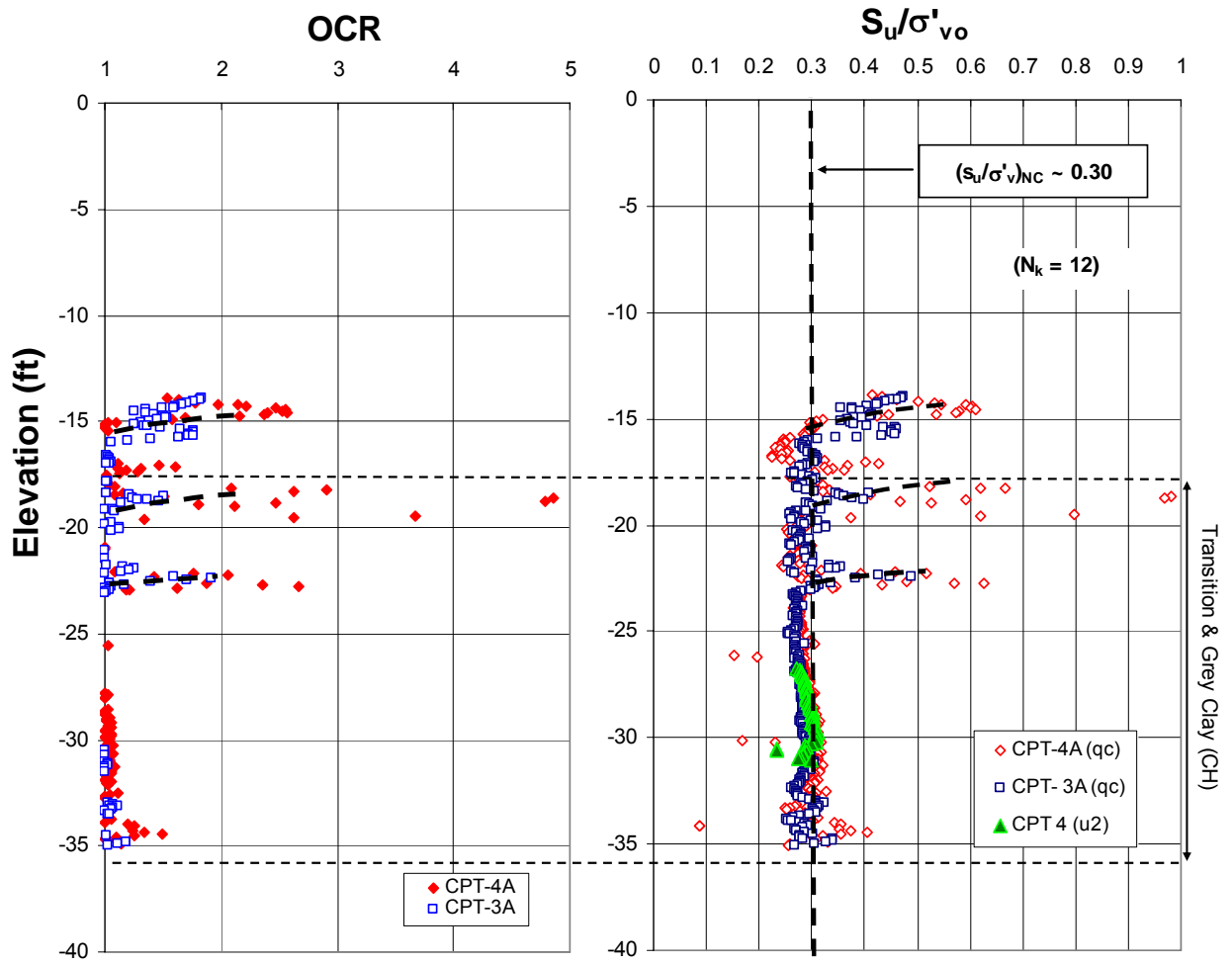


Figure 8.42: Plots of (a) OCR vs. Depth and (b) S_u vs. Depth for the soft gray marsh clay (CH) beneath the full embankment overburden pressure.

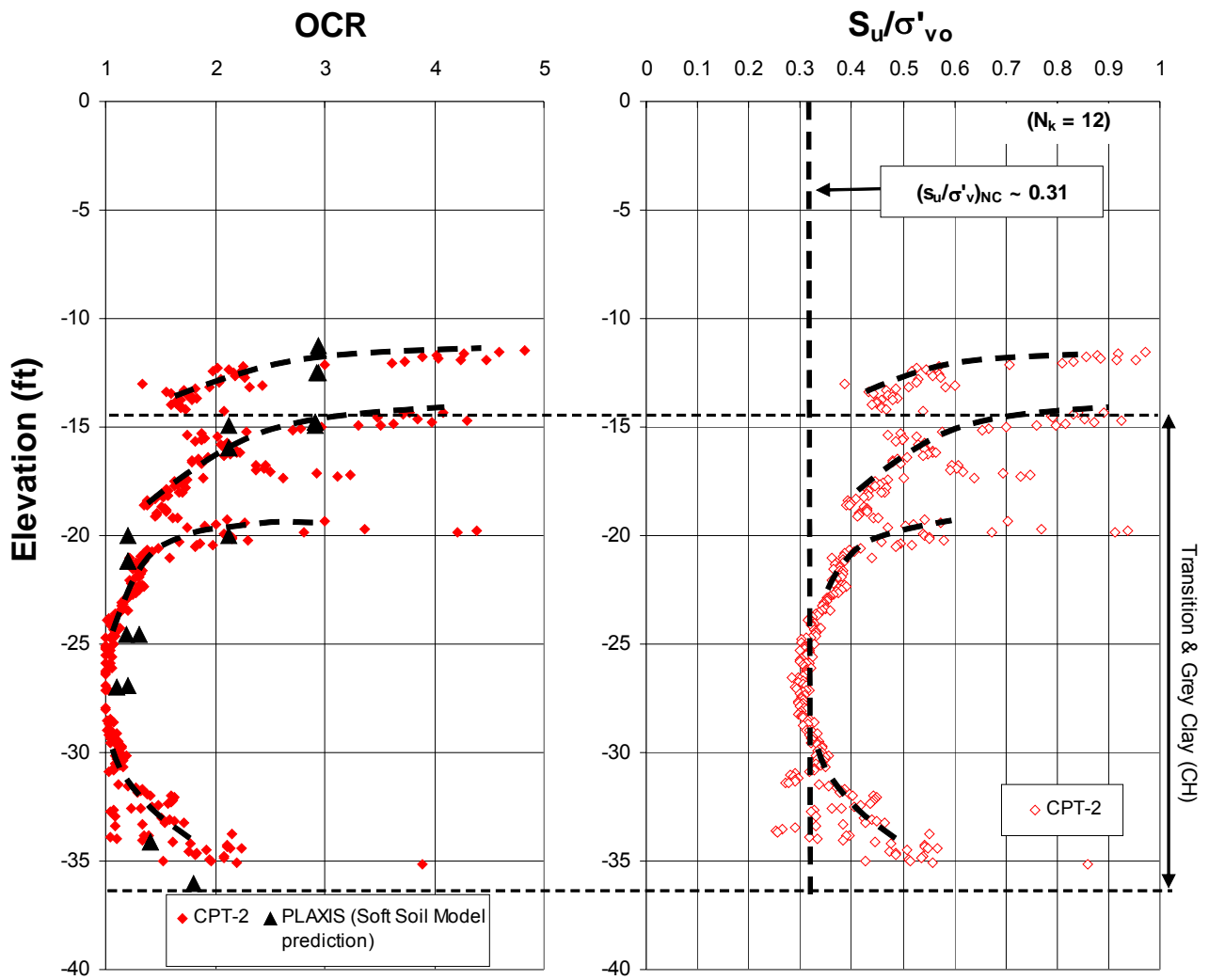


Figure 8.43: Plots of (a) OCR vs. Depth and (b) S_u vs. Depth for the soft gray marsh clay (CH) at the inboard toe and further to the landside (not under levee embankment overburden pressure) – 17th Street Canal breach site.

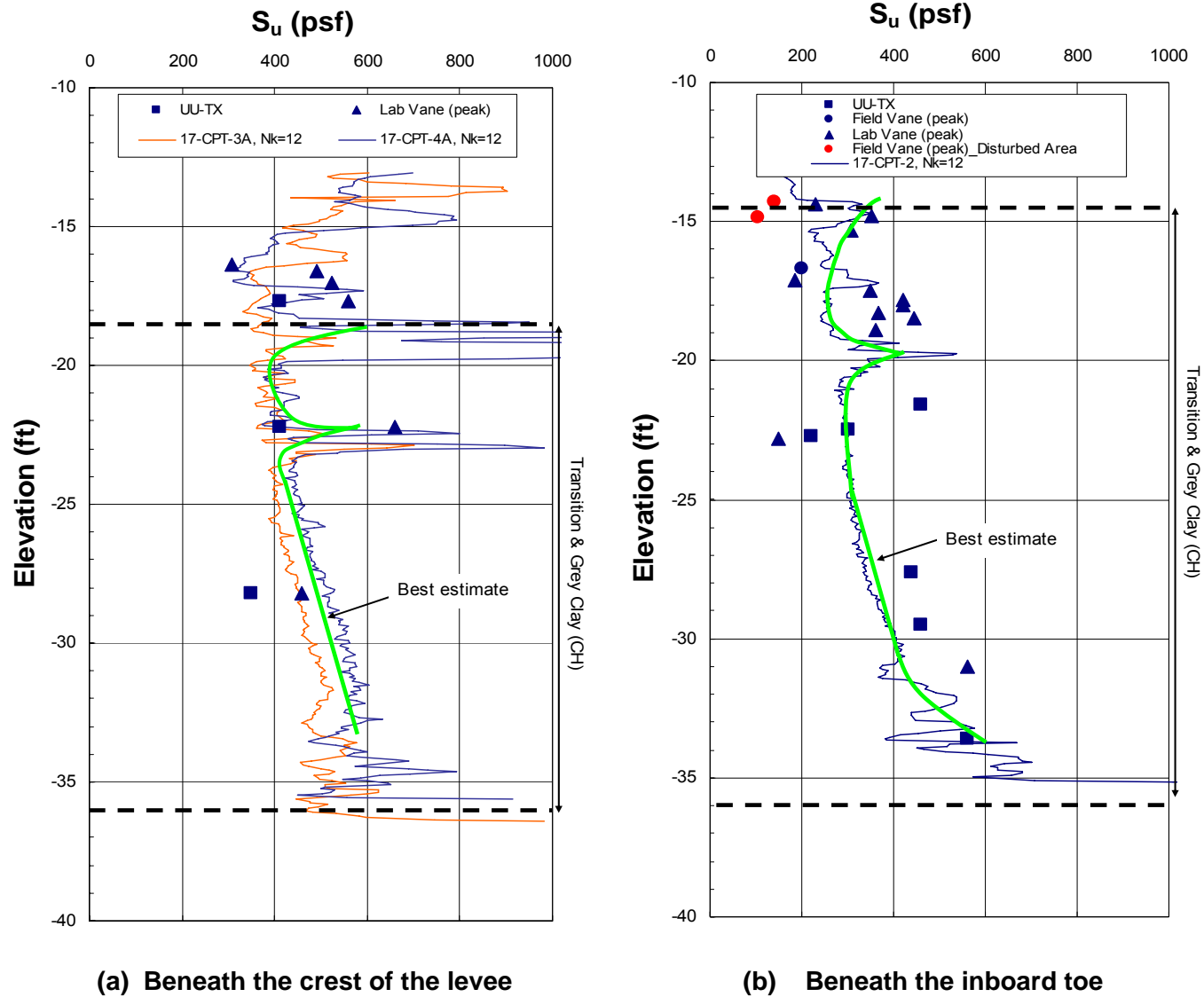


Figure 8.44: Profiles of shear strength vs. depth within the soft gray foundation clay at the 17th Street Canal breach site (a) beneath the crest of the levee, and (b) inboard of the toe of the levee.

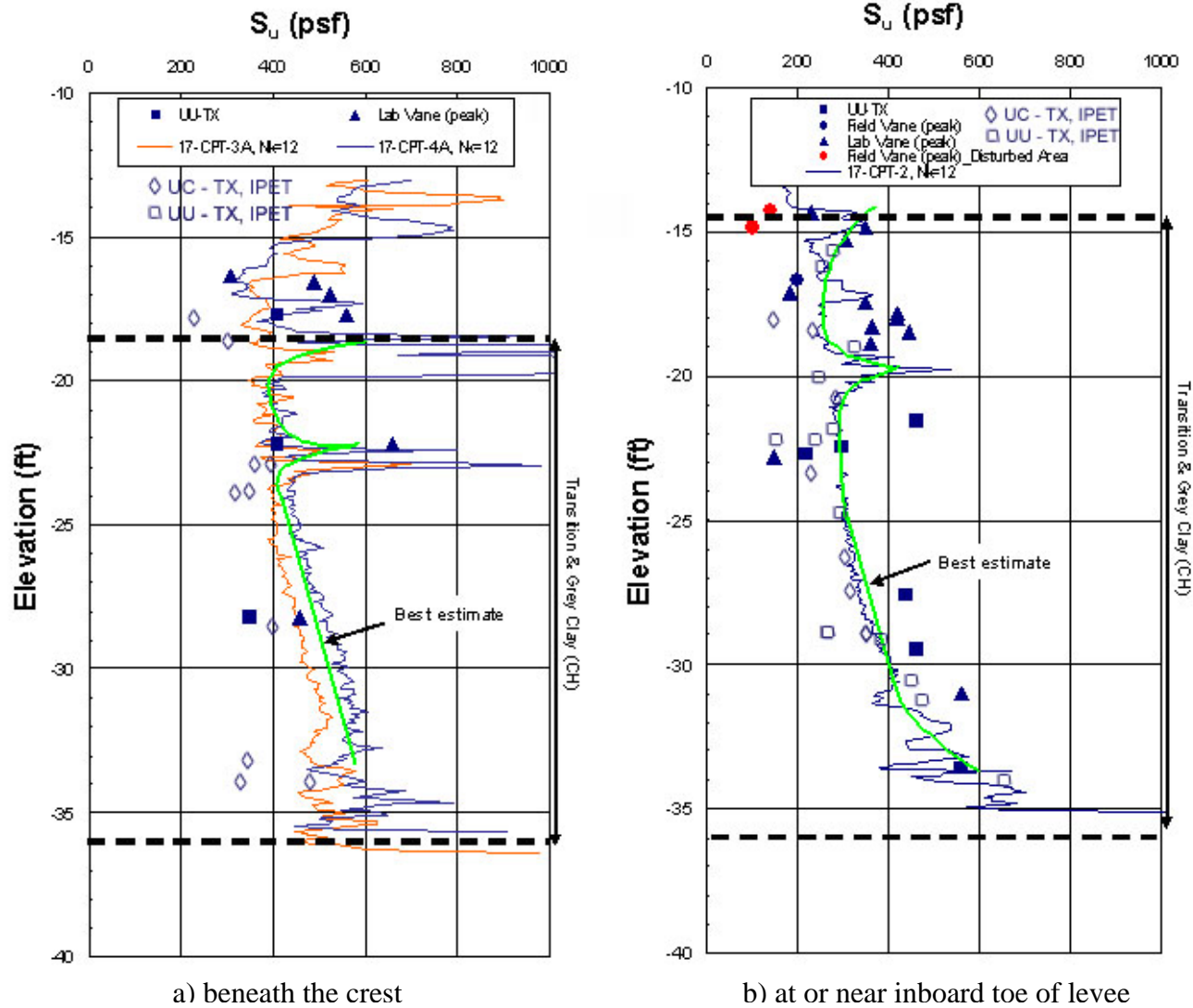


Figure 8.45: Profiles of shear strength vs. depth within the soft gray foundation clay at the 17th Street Canal breach site (a) beneath the crest of the levee, and (b) at and near the inboard toe of the levee, including the ILIT, IPET and pre-Katrina data.

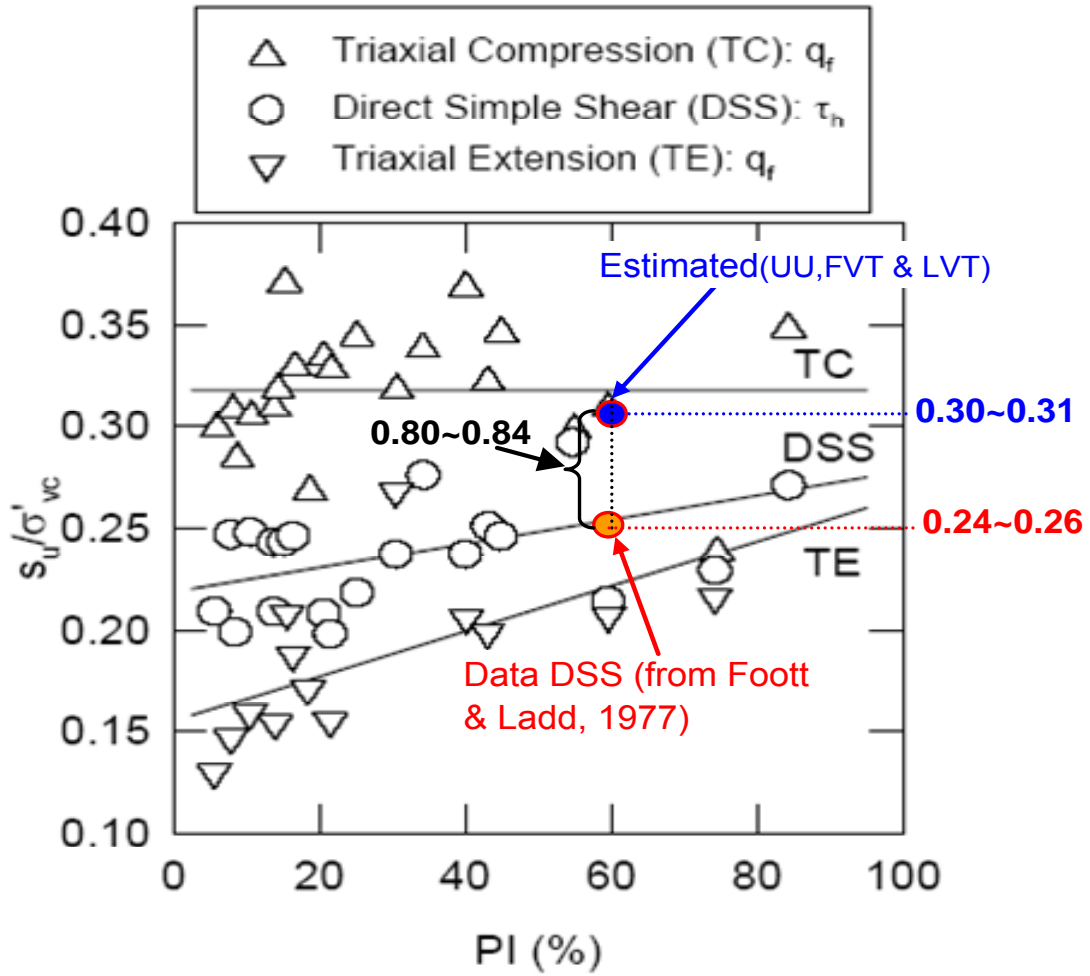


Figure 8.46: Undrained shear strength for UU-triaxial loading vs. undrained shear strength for DSS loading. [Base figure from Ladd, 2003]

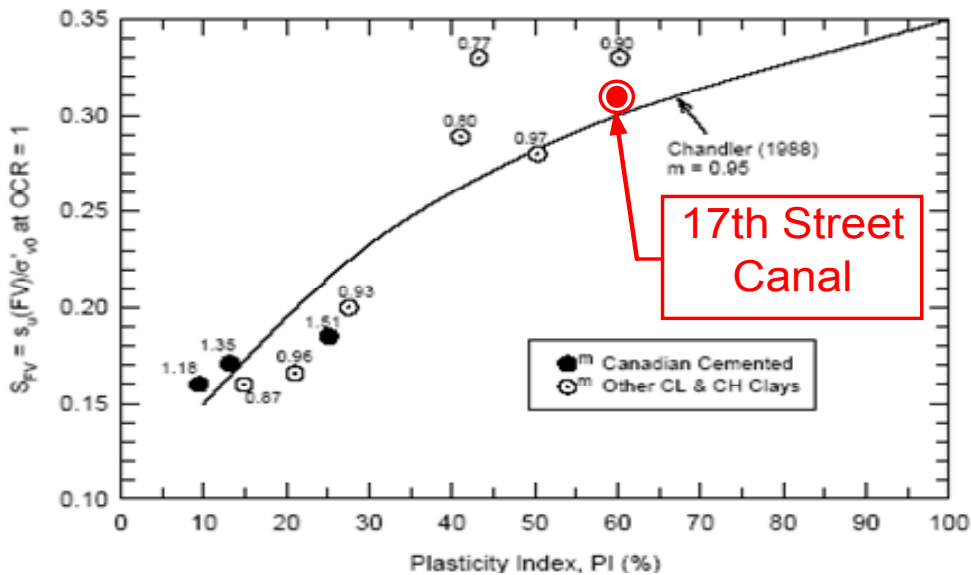


Figure 8.47: S_u/P for in situ field vane testing vs. Plasticity Index (PI) for normally consolidated clays (OCR = 1). [Base Figure from Ladd, 2003]

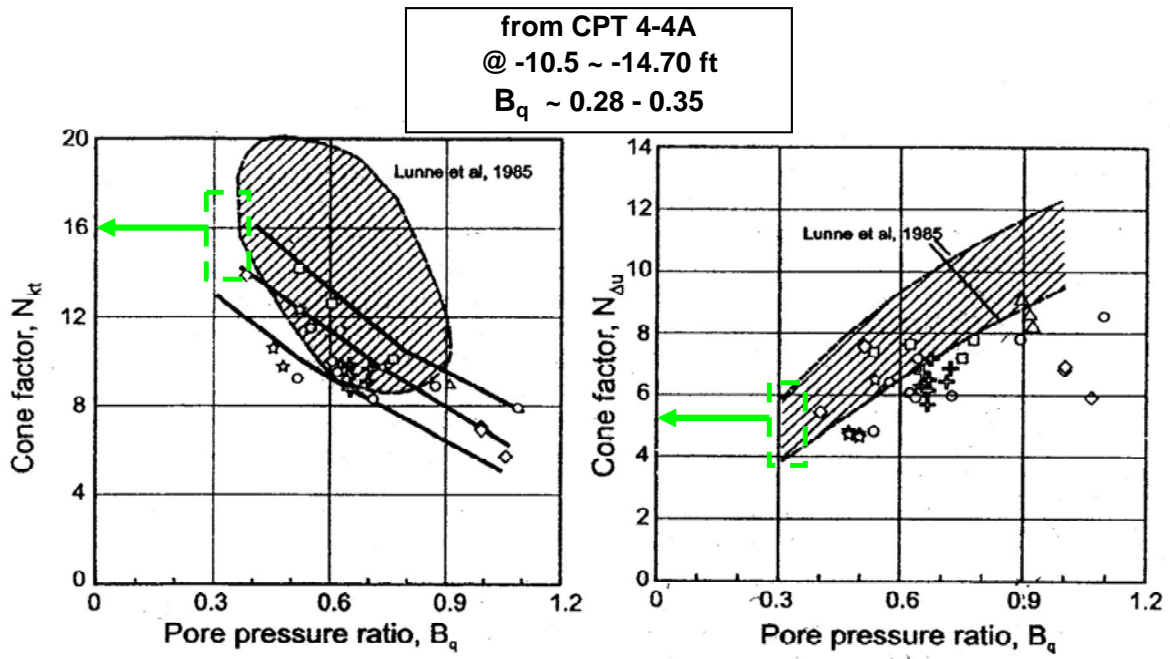


Figure 8.48: CPT cone factor N_{kt} based on B_q (after Lunne et al., 1985 and Karlsrud et al., 1996) for the marsh deposits under full embankment overburden load; 17th Street Canal breach site.

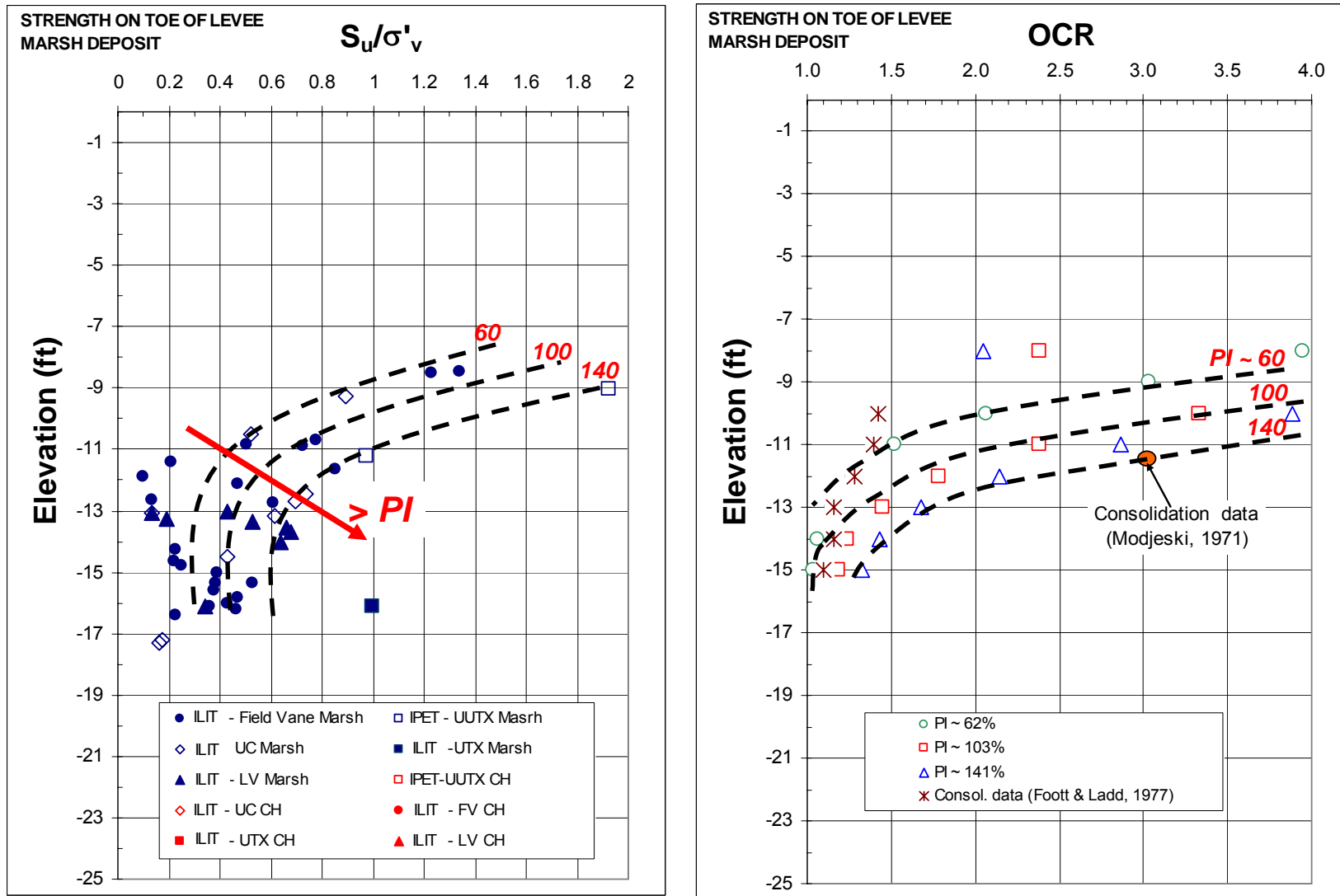


Figure 8.49: Undrained shear strength vs. depth, and OCR vs. depth, within the marsh deposits beneath the inboard toe based on Mayne and Mitchell (1988) – 17th Street Canal breach site.

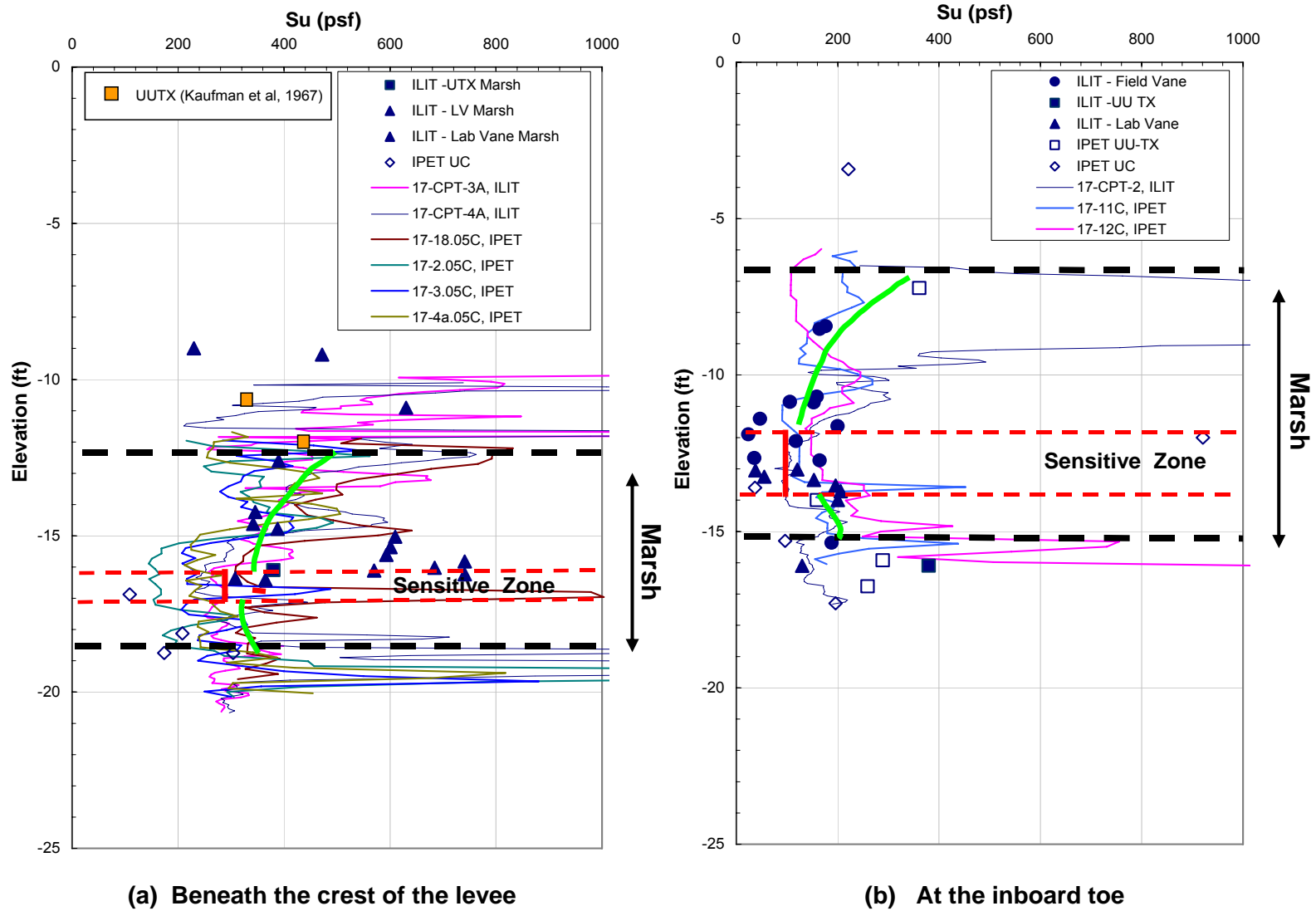


Figure 8.50: Shear strength vs. depth within the marsh deposits at the 17th Street Canal breach site (a) beneath the crest of the levee, and (b) at the inboard toe.



Figure 8.51: Shiny dark brown to black sensitive organic clay on auger stem and (inset) closeup view of leaves and twigs; 17th Street Canal breach site.



Figure 8.52: Shear zone within disturbed area, middle of 17th Street Canal breach, adjacent to displaced block at Elev. -9 feet (MSL).

17th Str. Canal, West Bank



Figure 8.54: Photo of an “undisturbed” sample of the sensitive organic silty clay.



Figure 8.55: Laboratory vane shear testing of the thin layer of sensitive organic silty clay.

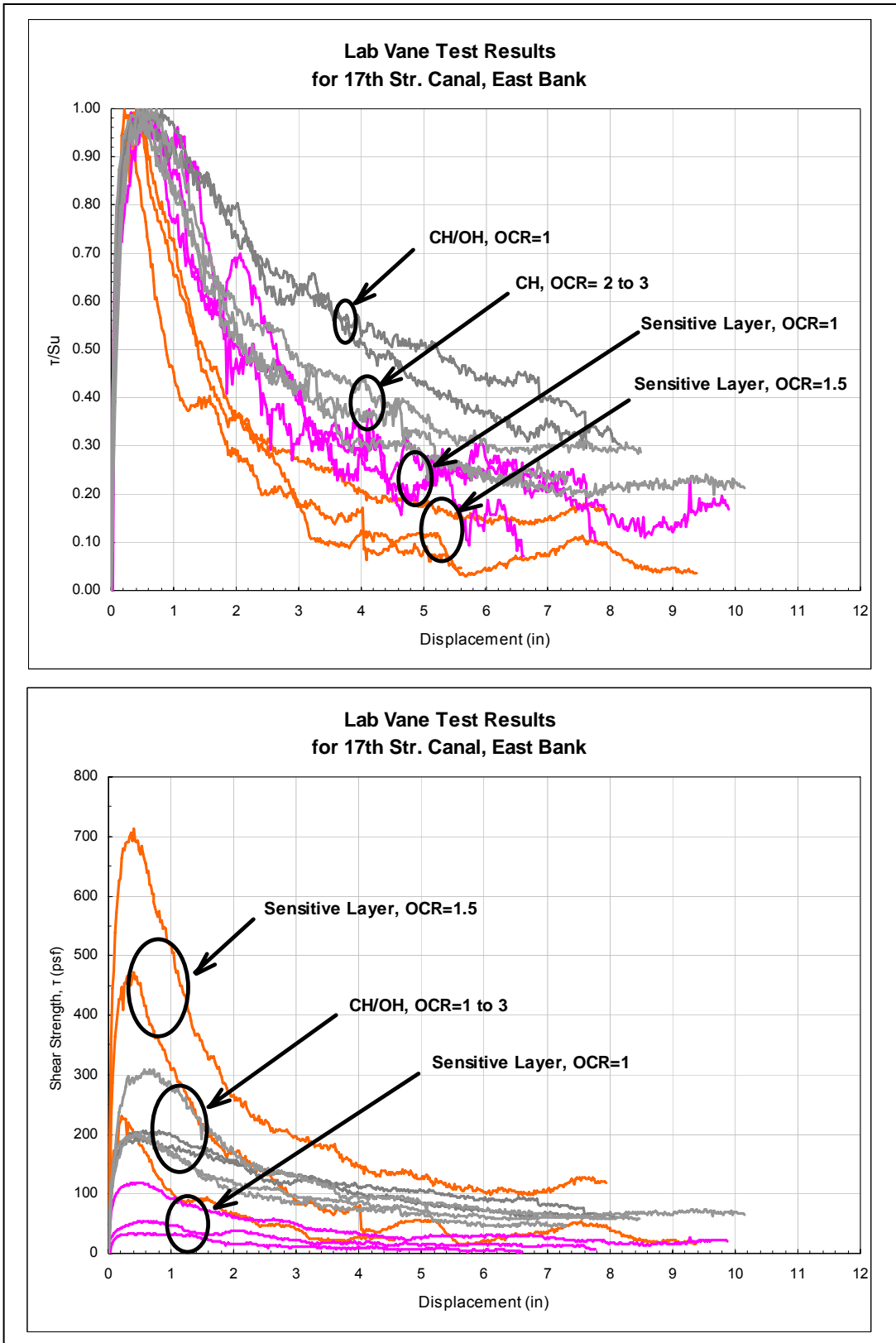


Figure 8.56: Stress-displacement behavior for soft gray clay (CH and CH/OH) and “sensitive” layer of organic clay within marsh deposit.

Geotechnical parameters for the Finite Element Analysis Model

ID	Soil Model	Name	Type	g_unsat [lb/ft^3]	g_sat [lb/ft^3]	k_x [ft/day]	k_y [ft/day]	nu [-]	E_ref [lb/ft^2]	c_ref [lb/ft^2]	phi [°]
CF Upper CH SC	Mohr Coulomb	ML-silt (Compacted Fill)	Undrained	105	115	0.0028	0.00028	0.35	234000	900	0.001
		CH-Upper Fat Clay	Undrained	90	95	0.00028	0.000028	0.35	180000	600	0.001
		SC (Sand)	Drained	110	110	0.28	0.28	0.30	1000000	0.01	38

ID	Soil Model	Name	Type	g_unsat [lb/ft^3]	g_sat [lb/ft^3]	k_x [ft/day]	k_y [ft/day]	lambda* [-]	kappa* [-]	n_ur [-]	K0nc [-]	M [-]	c_ref [lb/ft^2]	phi @ pref [°]	OCR
M2	Soft Soil	Marsh 2	Undrained	80	80	28.3	2.8	0.21	0.033	0.15	0.60	1.90	0	36	2.25
M1		Marsh 1	Undrained	80	80	28.3	2.8	0.21	0.033	0.15	0.60	1.90	0	36	1.1
IZ		Intermixing zone	Undrained	85	85	28.32	2.8	0.10	0.02	0.15	0.61	1.27	0	23	3
CH1		Grey Clay	Undrained	90	95	0.00028	0.000028	0.17	0.03	0.15	0.63	1.24	0	22	2.2
CH2-a		Grey Clay	Undrained	90	95	0.00028	0.000028	0.17	0.03	0.15	0.63	1.24	0	22	1.25
CH2-b		Grey Clay	Undrained	90	95	0.00028	0.000028	0.17	0.03	0.15	0.63	1.24	0	22	1.5

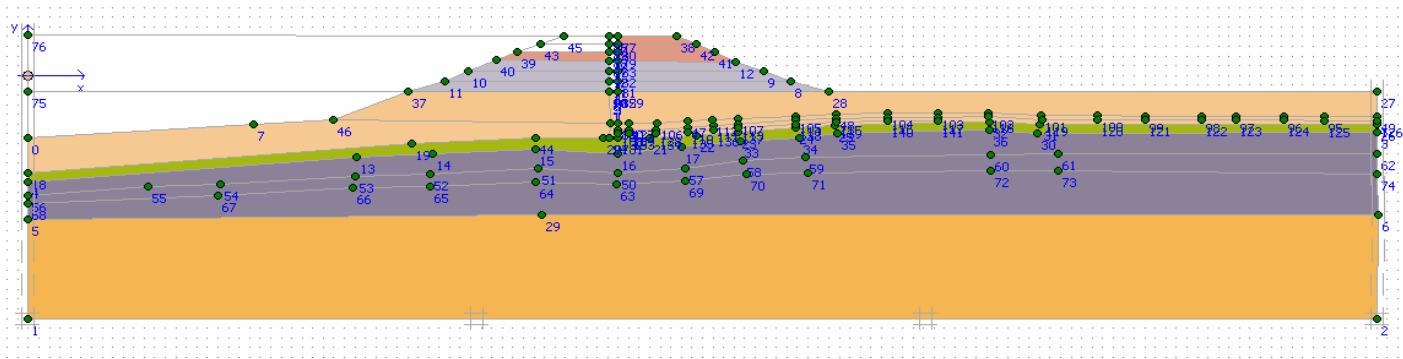


Figure 8.57: Parameters (and model) used in PLAXIS model for the 17th Street Canal breach site.

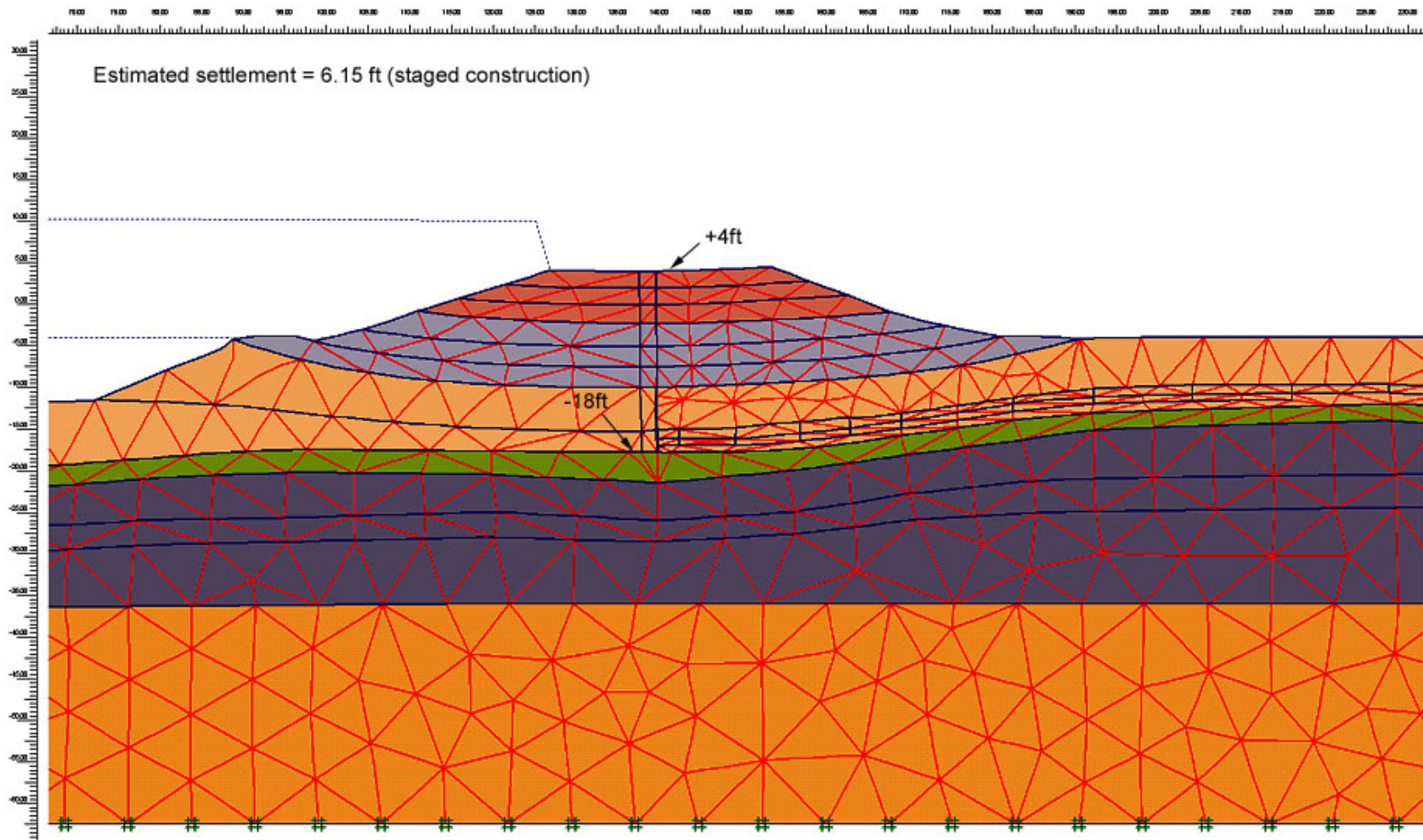


Figure 8.58: Deformed mesh at the end of initial construction of embankment and consolidation; 17th Street Canal breach section.

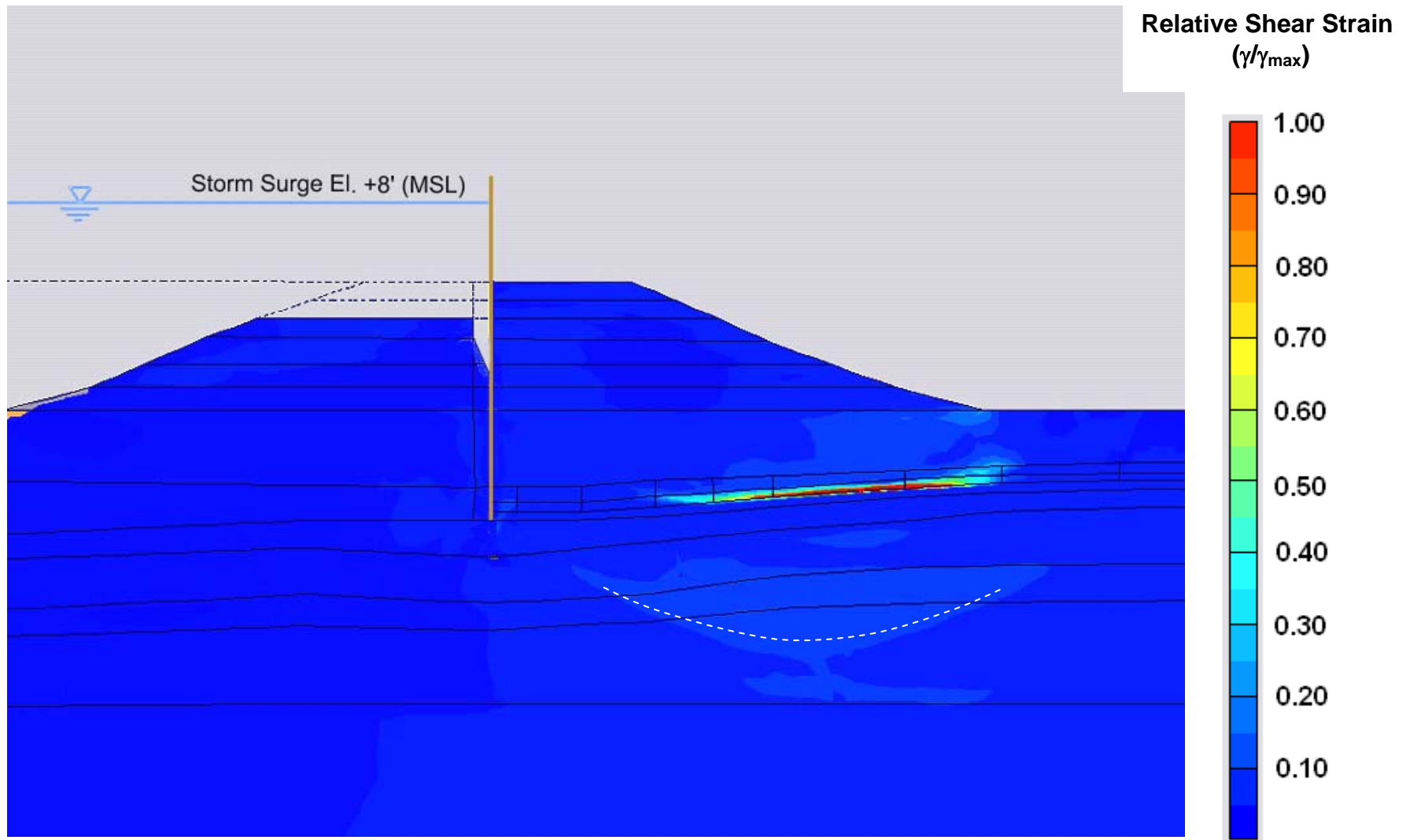


Figure 8.59: Normalized shear strain contours (shear strain divided by strain to failure) for a storm surge at Elev. + 8 feet (MSL) At the 17th Street Canal breach site; initiation of gapping at outboard toe of floodwall.

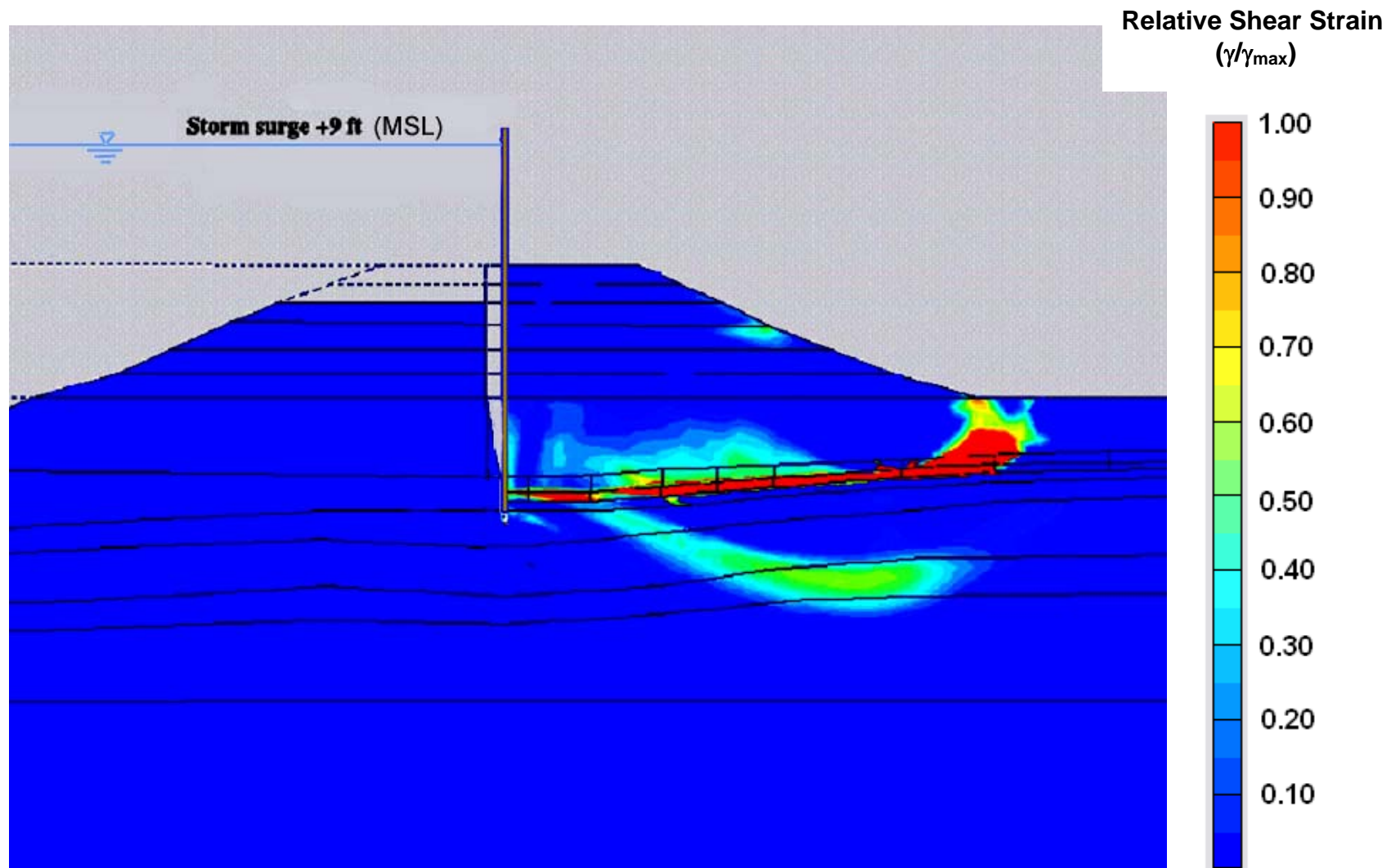


Figure 8.60: Normalized shear strain contours (shear strain divided by strain to failure) for a storm surge at Elev. + 8 feet (MSL) at the 17th Street Canal breach site; gapping at outboard toe of floodwall is now developed to full depth.

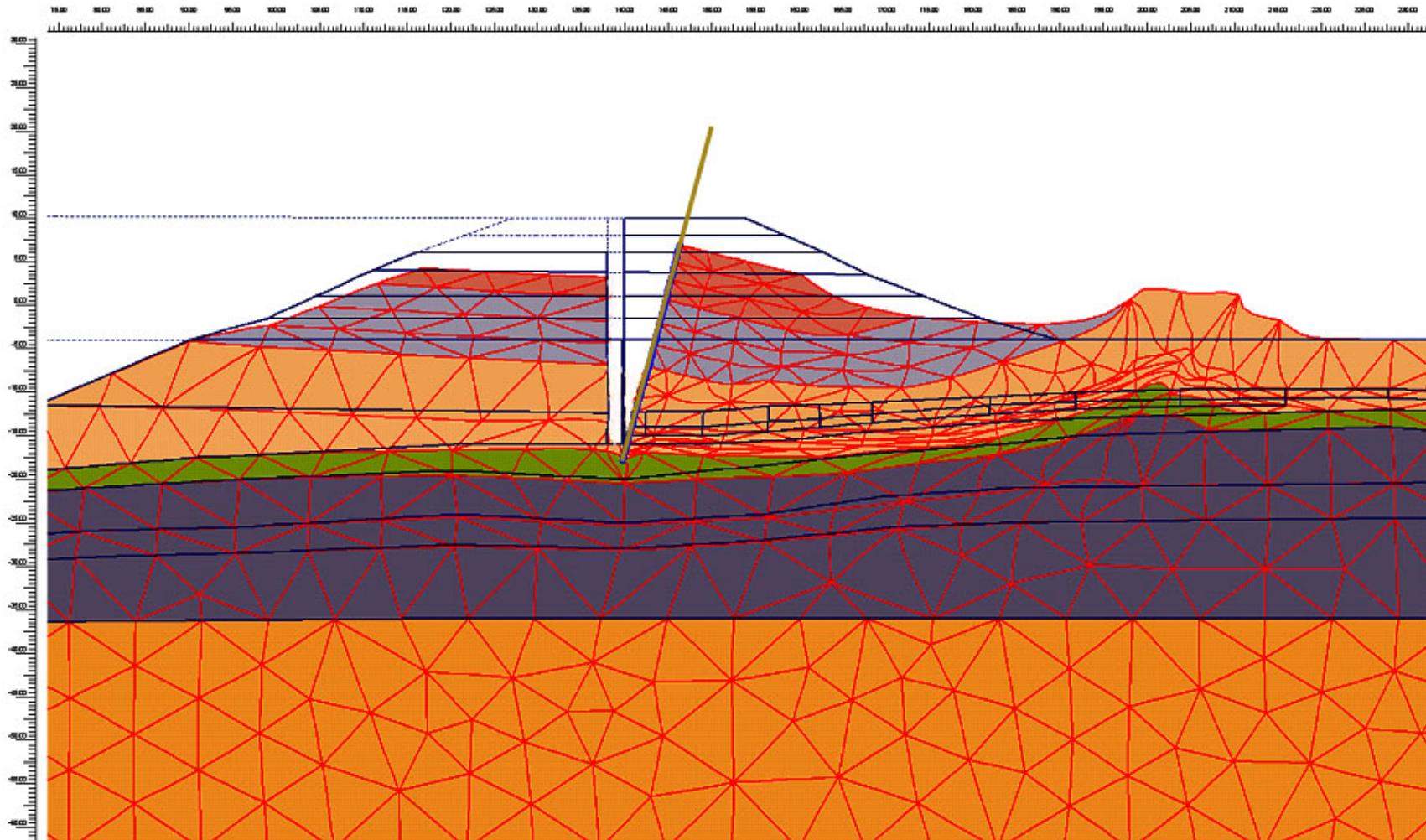


Figure 8.61: Displaced mesh for storm surge height at Elev. + 8.5 feet (MSL) at the 17th Street Canal breach site; displacements are increased by a factor of 3 in this figure.

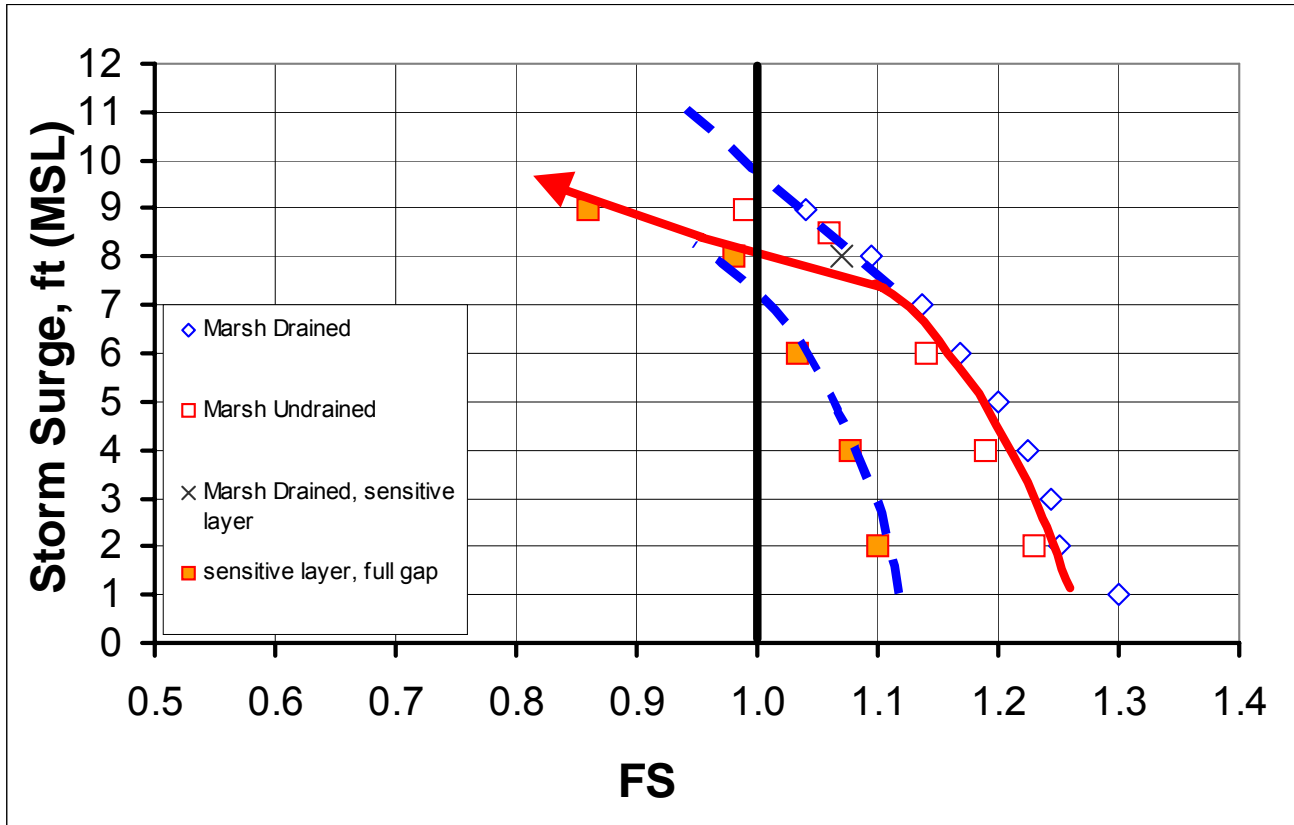


Figure 8.62: Calculated Factors of Safety for three modes based on PLAXIS analyses of the 17th Street Canal breach section for various canal water elevations; showing the best-estimated path to failure.

ID	Soil Model	Type	γ	c	ϕ	Su/p'
			[lb/ft ³]	[lb/ft ²]	[°]	
Upper fill	Mohr-Coulomb	Undrained	110	800	0	
Lower fill	Mohr-Coulomb	Undrained	85	550	0	
Marsh, beneath crest	Mohr-Coulomb	Undrained	80	375	0	
Marsh, free field	Mohr-Coulomb	Undrained	80	200	0	
Sensitive layer, beneath crest	Mohr-Coulomb	Undrained	80	240	0	
Sensitive layer, beneath toe	Mohr-Coulomb	Undrained	80	180	0	
Sensitive layer, free field	Mohr-Coulomb	Undrained	80	70	0	
Overconsolidated Grey CH	Mohr-Coulomb	Undrained	90	400	0	
Normally consolidated Grey CH	SHANSEP	Undrained	90			0.26
Sand	Mohr-Coulomb	Drained	110	0	33	

Geotechnical Parameters for the Limit Equilibrium Analyses for 17th Street Canal levee, East Bank.

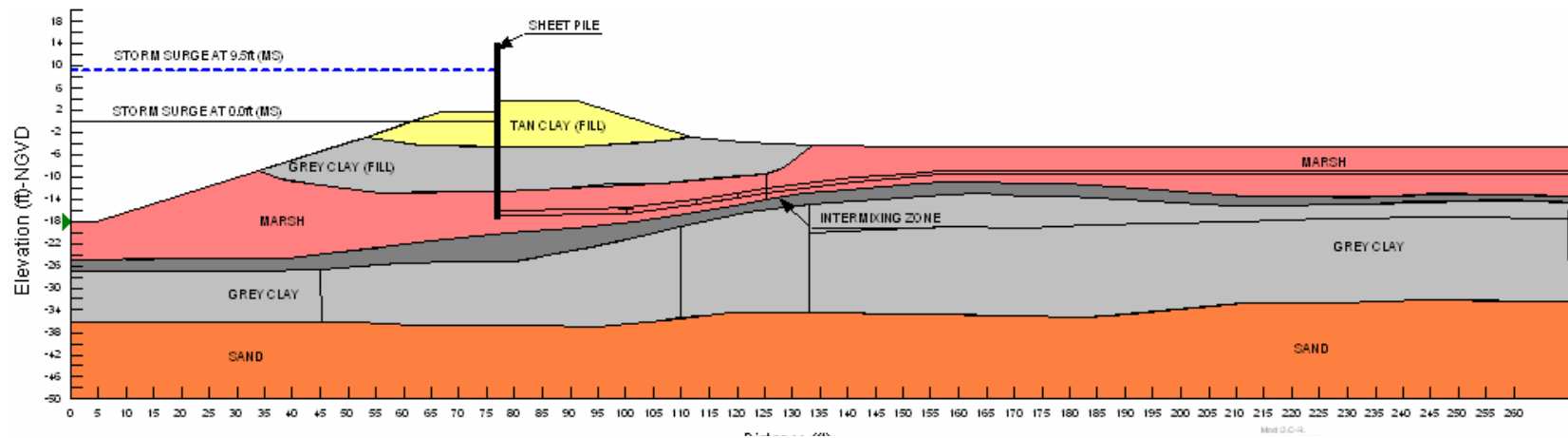


Figure 8.63: Cross-section and parameters used for conventional stability analyses of the breach section on the east side of the 17th Street Canal.

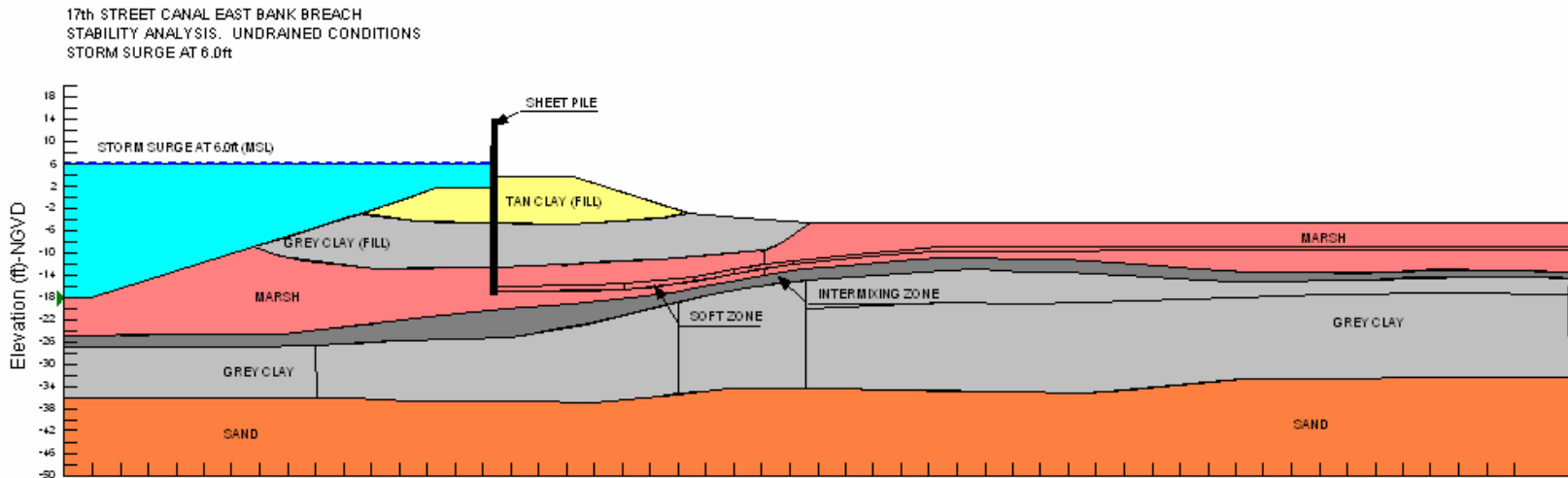


Figure 8.64: Cross-section at 17th Street Canal breach site for static slope stability analyses.

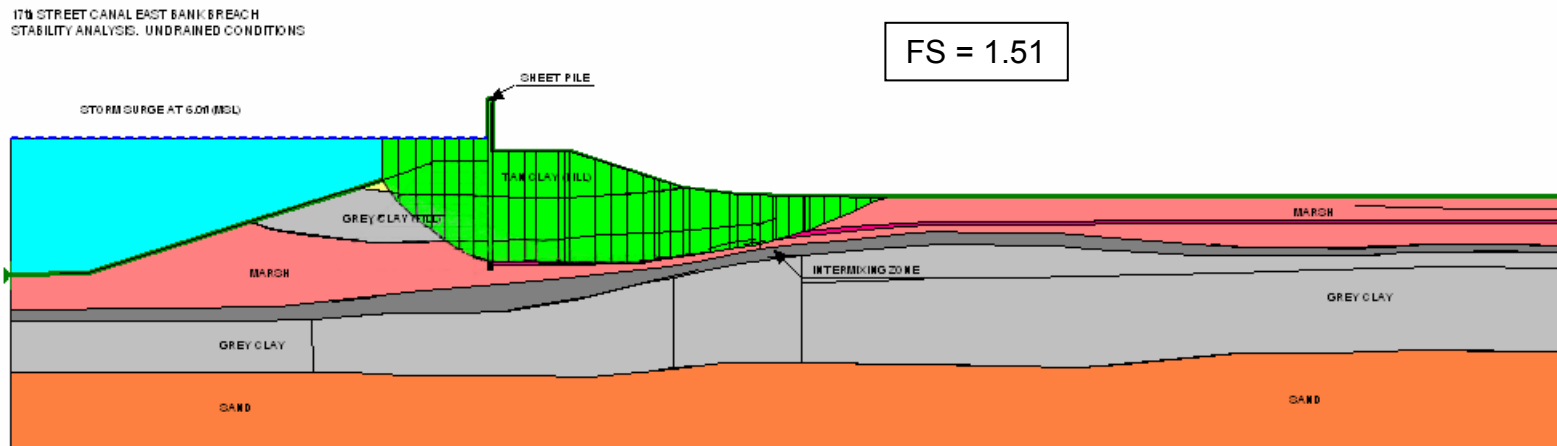


Figure 8.65: Stability analysis (worst case) for storm surge to Elev. + 6 feet (MSL) at the 17th Street Canal breach section.

17th STREET CANAL EAST BANK BREACH
STABILITY ANALYSIS. UNDRAINED CONDITIONS

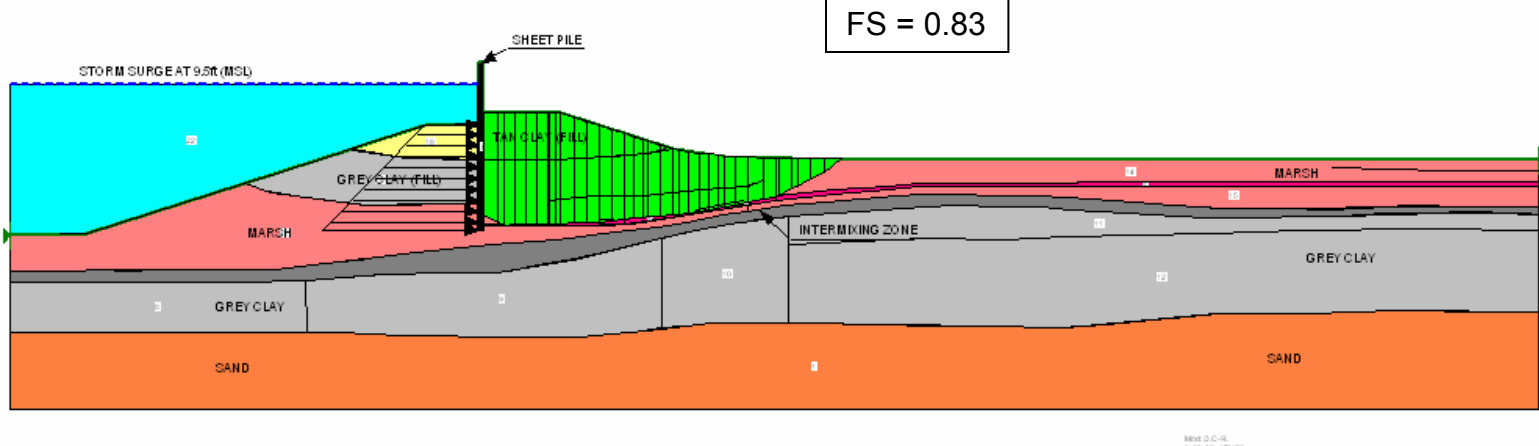


Figure 8.66: Stability analysis for actual observed failure mechanism at the 17th Street Canal breach section, with storm surge at Elev. + 9.5 feet (MSL) and with fully developed crack at the outboard side of the sheetpile/floodwall.

17th STREET CANAL EAST BANK BREACH
STABILITY ANALYSIS. UNDRAINED CONDITIONS

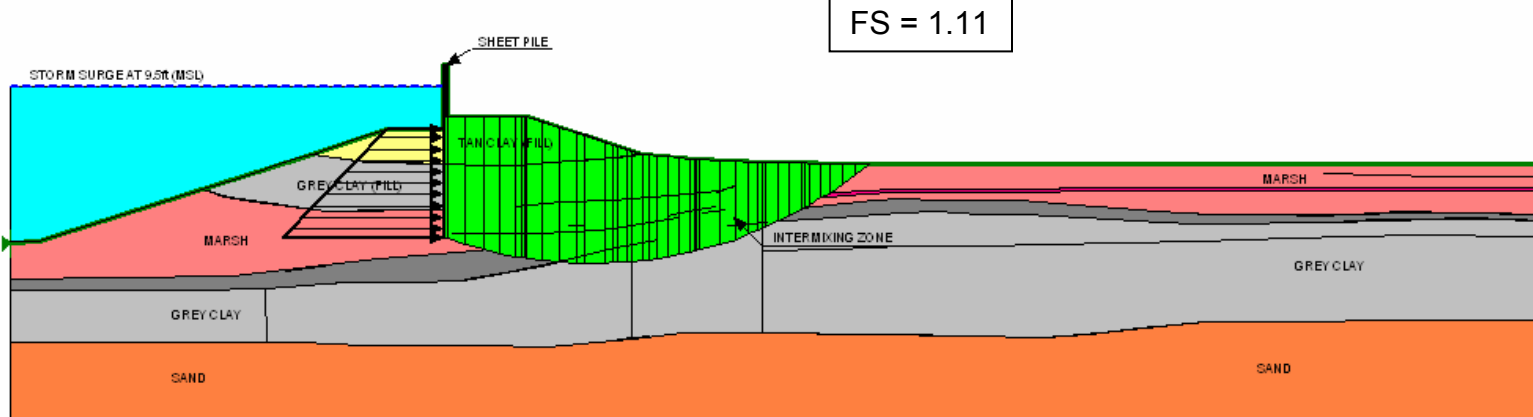


Figure 8.67: Stability analysis for shear failure through the deeper soft gray clays (CH) at the 17th Street Canal breach section, with storm surge at Elev. + 9.5 feet (MSL) and with fully developed crack at the outboard side of the sheetpile/floodwall.

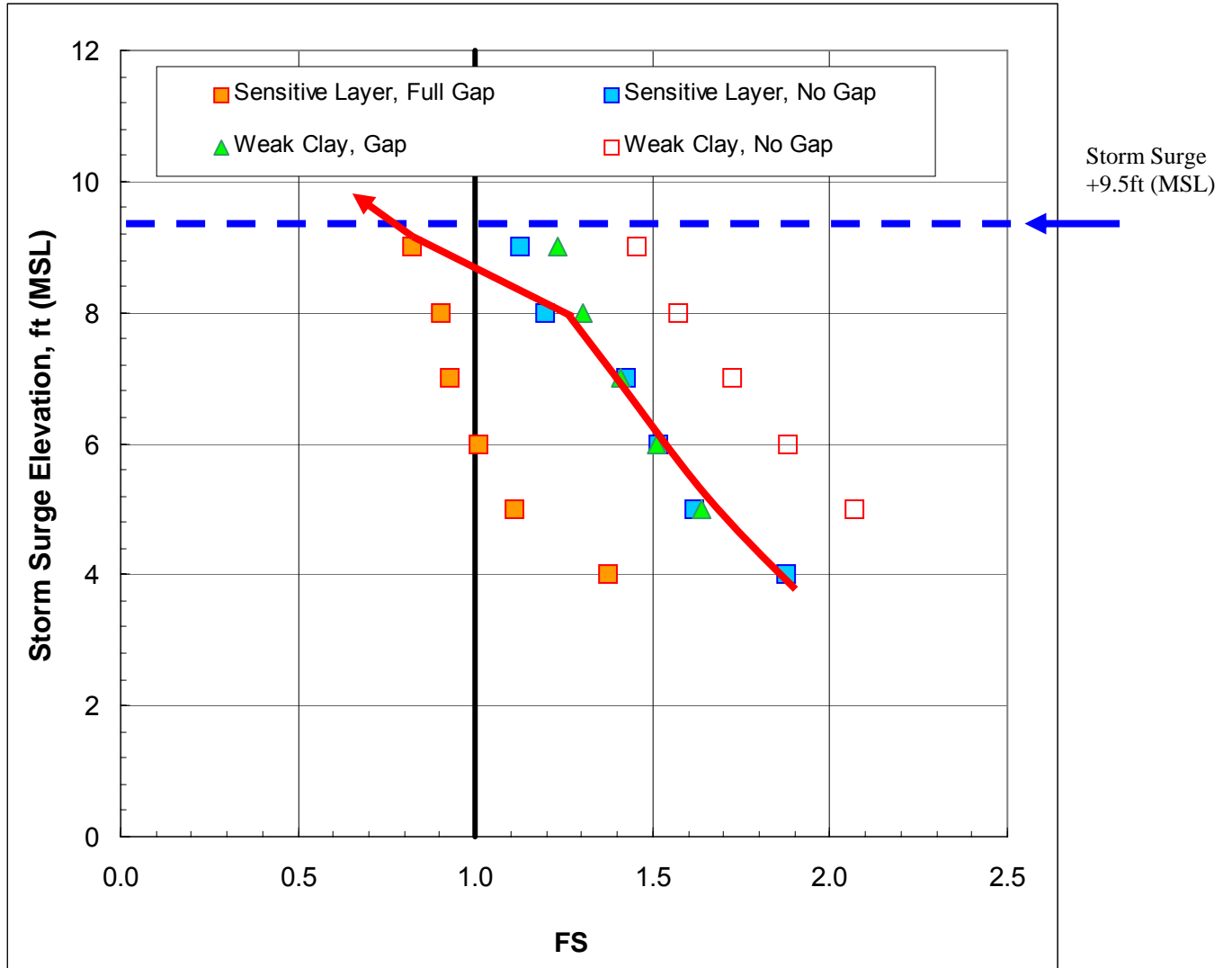


Figure 8.68: Factor of safety for four modes of failure at the 17th Street Canal breach site as a function of canal water elevation based on static Limit Equilibrium slope stability analyses: again showing the best-estimated path to failure.

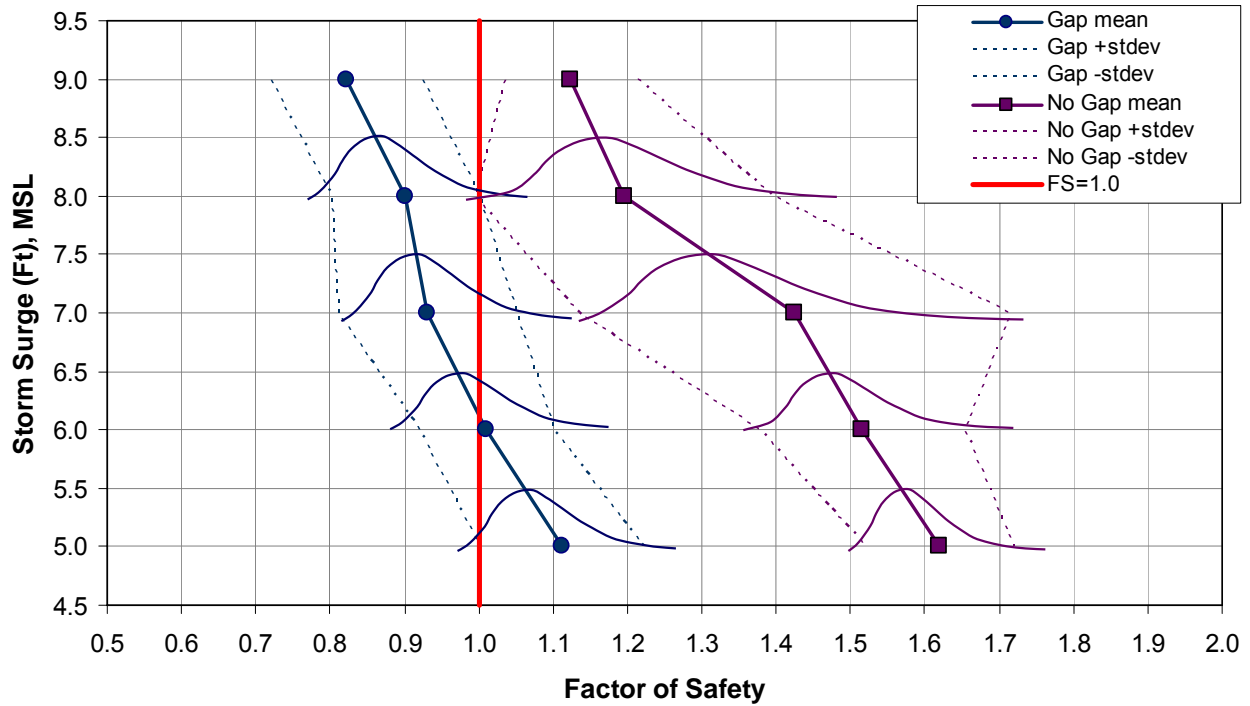


Figure 8.68(a): Distributions of Factor of Safety for the Ungapped and Water-Filled Gap Cases as a function of increasing canal water level; 17th Street Drainage Canal, east bank breach section.

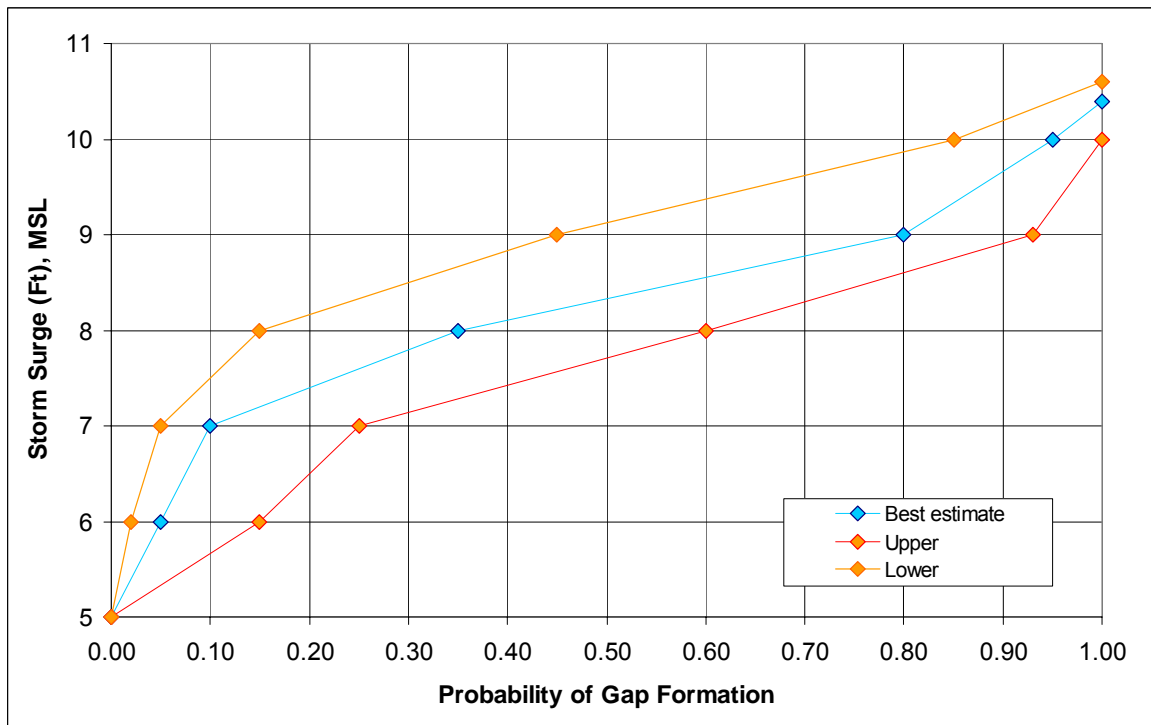


Figure 8.68(b): Estimated probabilities of formation of a significant water-filled gap as a function of increasing canal water level; 17th Street Drainage Canal, east bank breach section.

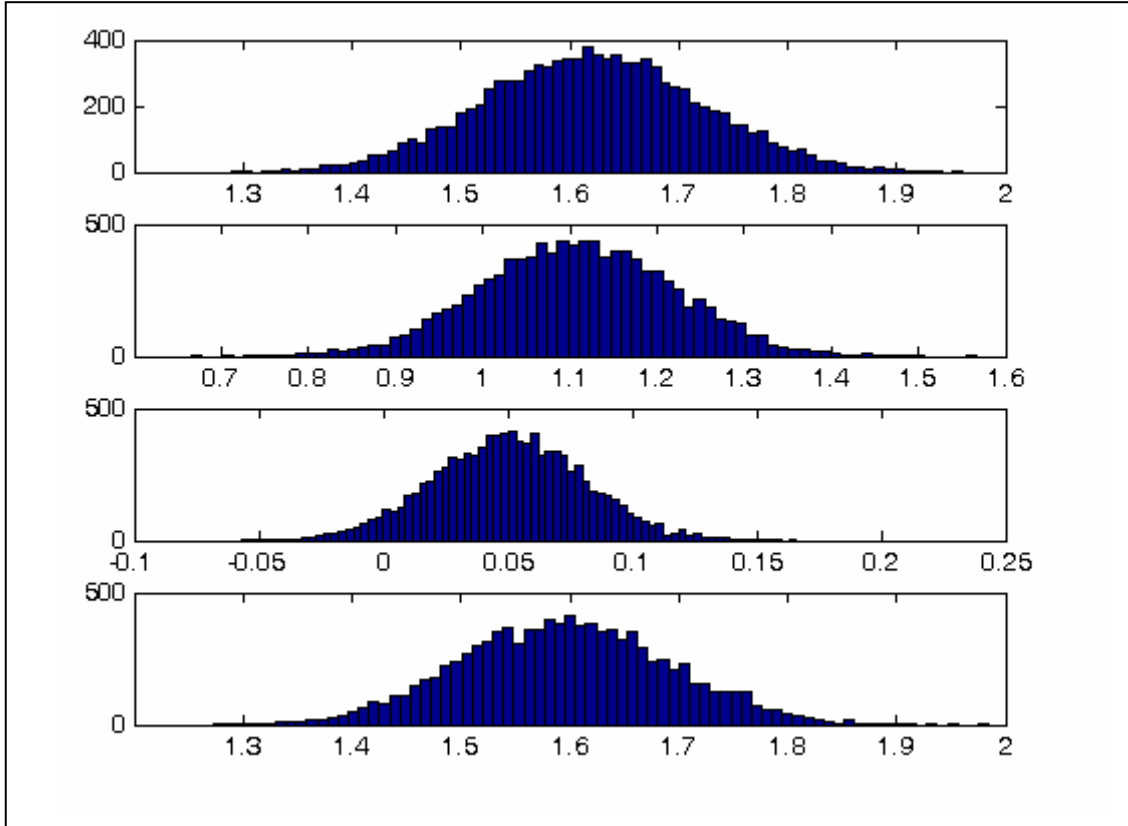


Figure 8.68(c): Example calculation (Monte Carlo simulation) for a canal water elevation of +5 feet (MSL).

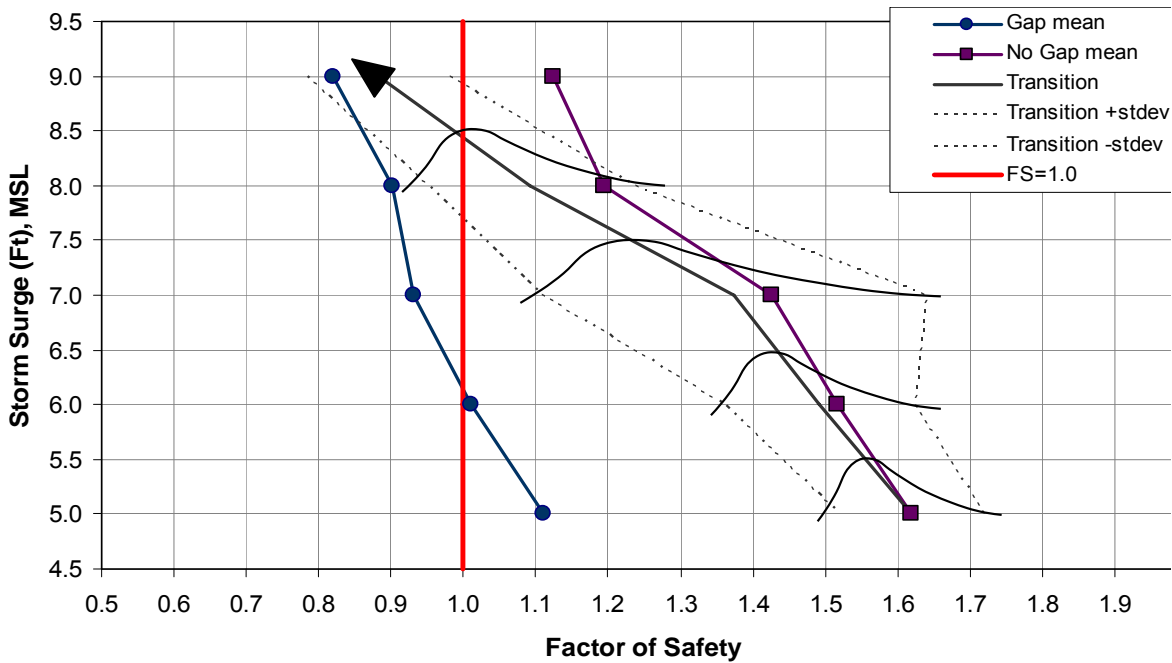


Figure 8.68(d): Distribution of Factor of Safety vs. canal water level with progressive transition from ungapped to water-filled gap conditions; 17th Street Canal, east bank breach section.

Storm Surge Elevation (ft), MSL	Probability of Failure
9	88.1%
8	25.6%
7	7.9%
6	0.01%
5	0.00%

Table 8.1: Probability of failure for 17th Street Canal, East Bank

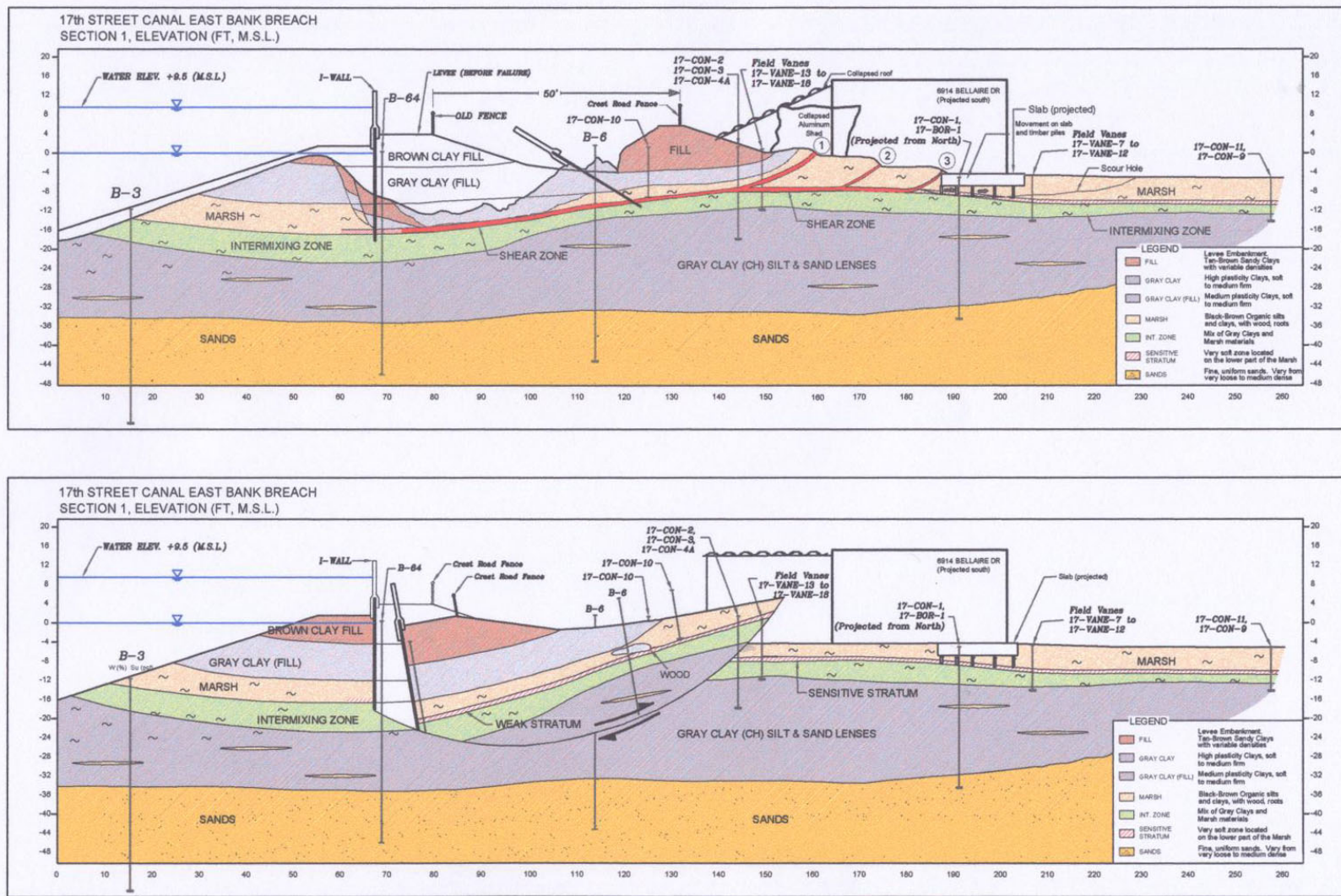


Figure 8.69: Comparison between deep rotational failure through the soft gray clay (CH) and translational failure along the sensitive clay layer within the marsh deposits as actually observed.

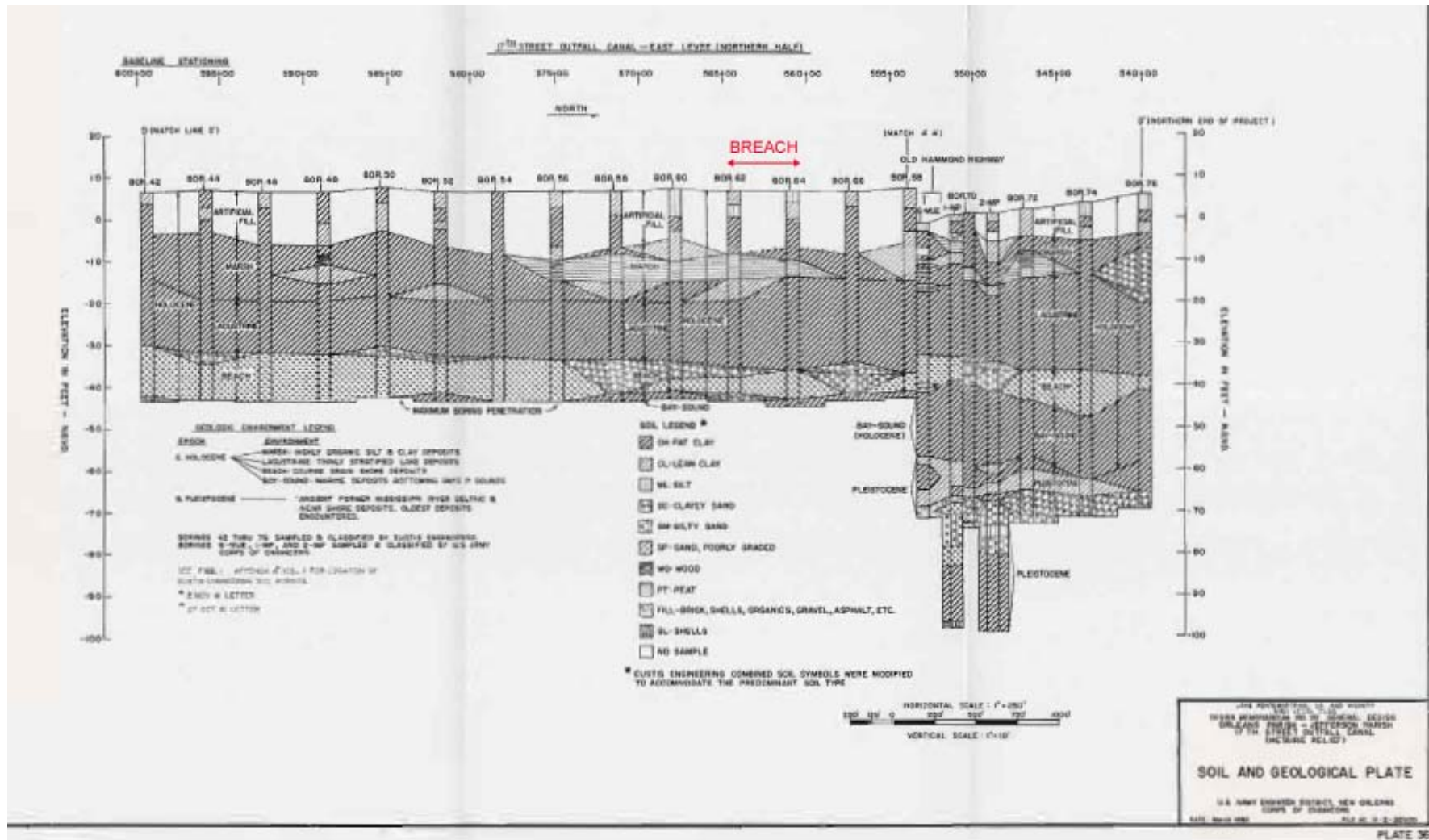


Figure 8.70: Initial longitudinal subsurface profile used for initial design at the 17th Street Canal breach site. [USACE, DM-20, Vol. 1, 1990]

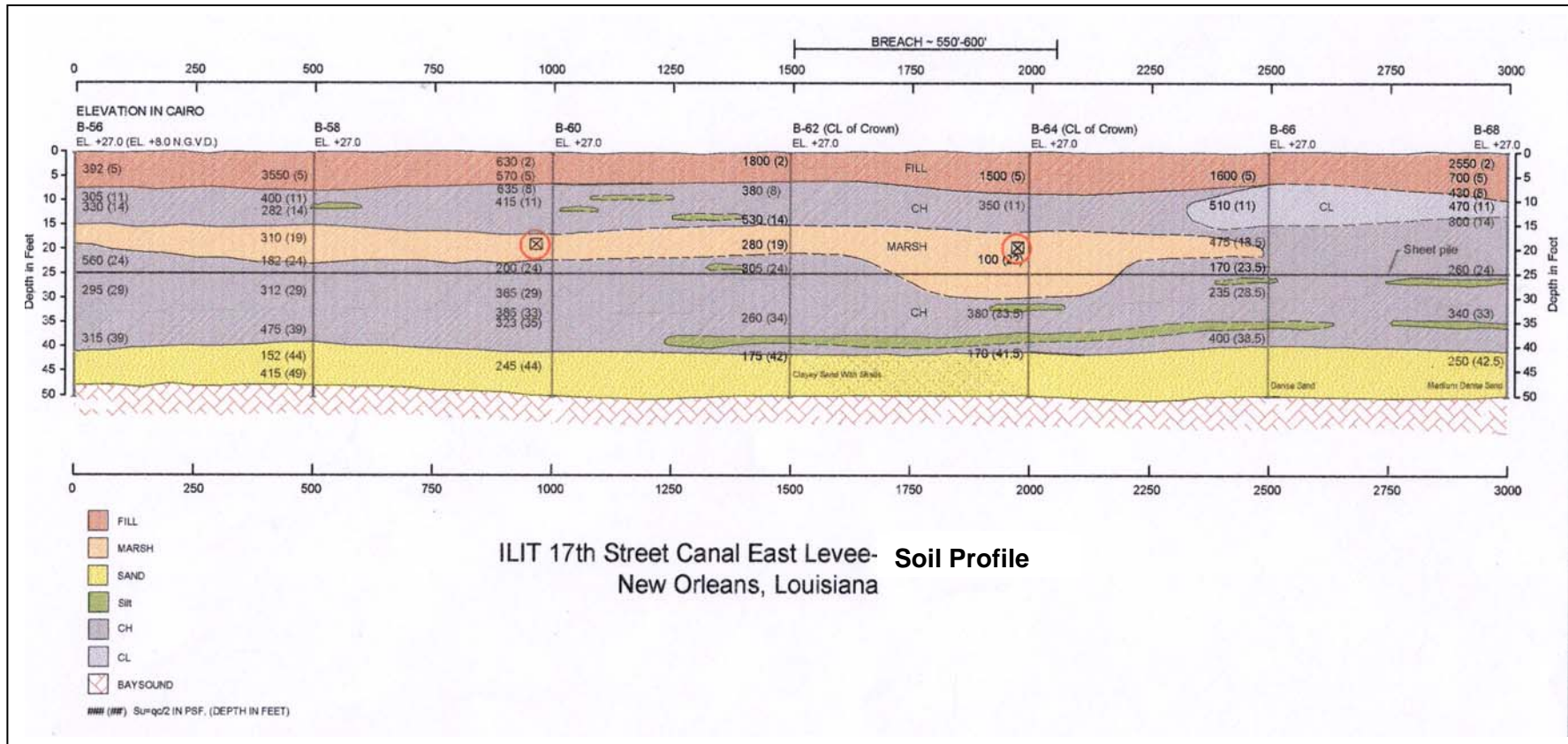


Figure 8.71: Re-interpreted longitudinal subsurface soil profile, showing location of breach section on the east side of the 17th Street Canal, and with non-tested samples highlighted.

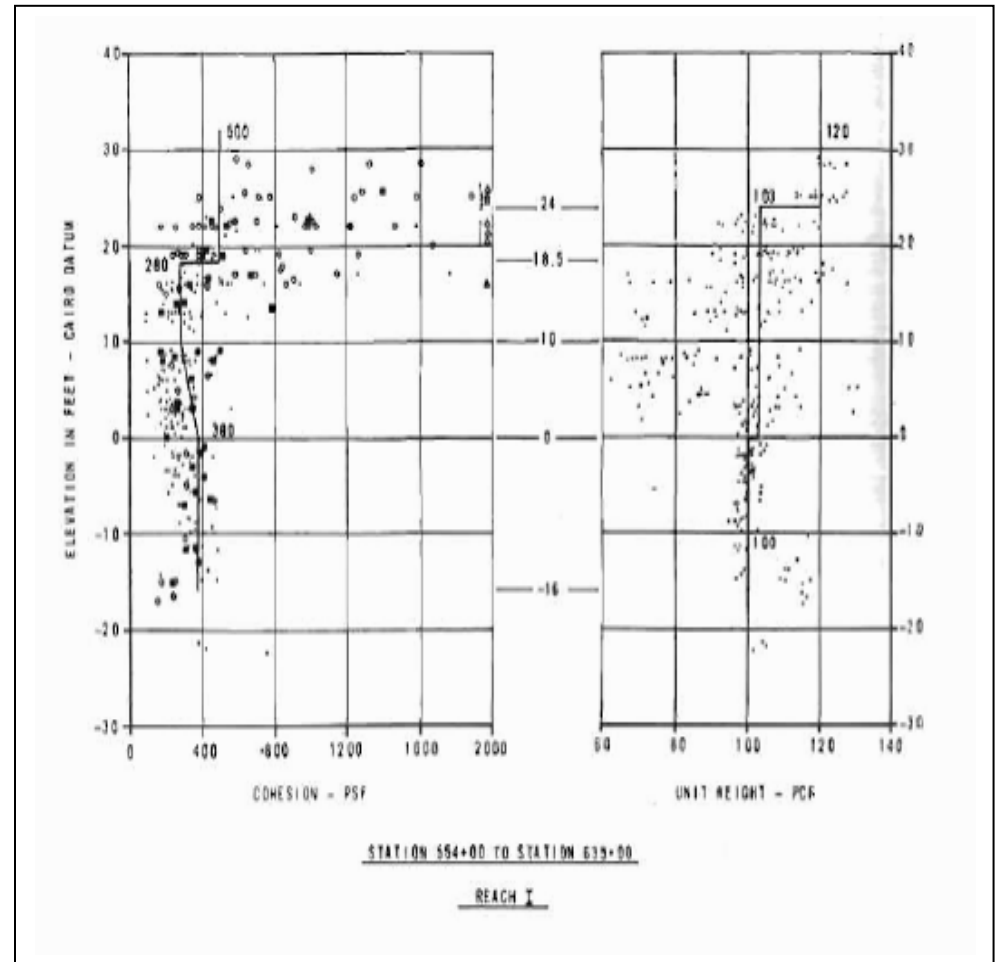
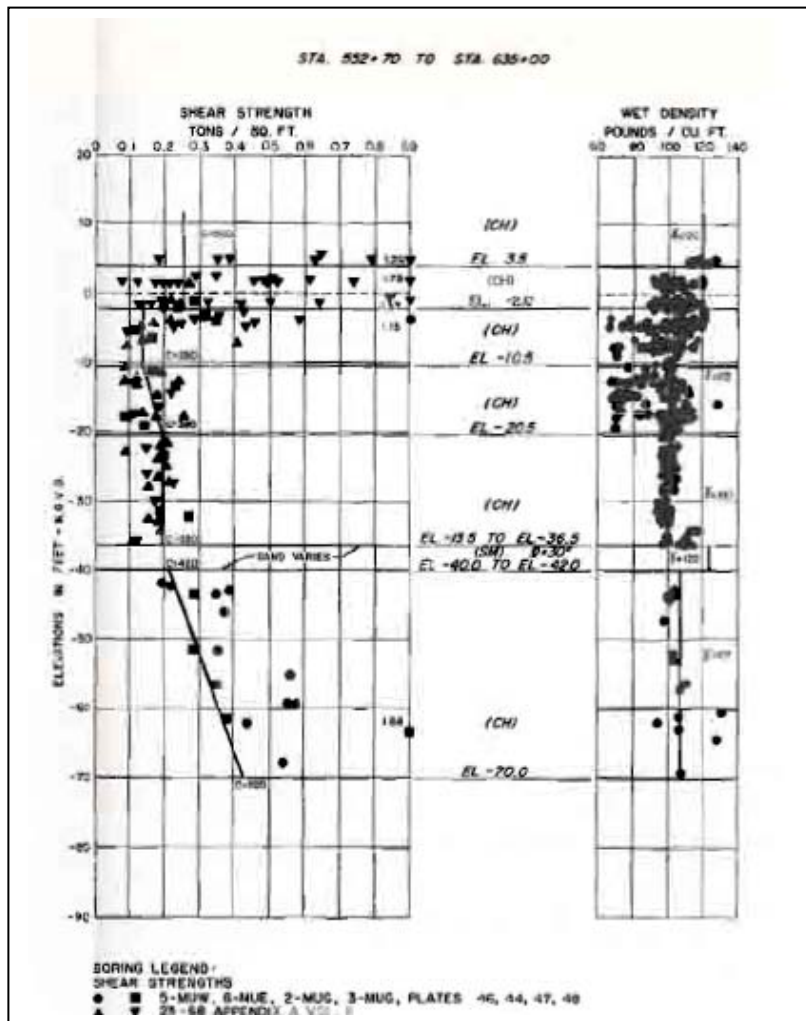


Figure 8.73: Profile of shear strength vs. depth used in original stability analyses for design at the 17th Street Canal breach site.
[USACE, DM-20, Vol.1 & 2, 1990]

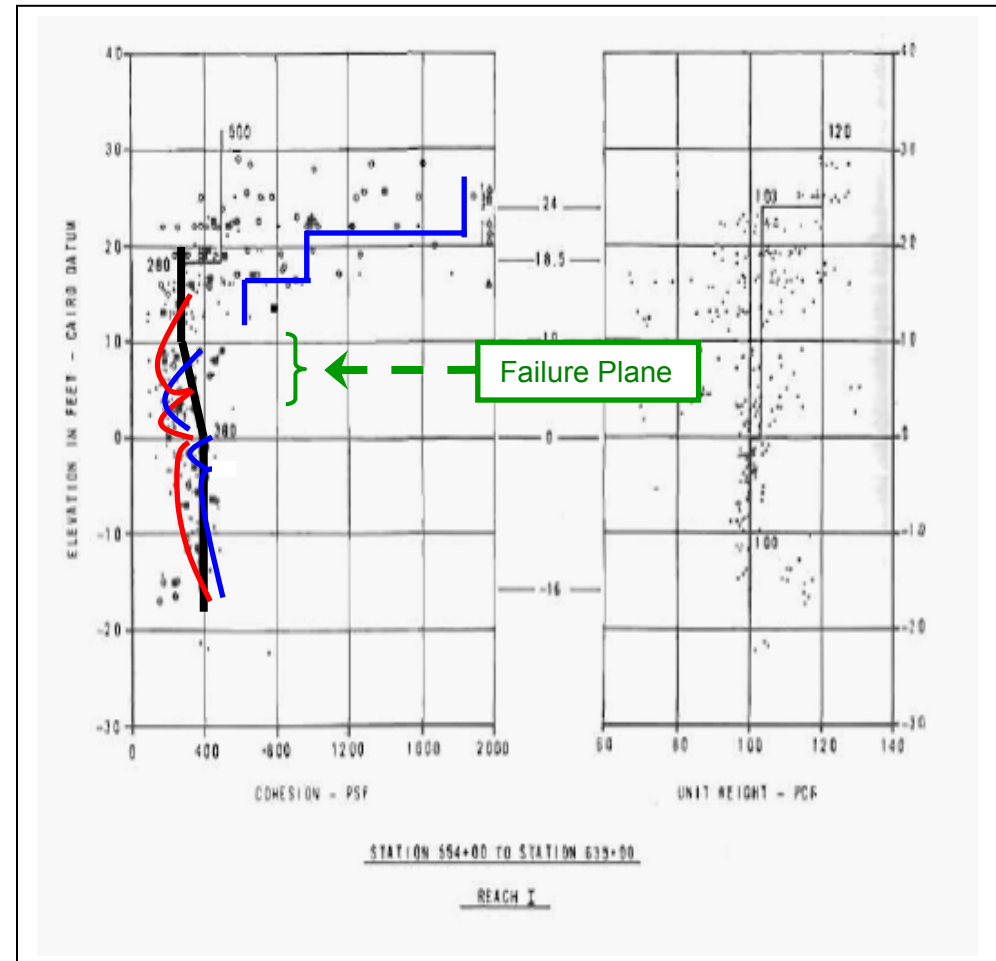
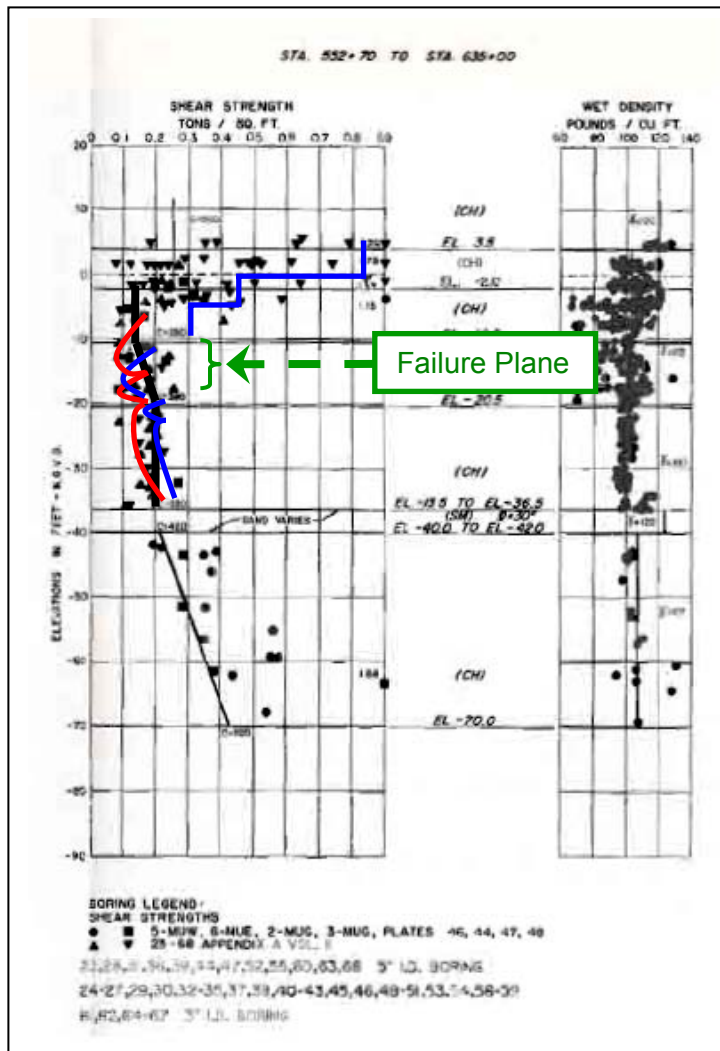


Figure 8.74: Profile of shear strength vs. depth used in original stability analyses for design at the 17th Street Canal breach site, and this investigation team's best estimated profiles of undrained shear strength vs. elevation (a) beneath levee crest [blue line], and (b) beneath levee toe [red line].

[USACE, DM-20, Vol.1 & 2, 1990]



Figure 8.75: View of floodwall displacement on the west bank of the 17th Street Canal.

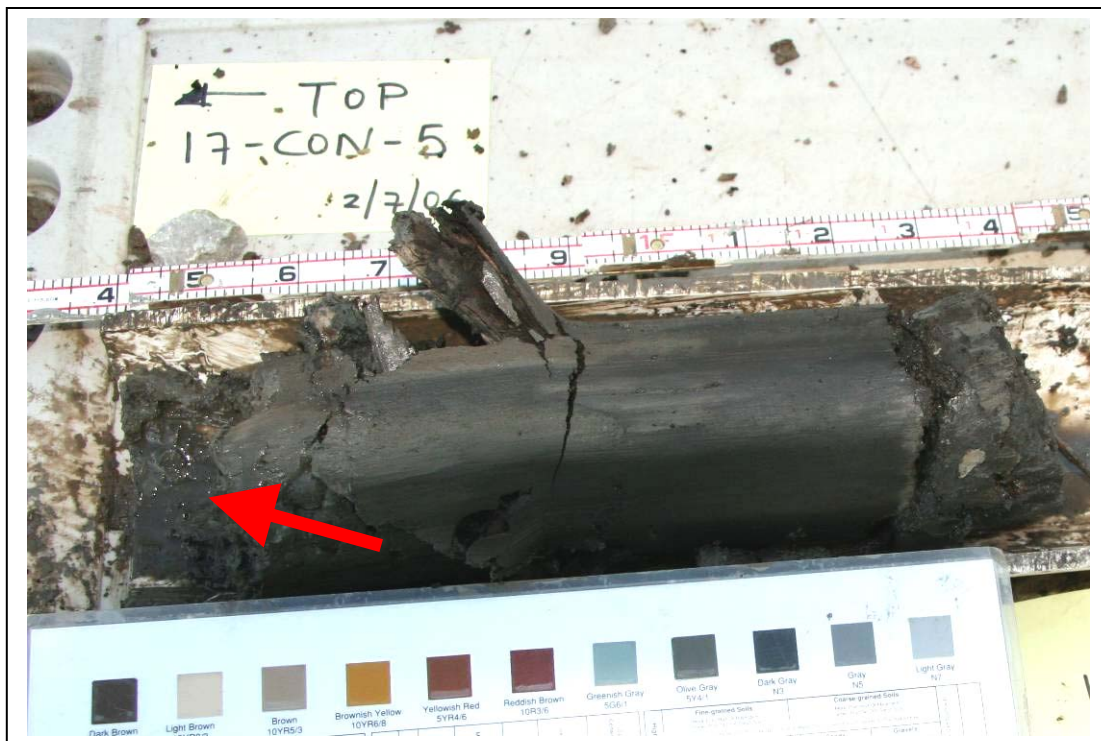


Figure 8.76: View of sample of “sensitive” clay layer within the marsh soils at the west side of the 17th Street Canal.

17th STREET CANAL WEST BANK BREACH
ANALYSIS SECTION

Elevation (ft, N.A.V.D.)

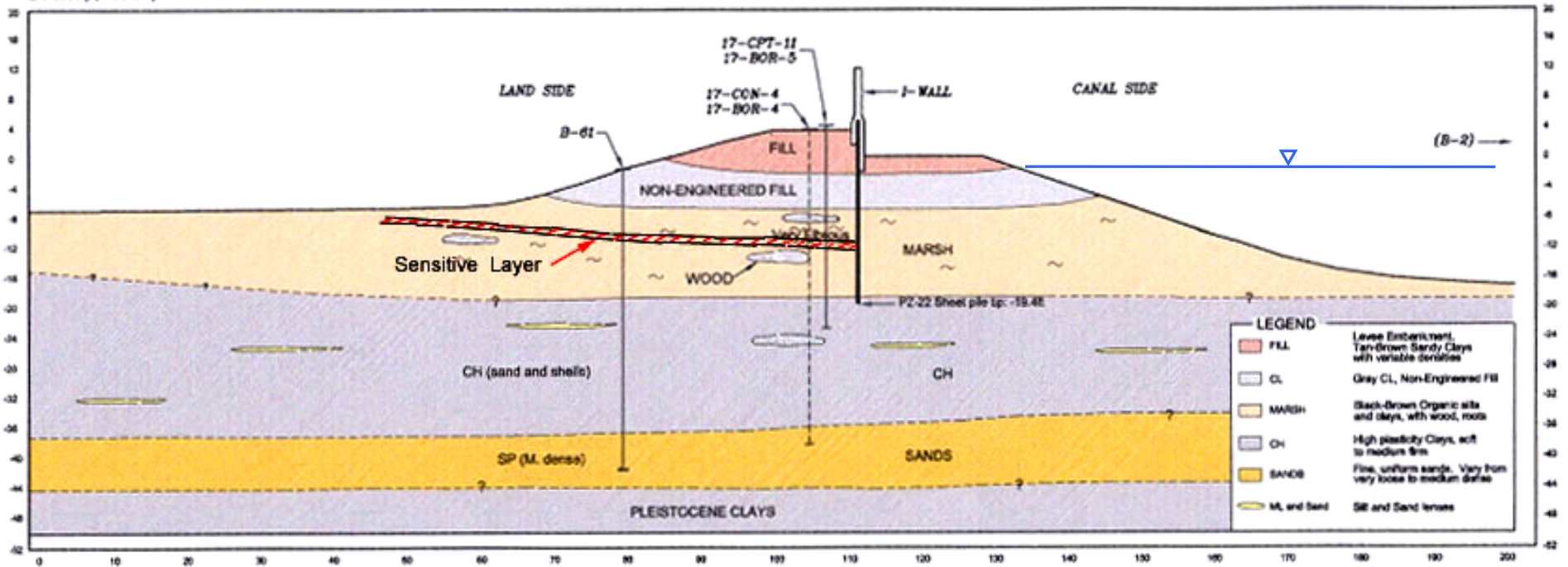


Figure 8.77: Analysis cross-section for the site on the west bank of the 17th Street Canal.

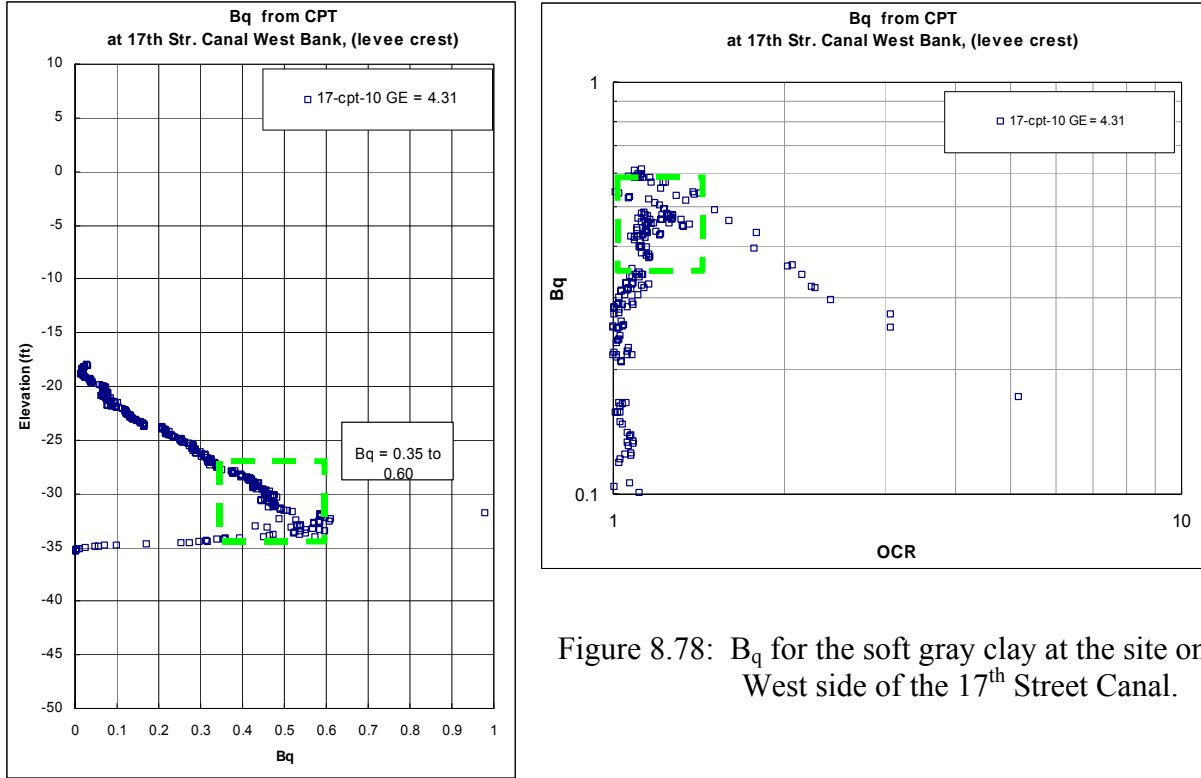


Figure 8.78: B_q for the soft gray clay at the site on the West side of the 17th Street Canal.

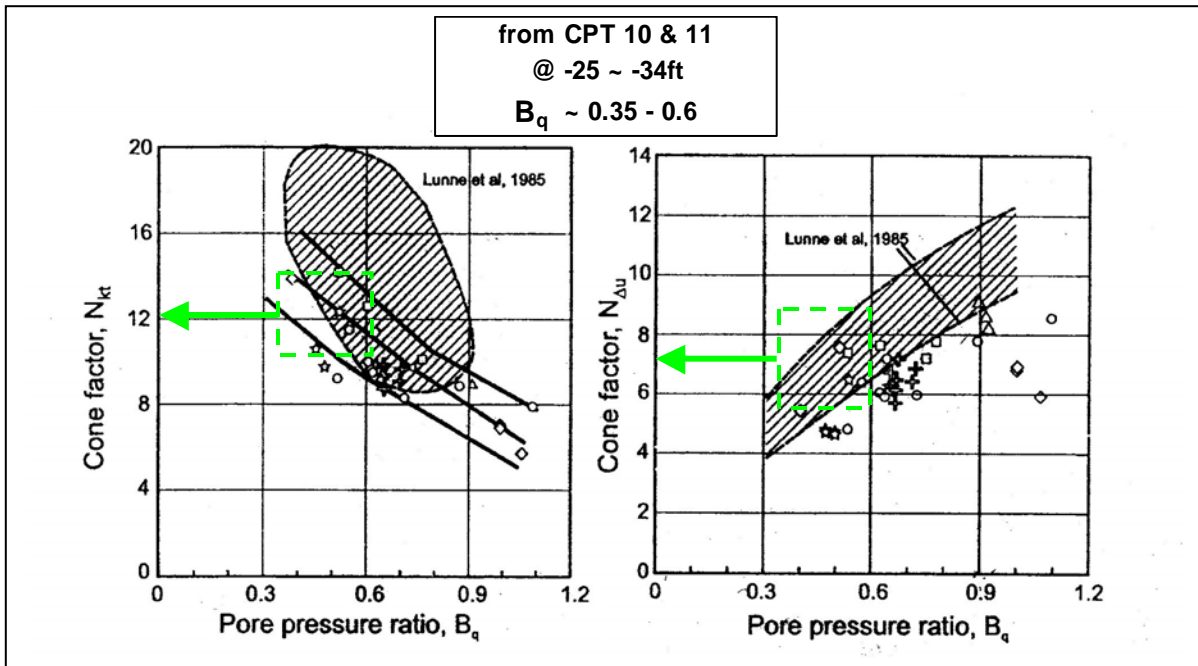


Figure 8.79: N_{kt} and N_{du} for the soft gray clay at the site on the west side of the 17th Street Canal based on CPTU.

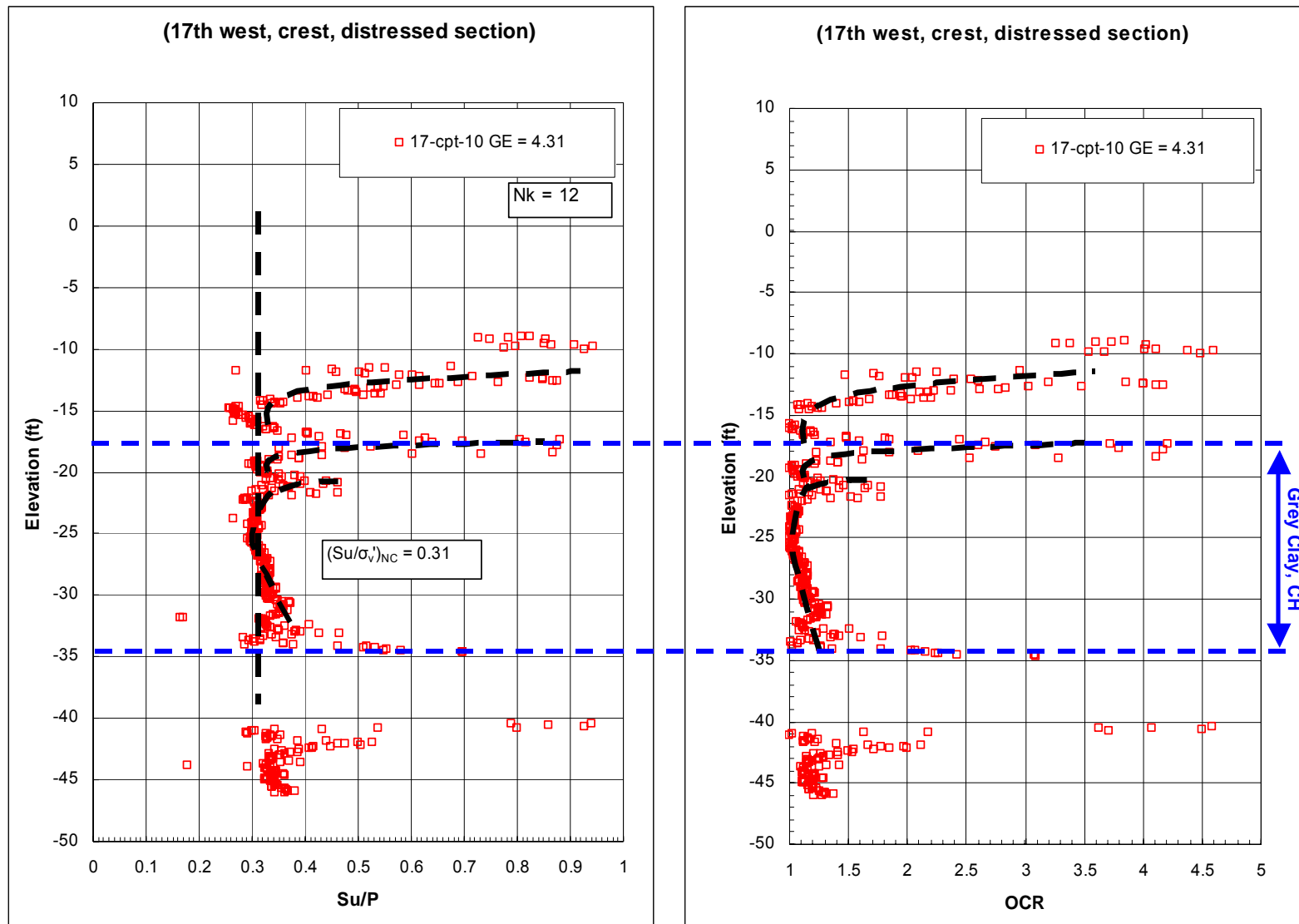


Figure 8.80: S_u/P vs. depth and OCR vs. depth for soft gray clay (CH) beneath the crest of the embankment for the site on the west side of the 17th Street Canal.

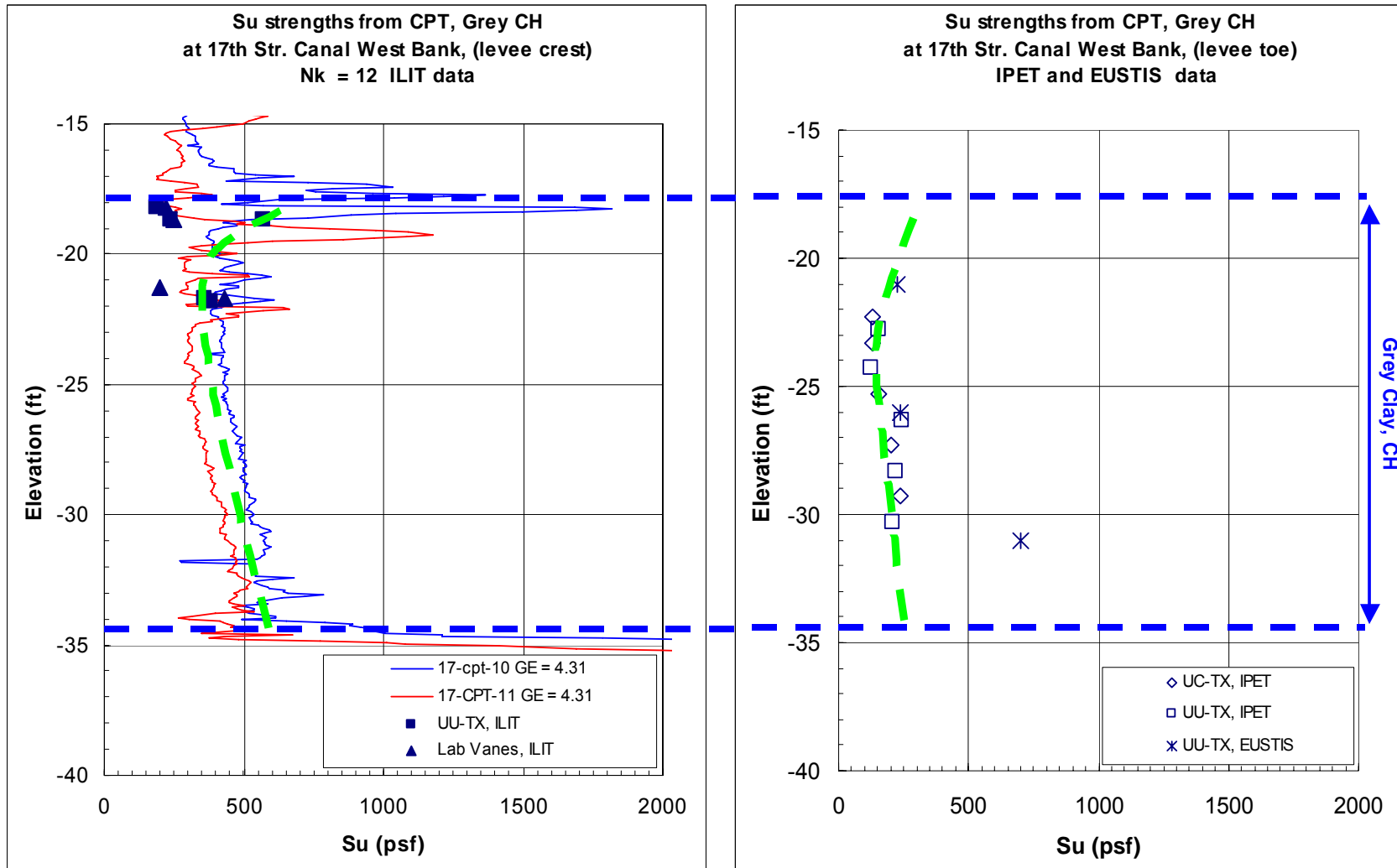
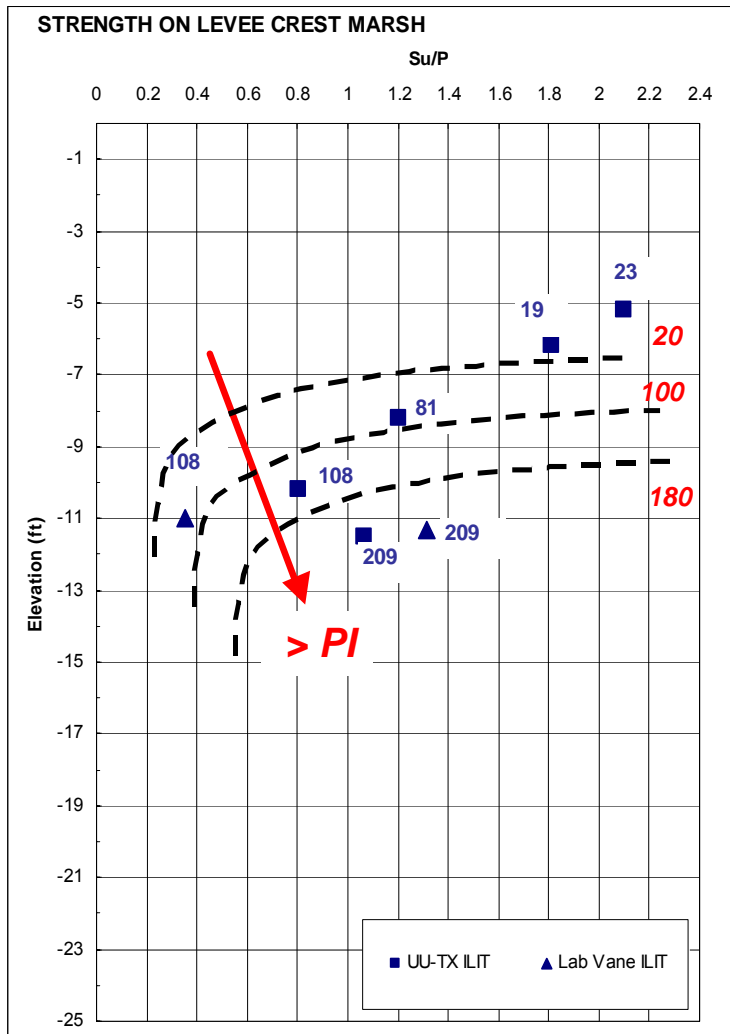


Figure 8.81: Shear strength vs. depth within the soft gray clay (CH) for the site on the west side of the 17th Street Canal (a) beneath the crest of the levee, and (b) beneath the inboard side toe of the levee embankment.

Ref: Mayne, P.W and Mitchell,
J.K (1988)



elev (ft)	S _u /σ' _v			OCR = α _{VST} (S _u /σ' _v)		
	PI (%)			α _{VST} = 22 PI ^{-0.48}		
-5	2.4			5.2	2.4	1.8
-6	2.2			5.2		
-7	1.2			5.2		
-8	0.6	2.2		5.2	2.4	1.8
-9	0.34	0.9	3	5.2	2.4	1.8
-10	0.27	0.6	1.4	5.2	2.4	1.8
-11	0.22	0.4	0.8	5.2	2.4	1.8
-12	0.2	0.4	0.6	5.2	2.4	1.8
-13	0.2	0.4	0.55	5.2	2.4	1.8
-14	0.2	0.4	0.55	5.2	2.4	1.8

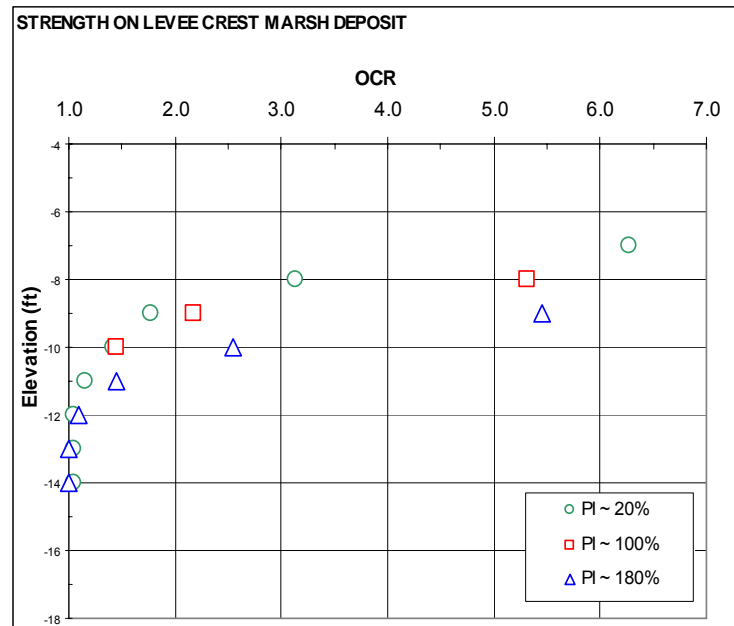
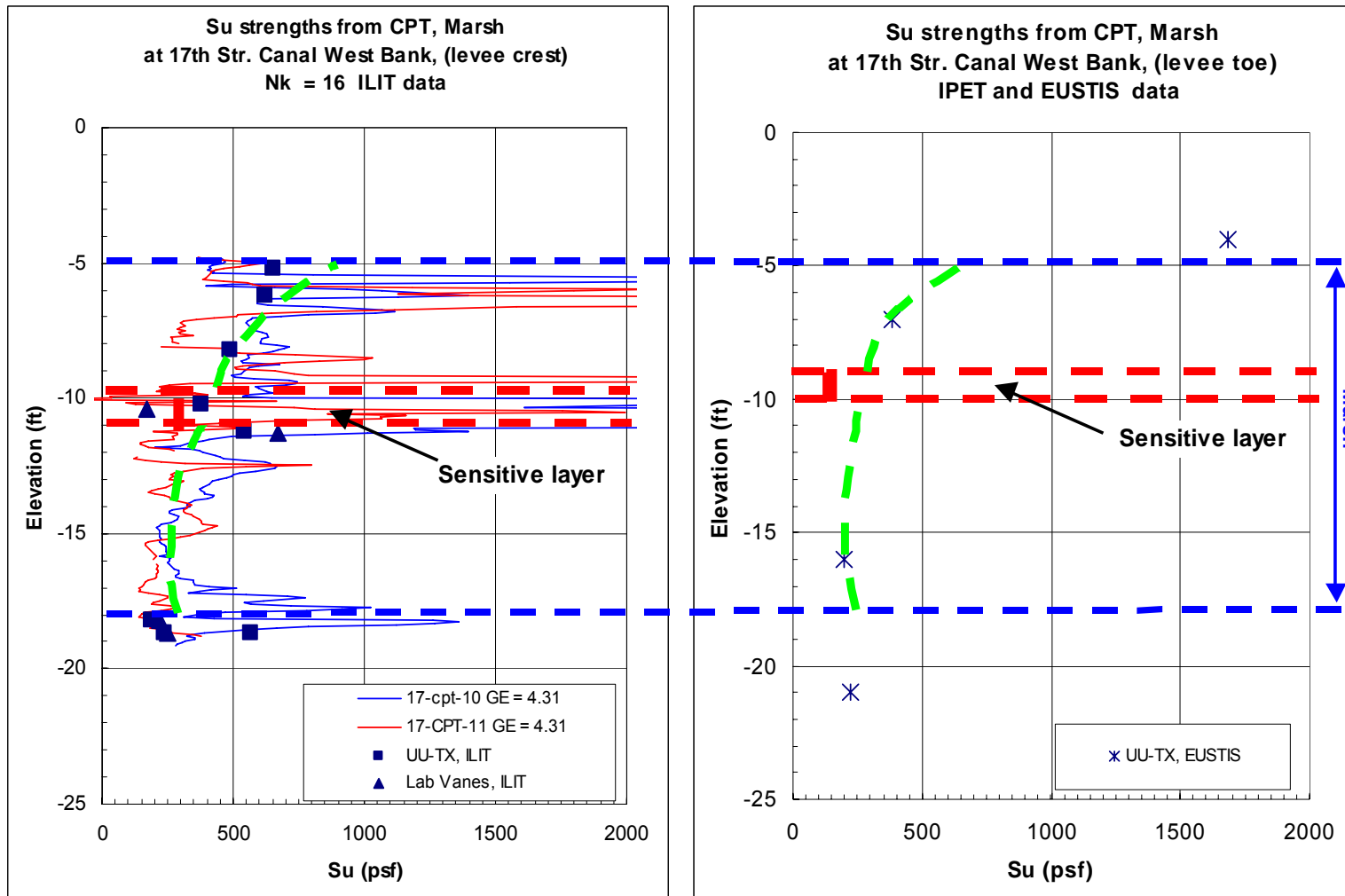


Figure 8.82: Su/P and OCR estimation from PI and vane shear tests for the marsh deposits at the site on the west side of the 17th Street Canal.



(a) Beneath the crest of the levee

(b) Beneath the inboard toe of the levee

Figure 8.83: Shear strength vs. depth within the marsh deposits at the site on the west side of the 17th Street Canal (a) beneath the crest of the levee, and (b) beneath the inboard toe of the embankment.

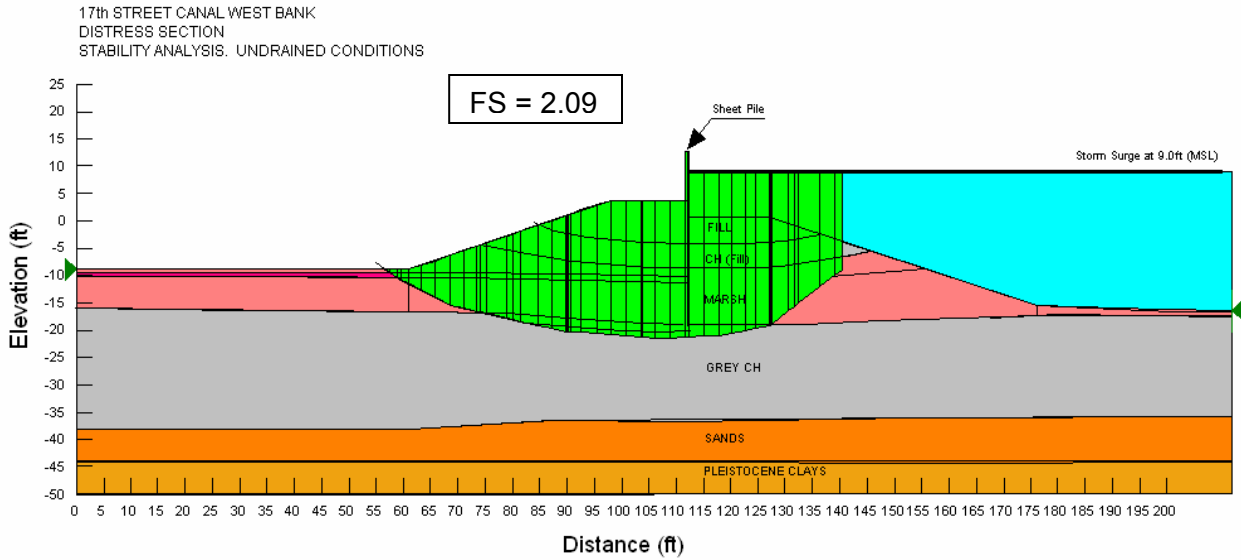


Figure 8.84: Stability analysis of the west side of the 17th Street Canal with water at Elev. + 9 feet (MSL) for case of rotational failure through the soft gray clay (CH) with no gap developed.

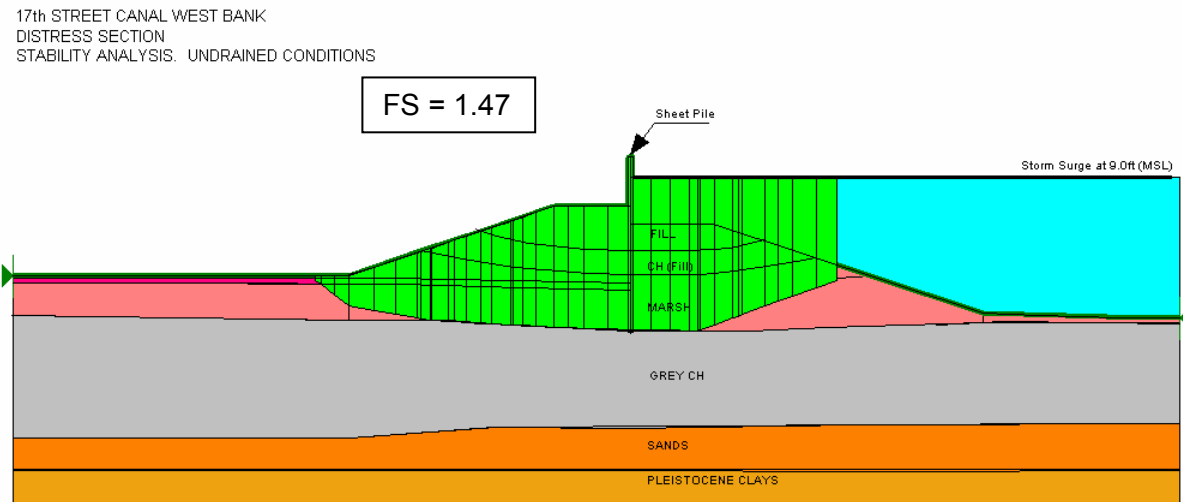


Figure 8.85: Stability analysis of the west side of the 17th Street Canal with water at Elev. + 9 feet (MSL) for case of failure through the base of the “marsh” layer (with no gap developed).

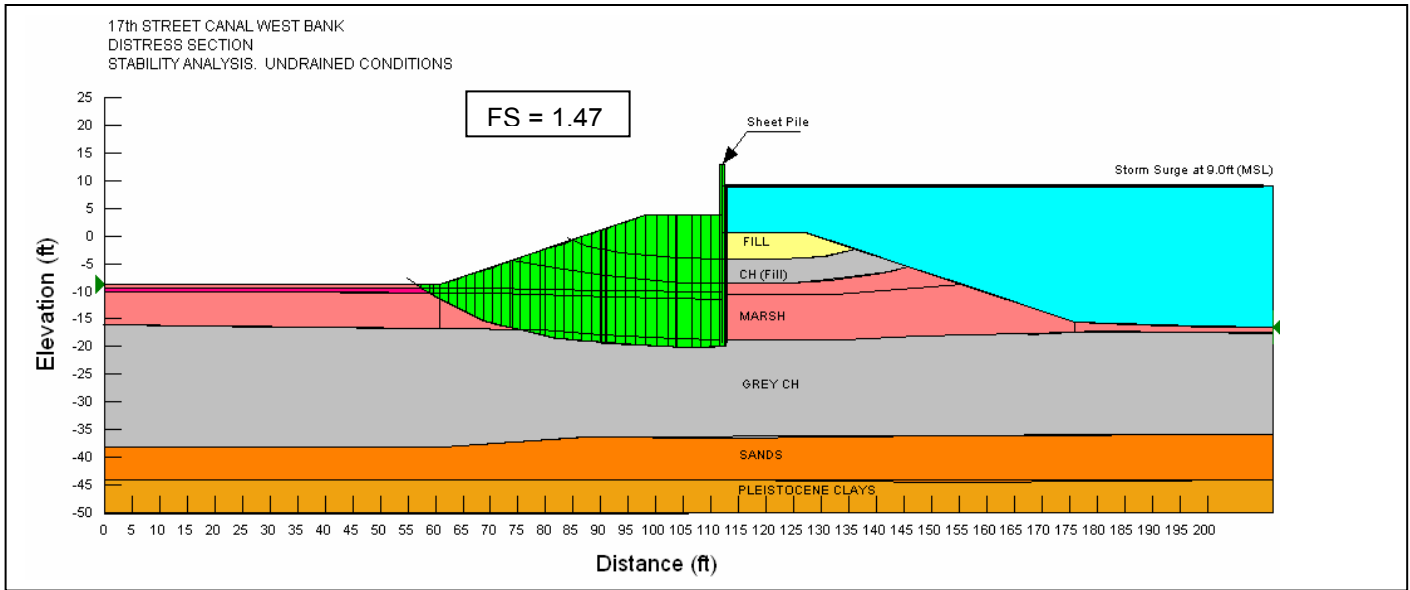


Figure 8.86: Stability analysis of the west side of the 17th Street Canal with water at Elev. + 9 feet (MSL) for case of rotational failure through the soft gray clay (CH) (with water-filled gap).

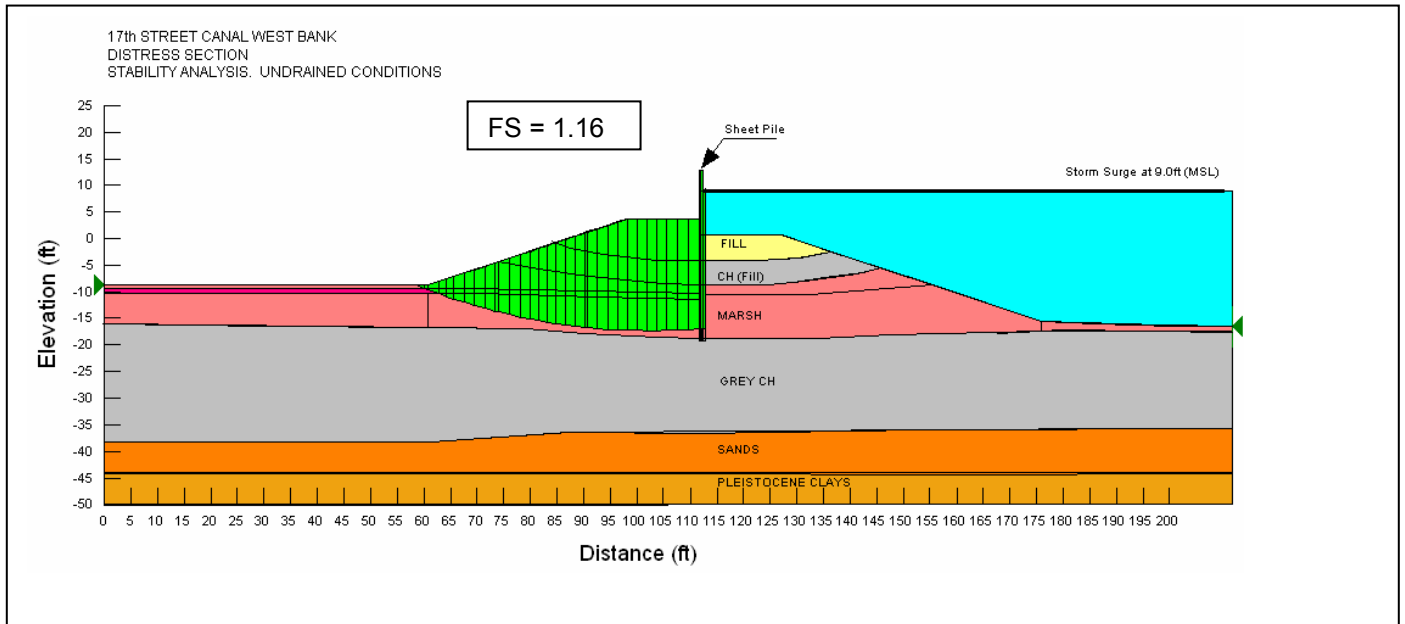


Figure 8.87: Stability analysis of the west side of the 17th Street Canal with water at Elev. + 9 feet (MSL) for case of failure along the base of the “marsh” layer (with water-filled gap).

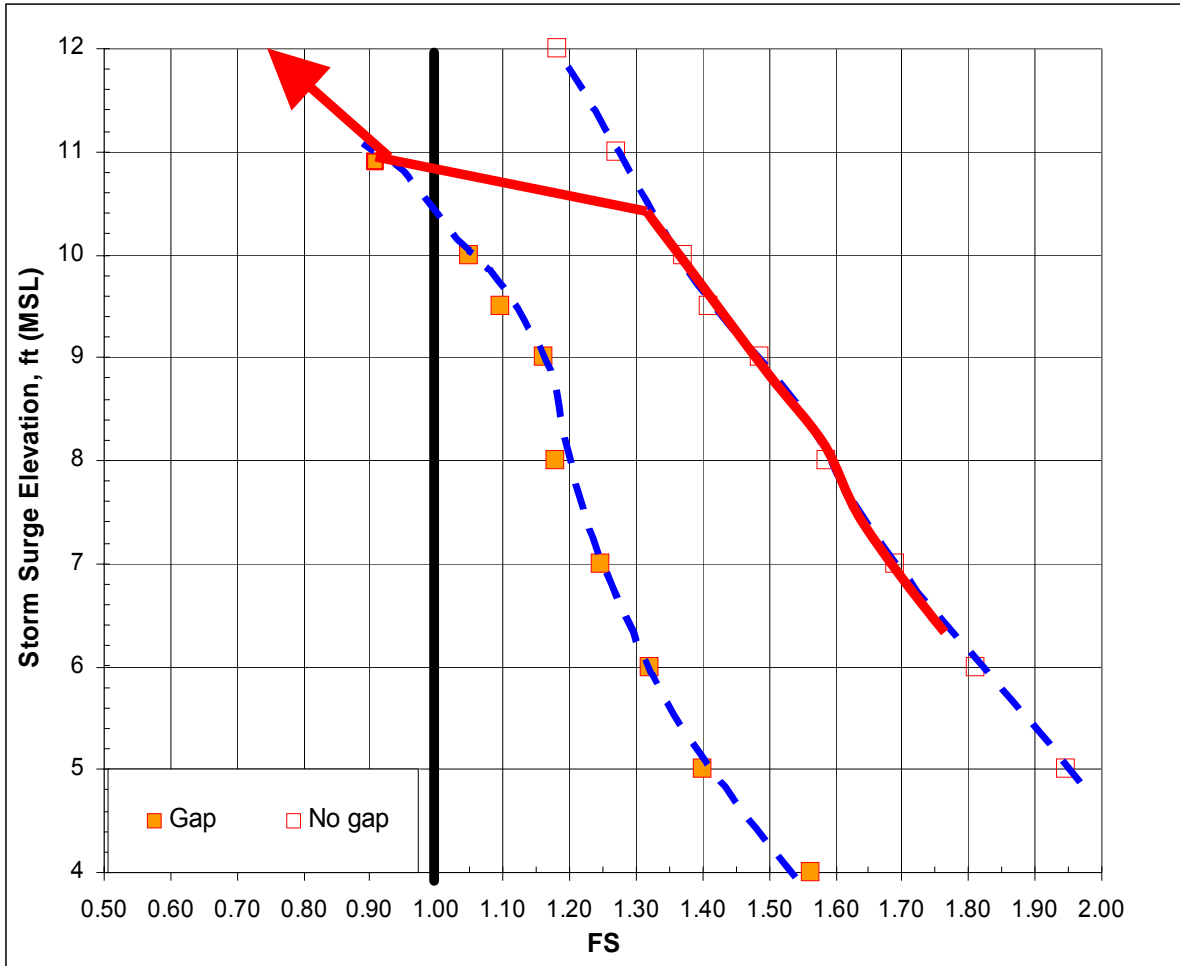


Figure 8.88: Factor of safety vs. water level on the west bank of the 17th Street Canal.

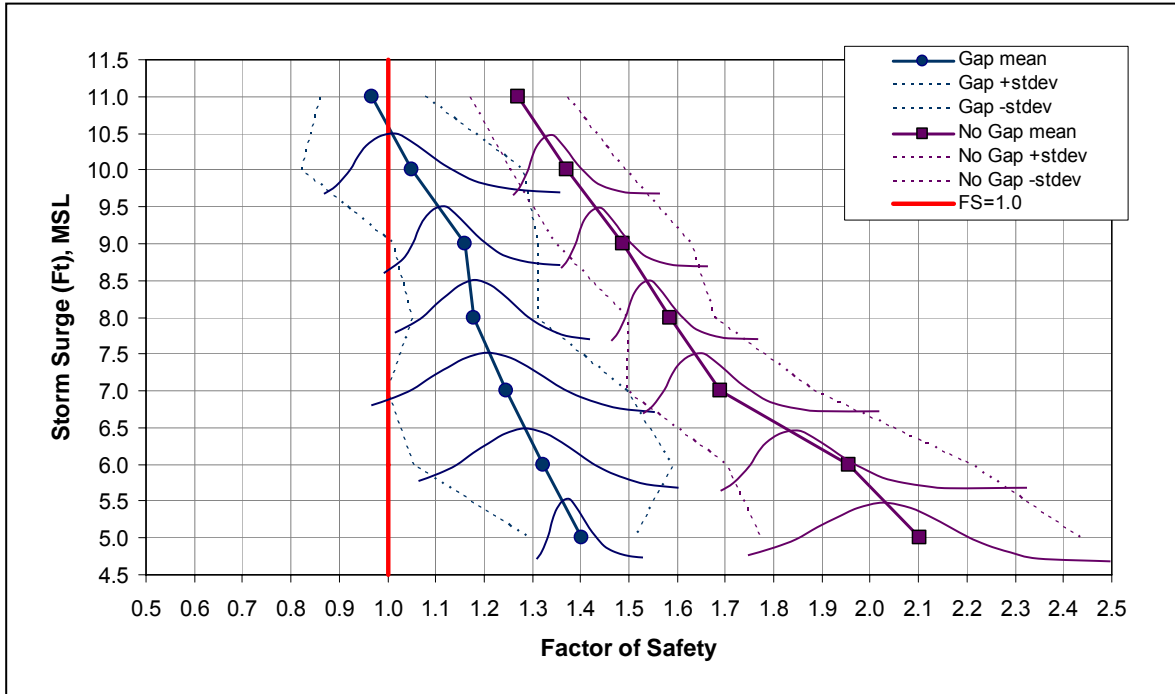


Figure 8.88(a): Distributions of factors of safety for the “Water-filled Gap” and the “Ungapped” cases as a function of rising canal water elevations; 17th Street Drainage Canal; west bank distressed section.

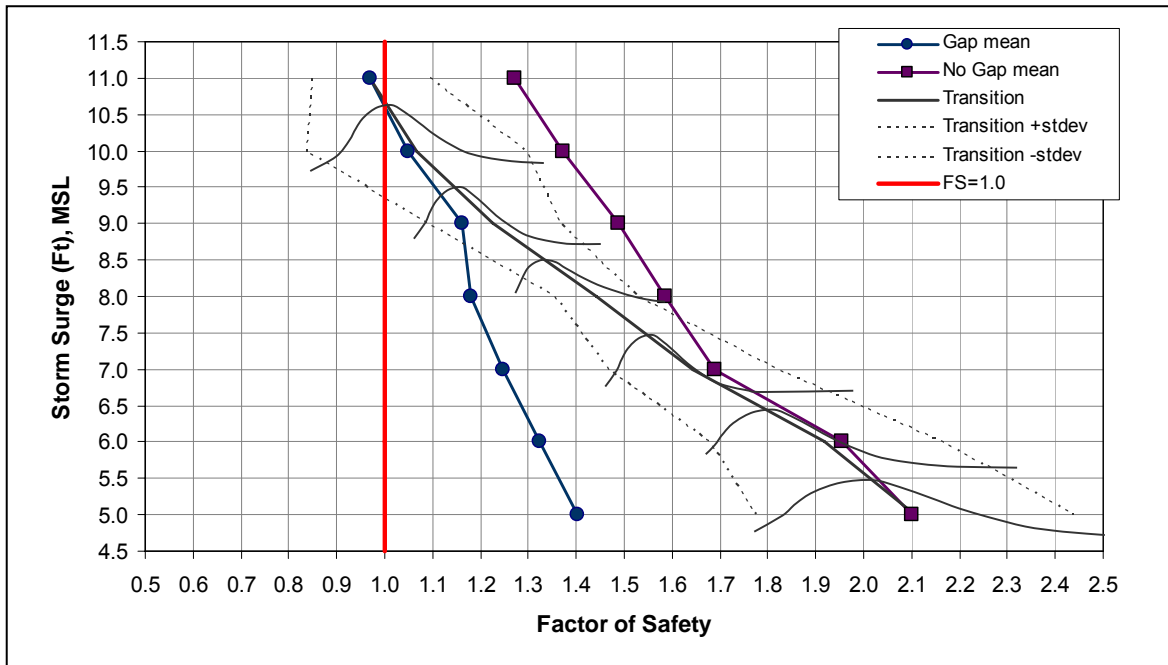


Figure 8.88(b): Distributions of conjugate overall factors of safety for the 17th Street Drainage Canal; west bank distressed section.

Storm Surge Elevation (ft), MSL	Probability of Failure
11	59.2%
10	38.7%
9	4.9%
8	0.10%
7	0.013%
6	0.007%
5	0.0%

Table 8.2: Probability of failure for 17th Street Canal, West Bank



Figure 8.89: View of failure and breach on the east bank near the south end of the London Avenue Canal.



Figure 8.90: View of sands piled in neighborhood inboard of the south London Avenue Canal breach.



Figures 8.91 and 8.92: Views of floodwall panels “dropping” into the eroded void at the north and south ends of the south London Avenue canal breach.



Figure 8.93: View of trees at the inboard levee toe immediately to the north of the end of the south breach in the London Avenue Canal.



Figure 8.94: View of toppled trees at the London Avenue Canal south breach site.

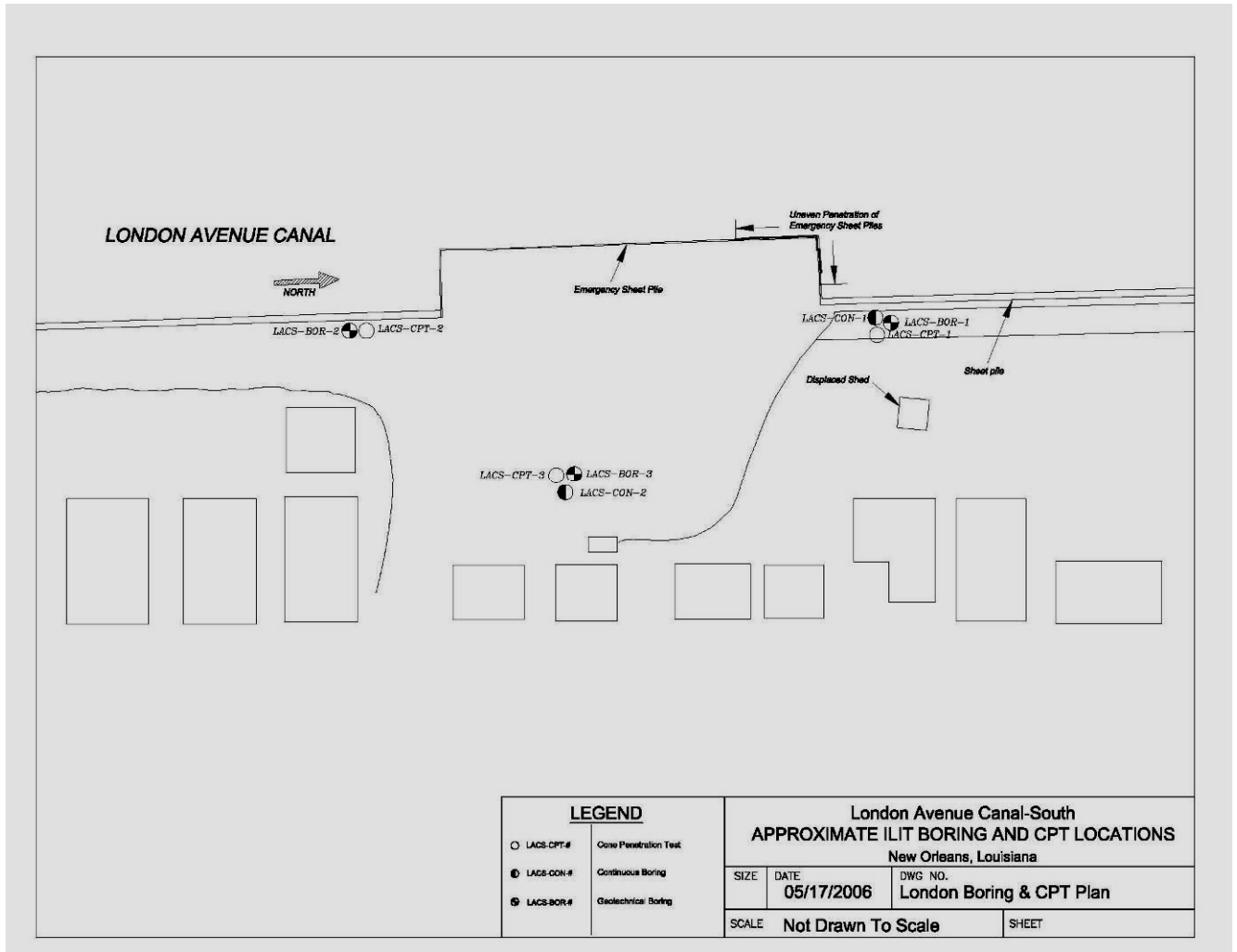


Figure 8.95: Plan view of the London Avenue Canal (South) breach site.

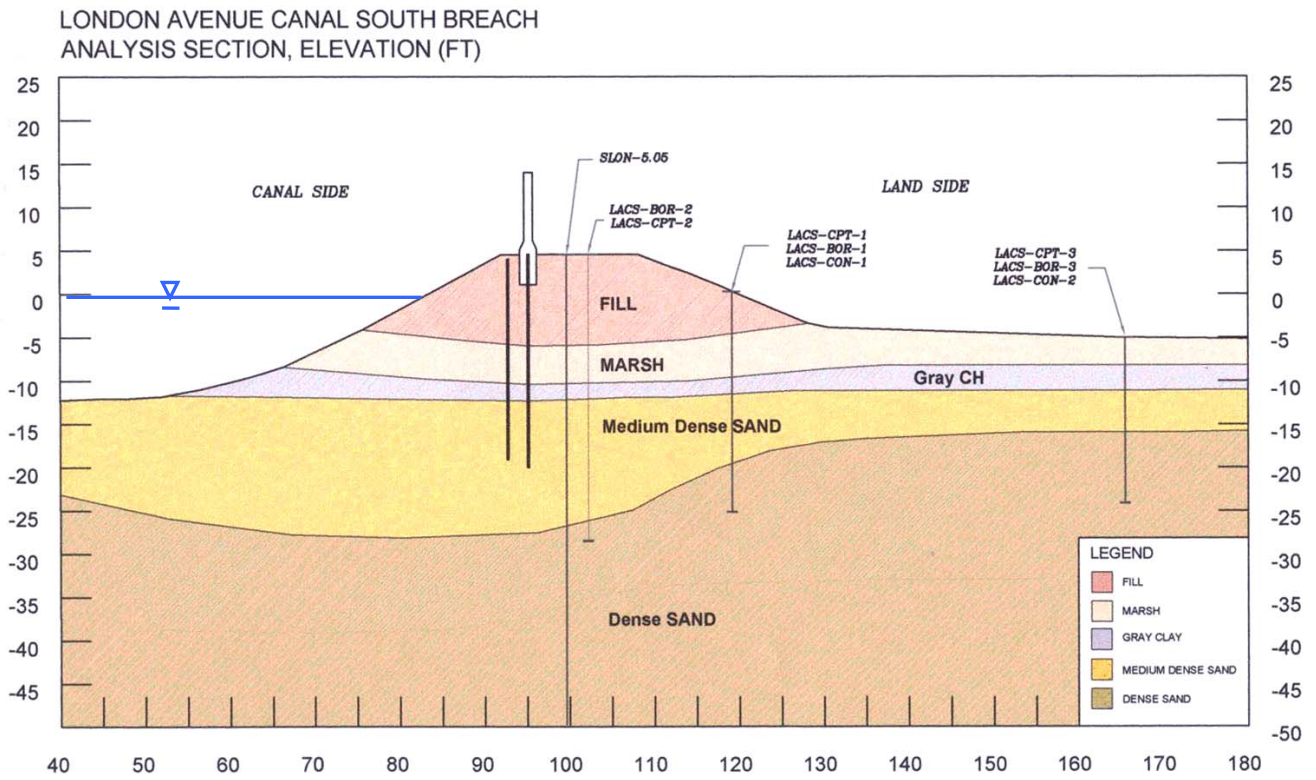
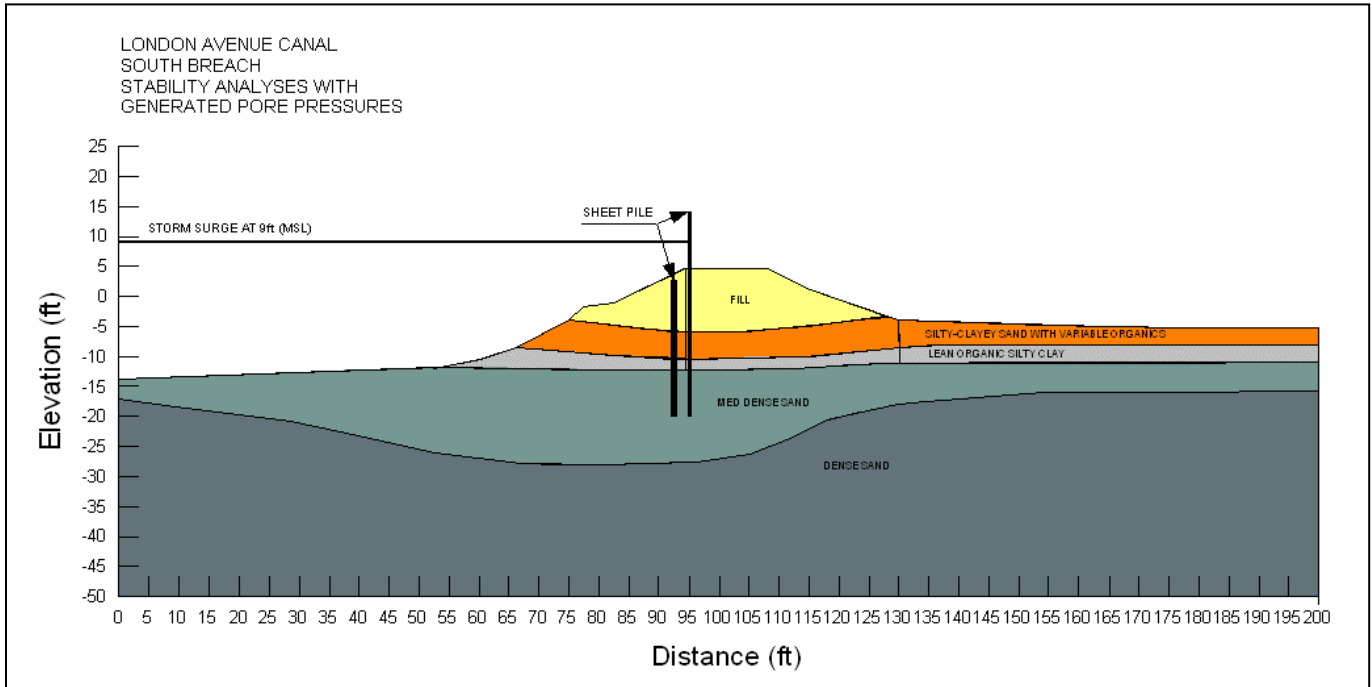


Figure 8.96: Cross-section through the breach near the south end of the London Avenue Canal.



ID	Soil Model	Type	γ	c	phi	k
			[lb/ft ³]	[lb/ft ²]	[°]	[ft/hr]
Upper fill	Mohr-Coulomb	Undrained	100	800	0	1.20E-03
SM/SC w/organics, crest	Mohr-Coulomb	Undrained	90	250	0	0.011
SM/SC w/organics, free field	Mohr-Coulomb	Undrained	90	200	0	0.011
Lean organic silty clay, crest	Mohr-Coulomb	Undrained	100	500	0	3.60E-03
Lean organic silty clay, free field	Mohr-Coulomb	Undrained	100	300	0	3.60E-03
Medium Dense Sand	Mohr-Coulomb	Drained	100	0	33	1.100
Dense Sand	Mohr-Coulomb	Drained	110	0	35	0.600

Figure 8.97: Geotechnical cross-section for analysis of the London Avenue south breach.

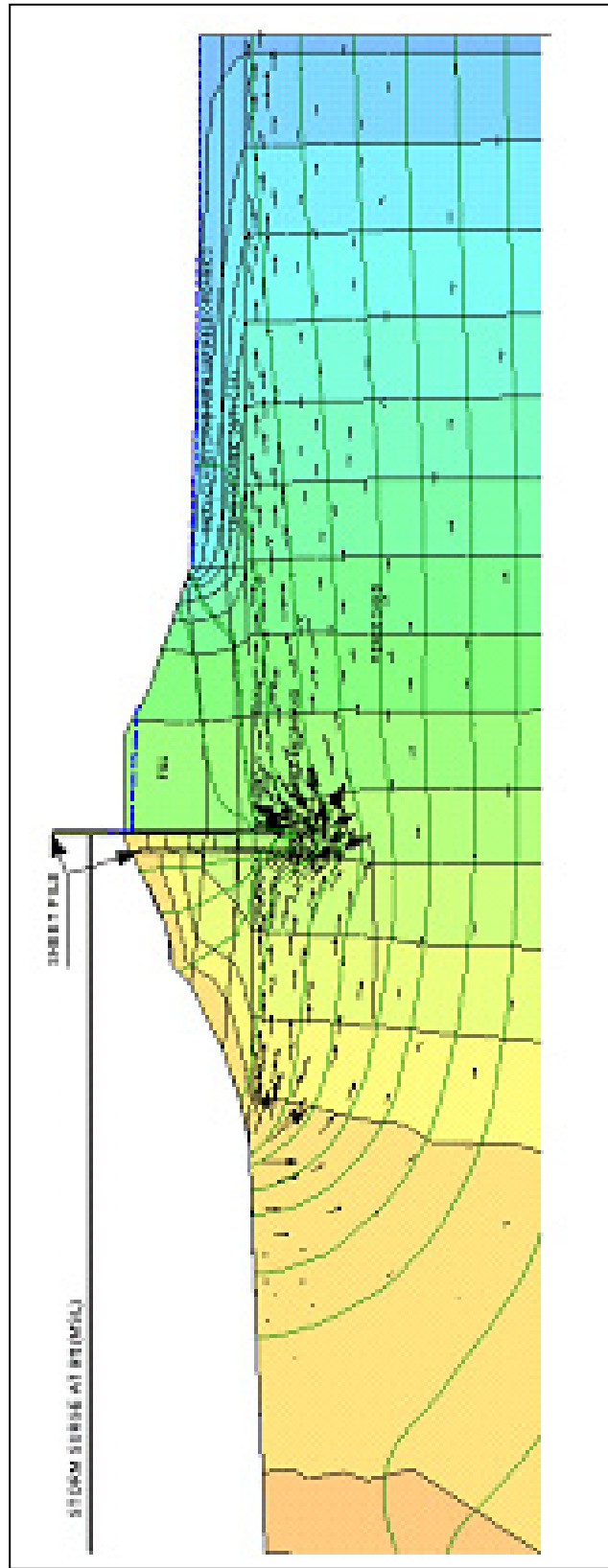


Figure 8.98: Flow vectors and head contours for seepage analysis of the south London Avenue Canal breach for a surge at Elev. + 9 feet (MSL).

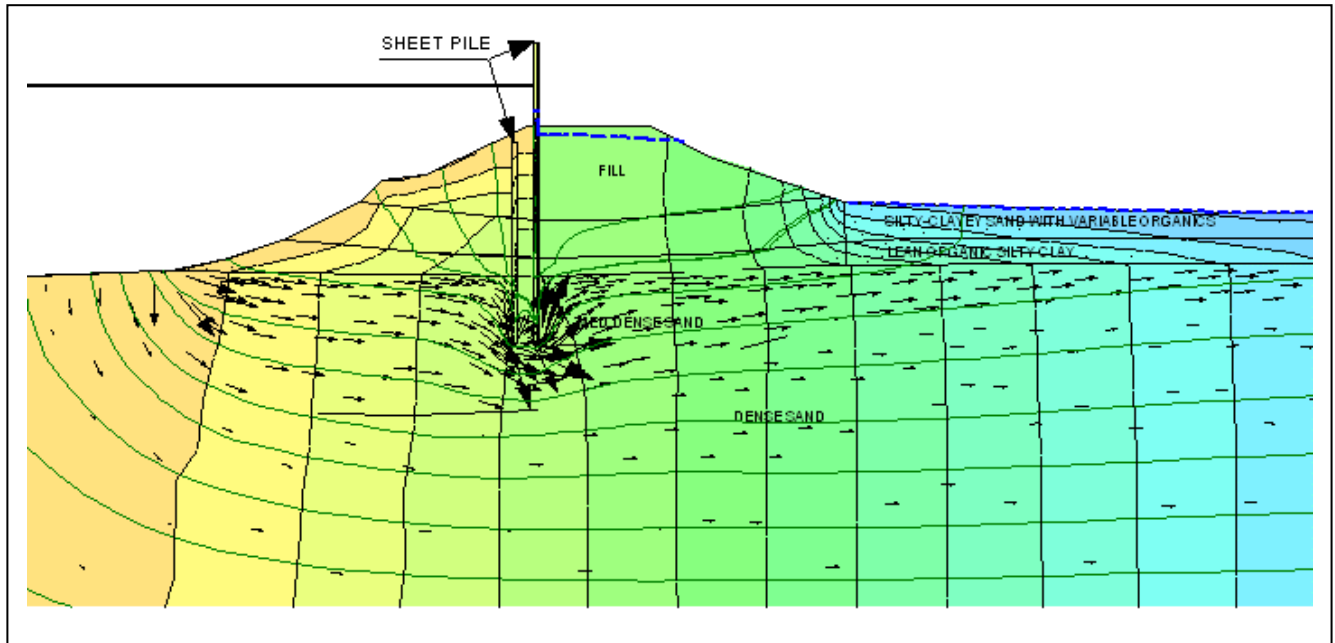


Figure 8.99: Closeup of flownet for storm surge at + 9ft (MSL) in the London Avenue Canal south breach. (Equipotential contours at intervals of one foot of head)

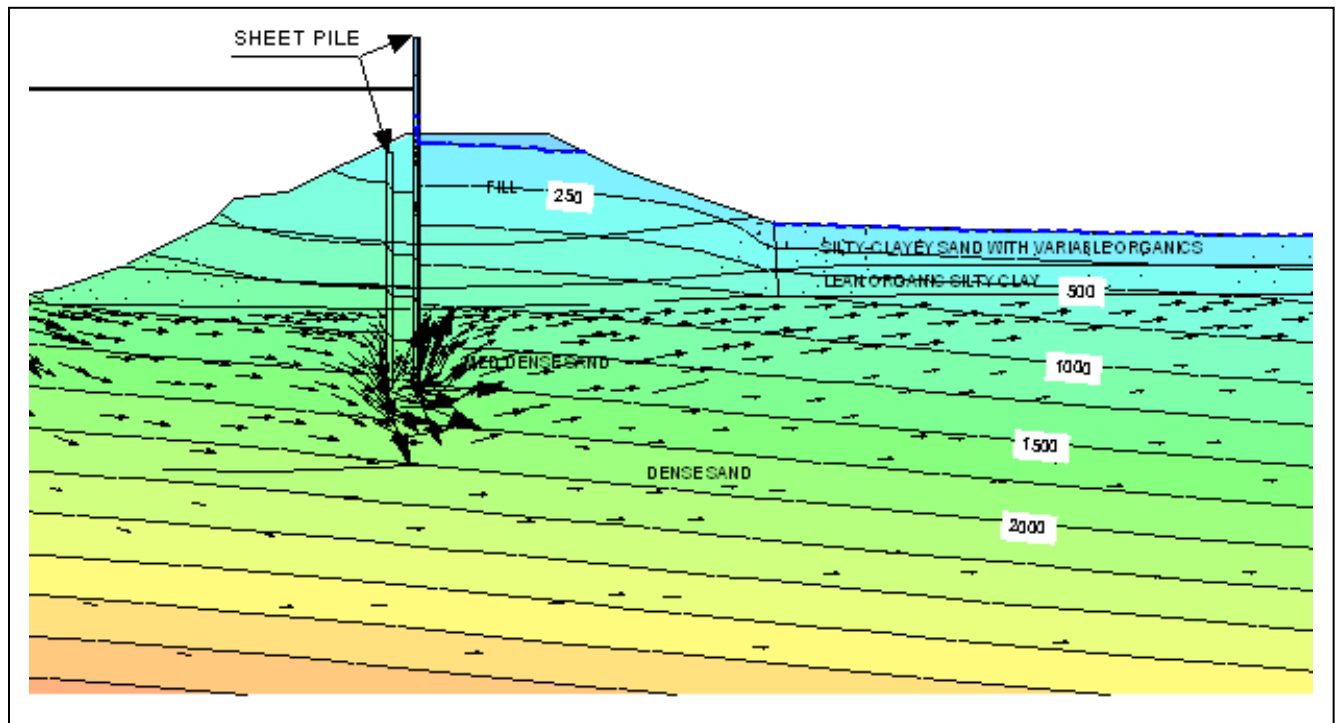


Figure 8.100: Pressure contours for Storm Surge at 9ft (MSL) in the London Avenue Canal South breach. (Pressure contours every 250 lb/ft²)

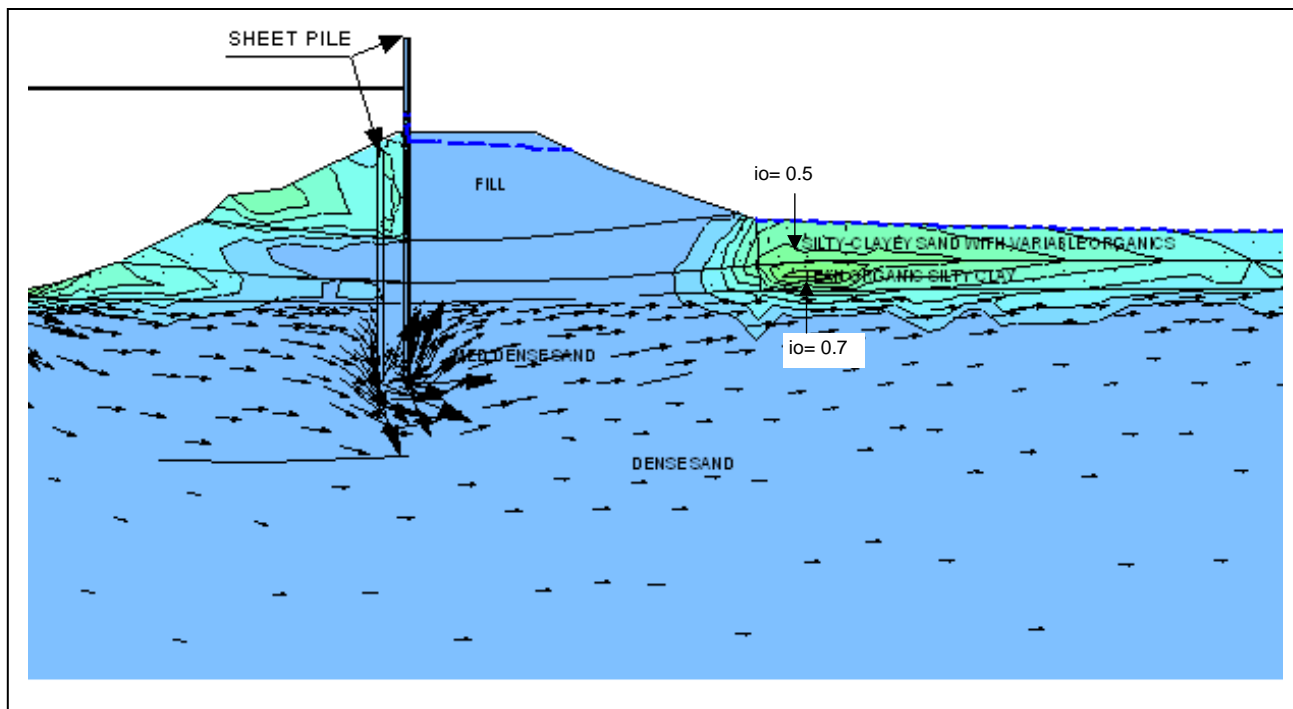


Figure 8.101: Hydraulic gradients for storm surge at +9ft (MSL) in the London Avenue Canal south breach. (Maximum toe exit gradient $i_o = 0.7$)

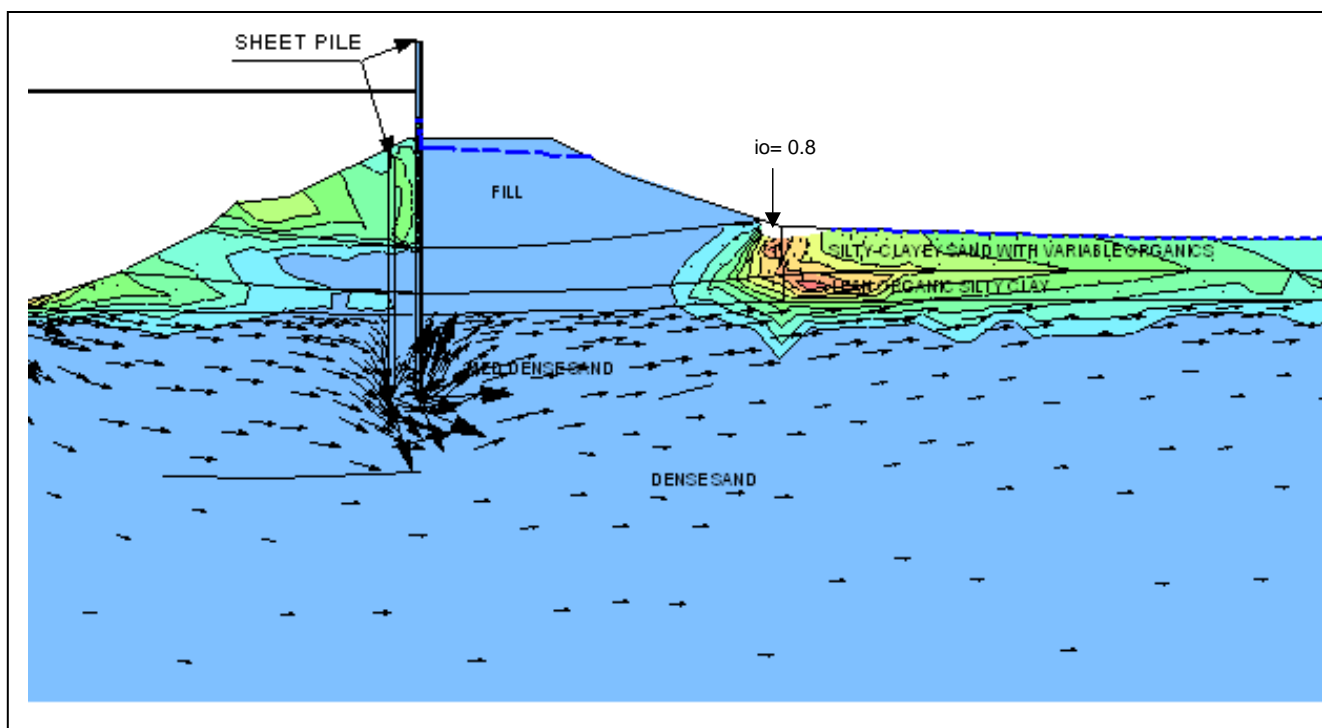


Figure 8.102: Hydraulic gradients for storm surge at +9ft (MSL) in the London Avenue Canal south breach: initiation of erosion at levee toe. (Maximum gradient $i_o = 0.8$)

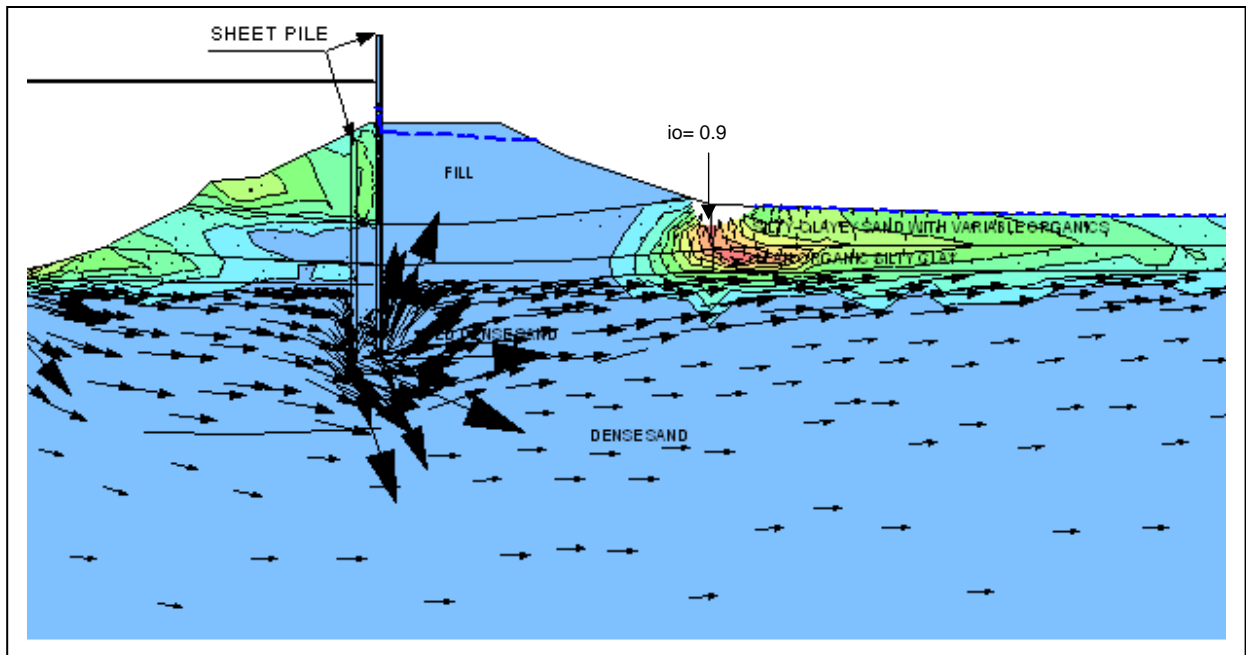


Figure 8.103: Hydraulic gradients for storm surge at +9ft (MSL) in the London Avenue Canal south breach; development of erosion at levee toe. (Maximum gradient $i_o = 0.9$).

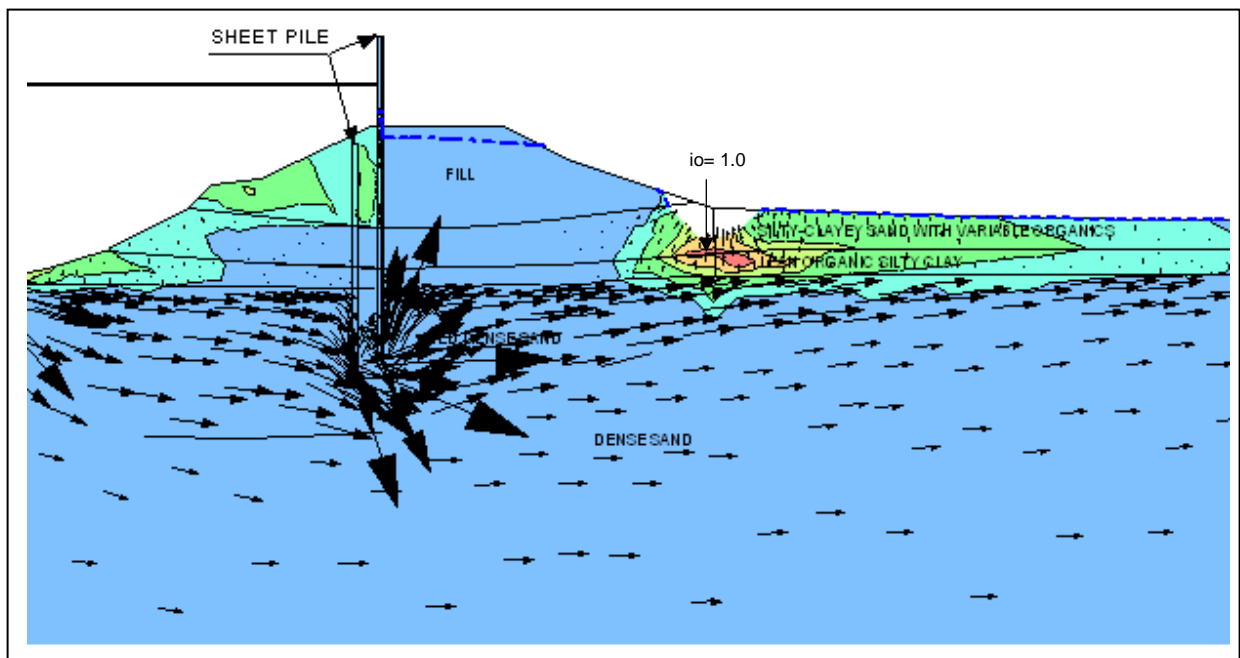


Figure 8.104: Hydraulic gradients for storm surge at +9ft (MSL) in the London Avenue Canal south breach; development of erosion at levee toe. (Maximum gradient $i_o = 1.0$).

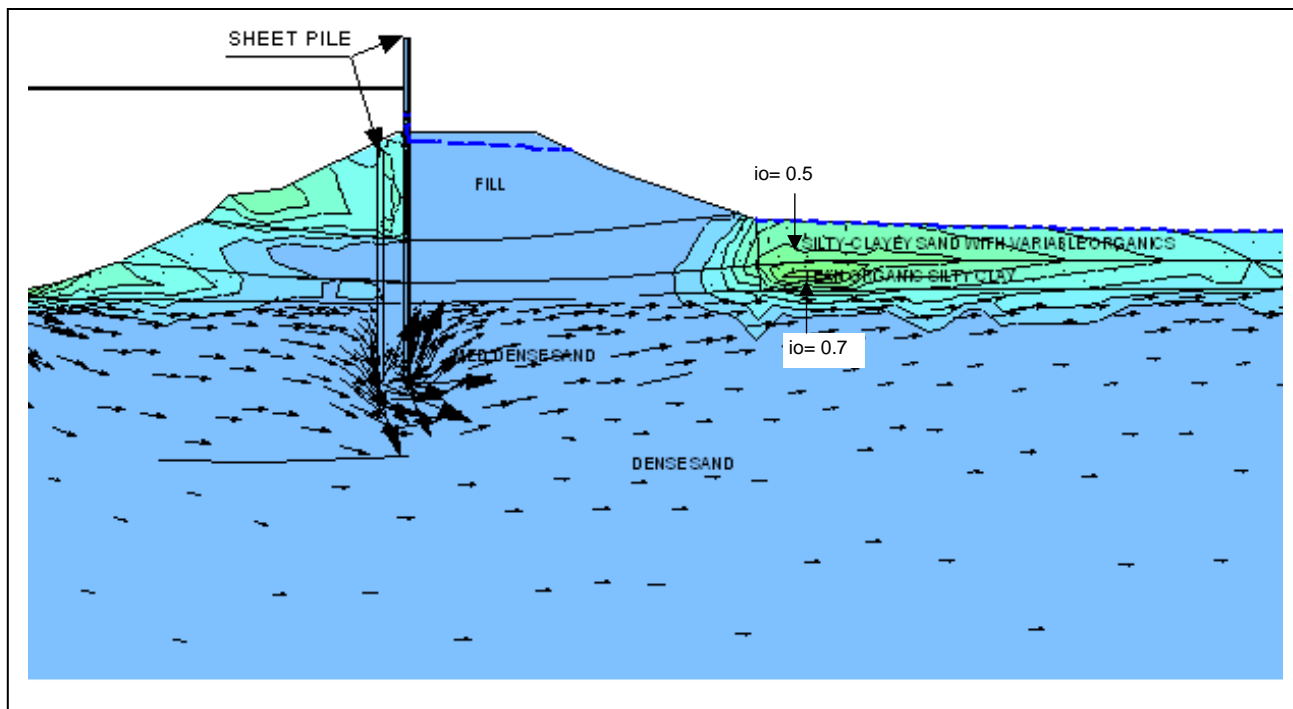


Figure 8.101: Hydraulic gradients for storm surge at +9ft (MSL) in the London Avenue Canal south breach. (Maximum toe exit gradient $i_o = 0.7$)

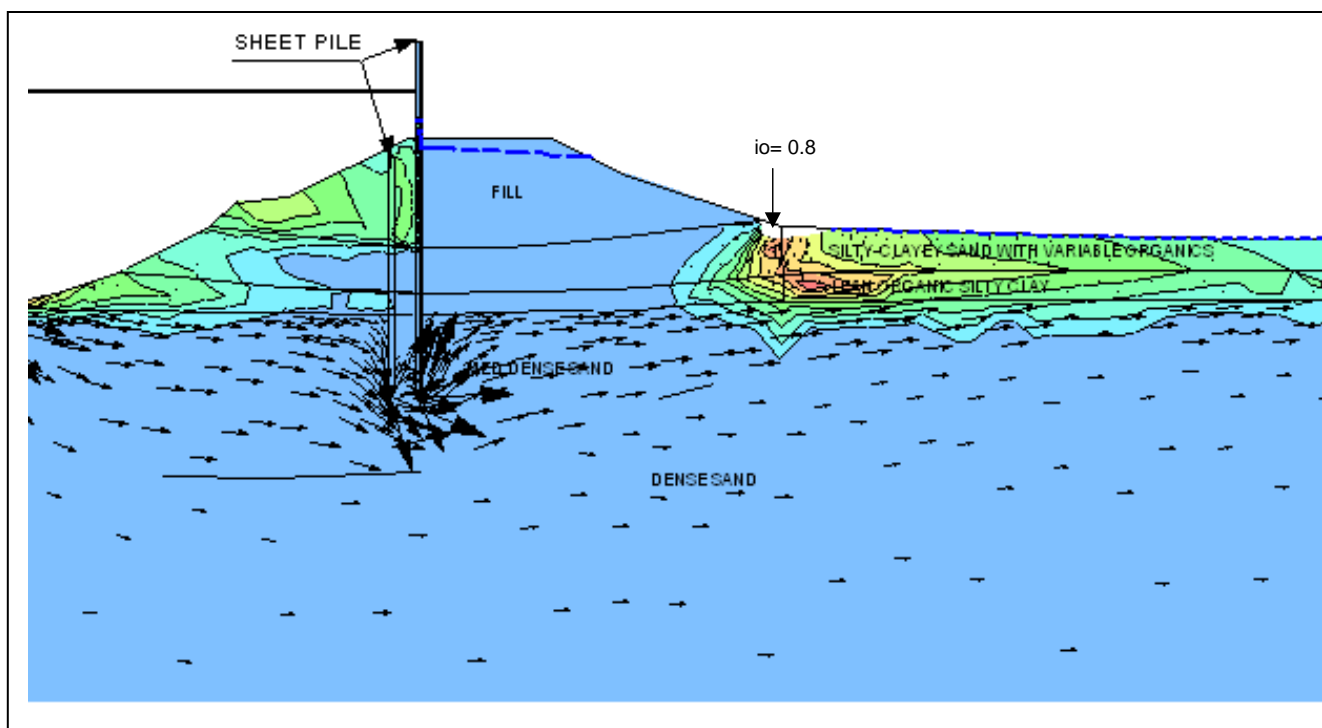


Figure 8.102: Hydraulic gradients for storm surge at +9ft (MSL) in the London Avenue Canal south breach: initiation of erosion at levee toe. (Maximum gradient $i_o = 0.8$)

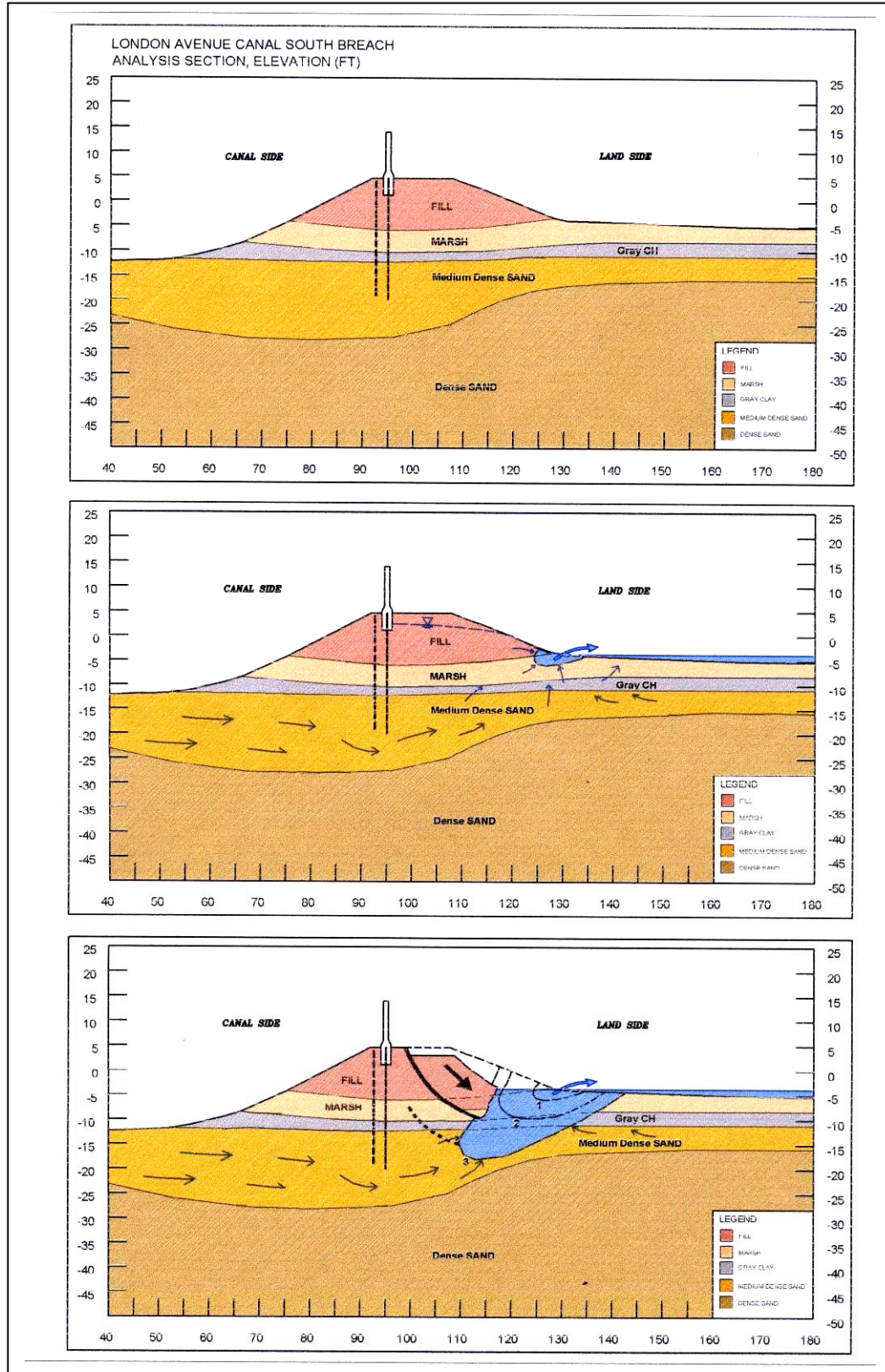


Figure 8.107: Schematic illustration of progressive erosion development at inboard toe.

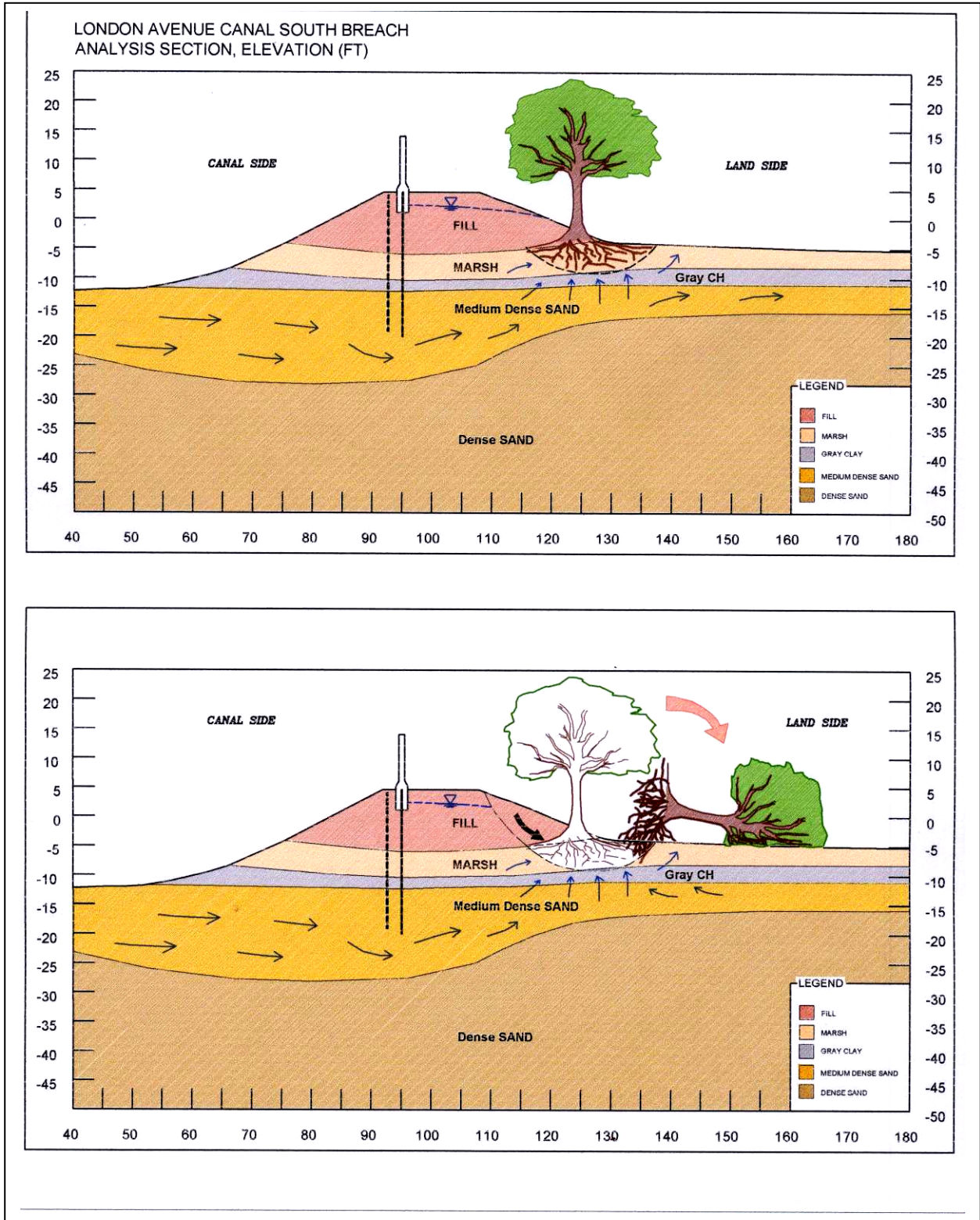


Figure 8.108: Schematic illustration of toppling of tree at inboard toe of levee.



Figure 8.109: View of the breach near the south end of the London Avenue Canal from the canal side in late September of 2005.



Figure 8.109(a): Sample across transition zone at London Avenue Canal, South Breach Section



Figure 8.110: Overhead view of the breach section on the west bank near the north end of the London Avenue Canal.



Figure 8.111: Oblique aerial view of the breached section on the west bank of the London Avenue Canal (North) and the “distressed” section on the east bank (on the left in this photo, which is taken looking to the south.)



Figure 8.112: View of the west bank breach near the north end of the London Avenue Canal from the south end showing the outboard side embankment section still in place.

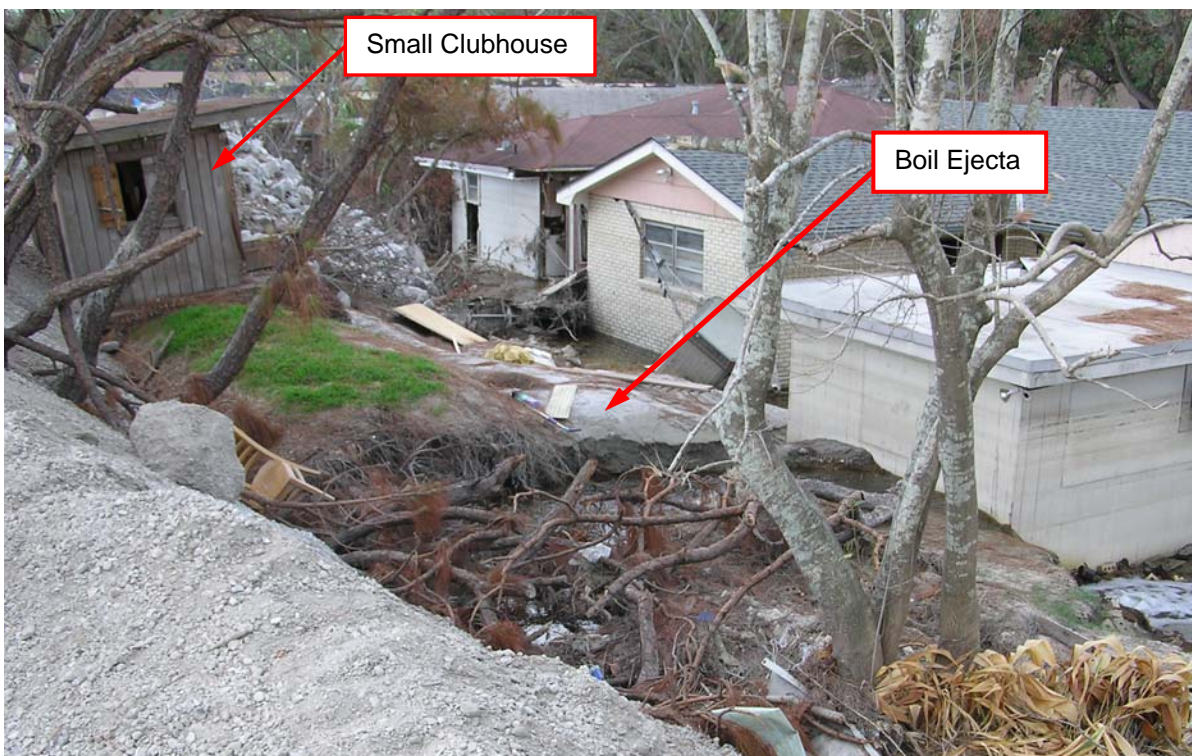


Figure 8.113: View of the inboard of the displaced embankment on the west side of the London Avenue canal showing heaving at the toe (and beneath the small wooden clubhouse), and the boil ejecta in front of the heave feature.



Figure 8.114: Water-filled gap at outboard side of east bank distressed section.

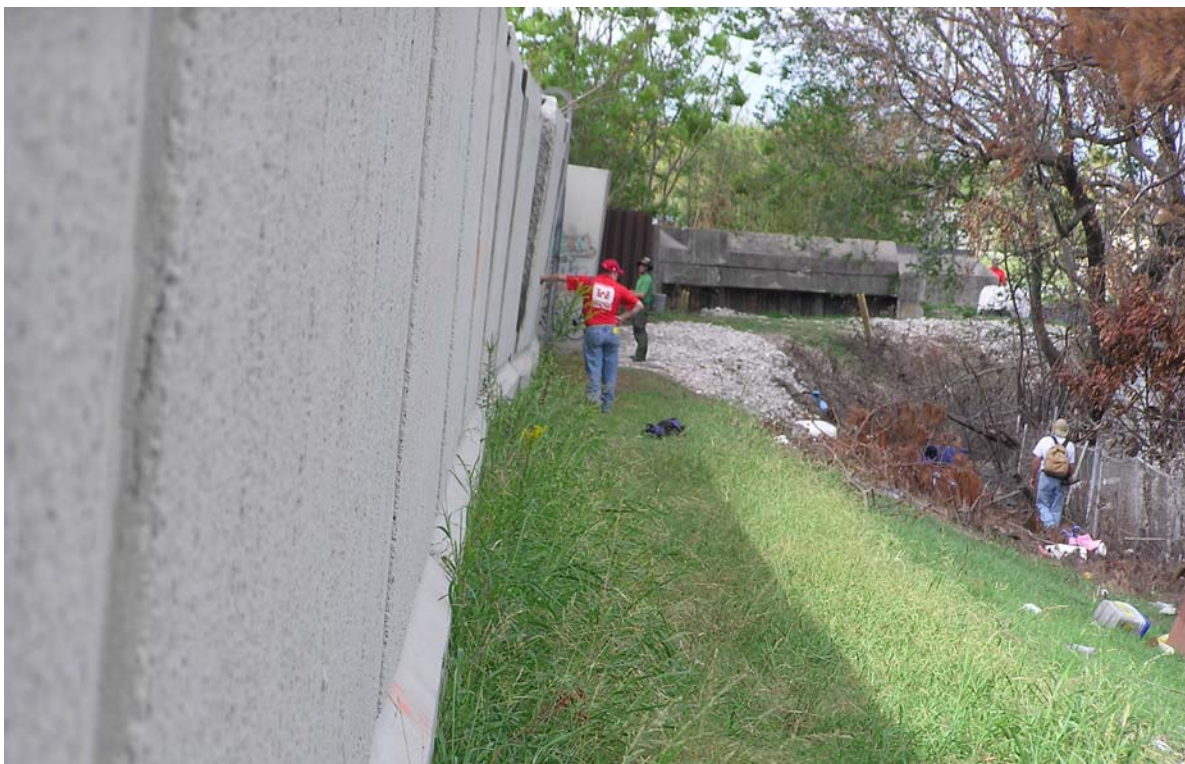


Figure 8.115: Inboard leaning floodwalls on the other side of the floodwalls shown above in Figure 8.112.



Figure 8.116: Sinkholes along the contact at the inboard side base of the floodwall and the levee crest.



Figure 8.117: Sand ejecta from toe boil, and edge of toe thrust feature; London Avenue canal (north) east bank distressed section.

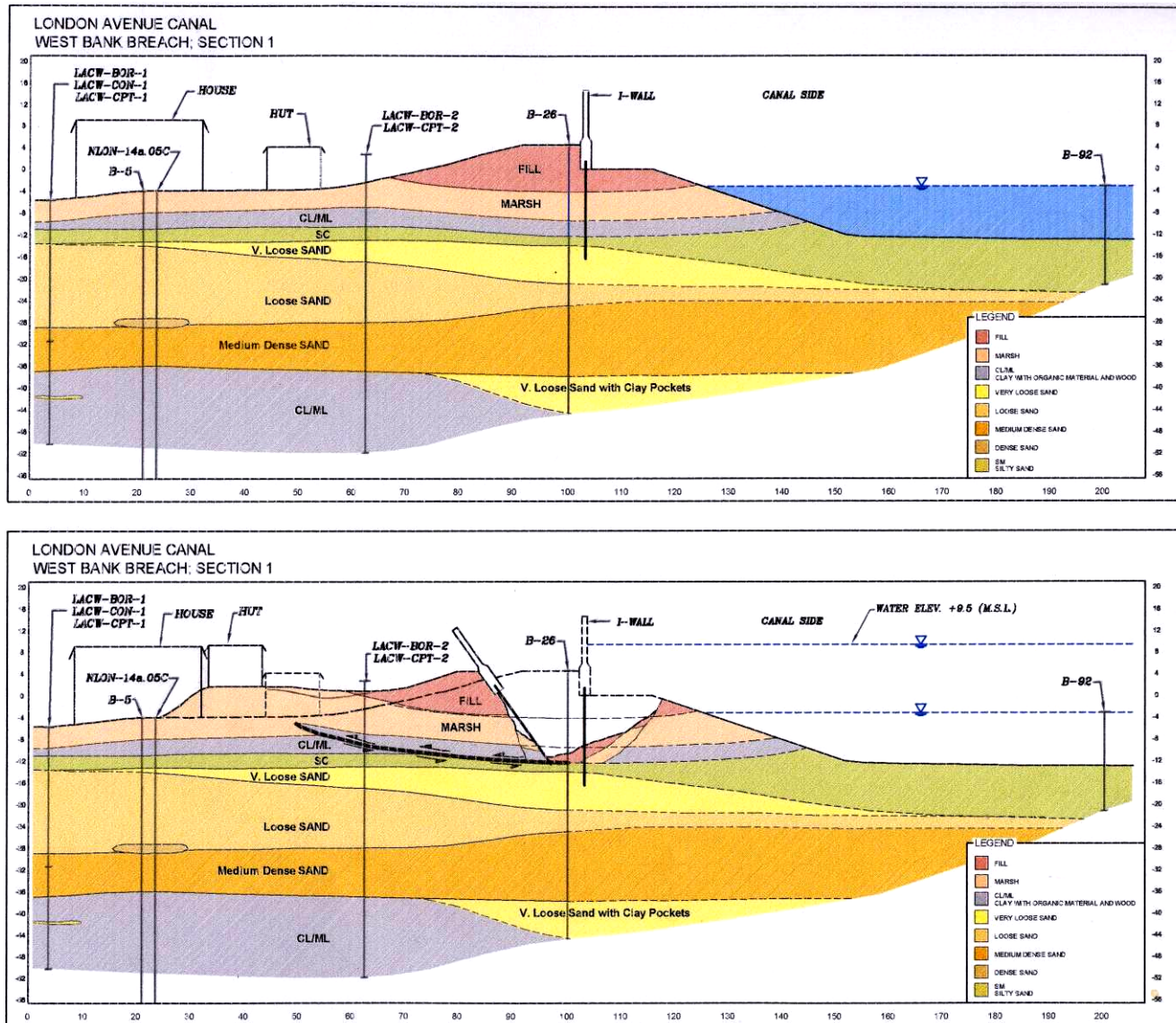


Figure 8.118: Pre-Katrina and Post-Katrina cross-section for London Avenue Canal North, west bank breach section.

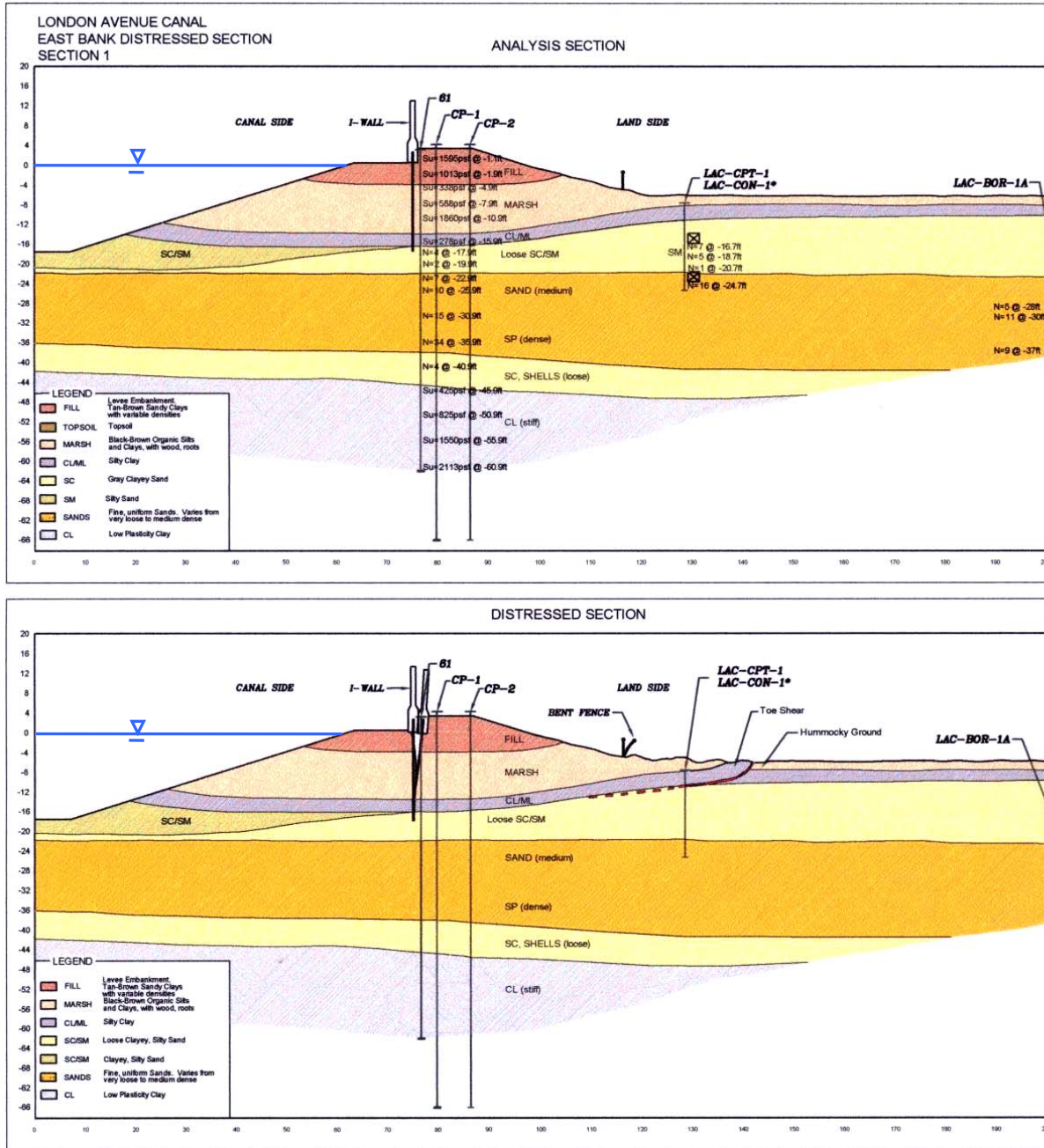


Figure 8.119: Pre-Katrina and Post-Katrina cross-section for London Avenue Canal North, east bank, distressed section.

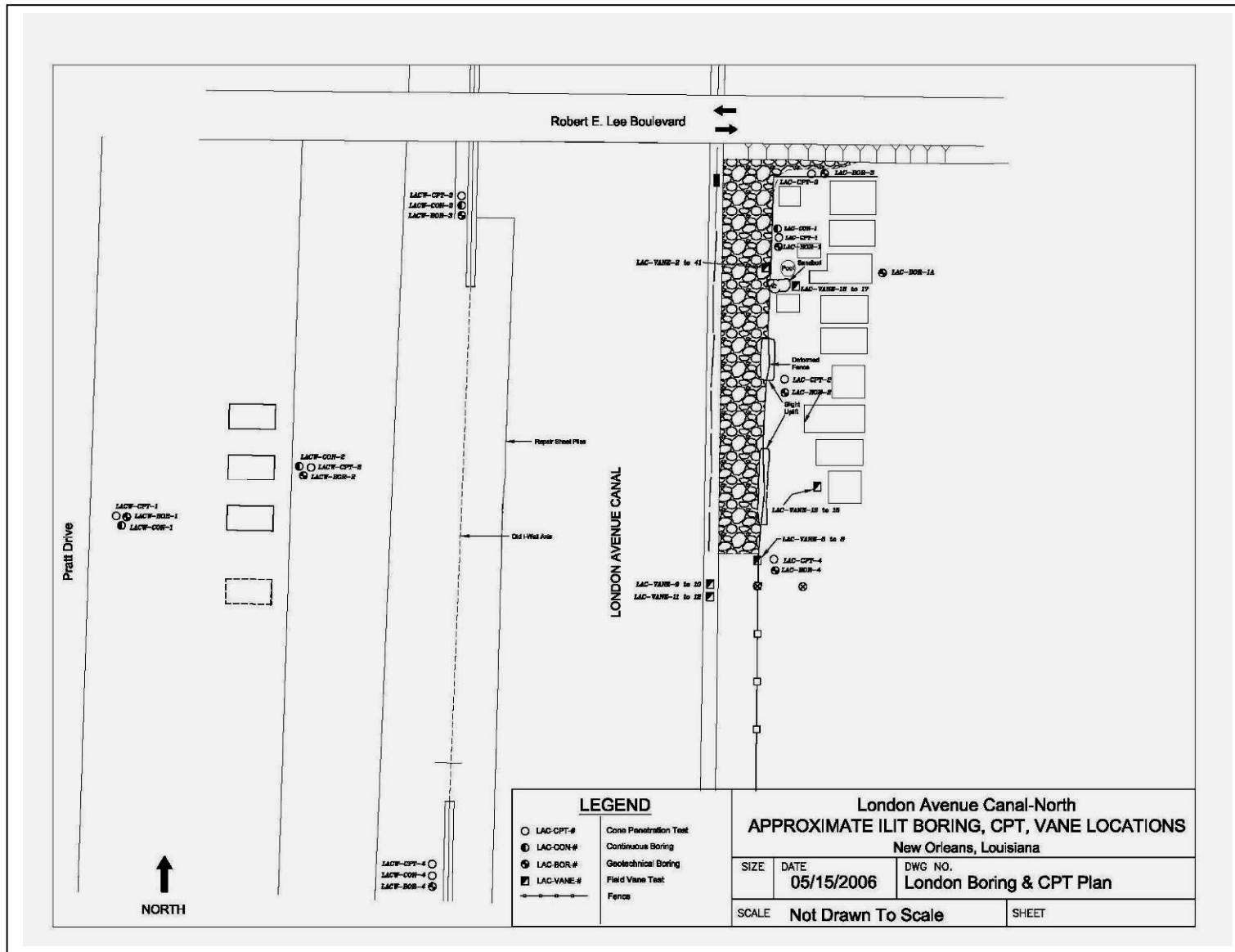


Figure 8.120: Approximate plan-view of London Avenue Canal, North, showing location of borings and CPT.

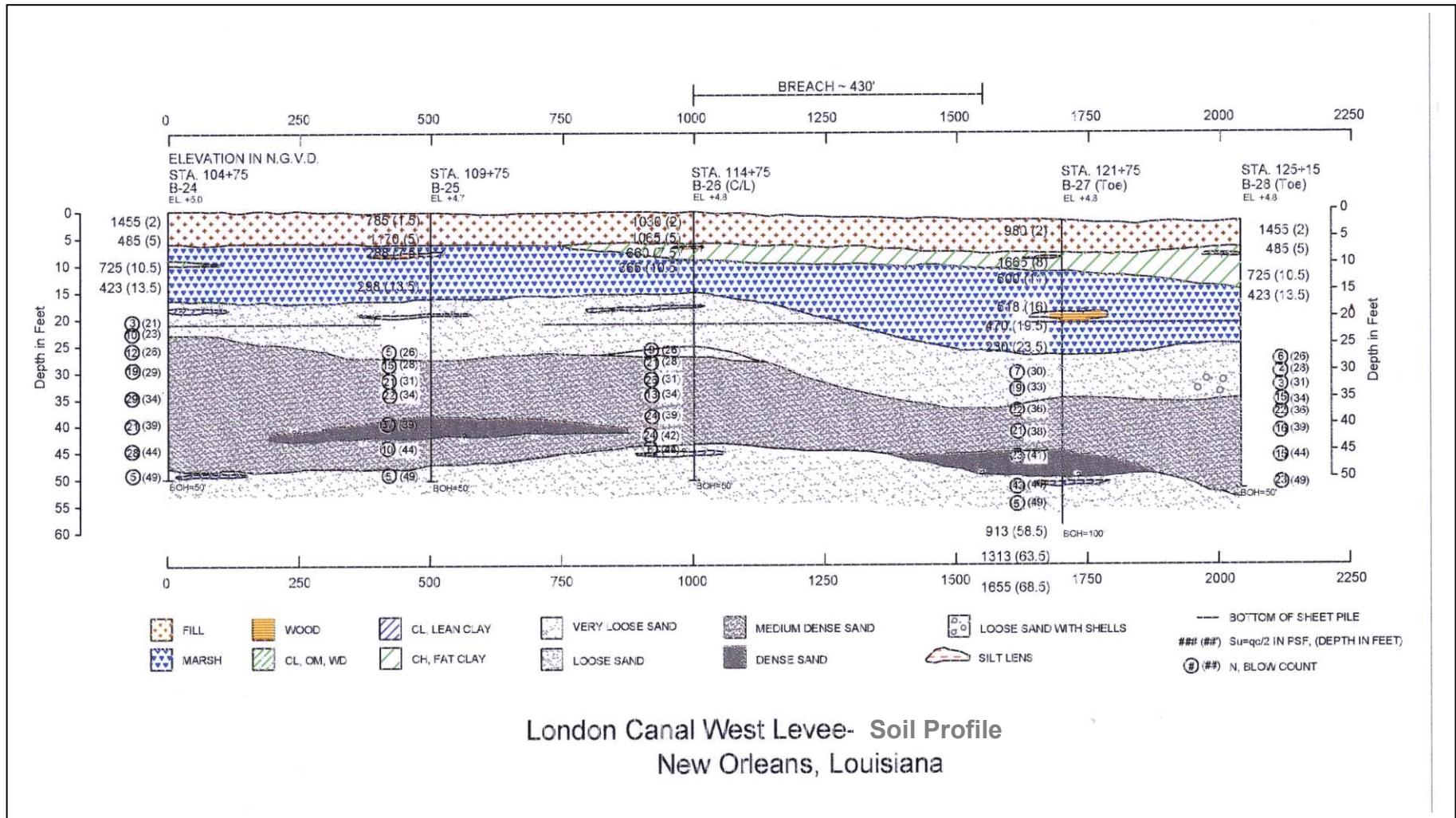


Figure 8.122: Re-interpreted longitudinal subsurface soil profile, showing location of breach section on the west bank of the London Avenue Canal, North.

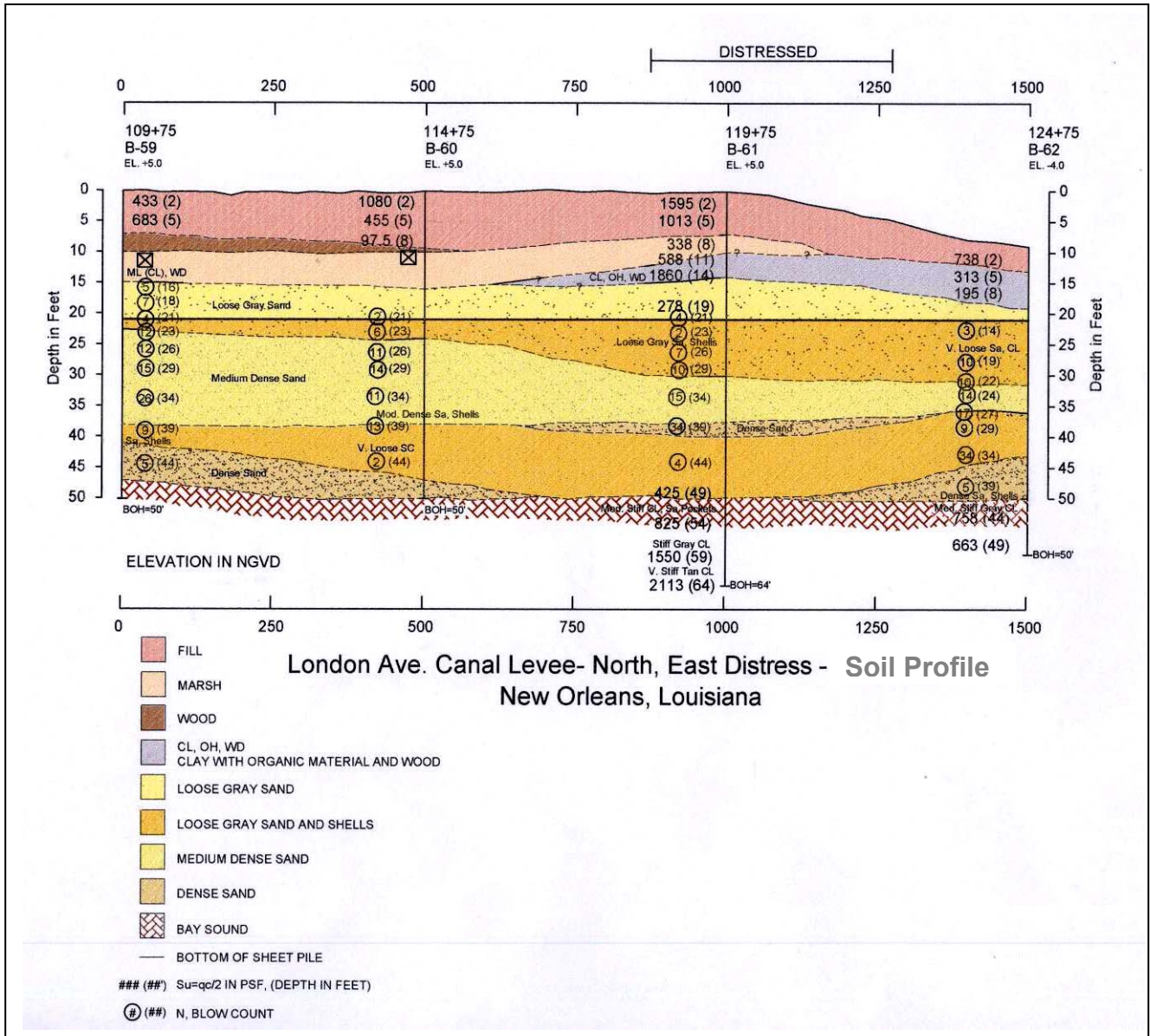
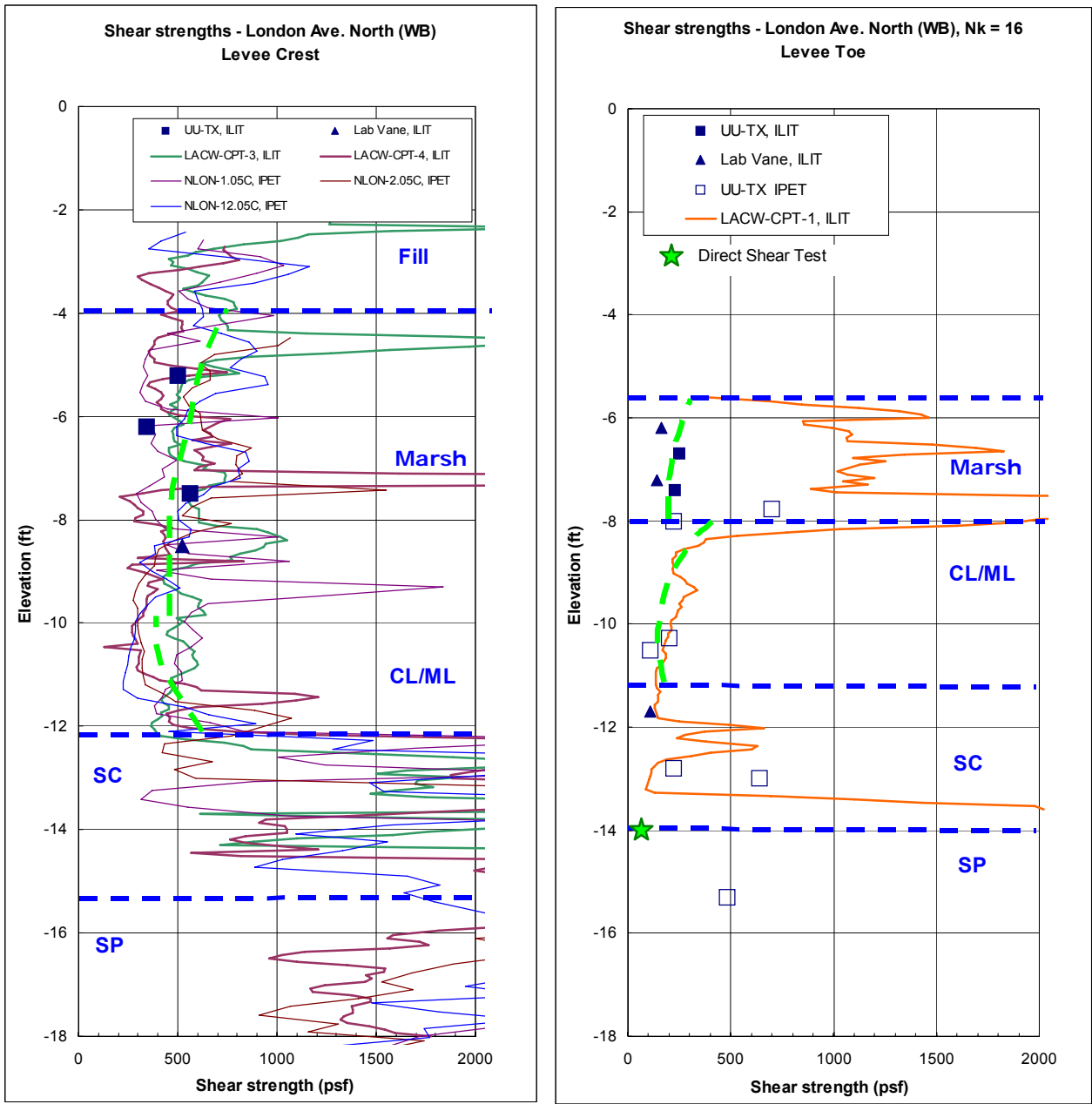


Figure 8.124: Re-interpreted longitudinal subsurface soil profile, showing location of distressed section on the east bank of the London Avenue Canal.



a) beneath crest of levee

b) at or near toe of levee

Figure 8.125: Best-estimate for shear strength (S_u) from CPT-data for London Avenue Canal west bank breach section (a) beneath the crest of the levee and (b) at or near the toe of the levee.

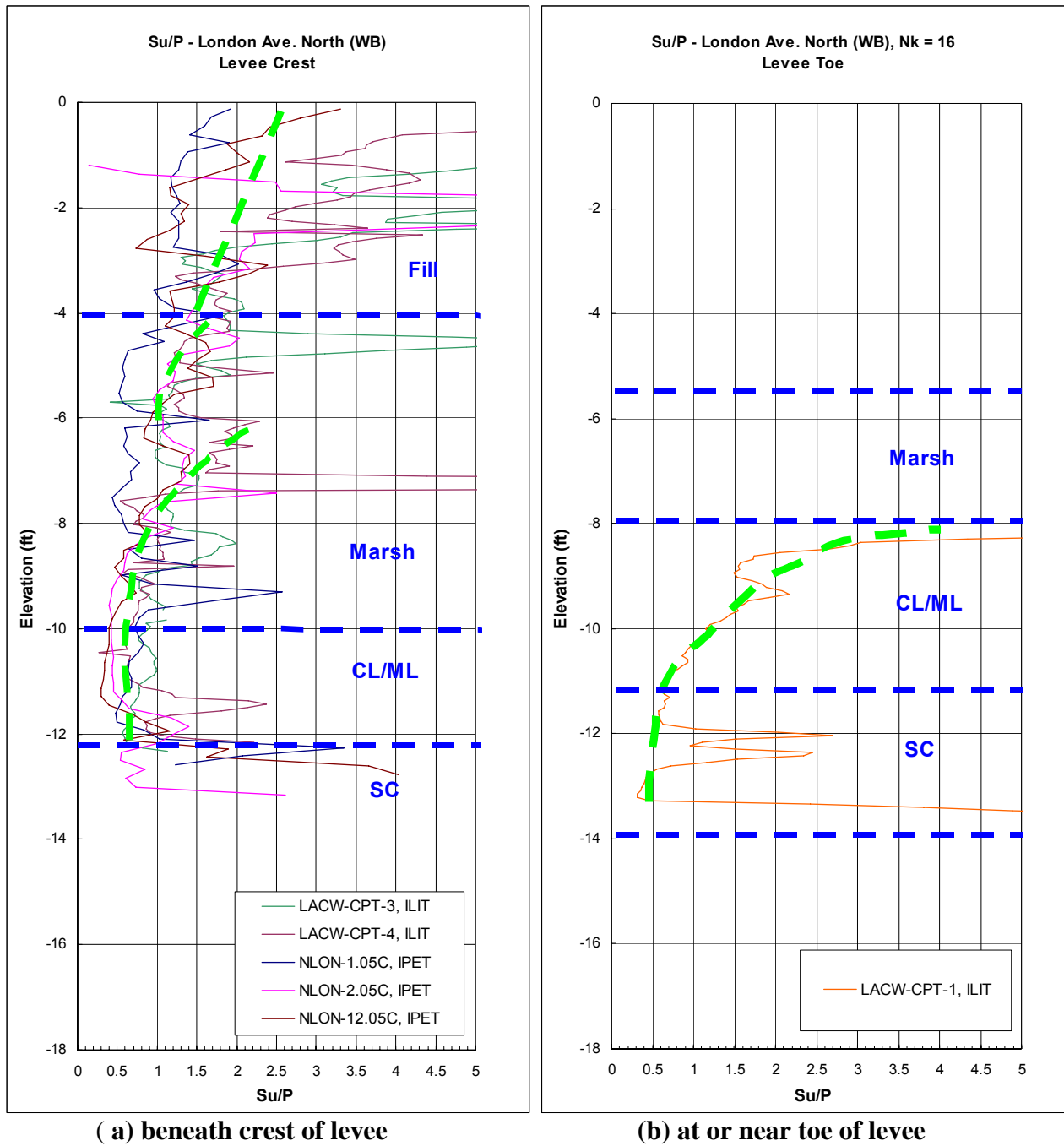


Figure 8.126: Best-estimate for Su/P from CPT-data for London Avenue Canal west bank breach section a) beneath the crest of the levee and b) at or near the toe of the levee.

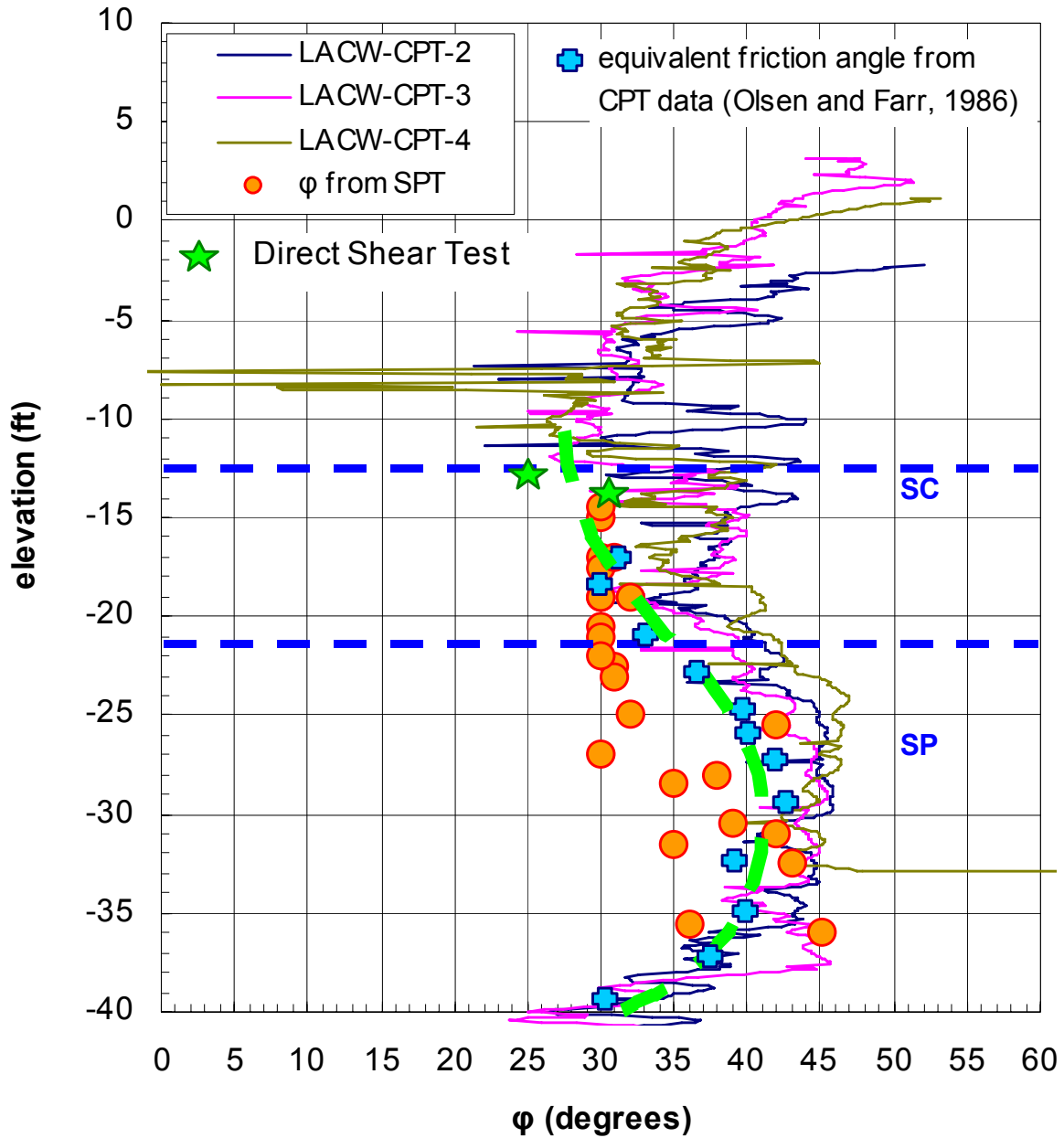
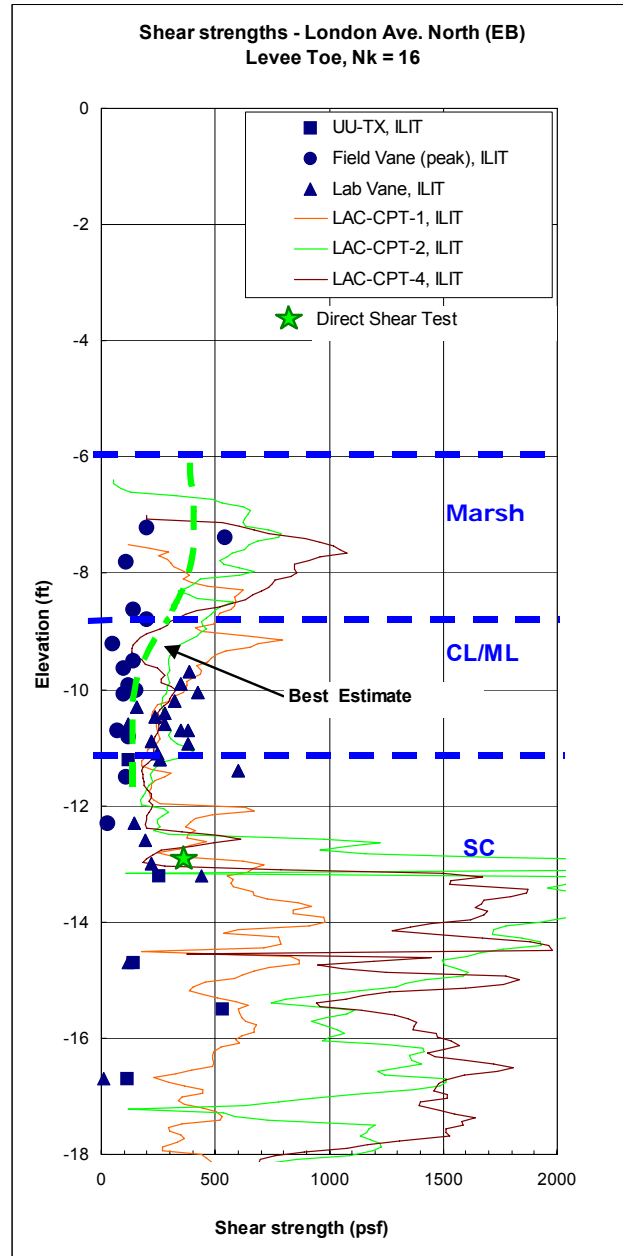
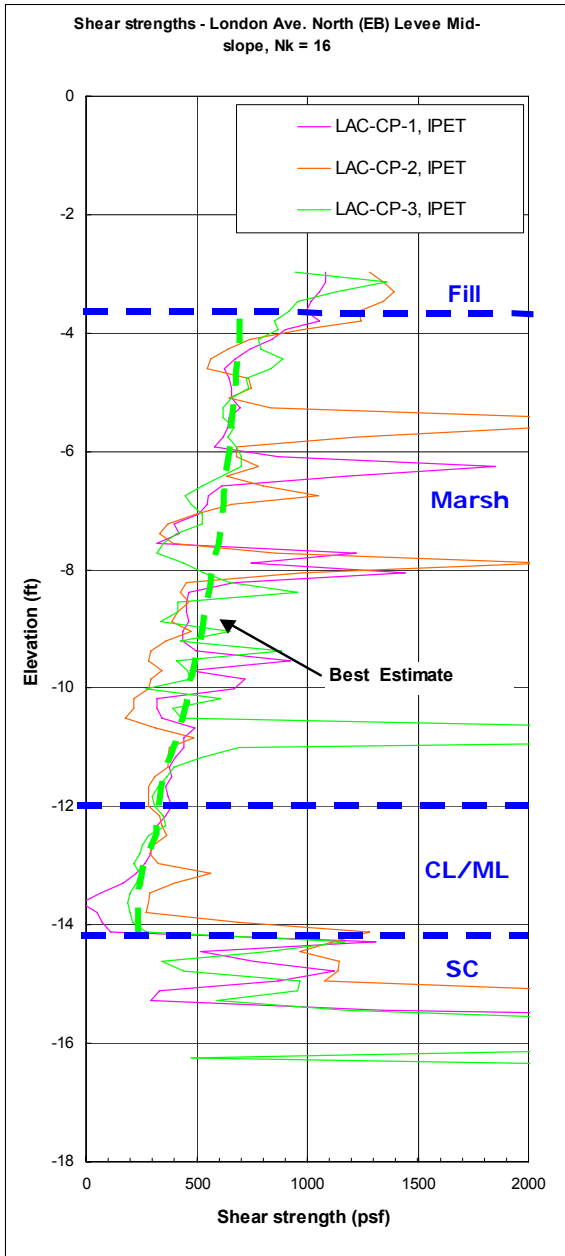


Figure 8.127: Estimation of friction angle for cohesionless materials for London Avenue Canal west bank breach section.

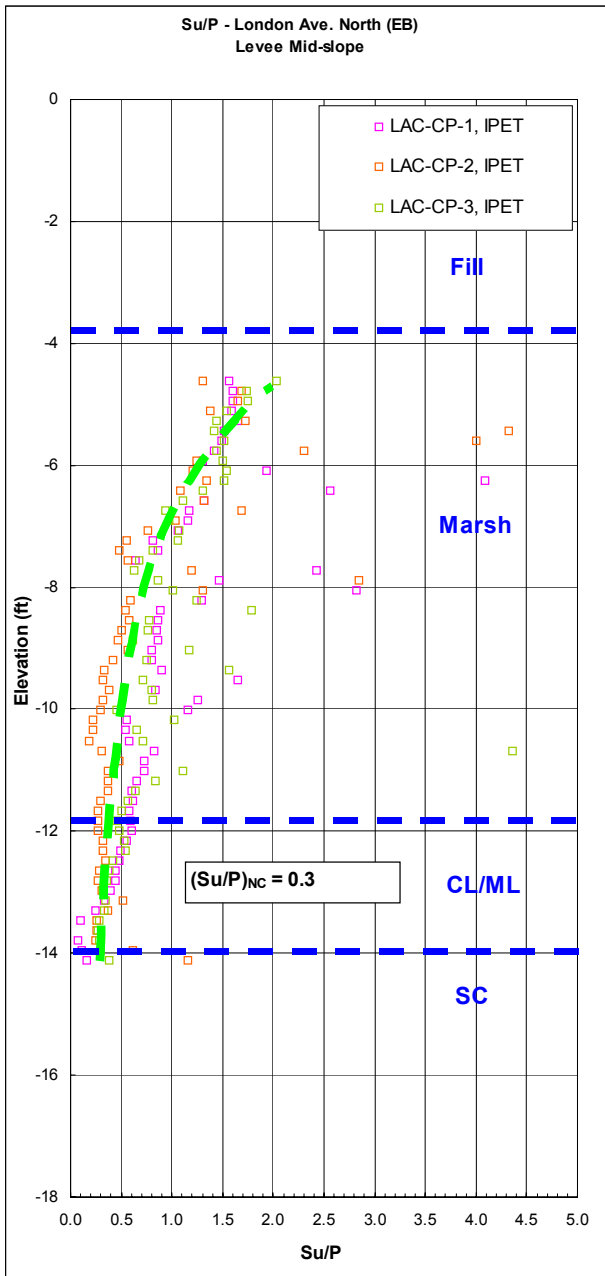
- Notes: a) The continuous lines are from Robertson and Campanella (1983)
- b) Friction angle from SPT is based on R.B. Seed's table
- c) The direct shear test was performed at the UC Berkeley geotechnical laboratory



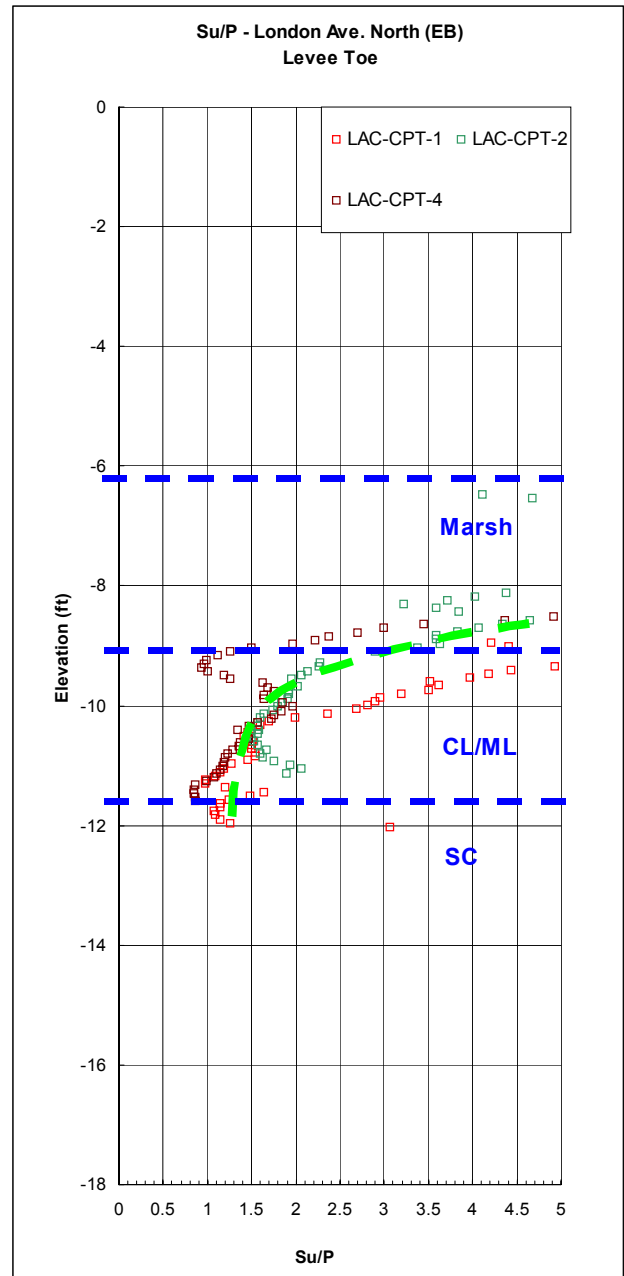
a) beneath crest of levee

b) at or near toe of levee

Figure 8.128: Best-estimate for shear strength (S_u) from CPT-data for London Avenue Canal distressed section (east bank) a) beneath the crest of the levee and b) at or near the toe of the levee.



a) beneath crest of levee



b) at or near toe of levee

Figure 8.129: Best-estimate for Su/P from CPT-data for London Avenue Canal distressed section (east bank) a) beneath the crest of the levee and b) at or near the toe of the levee

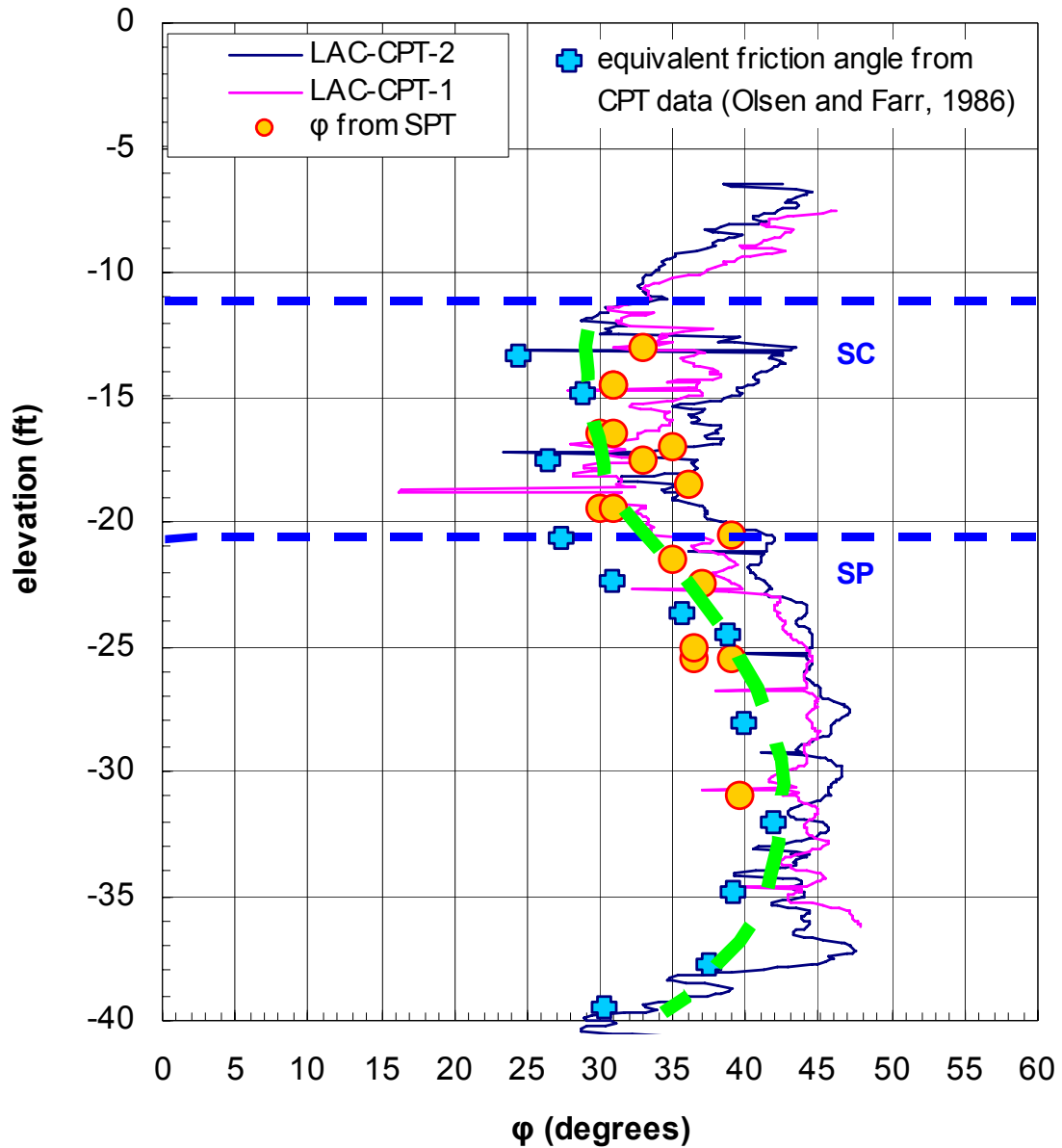


Figure 8.130: Estimation of friction angle for cohesionless materials for London Avenue Canal distressed section (east bank).

- Notes: a) The continuous lines are from Robertson and Campanella (1983)
- b) Friction angle from SPT is based on R.B. Seed's table

London Avenue Canal, North, East Bank

Geotechnical parameters for the Finite Element Analysis Model

ID	Soil Model	Description	Type	γ_{unsat} [lb/ft ³]	γ_{sat} [lb/ft ³]	k_x [ft/day]	k_y [ft/day]	ν [-]	E_{ref} [lb/ft ²]	c_{ref} [lb/ft ²]	ϕ [°]
fill	Mohr Coulomb	(Non-engineered Fill / Fill)	Undrained	70	90	2.80E-03	2.80E-04	0.35	1.00E+06	800	0.001
marsh		marsh	Undrained	50	80	28.3	2.83	0.35	2.80E+05	550	0.001
CL/ML		silty low-PI clay (traces organic)	Undrained	70	90	2.80E-03	2.80E-04	0.35	9.00E+05	250	0.001
SC/SM		clayey, silty sand	Drained	90	100	2.33	1.15	0.3	5.00E+05	0.001	30
SP_1		loose sand	Drained	90	100	2.33	2.33	0.25	9.00E+05	0.001	33
SP_2		medium dense sand	Drained	100	110	2.33	2.33	0.25	1.00E+06	0.001	36
SP_3		dense sand	Drained	110	115	2.33	2.33	0.25	1.50E+06	0.001	40
CH		grey clay (Bay Sound)	Undrained	95	105	2.80E-03	2.80E-04	0.35	1.00E+06	600	0.001

London Avenue Canal, North, West Bank

Geotechnical parameters for the Finite Element Analysis Model

ID	Soil Model	Description	Type	γ_{unsat} [lb/ft ³]	γ_{sat} [lb/ft ³]	k_x [ft/day]	k_y [ft/day]	ν [-]	E_{ref} [lb/ft ²]	c_{ref} [lb/ft ²]	ϕ [°]
fill	Mohr Coulomb	(Non-engineered Fill / Fill)	Undrained	70	90	2.80E-03	2.80E-04	0.35	1.00E+06	800	0.001
marsh		marsh	Undrained	50	80	28.3	2.83	0.35	2.80E+05	450	0.001
CL/ML		silty low-PI clay (traces organic)	Undrained	70	90	2.80E-03	2.80E-04	0.35	9.00E+05	300	0.001
SC/SM		clayey, silty sand	Drained	90	100	2.33	1.15	0.3	5.00E+05	0.001	29
SP_1		loose sand	Drained	90	100	2.33	2.33	0.25	9.00E+05	0.001	33
SP_2		medium dense sand	Drained	100	110	2.33	2.33	0.25	1.00E+06	0.001	36
SP_3		dense sand	Drained	110	115	2.33	2.33	0.25	1.50E+06	0.001	40
CH		grey clay (Bay Sound)	Undrained	95	105	2.80E-03	2.80E-04	0.35	1.00E+06	600	0.001

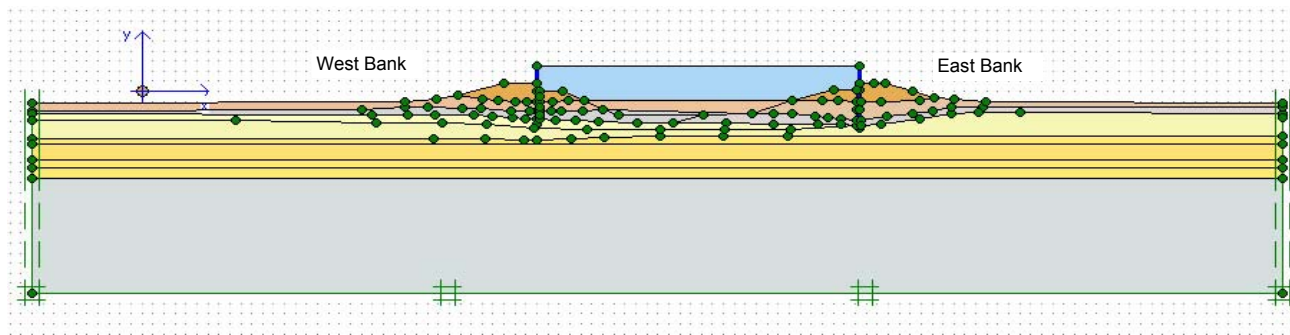


Figure 8.131: Geometry and input parameters for FEM analyses for London Avenue Canal, North (east and west banks)

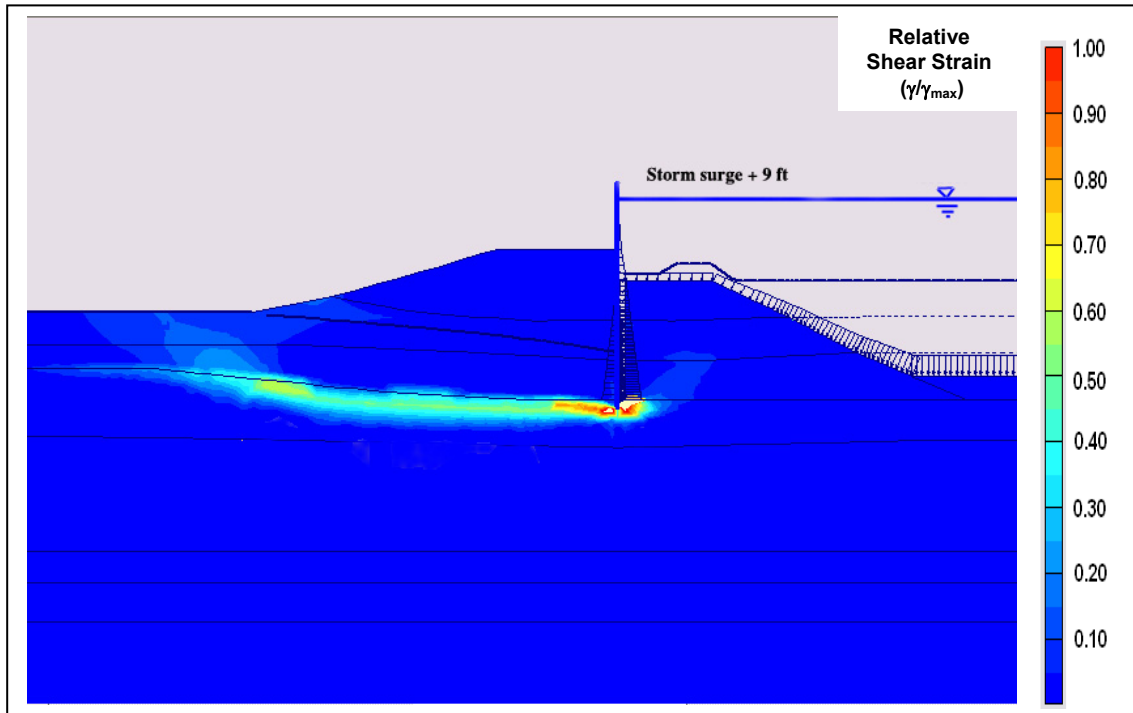


Figure 8.132: Normalized shear strain contours (shear strain divided by strain to failure) for a storm surge at Elev. + 9 feet (MSL) at the London Avenue Canal breach site (west bank); gapping at outboard toe of floodwall is developed to full depth.

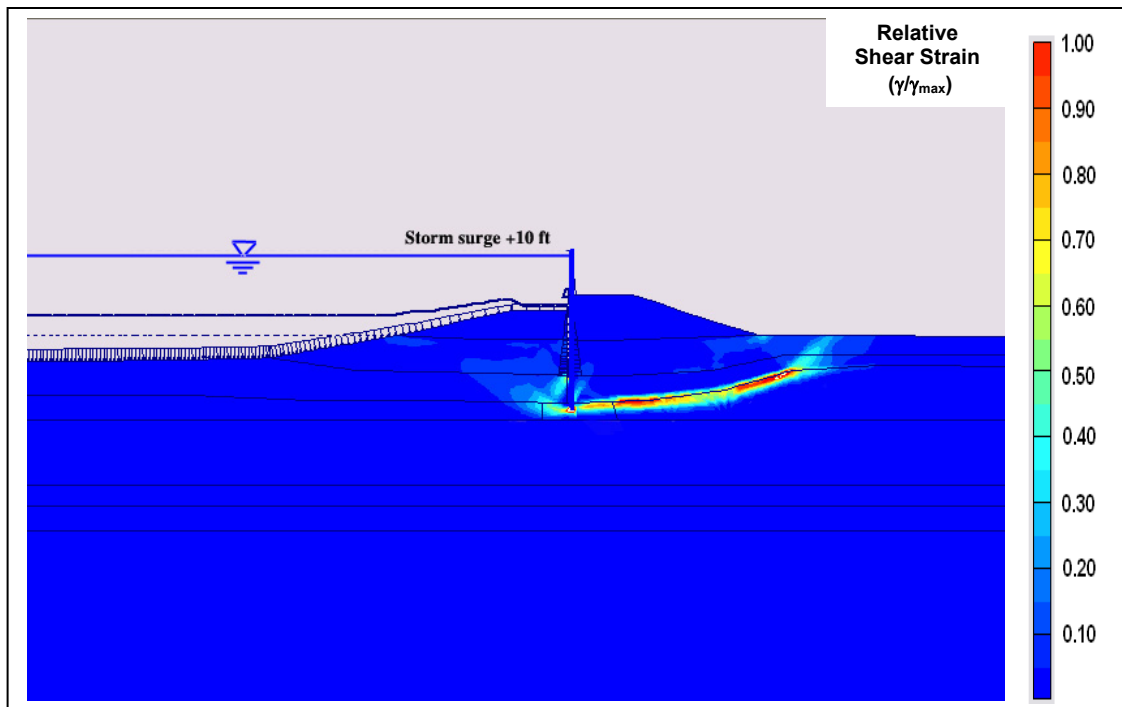


Figure 8.133: Normalized shear strain contours (shear strain divided by strain to failure) for a storm surge at Elev. + 10 feet (MSL) at the London Avenue Canal distressed site (east bank); gapping at outboard toe of floodwall is developed.

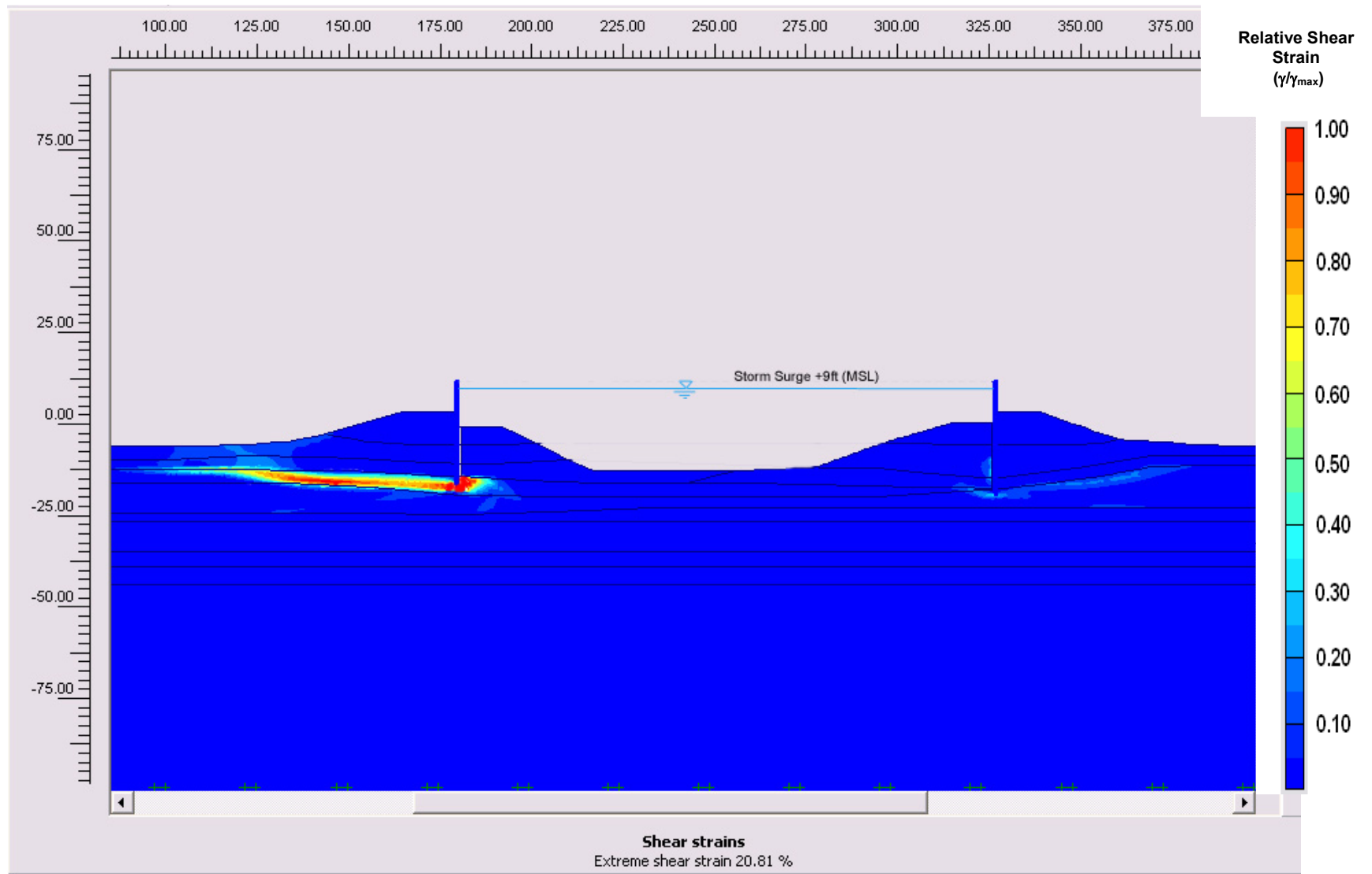


Figure 8.134: Normalized shear strain contours (shear strain divided by strain to failure) for a storm surge at Elev. + 9 feet (MSL) at the London Avenue Canal (east and west banks).

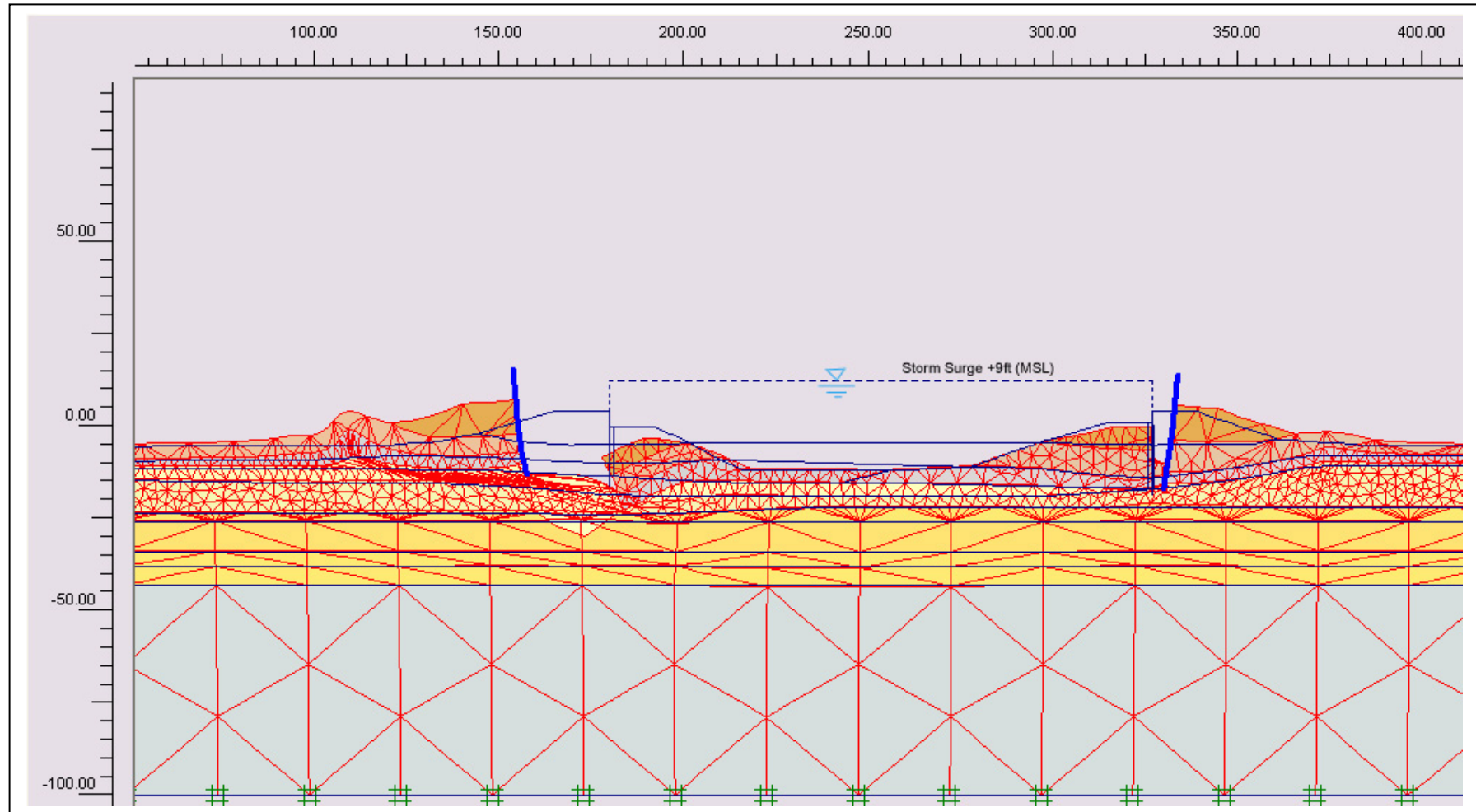


Figure 8.135: Deformed mesh for a storm surge elevation + 9 feet (MSL), London Avenue Canal (east and west banks). Displacements are exaggerated for clarity.

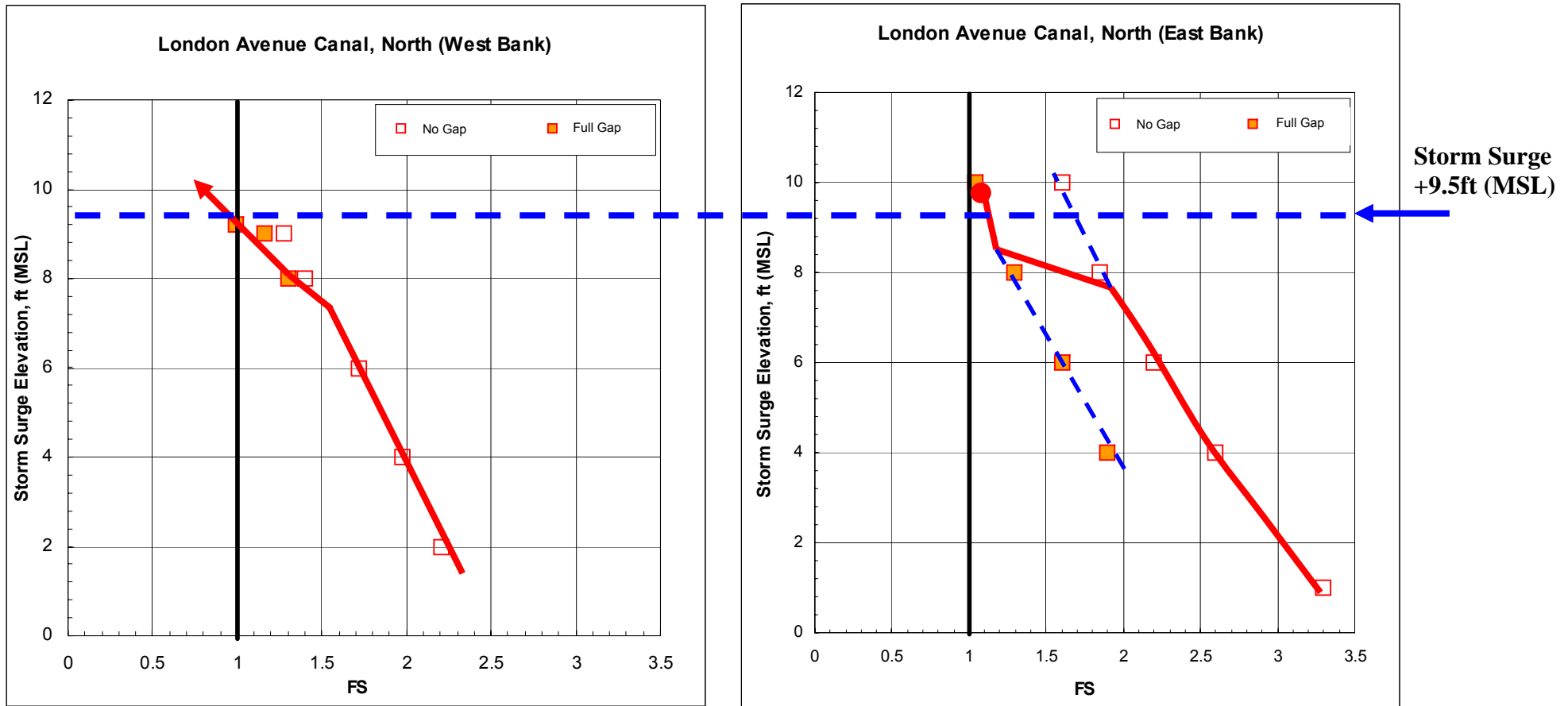


Figure 8.136: Calculated Factors of Safety for two modes based on PLAXIS analyses of the London Avenue Canal breach and distressed section for various canal water elevations; showing the best-estimated path to failure.

ID	Soil Model	Type	γ	c	ϕ	k
			[lb/ft ³]	[lb/ft ²]	[°]	[ft/hr]
Upper fill	Mohr-Coulomb	Undrained	100	800	0	1.17E-04
Marsh, crest	Mohr-Coulomb	Undrained	80	475	0	1.17
Marsh, free field	Mohr-Coulomb	Undrained	80	200	0	1.17
CL/ML, crest	Mohr-Coulomb	Undrained	85	500	0	2.00E-04
CL/ML, free field	Mohr-Coulomb	Undrained	85	300	0	2.00E-04
SC	Mohr-Coulomb	Drained	100	0	30	0.097
Loose Sand	Mohr-Coulomb	Drained	100	0	33	0.333
Dense Sand	Mohr-Coulomb	Drained	105	0	36	0.09
Stiff Clay	Mohr-Coulomb	Undrained	90	600	0	2.00E-04

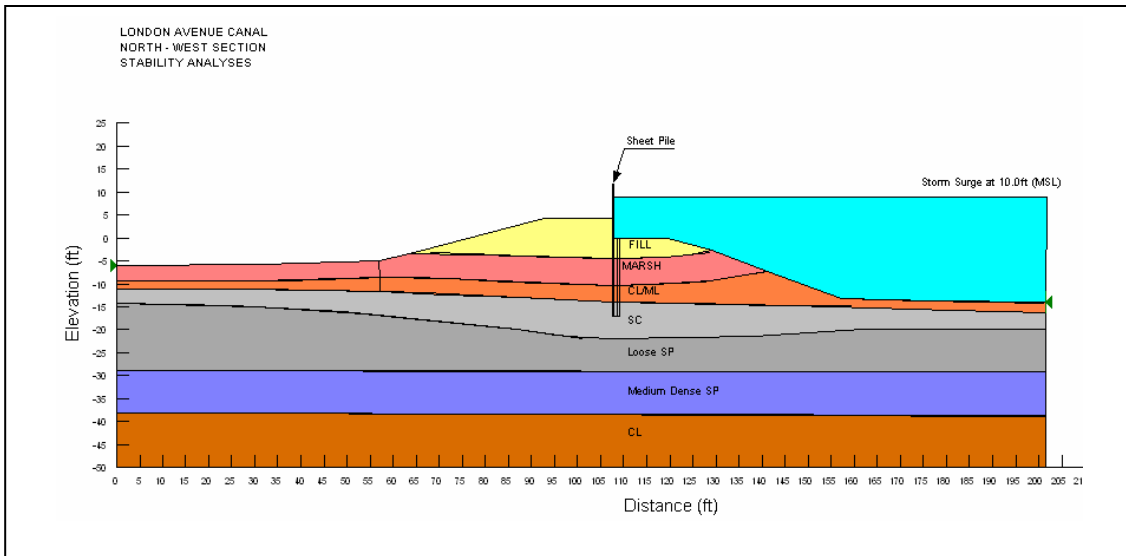


Figure 8.137: Geometry and input parameters for Limit Equilibrium and Steady State seepage analyses for London Avenue Canal North, West bank.

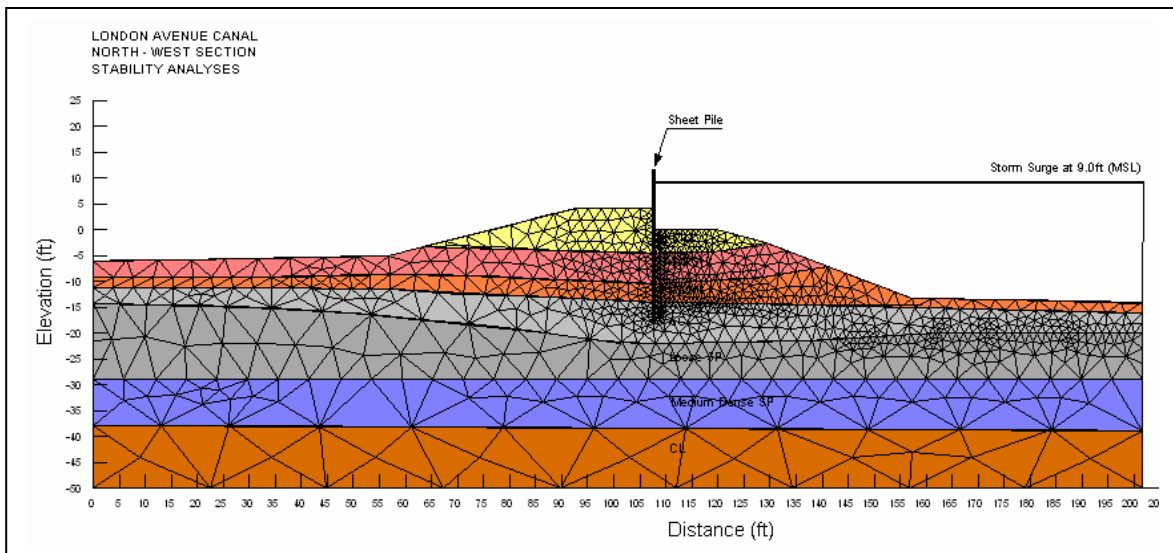


Figure 8.138: Finite Difference mesh for Steady State seepage Analyses for London Avenue Canal North, West bank.

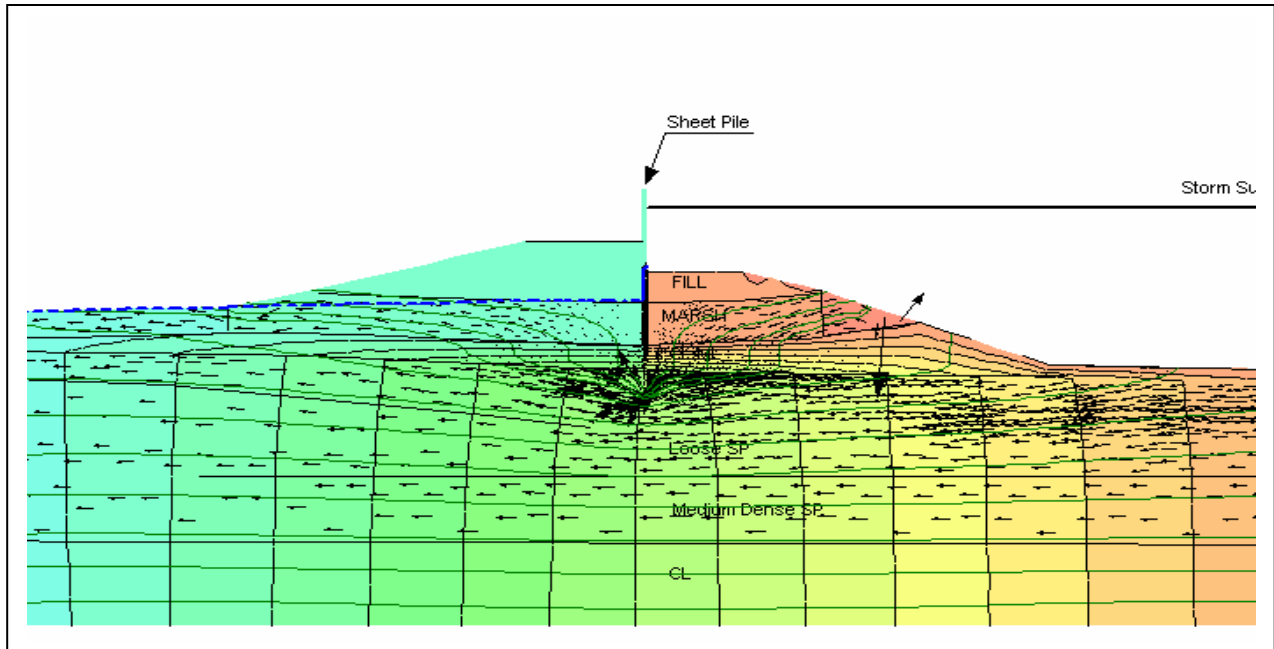


Figure 8.139: Flow net generation without the gapping in the outboard toe of the floodwall, London Avenue Canal North, West bank. Storm surge at 9ft (MSL).

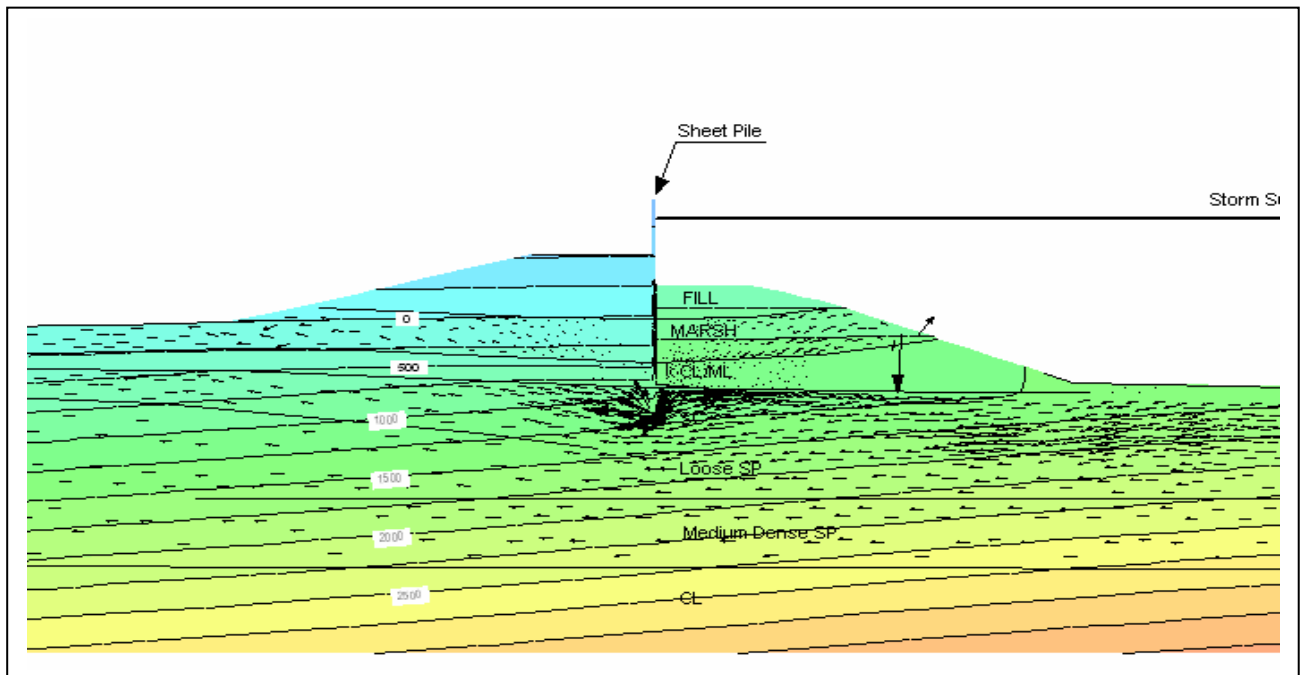


Figure 8.140: Pore water pressure contours without the gapping in the outboard toe of the floodwall, London Avenue Canal North, West bank. Storm surge at 9ft (MSL).

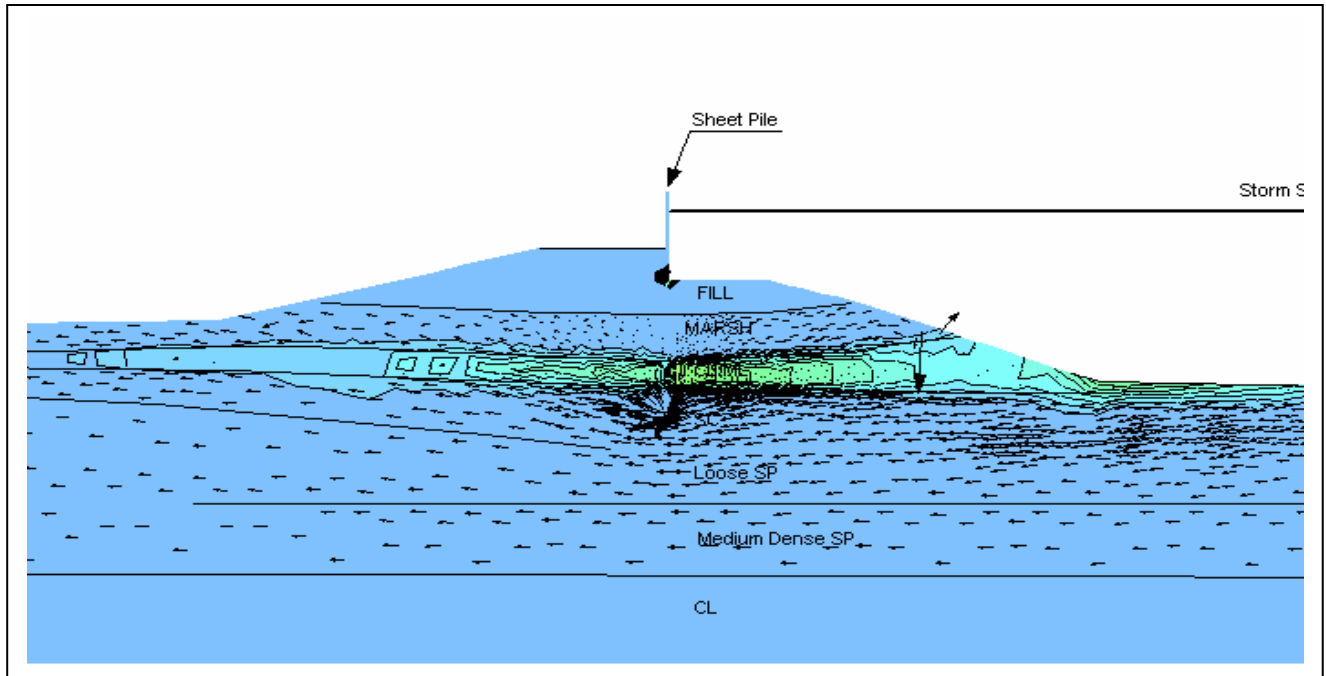


Figure 8.141: Hydraulic gradient contours without the gapping in the outboard toe of the floodwall, London Avenue Canal North, West bank. Storm surge at 9ft (MSL). Exit gradient at the inboard toe is 0.20.

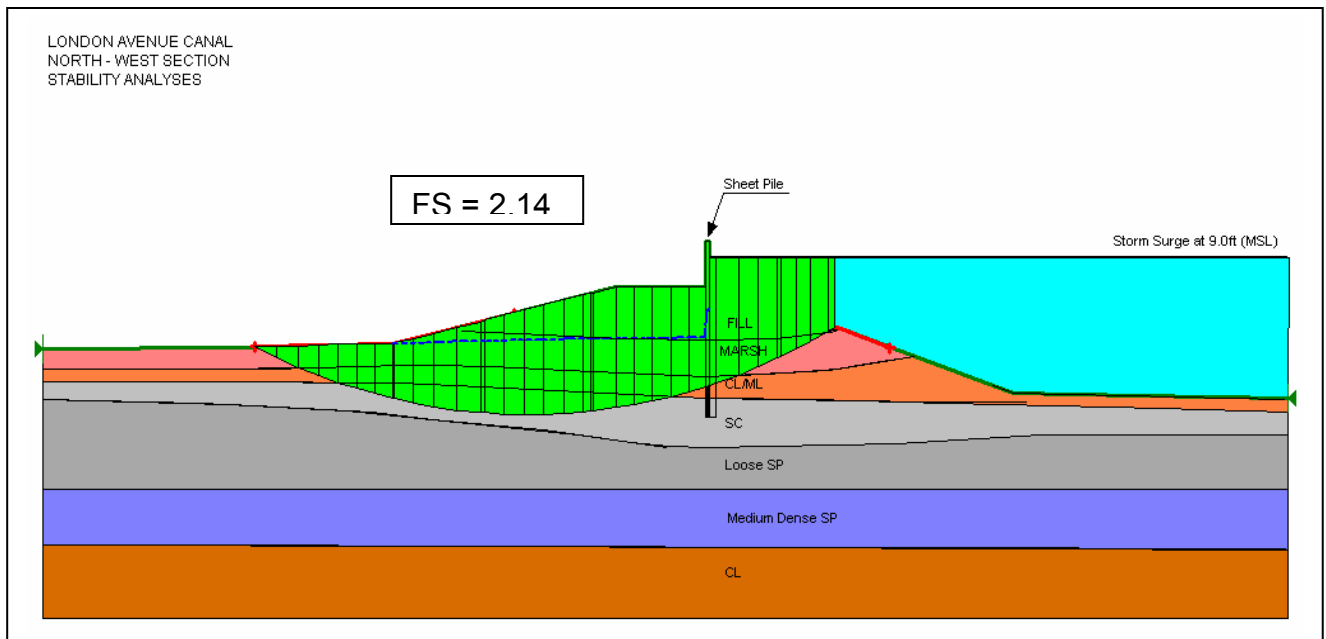


Figure 8.142: Critical failure surface without the gapping in the outboard toe of the floodwall, London Avenue Canal North, West bank. Storm surge at 9ft (MSL).

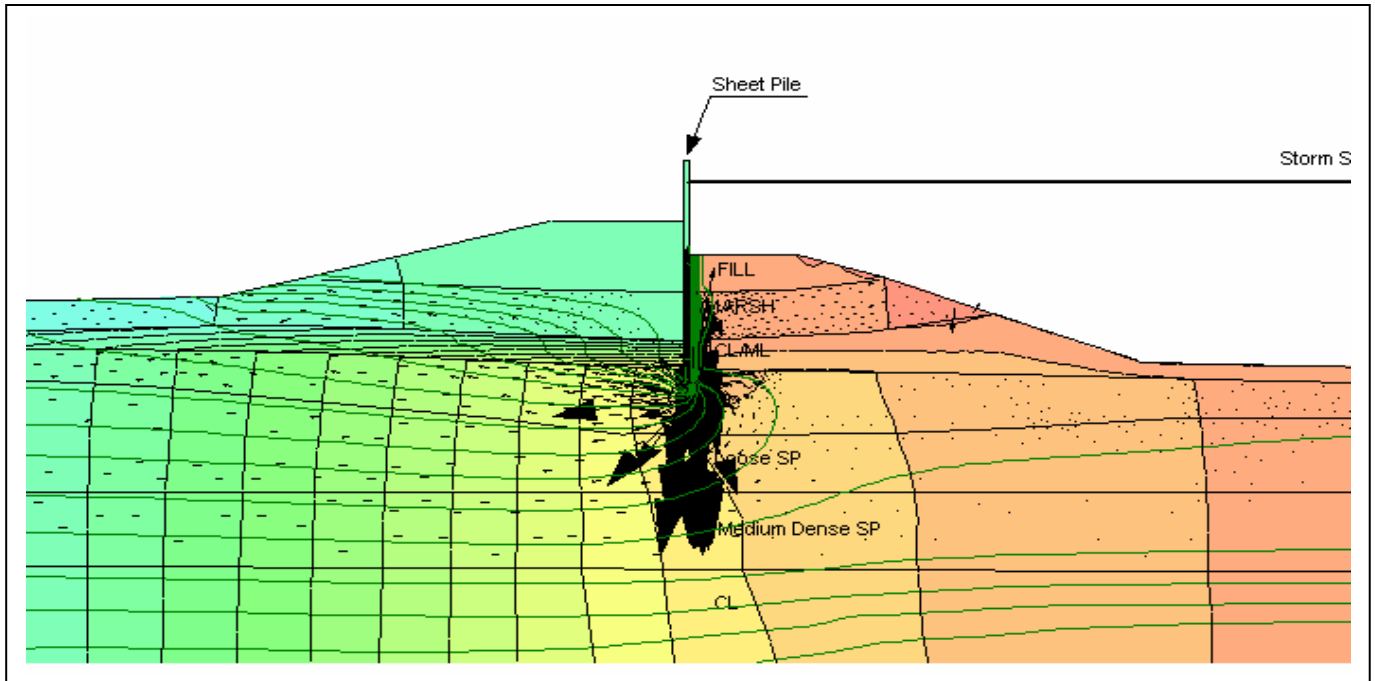


Figure 8.143: Flow net generation with the gapping in the outboard toe of the floodwall, London Avenue Canal North, West bank. Storm surge at 9ft (MSL).

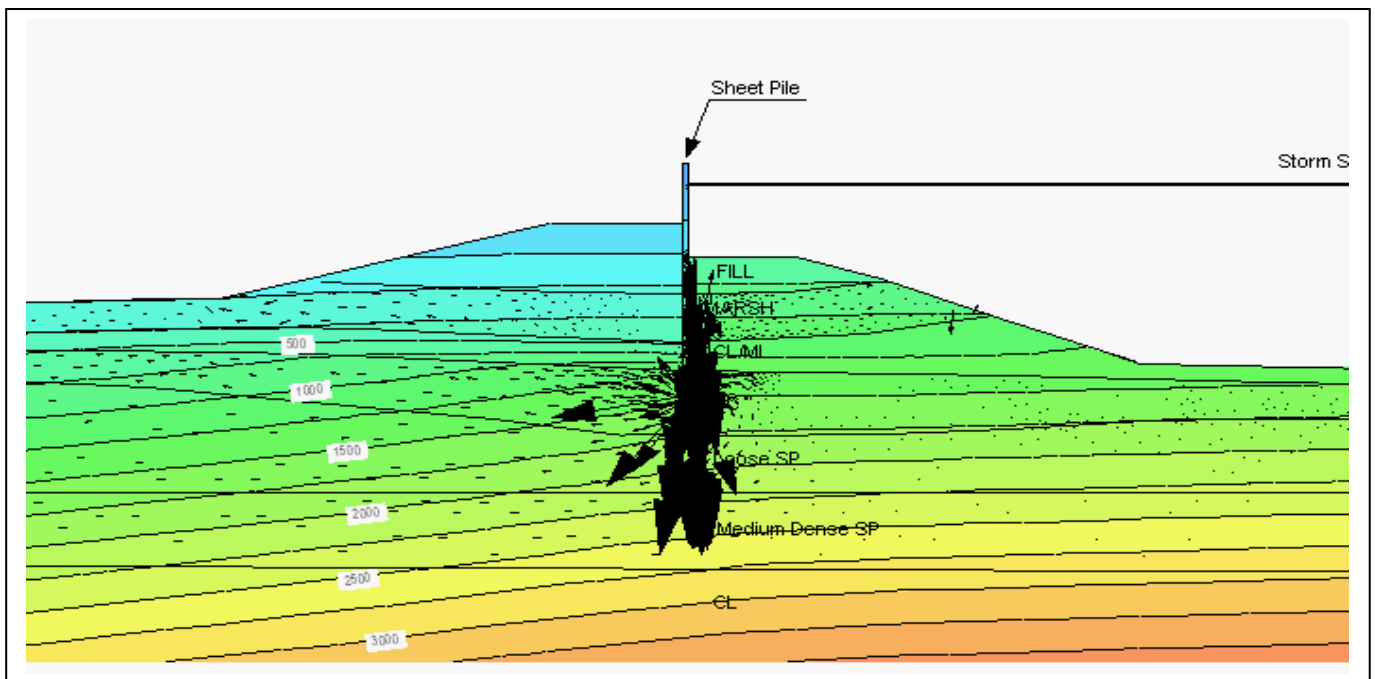


Figure 8.144: Pore water pressure contours with the gapping in the outboard toe of the floodwall, London Avenue Canal North, West bank. Storm surge at 9ft (MSL).

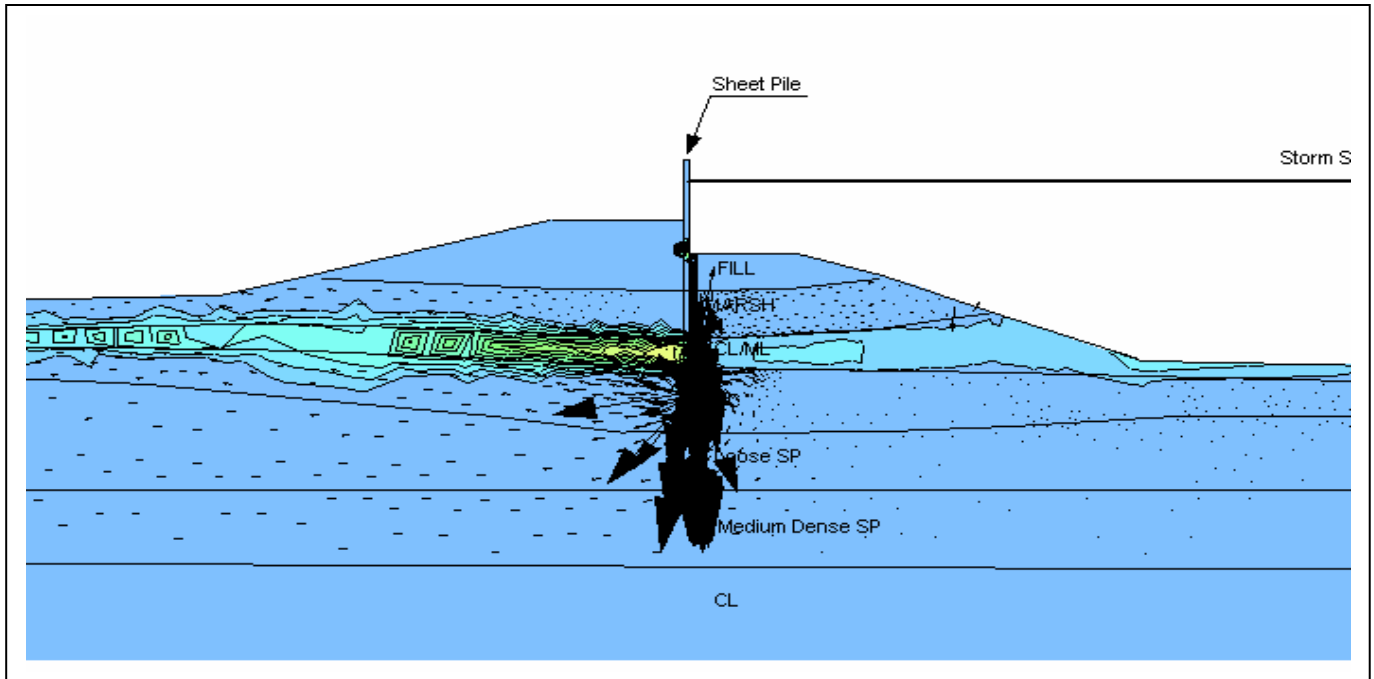


Figure 8.145: Hydraulic gradient contours with the gapping in the outboard toe of the floodwall, London Avenue Canal North, West bank. Storm surge at 9ft (MSL). Exit gradient at the inboard toe is 0.32.

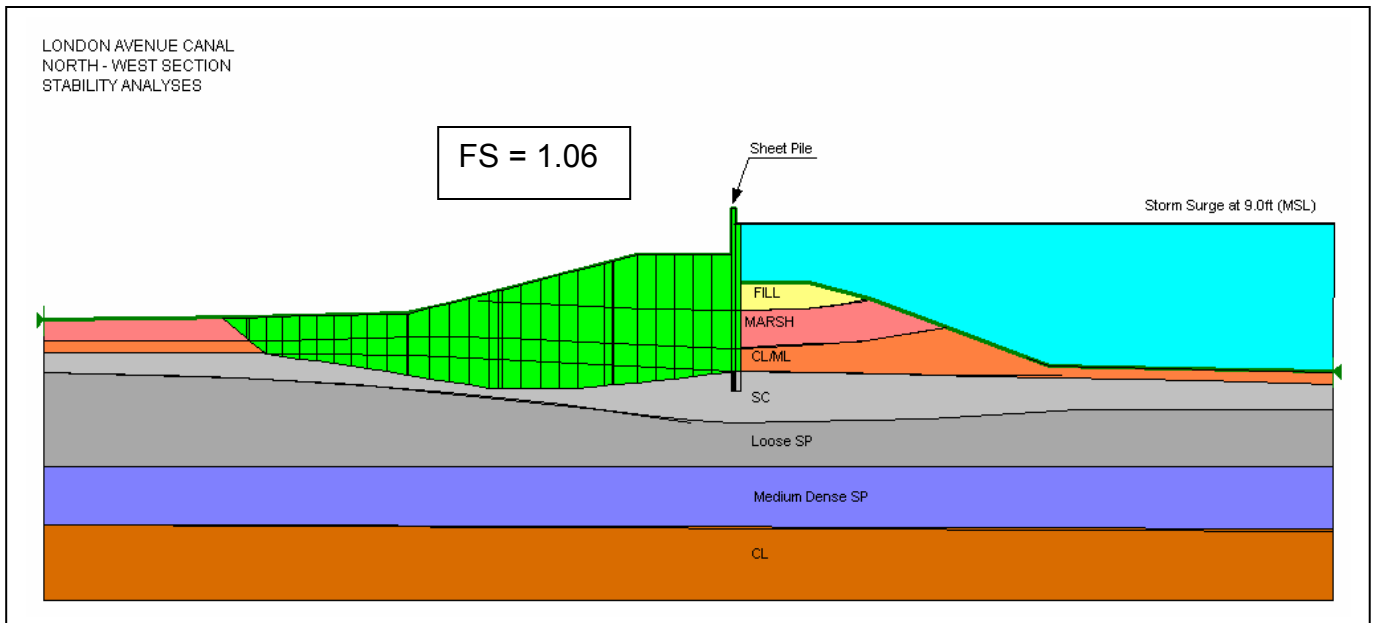


Figure 8.146: Critical failure surface with the gapping in the outboard toe of the floodwall, London Avenue Canal North, West bank. Storm surge at 9ft (MSL).

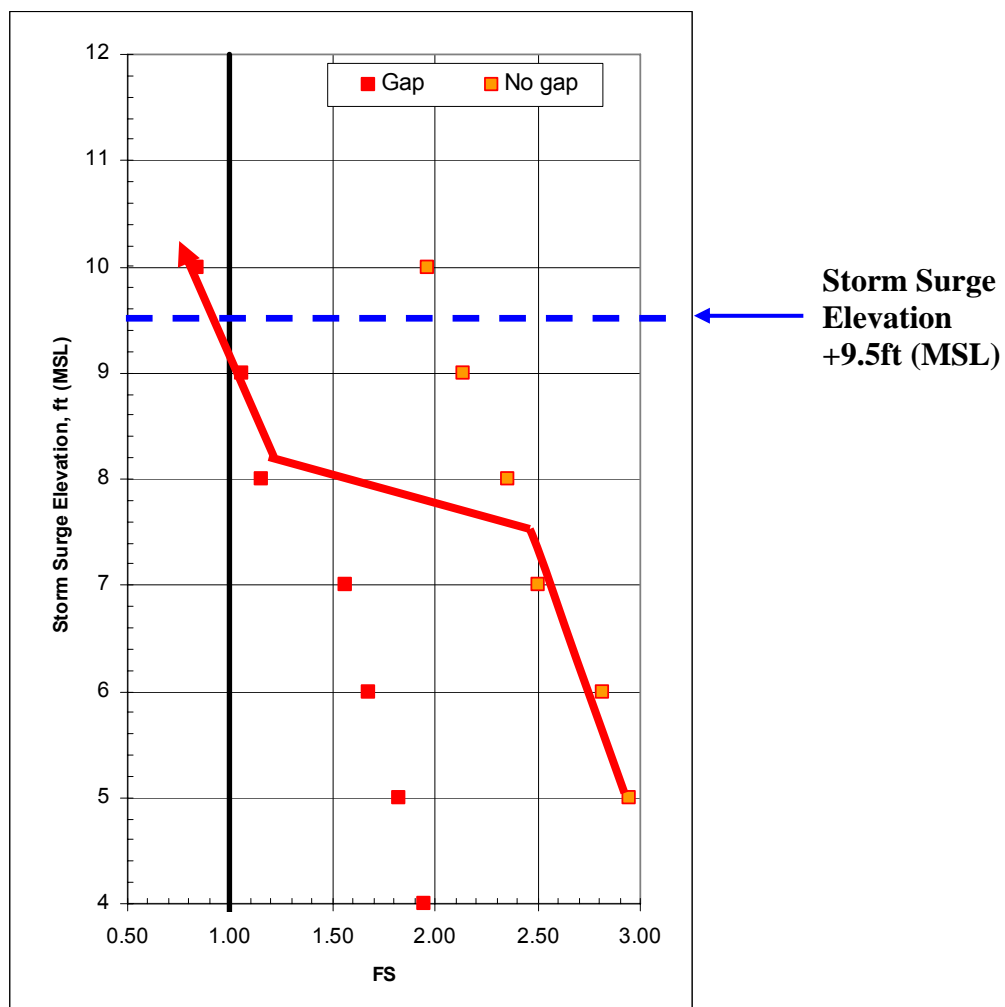


Figure 8.147 : Calculated Factors of Safety for two models based on Limit Equilibrium Analyses of the London Avenue Canal, North West bank.

ID	Soil Model	Type	γ	c	ϕ	k
			[lb/ft ³]	[lb/ft ²]	[°]	[ft/hr]
Upper fill	Mohr-Coulomb	Undrained	100	800	0	1.17E-04
Marsh, crest	Mohr-Coulomb	Undrained	80	550	0	1.17
Marsh, free field	Mohr-Coulomb	Undrained	80	300	0	1.17
CL/ML, crest	Mohr-Coulomb	Undrained	85	275	0	2.00E-04
CL/ML, free field	Mohr-Coulomb	Undrained	80	200	0	2.00E-04
SC	Mohr-Coulomb	Drained	100	0	30	0.097
Loose Sand	Mohr-Coulomb	Drained	100	0	33	0.333
Dense Sand	Mohr-Coulomb	Drained	115	0	36	0.09
Stiff Clay	Mohr-Coulomb	Undrained	95	600	0	2.00E-04

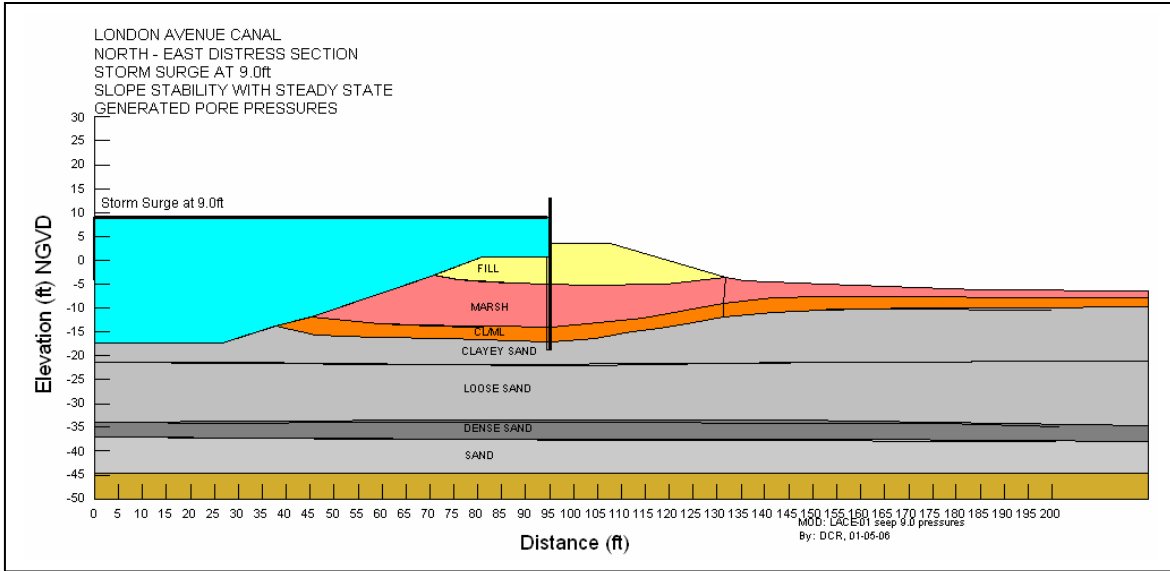


Figure 8.148: Geometry and input parameters for Limit Equilibrium and Steady State seepage Analyses for London Avenue Canal North, East bank.

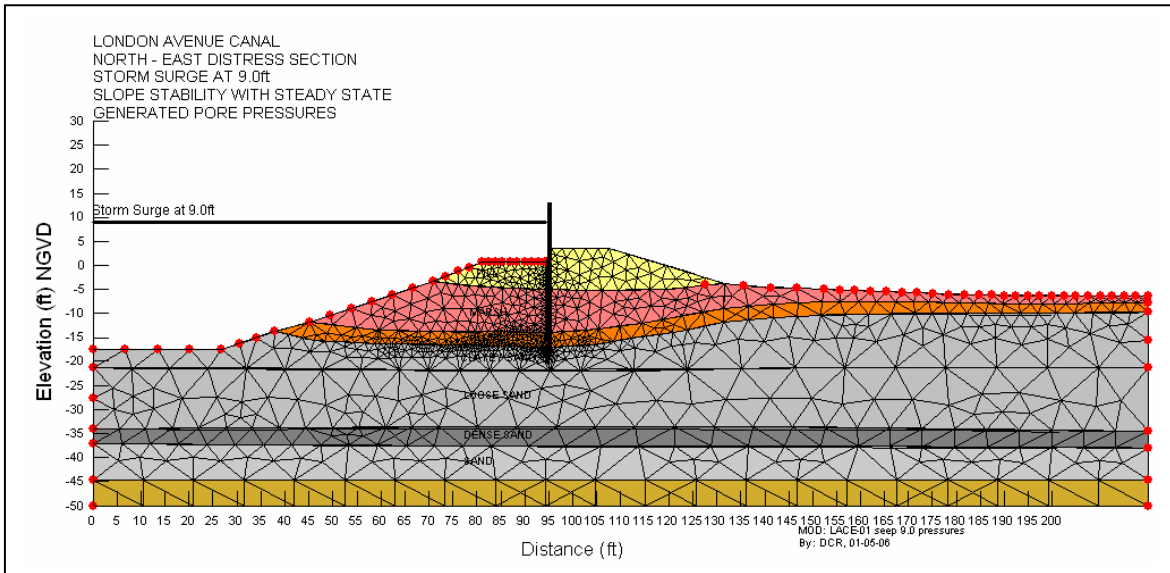


Figure 8.149: Finite Difference mesh for Steady State seepage Analyses for London Avenue Canal North, East bank.

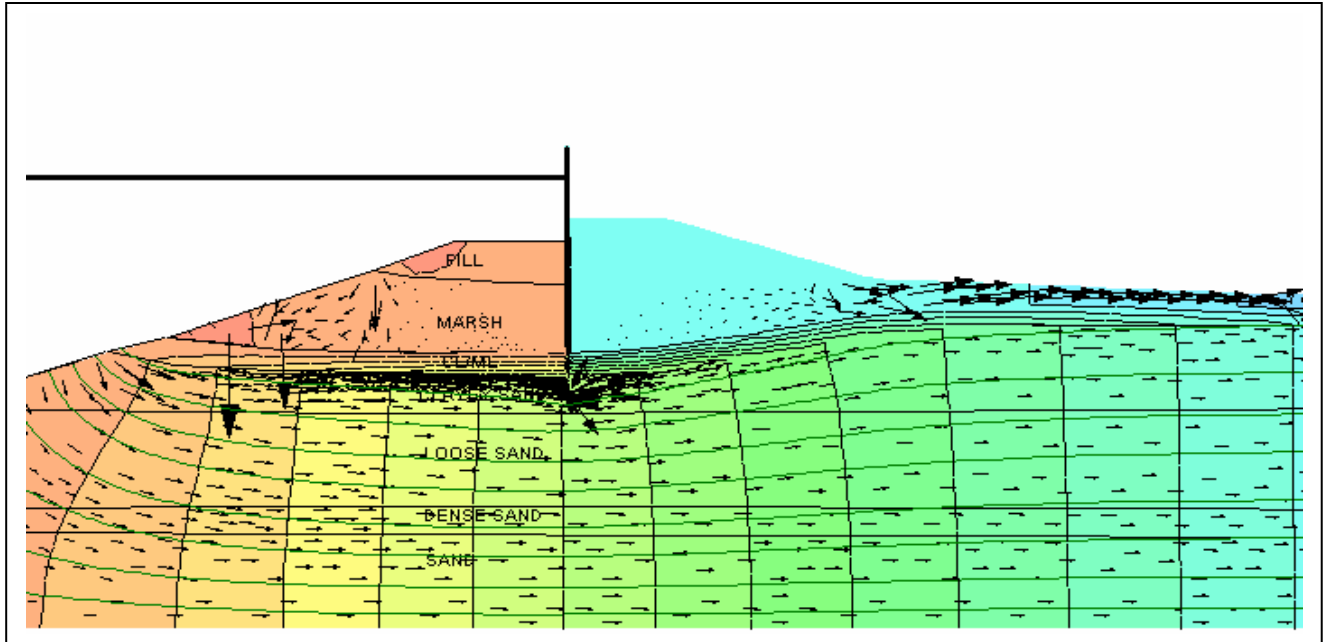


Figure 8.150: Flow net generation without the gapping in the outboard toe of the floodwall, London Avenue Canal North, East bank. Storm surge at 9ft (MSL).

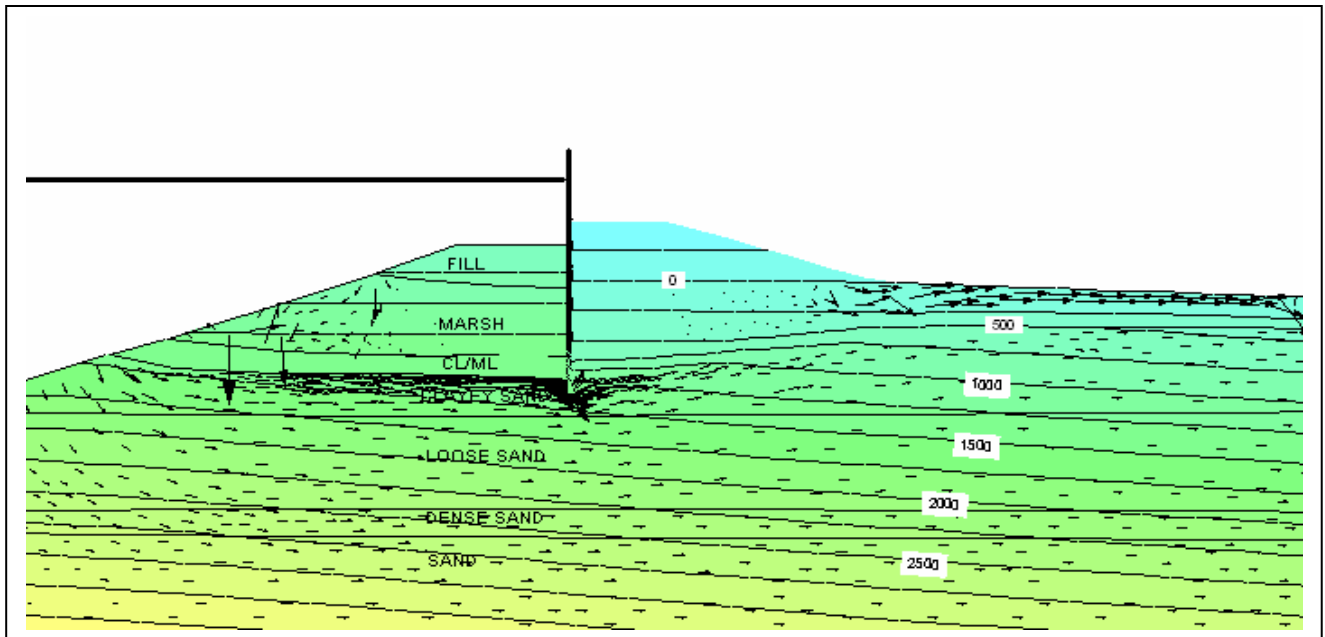


Figure 8.151: Pore water pressure contours without the gapping in the outboard toe of the floodwall, London Avenue Canal North, East bank. Storm surge at 9ft (MSL).

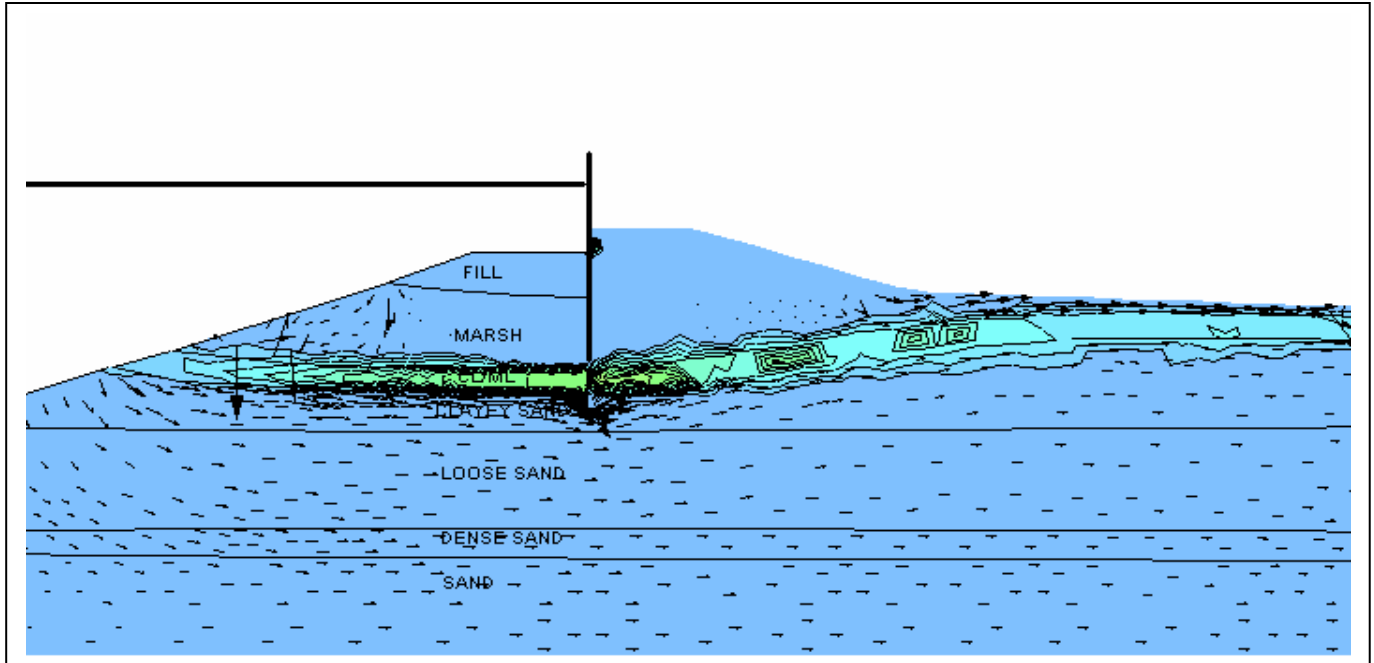


Figure 8.152: Hydraulic gradient contours without the gapping in the outboard toe of the floodwall, London Avenue Canal North, East bank. Storm surge at 9ft (MSL). Exit gradient at the inboard toe is 0.20.

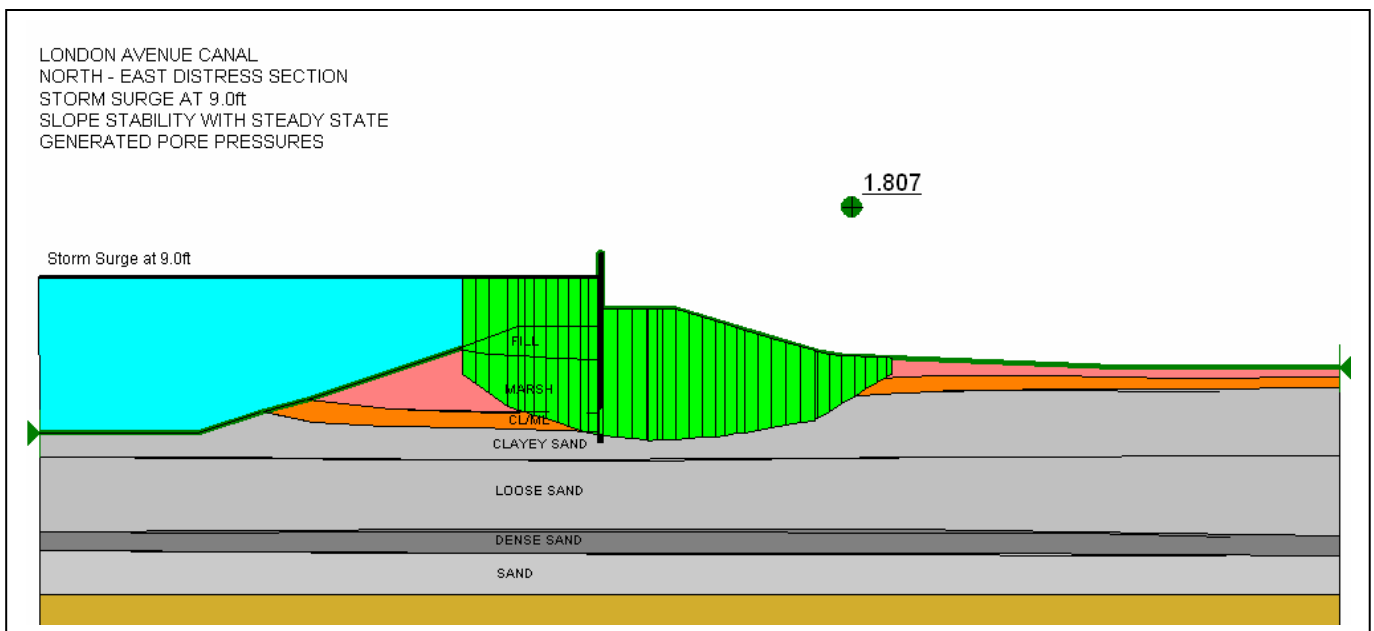


Figure 8.153: Critical failure surface without the gapping in the outboard toe of the floodwall, London Avenue Canal North, East bank. Storm surge at 9ft (MSL).

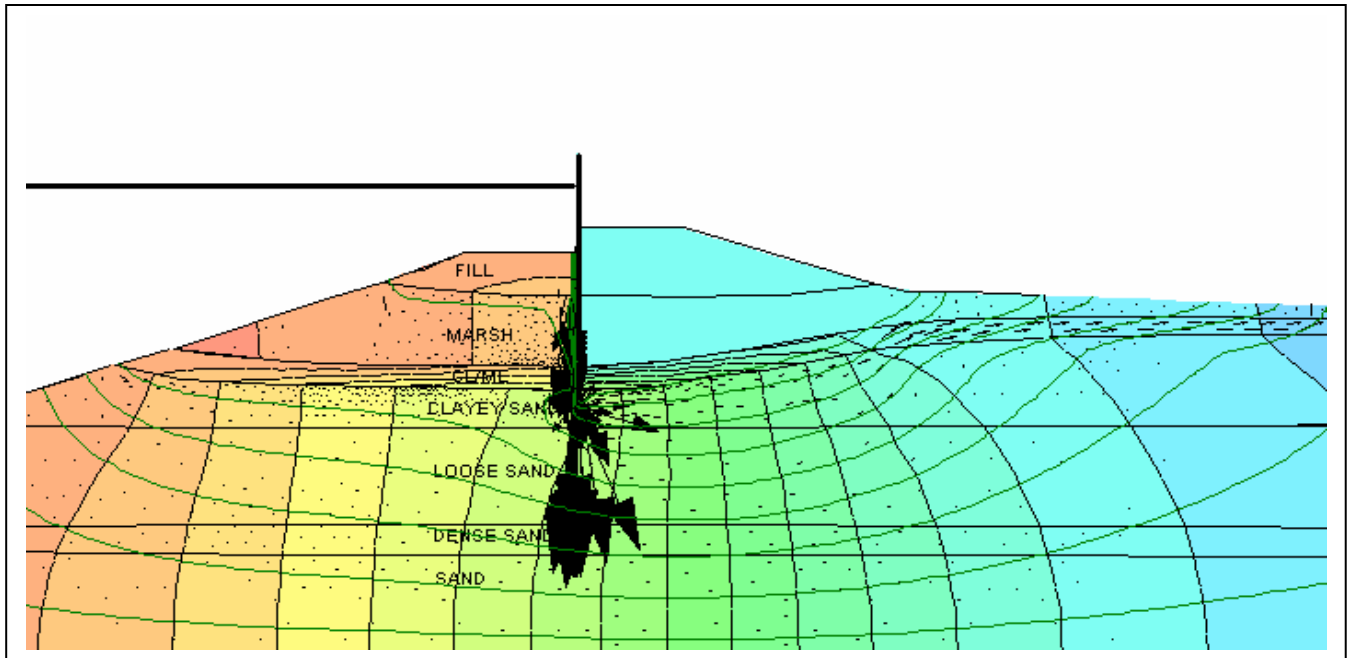


Figure 8.154: Flow net generation with the gapping in the outboard toe of the floodwall, London Avenue Canal North, East bank. Storm surge at 9ft (MSL).

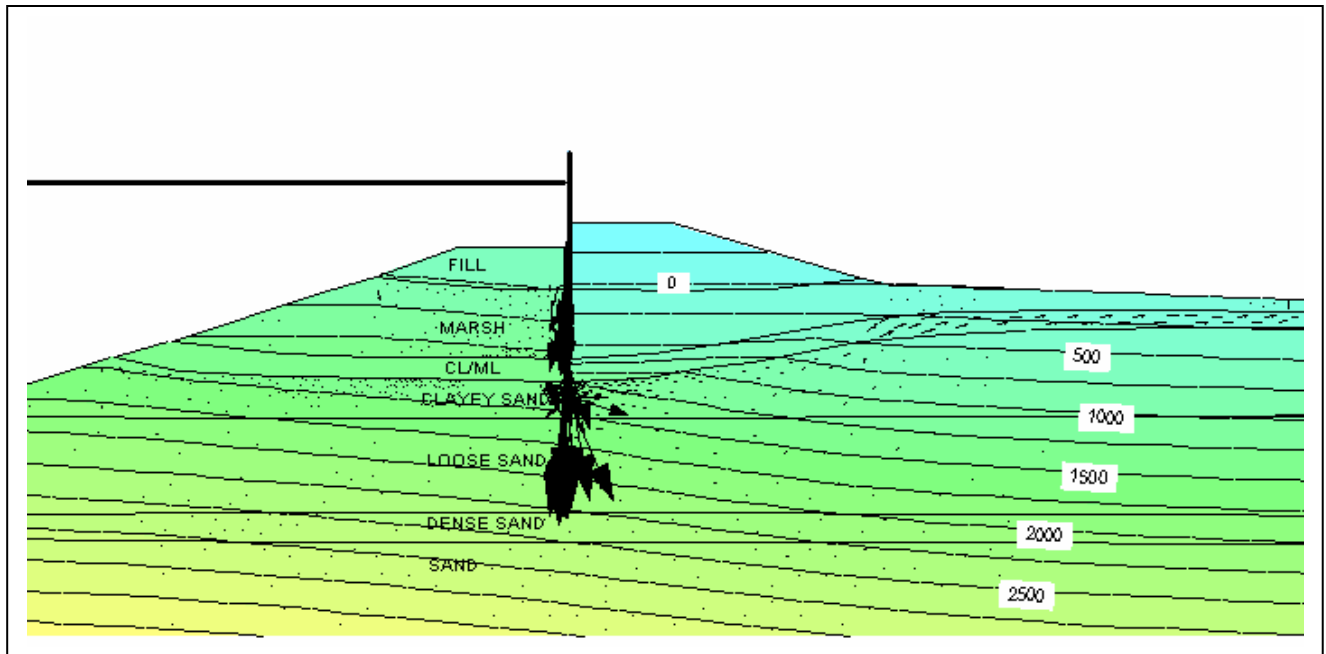


Figure 8.155: Pore water pressure contours with the gapping in the outboard toe of the floodwall, London Avenue Canal North, East bank. Storm surge at 9ft (MSL).

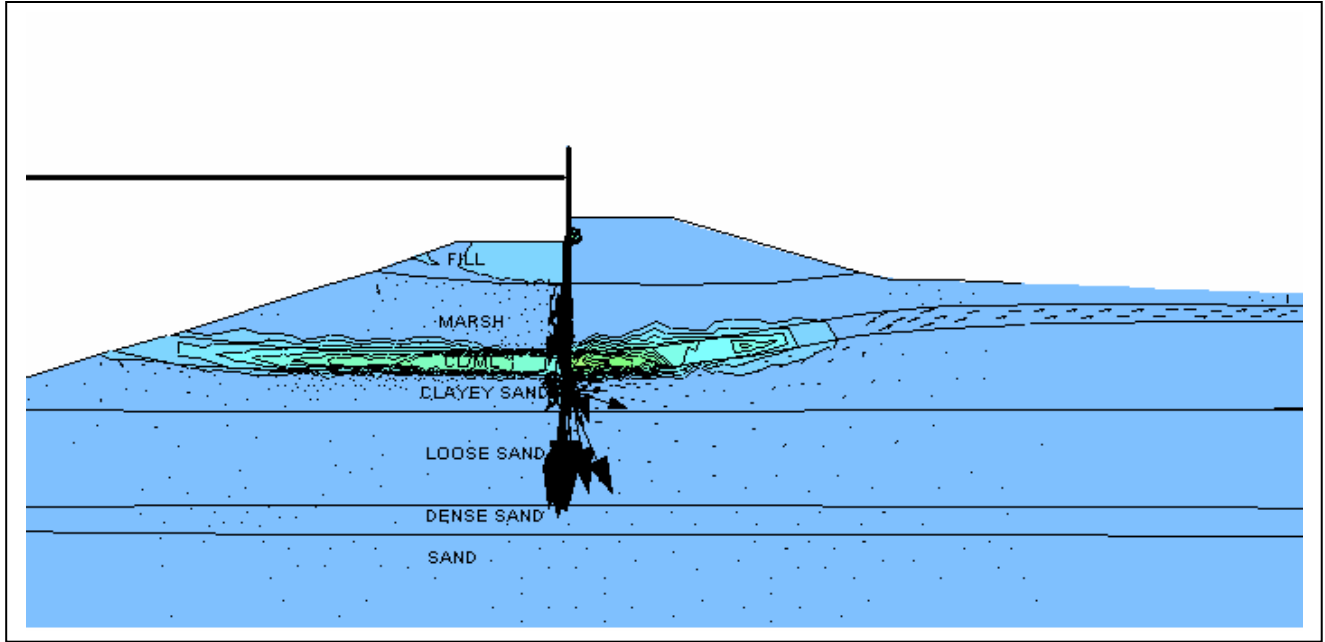


Figure 8.156: Hydraulic gradient contours with the gapping in the outboard toe of the floodwall, London Avenue Canal North, East bank. Storm surge at 9ft (MSL). Exit gradient at the inboard toe is 0.25.

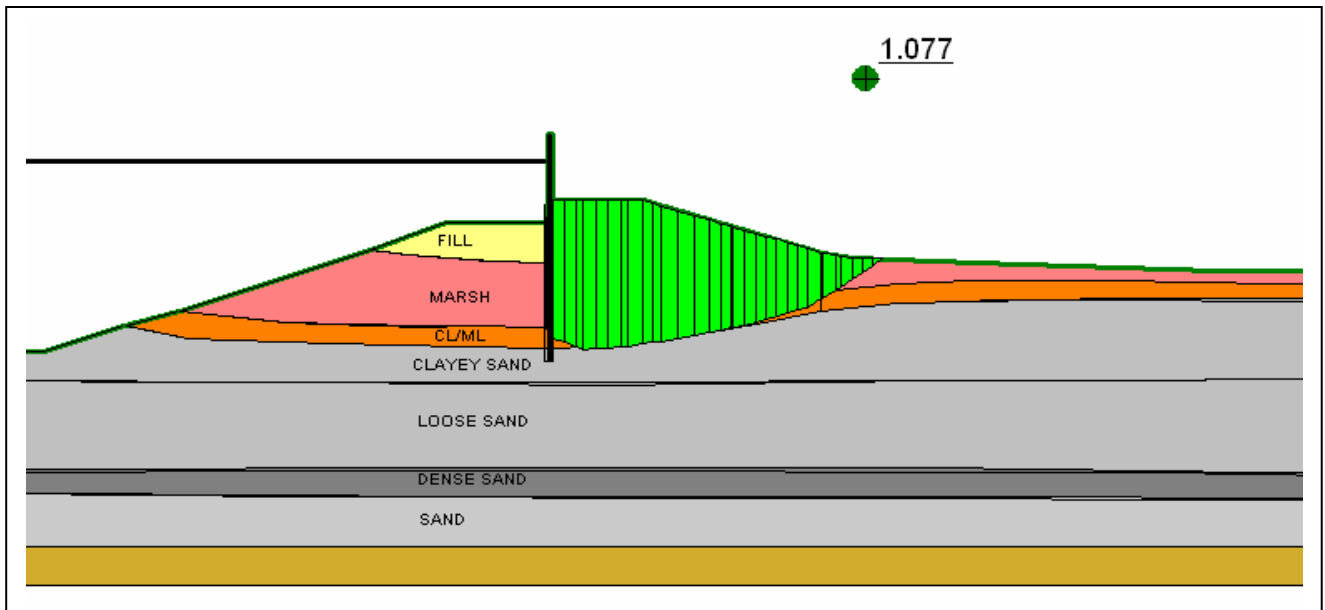


Figure 8.157: Critical failure surface with the gapping in the outboard toe of the floodwall, London Avenue Canal North, East bank. Storm surge at 9ft (MSL).

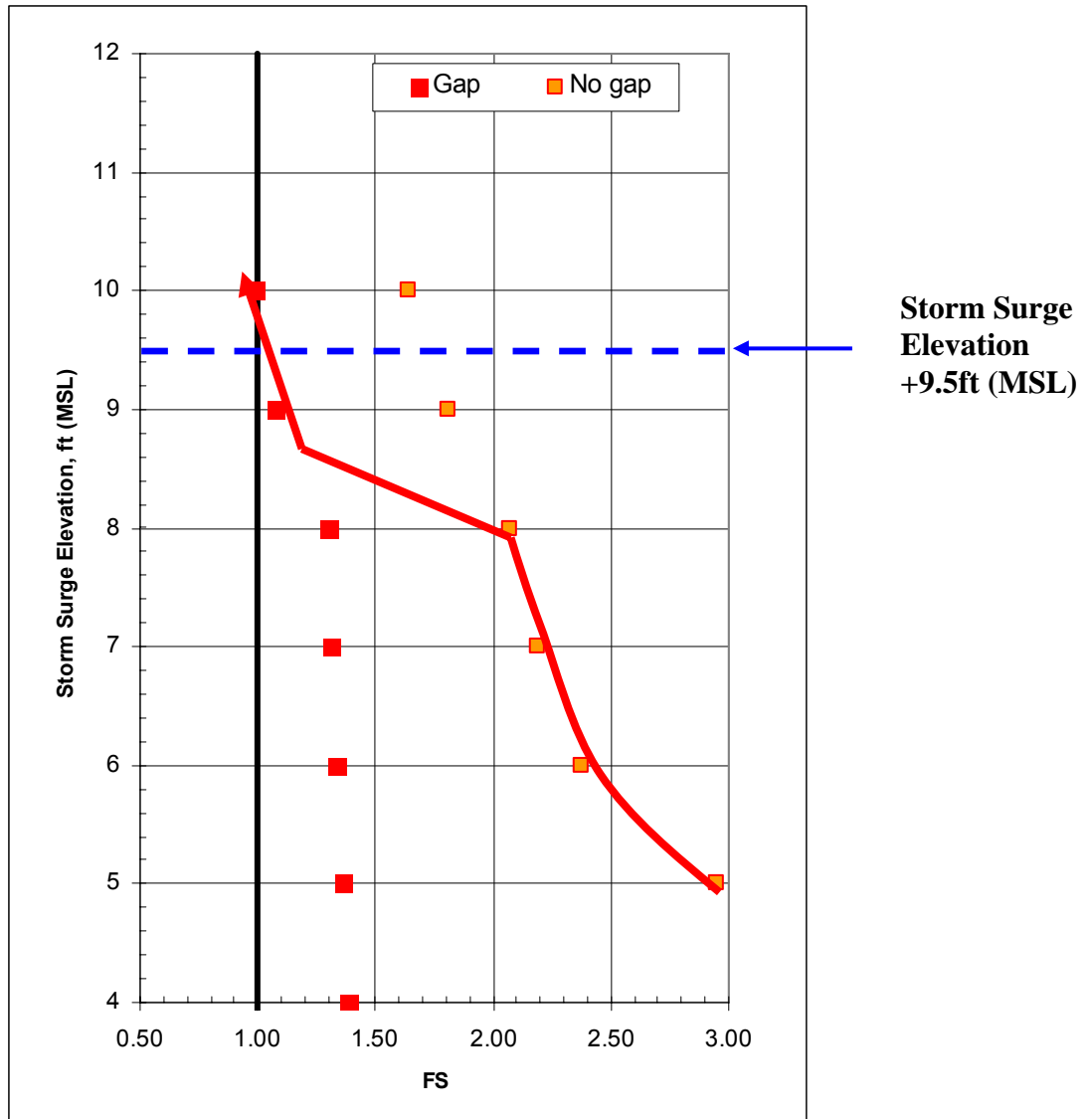


Figure 8.158 : Calculated Factors of Safety for two models based on Limit Equilibrium analyses of the London Avenue Canal, North East bank.

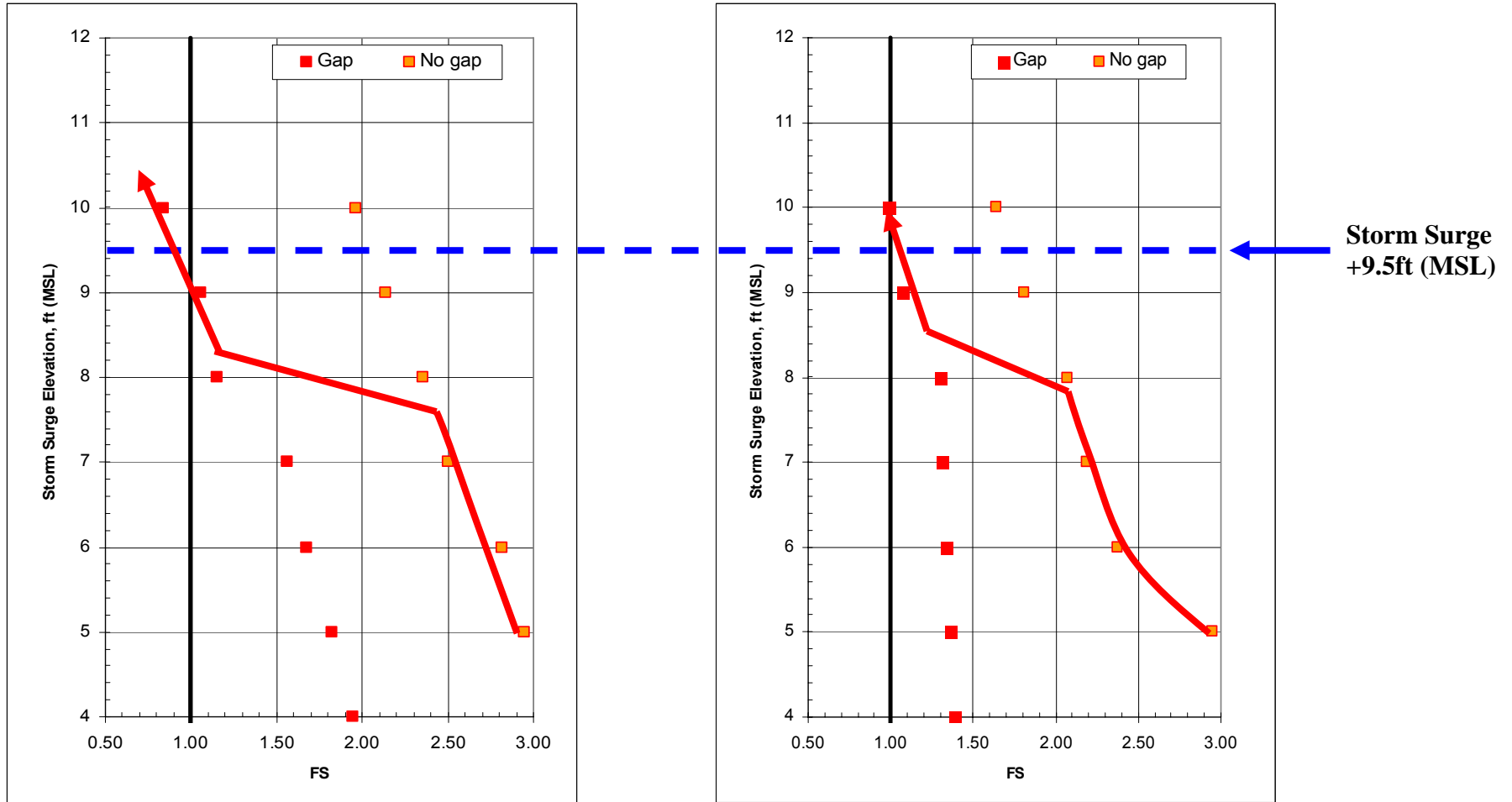


Figure 8.159: Calculated Factors of Safety for two modes based on Limit Equilibrium Analyses of the London Avenue Canal breach and distressed section for various canal water elevations; showing the best-estimated path to failure.